ABSTRACT

Title of Thesis:	EVALUATION OF NUTRIENTS AND SUSPENDED SOLIDS REMOVAL BY STORMWATER CONTROL MEASURES USING HIGH FLOW MEDIA
	Matthew Robert Landsman, Master of Science, 2017
Thesis directed by:	Dr. Allen P. Davis Department of Civil and Environmental Engineering

High Flow Media (HFM) is able to treat large runoff volumes using small-footprint systems. Seven full-scale HFM Stormwater Control Measures (SCMs) in a residential area were monitored over 11 months to assess the removal of Total Suspended Solids (TSS), Nitrogen, and Phosphorus in First Flush (FF) stormwater runoff. Excellent removal of TSS and particulate-bound nutrients was noted, but, in most SCMs, removal of dissolved species was limited. Sorption of dissolved P occurred, although most likely on captured and suspended sediment and not on the HFM itself. Mineralization and nitrification of dissolved N species during dry periods led to nitrate export. HFM grain size and organic content did not significantly impact TSS or P removal, but higher organic content was associated with higher N removal. FF was present in TSS (strongest), TN, and TP (weakest). Optimal HFM SCM design incorporates sedimentation before filtration.

EVALUATION OF NUTRIENTS AND SUSPENDED SOLIDS REMOVAL BY STORMWATER CONTROL MEASURES USING HIGH FLOW MEDIA

by

Matthew Robert Landsman

Thesis submitted to the Faculty of the Graduate School of the
University of Maryland, College Park, in partial fulfillment
of the requirements for the degree of
Master of Science
2017

Advisory Committee:
Dr. Allen P. Davis, Chair
Dr. Richard H. McCuen
Dr. Alba Torrents

ACKNOWLEDGEMENTS

Sincere thanks to Prince George's County Department of Environment for funding this work. The author would also like to thank all faculty and staff of the Civil and Environmental Engineering Department at the University of Maryland, College Park, especially Drs. Allen Davis, Richard McCuen, and Alba Torrents, for their much-appreciated support and guidance. Finally, a special thanks to all family and friends for their love and support over the years.

TABLE OF CONTENTS

LIST OF TABLES

LIST OF FIGURES

CHAPTER ONE: INTRODUCTION

1.1 Background

Stormwater runoff is a leading cause of environmental degradation in water bodies throughout the United States, and its impacts are intensifying alongside rapid urbanization, evolving regulations, and an uncertain climate (Kerkez et al. 2016). Land development to support urban sprawl alters hydrologic site conditions, creating flashy flood runoff and increased pollutant fluxes in local waterways. These changes are accountable for the degradation of approximately 13,000 square kilometers (5,000 square miles) of estuaries, 5,500 square kilometers (1.4 million acres) of lakes, and 48,000 kilometers (30,000 miles) of rivers in the United States (U.S. EPA 2009). The increased amount and variability of nutrients and sediment in runoff has negative aesthetic and biological effects on the environment; in particular, excess phosphorus and nitrogen loading can produce nuisance algae blooms via eutrophication (Hsieh et al. 2007). For these reasons, Section 303(d) of the Clean Water Act was introduced to allow states to implement Total Maximum Daily Loads (TMDLs) of pollutants to impaired bodies of water.

In order to meet local TMDLs, states are implementing Low Impact Development (LID) techniques to control urban rainfall and stormwater runoff. Best Management Practices (BMPs), also known as Stormwater Control Measures (SCMs), are becoming one of the most widely accepted approaches to LID. These systems were first developed by Prince George's County, Maryland in the 1990s and have been shown to improve stormwater quality and reduce runoff volumes and peak flows from urban environments (Pitt et al. 1995). SCMs are engineered systems that treat runoff at the source, in contrast to traditional end-of-pipe approaches that are located at the drainage outlet. This promotes decentralized runoff control

and has been proven effective in improving the environmental health of urban watersheds (Hunt et al. 2012). In SCMs, the removal of pollutants from stormwater is achieved through a combination of physical, chemical, and biological treatment processes, including filtration, sorption, sedimentation, plant uptake, and microbial degradation. Bioretention is a common SCM in which stormwater runoff is directed to flow through porous media and percolate as a treatment (Li and Davis 2009).

Treatment of stormwater runoff often focuses on the removal of total suspended solids (TSS) and nutrients; specifically, in the Chesapeake Bay, nitrogen and phosphorus. TSS removal is primarily based on sedimentation and filtration mechanisms. Larger, high-density particles are effectively trapped by sedimentation or strained out as runoff infiltrates the filter bed, and particles smaller than the pore size are captured by the media through sedimentation, interception, and diffusion-transport (Hunt et al. 2012). Davis (2007) found a median event mean concentration (EMC) of influent TSS in parking lot runoff into two bioretention cells on the University of Maryland campus to be 34 mg/L and effluent values from these cells to be 18 mg/L and 13 mg/L, representing 47% and 62% reductions in influent-to-effluent EMCs, respectively. Li and Davis (2009) found median influent and effluent EMCs of TSS from bioretention cells treating parking lot runoff to be 66 mg/L and 6 mg/L in College Park, Maryland, and 17 mg/L and 4 mg/L in Silver Spring, Maryland. Both represent >96% pollutant mass removal from influent to effluent. In these studies, the median TSS output was lower than the input, indicating successful water quality improvements in full scale bioretention. Davis and McCuen (2005) indicate that water in the Potomac River Basin, Maryland, with TSS below 25 mg/L can be considered to have excellent water quality.

Capture of TSS is important because many pollutants attach to and are mobilized by sediment. Phosphorus in stormwater runoff is generally particulate-bound, so SCMs that promote particulate removal will also perform well in terms of phosphorus removal. Primary phosphorus removal mechanisms include filtration of particulate-bound P and chemical sorption of dissolved P. Davis (2007) found median influent and effluent EMCs of total phosphorus (TP) in parking lot runoff treated with bioretention at the University of Maryland to be 0.61 mg/L and 0.15 mg/L from Cell A (75% EMC reduction) and 0.17 mg/L from Cell B (72% EMC reduction). In categorization of water quality in the Potomac River Basin, TP levels between 0.05-0.25 mg/L as P represent good water quality (Davis and McCuen 2005).

The fate of nitrogen in stormwater systems is very complex and it is difficult to treat, for it is affected by several treatment mechanisms. Particulate-bound N in stormwater, including ammonium and particulate organic N, can be effectively removed via filtration, sedimentation, and adsorption processes, and nitrite (NO_2^-) is effectively removed via reduction-oxidation reactions (Li and Davis 2014). With this, plant uptake, internal nitrogen cycling, and biological transformations cause other forms of nitrogen to be released, including nitrate (NO_3^-) and dissolved organic N (DON). Li and Davis (2014) found only 9% net overall reductions in total nitrogen (TN) concentrations in stormwater runoff from an asphalt parking lot that was treated using bioretention in College Park, Maryland, and effluent N was dominated by NO_3^- and DON, each comprising 42% of TN by mass. Davis et al. (2006) found poor NO_3^- reduction (<20%) in urban stormwater by bioretention and, in several cases, NO_3^- production was noted, most likely from nitrification of organic N.

As noted above, the composition of stormwater runoff is highly variable, and depends on factors that incorporate both watershed and rainfall characteristics. Larger drainage areas

and more-impervious watersheds generate larger runoff volumes; land use (residential, commercial, and industrial) affects pollutant compositions; length of dry periods impacts accumulation of pollutants on impervious surfaces; and the depth, duration, and intensity of rainfall impacts both the flow and composition of runoff. Termed first flush, it has been found that stormwater runoff in the initial part of a rainfall-runoff event is more polluted than that of the later periods (Deletic 1998). Conceptually, first flush occurs when pollutants build up on impervious surfaces during antecedent dry days and are mobilized by contact with runoff, generating high pollutant concentrations in initial runoff. Understanding the first flush is extremely important in designing treatment systems, but quantifying first flush is complex, inconsistent, and highly debated. An early definition of first flush offered by Bertrand-Krajewski et al. (1998) suggests the existence of a first flush when 80% or more of the pollutant mass is delivered in the first 30% of runoff volume (referred to as 80/30). Other definitions have been adapted over time (Saget et al. 1996, Sansalone et al. 1998), each with site-specific first flush definitions ranging from a 70/40 first flush to a 90/20 first flush. There is a lack of standardization in first flush characterization. Depending on the criteria chosen, in addition to the rainfall characteristics, background pollutant levels, and antecedent dry periods, there will always be varying conclusions on the presence of first flush. Additionally, first flush is pollutant species-dependent. TSS has been shown to exhibit the strongest first flush and nitrogen species have stronger first flush effects than phosphorus (Hathaway et al. 2012).

In designing SCMs for control of first flush, a balance between media hydraulic conductivity (flow rate) and pollutant removal must be maintained. Hydraulic conductivity of bioretention media depends primarily on the pore size; generally, larger

pores conduct water more rapidly (Hillel 1998). Coarse/sandy media is favored for high infiltration rates and mitigation of peak flow from infrequent storm events (Hartsig and Szatko 2012). Meanwhile, finer fractions (clay) tend to be the most chemically active and provide higher nutrient removals (Hiesh and Davis 2005).

High flow bioretention media (HFM) represents a fairly new, yet emerging, technology in SCM design. HFM systems are designed to infiltrate stormwater runoff at high flow rates without comprising pollutant removal efficiencies. HFM SCMs provide the opportunity to treat large runoff volumes with small-footprint SCMs, resulting in significant cost savings through decentralized stormwater mitigation. There are two major commercial HFM designs on the market: Filterra® by Contech Engineered Solutions and FocalPoint by Convergent Water Technologies. While Hunt et al. (2012) recommends an infiltration rate of 15.2 cm/hr (6.0 in./hr) for traditional bioretention systems, both of these HFM designs are claimed to have infiltration rates greater than 254 cm/hr (100 in./hr). Lenth et al. (2010) found Filterra® to have TSS removal efficiency between 83-88%, TP removal efficiency between 9-70%, and TN removal efficiency at 40% for bioretention systems in Maryland, Virginia, and Washington treating parking lot runoff. Convergent (n.d.) found FocalPoints' removal efficiencies in bioretention treating residential stormwater runoff to be 80% for TSS, 60% for phosphorus, and 48% for nitrogen.

1.2 Research Goals and Objectives

As HFM is a fairly new technology, performance data on stormwater treatment using HFM SCMs is sparse. An ongoing need exists to fill research gaps and continue

studying HFM as an effective treatment method. Specifically, peer-reviewed literature shows that HFM is highly effective in removing TSS and particulate-bound nitrogen and phosphorus from stormwater, but data on removal of dissolved nutrients, configuration of HFM SCM facilities, and long-term performance is much less clear. The goal of this research was to explore the future of HFM for full removal of nitrogen, phosphorus, and suspended solids in runoff.

Additionally, this study explores the characterization of first flush and how first flush affects system design and performance. By understanding the mechanisms of water quality transformations occurring within HFM SCMs, system design can be optimized for effective and efficient control of first flush. Specific objectives of this work are:

1. Analyze the efficiency of HFM SCMs for removal of suspended solids, nitrogen, and phosphorus in first flush stormwater runoff.
2. Characterize first flush and explore the relationship between first flush and HFM SCM treatment performance.
3. Investigate HFM as a potential advancement to current SCM design.
4. Provide recommendations for optimal SCM characteristics and configurations that maximize removal of solids and nutrients in stormwater runoff.

To meet these objectives, this study presents a field assessment on seven full-scale HFM SCMs in Prince George's County, Maryland, to analyze the removal of suspended solids, nitrogen, and phosphorus from stormwater runoff in an urban residential community. The seven monitored SCMs differ in watershed considerations and facility configurations, including HFM characteristics, drainage and impervious areas, storage and filtration configurations, and the presence of vegetation. Rainfall data

were also collected to evaluate system performance as a function of storm event characteristics. The findings will refine SCM design using HFM to address the long-term sustainability of these SCMs as stormwater management practices.

CHAPTER TWO: METHODOLOGY

2.1 Site Description

The seven monitored SCMs are located in the Camelot subdivision of Glenn Dale, Maryland. Camelot is located north of the intersection of Glenn Dale Boulevard (MD-193) and Annapolis Road (MD-450), as presented in Figures 2-1 and 2-2. The sites are all located in the Upper Patuxent River Watershed, which discharges into the Chesapeake Bay (CBF n.d.). A total of 32 SCM facilities were designed and constructed in Camelot by the Prince George's County Department of the Environment. Of the seven monitored systems, six are underground roadside facilities (SCMs A-F) and one is a water quality swale (SCM G). Brief site narratives are in Table 2-1 and configurations are expanded upon below. See Appendix A for additional photographs and site information.

Figure 2-1. Map of the state of Maryland showing the location of Camelot subdivision (Adapted from *USA Maryland Location Map*, n.d.).

Table 2-1. SCM site summary.

SCM[1]	PGC[2] Nota-tion[+]	Latitude / Longitude	DA[3] in ac (ha)[+]	IA[4] in ac. (ha)[+] [% of DA]	HFM[5]	CN[6] (HSG[7*])	Storage Volume in m^3 (ft^3)	Storage Runoff Depth in cm (in.)	DA/SA[8] (%SA/ DA)	Design Narrative
A	7-6	38°58'30" N 76°47'29" W	0.62 (0.25)	0.35 (0.14) [57%]	Y	85 (B)	13.9 (490)	0.55 (0.22)	116 (0.86)	Filtering before storage
B	7-8	38°58'29" N 76°47'29" W	0.36 (0.15)	0.19 (0.08) [53%]	Y	86 (B)	8.8 (311)	0.61 (0.24)	81 (1.2)	Storage before filtering
C	4-1	38°58'25" N 76°47'48" W	0.46 (0.19)	0.25 (0.10) [54%]	Y	86 (B)	10.0 (352)	0.54 (0.21)	67 (1.5)	HFM below pipe storage
D	2-7	38°58'14" N 76°47'27" W	0.59 (0.24)	0.24 (0.10) [41%]	Y	89 (B)	13.5 (478)	0.57 (0.22)	107 (0.93)	HFM around pipe storage
E	3-3	38°58'20" N 76°47'46" W	0.68 (0.28)	0.34 (0.14) [50%]	X	87 (B)	15.2 (537)	0.55 (0.22)	93 (1.1)	HFM around pipe storage, serving large DA
F	9-6	38°58'15" N 76°47'19" W	0.75 (0.30)	0.35 (0.14) [47%]	X	87 (B)	26.1 (921)	0.86 (0.34)	54 (1.8)	Tree box
G	Swale -1	38°58'16" N 76°47'32" W	4.12 (1.67)	2.13 (0.86) [52%]	Y	86 (B/C)	60.9 (2,151)	0.37 (0.14)	45 (2.2)	Bioswale

(1) Stormwater Control Measure. (2) Prince George's County. (3) Drainage Area. (4) Impervious Area. (5) High Flow Media. (6) Curve Number. (7) Hydrologic Soil Group. (8) Facility Surface Area.
(+) Information provided by Prince George's County. (*) Information per NRCS Web Soil Survey.

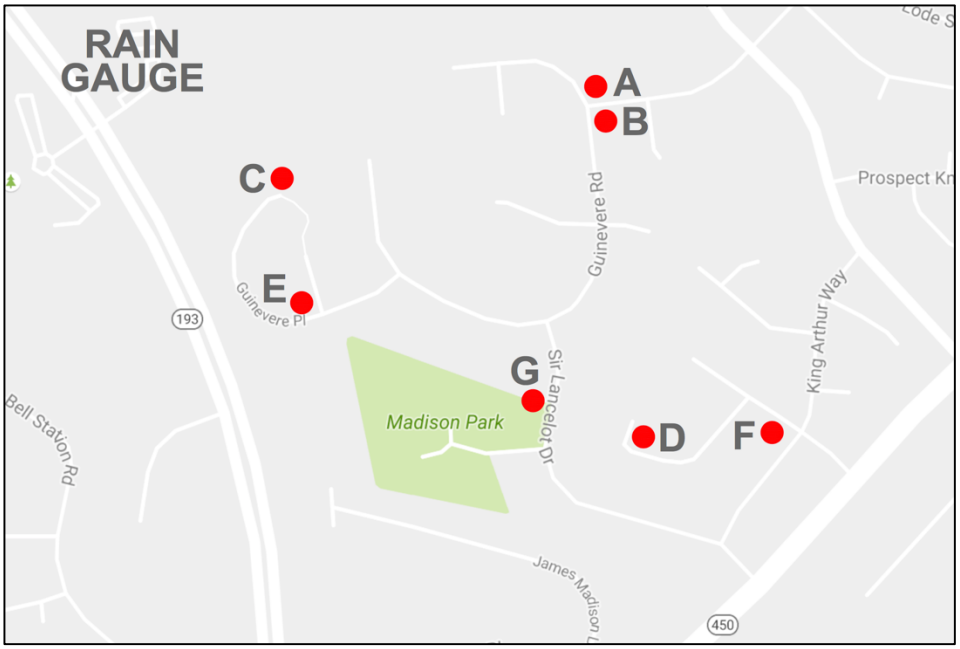

Figure 2-2. Aerial view of Camelot subdivision with SCMs and rain gauge labeled (Adapted from Google Maps).

2.1.1 Common SCM Elements

A general schematic of the six subsurface SCMs (SCMs A-F) is presented in Figure 2-3. All six subsurface SCMs receive runoff directly from the roadway via a Nyoplast Curb Inlet Structure, also called a forebay. They also receive water via infiltration from the surface through grass and porous sidewalks. The forebays are on-grade, meaning that they intercept runoff uphill of an existing inlet. The forebays are cylindrical with a diameter of 76.2 cm (30.0 in) and a depth of 1.7 m (5.5 ft). Connector pipes, located 0.8 m (2.5 ft) above the datum of the forebay, transport runoff from the forebay into the treatment chamber. Each of the SCMs have unique treatment chambers that are described below. Following the treatment chamber, treated runoff flows through an effluent monitoring well and discharges into existing inlets that connect to the existing storm drain network.

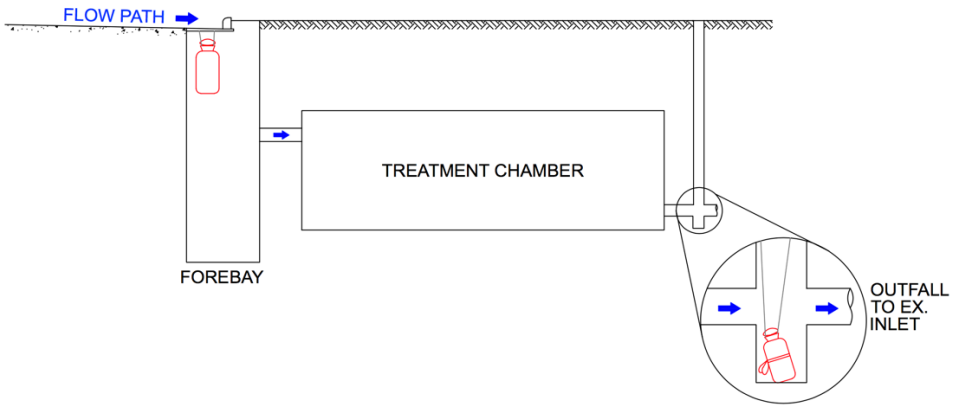

Figure 2-3. Schematic of subsurface SCMs, with flow path arrows in blue and influent and effluent samplers in red.

2.1.2 SCM A Design Narrative

The treatment chamber of SCM A features filtration before storage. The forebay connector pipe splits into two 15.2 cm (6.0 in.) perforated connector pipes that disperse runoff into a 45.7 cm (18.0 in.) deep matrix of HFM Y. After infiltrating the HFM matrix, runoff collects in two parallel 61.0 cm (24.0 in.) perforated cylindrical storage pipes. The sides and bottom of the treatment chamber of SCM A are impermeable. The storage pipes are perforated all around and surrounded by a gravel bed, creating a constant dead storage in the storage chamber below the invert of the effluent discharge pipe. A 15.2 cm (6.0 in.) effluent pipe is connected to the top of one of the storage pipes and transports treated runoff to an effluent monitoring well and into the existing storm drain network.

2.1.3 SCM B Design Narrative

The treatment chamber of SCM B features storage before filtration. The connector pipe transports runoff from the forebay into a perforated cylindrical storage pipe that is located in an impermeable gravel box. Two parallel perforated pipes are placed the gravel

box, both 76.2 cm (30.0 in.) in diameter and 7.3 m (24.0 ft) in length. The storage pipes and surrounding gravel bed act as one storage reservoir and have one influent and one effluent pipe. The storage reservoir is surrounded by impervious sheeting and has a drainage pipe to empty the chamber during dry periods. Once the storage reservoir is filled, runoff discharges into a 20.3 cm (8.0 in.) perforated pipe, located on the end cap of the storage pipe opposite of the influent pipe. This perforated pipe disperses runoff into 45.7 cm (18.0 in.) deep matrix of HFM Y that is 2.4 m (8.0 ft) wide and 3.1 m (10.0 ft) long. Below the HFM matrix is a 20.3 cm (8.0 in.) perforated effluent pipe. The filtration chamber is impervious, so groundwater infiltration cannot occur. All treated runoff enters the effluent pipe and outfalls into the existing inlet.

2.1.4 SCM C Design Narrative

The treatment chamber of SCM C features HFM below pipe storage. The forebay connector pipe transports runoff into a perforated storage pipe with a diameter of 76.2 cm (30.0 in.) and a length of 9.1 m (30.0 ft). The storage pipe is perforated around its entire length and circumference and sits in a gravel bed. In the first 3.1 m (10.0 ft) of length, measured laterally from where the connector pipe introduces runoff into the storage pipe, the gravel bed sits above natural soils. The latter 7.1 m (20.0 ft) sit above a HFM Y matrix. The treatment chamber in SCM C is surrounded by filter fabric, which makes it permeable. Therefore, discharge from the storage pipe in SCM C can infiltrate directly into surrounding soils, drain through the 45.7 cm (18.0 in.) deep HFM matrix and into surrounding soils, or drain through the HFM, into the effluent pipe, and outfall into the existing inlet.

2.1.5 SCMs D and E Design Narrative

SCMs D and E feature HFM around perforated pipe storage. From the forebay connector pipe, runoff splits into two perforated storage pipes. The storage pipes are all 76.2 cm (30.0 in.) in diameter. In SCM D, they are 7.3 m (24.0 ft) long and in SCM E, they are 9.1 m (30.0 ft) long. In all previously described SCMs, storage pipes are located within gravel beds, but, in SCMs D and E, the storage pipes are located within a bed of HFM. SCM D has HFM Y and SCM E has HFM X. Perforations in the storage pipes discharge runoff directly into HFM from the storage pipes. The HFM chamber is impermeable on the side adjacent to the roadway, but perforated on the bottom and side opposite of the roadway. The matrix of HFM is 45.7 cm (18.0 in.) deep and sandwiched between 15.2 cm (6.0 in.) gravel layers. Filtered runoff either infiltrates into surrounding soils or enters the effluent pipe and travels into the existing inlet.

2.1.6 SCM F Design Narrative

SCM F features a vegetated tree box. From the forebay connector pipe, runoff enters a perforated storage pipe that runs parallel with the roadway, 18.3 m (60.0 ft) in length and 61.0 cm (24.0 in.) in diameter. The storage pipe is perforated on the side opposite of the roadway, dispersing runoff into a gravel bed. The gravel bed is perforated on the side opposite of the roadway and on the bottom. As the storage pipe fills and runoff travels through the gravel bed, runoff will disperse outwardly from the roadway, toward treatment boxes. Four tree boxes are present, each 1.5 m (5.0 ft) long by 1.5 m (5.0 ft) wide by 1.5 m (5.0 ft) deep, and four HFM boxes, each 3.1 m (10.0 ft) long by 1.5 m (5.0 ft) wide by 1.5 m (5.0 ft) deep and filled with HFM X. The boxes are separated by

an open mesh boundary so that lateral flow is not restricted. Runoff infiltrates through the tree boxes and/or HFM matrices and either infiltrates into surrounding soils or enters an effluent pipe that sits at the bottom of the treatment boxes. The effluent pipe transports treated runoff into the existing storm drain network.

2.1.7 SCM G Design Narrative

A water quality swale is located in the northern edge of Camelot Community Park. The entire bioswale system is 83.8 m (275.0 ft) in length, and receives influent from an existing 61.0 cm (24.0 in.) storm drain pipe perpendicular to Sir Lancelot Drive. Runoff outfalls from the storm drain pipe into rip-rap and infiltrates into the first cell of the swale.

Four cells of HFM Y were installed in this system: cell one is 10.7 m (35.0 ft) long; and cells two through four are 13.7 m (45.0 ft) long. The entire system is 4.9 m (16.0 ft) wide, and cells are comprised of 1.2 m (4.0 ft) wide HFM matrices centered between two downward-sloped banks. This directs rainfall and runoff to infiltrate the treatment chambers. These cells follow the natural slope of the ground, and are isolated by berms. The berm sections separate the four cells with impermeable sheeting, and connect effluent pipes of successive cells with sloped PVC pipes. Runoff infiltrates the soil surface and through a 45.7 cm (18.0 in.) depth of HFM. Below the HFM matrix are several collection pipes in parallel. Cells one through three have six 45.7 cm (18.0 in) diameter collection pipes and cell four has eight 30.5 cm (12.0 in.) diameter pipes. After entering the collection pipes, treated runoff flows from cell one to cell four via a series of pipes and discharges into a plunge-pool that drains into an existing stream.

2.1.8 HFM Characterization

The monitored SCMs contain one of two types of media: Chesterfield-supplied HFM and Rotondo-supplied HFM. The two media are sand/gravel based and promote treatment primarily through physical filtration. A sieve analysis was performed on the media to obtain their grain size distributions. Additionally, a Loss-On-Ignition test (Heiri et al. 2001) was conducted to determine the organic content of these medias. Samples were heated to 500 and 1000^{o}C. By subtracting the masses between each step of the process, mass-percentages of organic matter (OM) and carbonate were determined.

2.1.9 Curve Numbers

Curve Numbers (CNs) measure the runoff potential of a site based on soil permeability and land cover / land use. CN is dimensionless and ranges from 30 to 99, where lower numbers indicate low runoff potential and CN=99 represents a completely impervious surface (Cronshey 1986).

A soil classification was performed to determine the soil characteristics of the Camelot subdivision. Soils were classified into Hydrologic Soil Groups (HSGs) according to their infiltration rates and textures. The Camelot subdivision is comprised of predominantly gently sloping soils and varying drainage characteristics (NRCS 2016). Using HSGs and IAs, weighted CNs were computed for each of the SCMs with equation (2-1) (McCuen 2004):

$$CN_w = (CN_i) * (f) + \left(CN_p\right) * (1 - f) \quad (2\text{-}1)$$

where CN_w is the weighted curve number, CN_i is the curve number for impervious surfaces, CN_p is the curve number for pervious surfaces, and f is the percentage of

impervious area in the DA. Impervious areas were assigned a CN of 98; a value typically associated with paved surfaces. For the pervious surfaces, land cover and land use was assumed as residential district, 1/4 acre lots. Therefore, a CN of 75 was assigned to sites in HSG B and a CN of 83 is assigned to sites in HSG C. In the case of SCM G, where multiple HSGs were present, the average of the two values was used.

2.1.10 Storage Calculations

To assess the amount of storage in the SCMs, calculations were made to estimate the available volume for water storage in each component of the SCMs, including the forebays, storage pipes, and gravel and HFM matrices. Storage within the SCMs were calculated using dimensions obtained from SCM design drawings provided by Prince George's County, Maryland, and presented in Appendix A.

First, the volume of runoff stored in the forebays was calculated based on the volume of a cylinder and the number of forebays. SCMs A through D have two forebays; SCMs E and F have one forebay; and SCM G has no forebay. All forebays are 1.5 m (5.0 ft) deep and 76.2 cm (30.0 in.) in diameter. Volumes in storage pipes were calculated using the volume of a cylinder. Lengths and diameters of the storage pipes varied from SCM to SCM. To calculate the volume of water storage in the gravel and HFM matrices, the volumes of storage pipes were subtracted from the total volume of gravel/HFM chambers and multiplied by a porosity. These calculations were dependent on SCM configurations; for example, in SCM A, the storage pipes are in a gravel chamber that is completely separated from the HFM matrix, while, in SCMs D and E, the storage pipes are located within the HFM. A porosity of 0.4 was assumed for both gravel and HFM.

Storage volumes of each SCM component were added together to provide an estimation of dead storage available in each SCM. Storage volumes were then converted into depths of runoff by dividing the storage volume by the drainage area of the SCM.

2.1.11 Drainage Area to Surface Area Calculations

Contributing drainage areas (DAs) were compared to facility surface areas (SAs) to assess the amount of space needed per amount of runoff treated in the SCMs. This was done by dividing DA over SA and by calculating the percentage of DA that SA occupied. Drainage areas were provided by Prince George's County, Maryland. Facility surface areas were calculated based on dimensions in SCM design drawings provided by Prince George's County, Maryland, and presented in Appendix A.

2.2 Simulation Model

A simulation model was developed in Fortran to assess the flow of runoff through HFM SCMs. The model generates rainfall-runoff volumes at one-minute increments and simulates runoff movement through the SCMs by performing water balances in four compartments of SCMs D and E (HFM around perforated pipe storage). Variables include rainfall characteristics (precipitation depths and durations), facility configurations (media characteristics, component sizing and design), and watershed characteristics (drainage areas, curve numbers). This model provides a quantitative assessment of facility performance as a function of these characteristics. More information about the simulation model is provided in Appendix B.

2.3 Sampling Methodology

Samples were taken using Thermo Scientific Nalgene Storm Water Samplers (Figure 2-4(a)). These samplers collect first flush samples using a ball valve that seals the sampler after one liter is collected. No adjustments were made to influent samplers for the six roadside facilities. Due to the buoyancy of the empty bottles, the influent sampler in SCM G and all seven effluent samplers were held in place using five 340-gram (12-ounce) fishing weights attached to the sides of the samplers using a hose clamp and zip ties (Figure 2-4(b)).

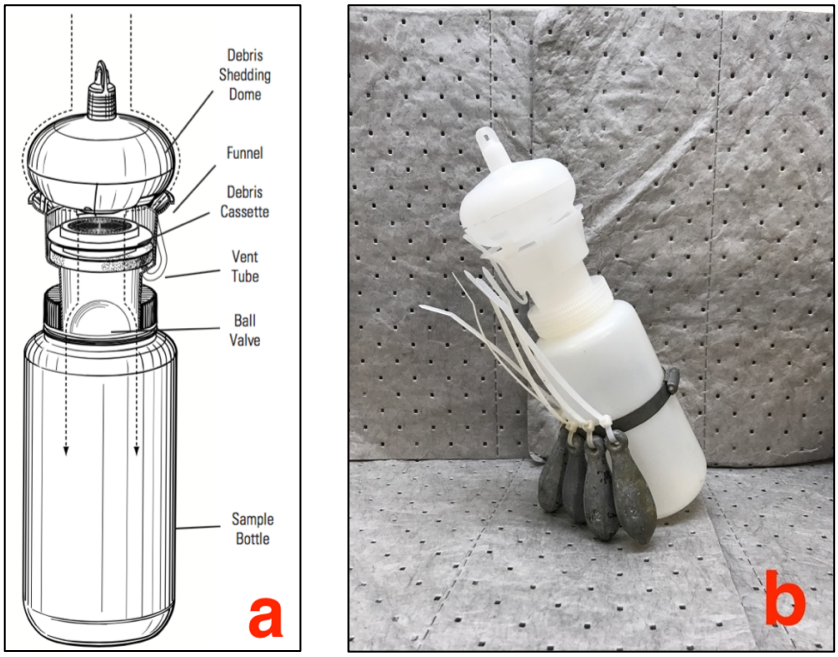

Figure 2-4 (a). Diagram of samplers (Thermo Scientific 2010).
(b). Effluent Sampler complete with fishing weights for stabilization in effluent monitoring wells.

Influent and effluent samples were collected from June 2016 to June 2017. Placement of influent and effluent samplers for SCMs A-F are shown in red in Figure 2-3. In all six roadside SCMs, influent samplers were hung from the inlet grates using fishing line, as seen in Figure 2-5, to collect runoff as it entered the forebay from the

roadway. In the bioswale, influent samples were collected at the outfall of the storm drain pipe, shown in Figure 2-6. Effluent samples for all seven SCMs were taken by placing the samplers into the monitoring wells using fishing line, as seen in Figure 2-7. Additional photographs showing sampling are provided in Appendix A.

Figure 2-5. Influent Sampling Methodology for SCMs A-F.

Between storm events, the tops of the samplers that were tied to fishing line were left in place and cleaned and rinsed with deionized water prior to the next storm event. This includes the debris shedding domes and funnels that are called out in Figure 2-4(a).

Figure 2-6. Influent sampling for SCM G.

Figure 2-7. Effluent sampling for all SCMs.

Figures 2-8 and 2-9 show influent and effluent sampler tops during dry periods, respectively. All other sampler components (bottles, ball valves, debris cassettes, and transport lids) were washed, soaked in acid baths overnight, and rinsed with deionized water prior to the next storm event.

Figure 2-8. Influent sampler during dry period.

Figure 2-9. Effluent sampler during dry period.

2.4 Weather Monitoring

Precipitation was measured using an Isco 674 Tipping Bucket Rain Gauge with 0.02 cm (0.01 in) sensitivity. The rain gauge is located approximately 0.8 km (0.5 mi) northwest of the Camelot subdivision, at the Glenn Dale Volunteer Fire Department, as presented in Figure 2-2. The rain gauge was connected to an Isco 4120 Flow Logger for data collection. For the first five monitored storm events, rainfall readings were taken in fifteen-minute intervals, but the flow logger was recalibrated to five-minute readings in August 2016. The field setup of the rain gauge is shown in Figure 2-10. Data from the flow logger was collected using an Isco 581 Rapid Transfer Device (RTD) and taken to the Environmental Engineering Laboratory at the University of Maryland, College Park. The RTD console connects to a computer and data was downloaded using Flowlink 4.2 software. In addition to field measurements, weather reports and local rainfall data were referenced for quality assurance purposes.

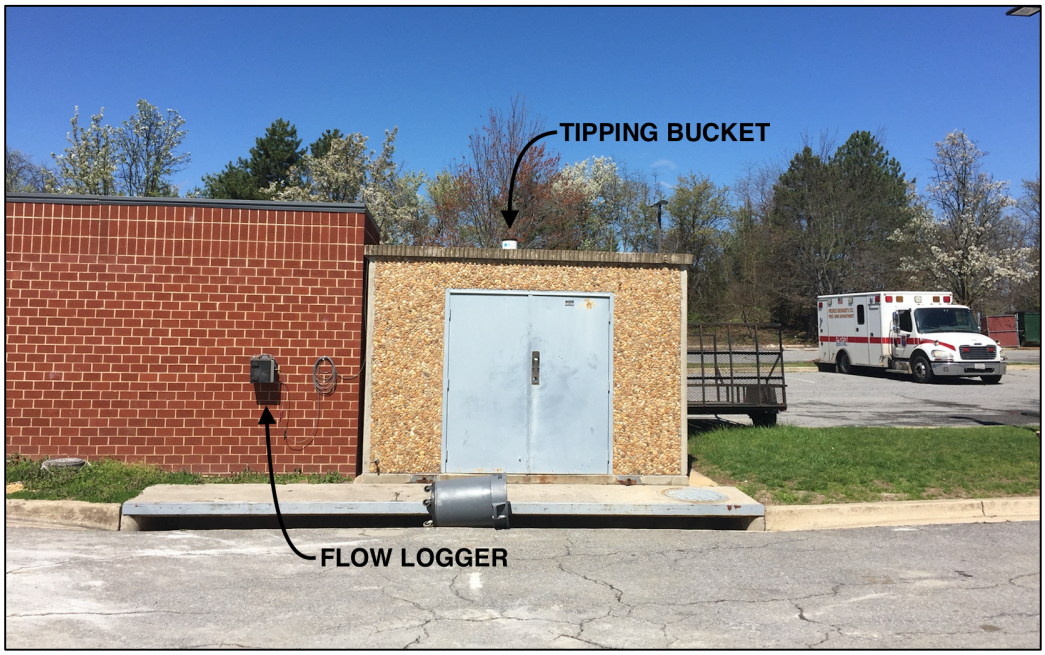

Figure 2-10. Rain gauge field setup.

2.5 Analytical Methodology

2.5.1 Water Quality Measurements

Influent and effluent samples from each of the seven SCMs were subjected to the following water quality tests: total suspended solids (TSS), total phosphorus (TP), total dissolved phosphorus (TDP), dissolved reactive phosphorus (DRP), total nitrogen (TN), total dissolved nitrogen (TDN), nitrate (NO_3^-), nitrite (NO_2^-) and ammonium (NH_4^+). All analyses followed the methods of *Standard Methods for the Examination of Water and Wastewater* (Eaton et al. 1998) and are summarized in Table 2-2.

Table 2-2. Summary of laboratory procedures for water quality measurements.

Parameter	Method*	Standard Method	Detection Limit (mg/L)	Accuracy (mg/L)
Total Suspended Solids	G	2540 D	1	1
Total Phosphorus	D, S	4500-P B.5 4500-P E	0.05 as P	0.01 as P
Dissolved Phosphorus	F, D, S	4500-P B.5 4500-P E	0.05 as P	0.01 as P
Dissolved Reactive Phosphorus (PO_4^{-3})	F, S	4500-P E	0.05 as P	0.01 as P
Total Nitrogen	D, S	4500-N C 4500-NO_3^-B	0.05 as N	0.01 as N
Total Dissolved N	F, D, S	4500-N C 4500-NO_3^-B	0.05 as N	0.01 as N
Nitrate	IC	4500-NO_3^-B	0.05 as N	0.01 as N
Nitrite	S	4500-NO_2^- B	0.05 as N	0.01 as N
Ammonium	S	4500-NH_3 F	0.05 as N	0.01 as N

*G = gravimetric, D = digestion, S = spectrophotometry, F = filtration, IC = ion chromatography

TSS was measured by passing 100 mL of sample through a preweighed 0.45 µm glass-fiber filter, drying the filter at 103 to 105°C for 1 hour, and computing the weight increase due to solids residue. In the cases where TSS was very high (greater than 2000

mg/L), lower amounts of sample were diluted and used to ensure that the filter would not clog prior to all of the sample passing through the filter.

TDP, DRP, TDN, NO_3, NO_2, and NH_4 samples were filtered through a 0.22 μm membrane filter prior to testing. All absorption measurements (TP, TDP, DRP, NO_2, and NH_4) were taken using a Shimadzu UV 160-VIS spectrophotometer. Phosphorus species were measured using the persulfate digestion and ascorbic acid methodology. TN and TDN measurements were made using the total nitrogen measuring unit of a Shimadzu TOC-L Analyzer. Nitrate measurements were made using an ICS-1100 Dionex ion chromatograph with a Dionex IonPac AS22 anion column. The eluent used for NO_3 measurements was 4.5 mM Na_2CO_3 / 1.4 mM $NaHCO_3$.

Dissolved organic phosphorus (DOP) and dissolved organic nitrogen (DON) were calculated by subtracting all measured species from the total dissolved concentrations, as shown in the following equations:

$$DOP = TDP - DRP \tag{2-4}$$

$$DON = TDN - [NO_3 - N] - [NO_2 - N] - [NH_4 - N] \tag{2-5}$$

where TDP is the measured concentration of total dissolved phosphorus, DRP is the Dissolved Reactive Phosphorus, DON is the dissolved organic nitrogen, and TDN is the total dissolved nitrogen.

2.5.2 Weighted Means

Mean influent and effluent concentrations of all pollutants were calculated in two ways: unweighted and weighted. Unweighted means represent the average of measured

values. Weighted means are the average of measured values normalized by individual storm sizes, as presented in the following equation:

$$\bar{x} = \frac{1}{P_{total}} \sum_{i=1}^{n} x_i P_i \qquad (2\text{-}6)$$

where $\bar{x}$ is the weighted average; P_{total} is the total rainfall depth for all monitored storms; i is the individual storm; n is the number of monitored storms; x_i is the measured pollutant concentration; and P_i is the rainfall depth of the individual storm. This allows for an analysis of the relationship between storm size and influent/effluent concentrations.

2.5.3 Probability Plots

Probability plots were created to present graphical distributions of pollutant concentrations for all monitored storm events. These plots are set up as cumulative normal distributions on a logarithmic scale. The x-axis represents the exceedance probability and the y-axis represents the pollutant concentration associated with that exceedance probability. For example, for the frequency curve of Figure 2-11, the probability of a TSS concentration being larger than 10 mg/L in one time period is 58%.

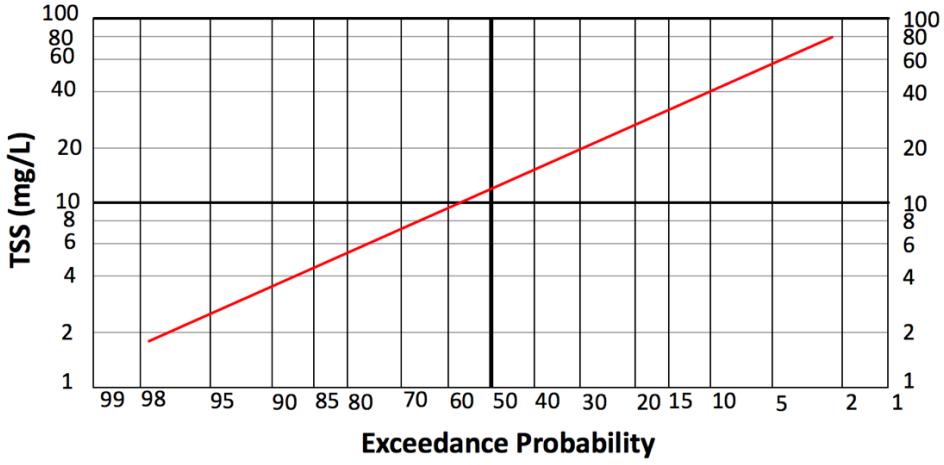

Figure 2-11. Example of an exceedance probability plot for a randomly-generated population of TSS concentrations.

2.5.4 Statistical Analyses

Statistical analyses were performed using the Mann-Whitney U test. This test is favored over the two-sample t-test because it does not require the assumption of normal populations. The Mann-Whitney test is a nonparametric test of the null hypothesis that randomly selected samples are taken from the same population (H_o: $\mu_1=\mu_2$). The alternative hypothesis can be one-sided (H_a: $\mu_1>\mu_2$) or two-sided (H_a: $\mu_1\neq\mu_2$). One-sided tests were used to determine a positive or negative shift in one population as compared to the other, such as comparing influent and effluent concentrations to determine if effluent concentrations were lower than influents. Two-sided tests were used to determine homogeneity in data sets, i.e., if effluent concentrations were different from SCM to SCM, or if individual storm characteristics affected influent and effluent concentrations.

The procedure for this test involves pooling all concentrations from the two samples into one combined sample set, while keeping track of which samples each concentration comes from, and then ranking from lowest to highest from 1 to n_1+n_2, where n_i is the number of values in the sample sets. Each sample set's rankings are summed and the Mann-Whitney U statistic is taken as the smaller of U_1 and U_2:

$$U_1 = n_1 n_2 + \frac{n_1(n_1+1)}{2} - R_1 \quad (2\text{-}7)$$

$$U_2 = n_1 n_2 + \frac{n_2(n_2+1)}{2} - R_2 \quad (2\text{-}8)$$

where U is the test statistic; n is the number of values in a sample set; R is the sum of the ranks; and subscripts 1 and 2 represent the two sample sets. Calculated U values were compared to critical values presented in McCuen (2003) to conclude whether or not differences were significant. All statistical analyses were performed at 5% level of significance (α=0.05), which indicates a 5% risk of concluding that a difference exists

when there is no actual difference (Type I error). When α is lower, a Type II error, which occurs when a null hypothesis is accepted when it is false, is more likely. There is no connection between this α value and the physical conditions of this study.

2.5.5 Simple Method

The Simple Method is a technique used for estimating pollutant loads in urban stormwater runoff (Schueler 1987). The Simple Method estimates annual pollutant loads as a product of runoff volumes and concentrations. A modified Simple Method, presented in equation (2-9), was used to estimate the pollutant loads for each storm event:

$$L = 0.226 * P * R_v * A * C \quad (2\text{-}9)$$

where L is the accumulated pollutant load, in lbs; 0.226 is the combined unit conversion for in to ft, L to ft^3, mg to lb, and ac to ft^2; P is the individual storm rainfall depth, in in; R_v is the dimensionless runoff coefficient; A is the drainage area, in ac; and C is the TSS FFC, in mg/L. R_v was calculated using the equation presented in the Maryland 10% Rule Guidance Manual (CWP 2003):

$$R_v = 0.05 + 0.009 * I \quad (2\text{-}10)$$

where I is the percentage of impervious cover expressed as a whole number. A mass balance was performed on TSS and all species of N and P to evaluate mass load reductions of each constituent through the SCMs. Since monitored storm events only account for a portion of total annual rainfall events, total input, output, and reduced mass loads of each constituent were converted into annual mass loads, based on the ratio of total annual rainfall over total recorded rainfall. Additionally, since not all rainfall events produce runoff, this ratio was multiplied by P_j. P_j was assumed to be 0.9; a value

presented in the Maryland 10% Rule Guidance Manual (CWP 2003) to represent the fraction of Maryland storms that are so minor that all of the rainfall is stored in surface depressions and eventually evaporates.

2.5.6 Sediment Accumulation Analysis

HFM samples from SCM G were collected at different stages of the project duration and analyzed to assess accumulation of sediment in HFM Y. SCM G has HFM matrices that begin on the ground surface, while HFM matrices from the other SCMs are subsurface and were inaccessible for media sampling. HFM samples were taken in the top 15 cm (6 in) of cells one and two of SCM G approximately one month into operation of the bioswale, on July 15, 2016, and in all four cells at the end of sampling, on May 15, 2017. Fresh HFM Y, provided by Prince George's County, was analyzed as a control to represent the HFM at the time of installation.

In the lab, 100 grams of well-mixed HFM samples were placed on a Number 8 sieve with a pore size opening of 2.38 mm. A preweighed metal collection dish was placed underneath the sieve to collect all particles that passed through the sieve's openings. This defines sediment as all particles less than 2.38 mm. On the sieve, samples were washed with deionized water and shaken to promote full washoff of sediment. After samples were fully washed and all sediment small enough had passed through the sieve, the metal dishes containing sediment and water were placed in a 104^{o}C oven overnight. The following day, dishes were weighed and the differences in masses of the dishes pre- and post-sieving was calculated to determine the amount of sediment in the 100 g

samples. By subtracting sediment masses taken at different stages of the project, an estimation of sediment accumulation in the bioswale HFM was determined.

2.6 Quality Assurance and Quality Control Measures

All sampling bottles and laboratory glassware were cleaned, soaked in acid overnight, rinsed with deionized water, and dried prior to use in the field and/or laboratory. Samplers were picked up within 24 hours of the start of the storm event and sealed, labeled and transported to the Environmental Engineering Laboratory at the University of Maryland in an iced cooler. All handling of sample bottles was done by gloved-personnel.

Field blanks were collected randomly with sample sets and subjected to the same processing and analytical procedures as samples. Field blank use deionized water brought from the Environmental Engineering Laboratory, College Park, MD. These blanks read below detection limits in all analytical tests. Additionally, samples were randomly selected to be processed in triplicates, to which the variation of these three measurements did not exceed ±10%. These cases are clearly marked in all text, tables, figures, and other use of the data in all reports, presentations, and documents.

In the lab, analysis was performed in a timely manner or samples were frozen until testing occurred. Each sample was recorded on the sampling master sheet, and a number/letter/color coding system was employed to ensure proper sample recording. All laboratory analytical measurements underwent calibrations every time they were used. At least five standards were used for calibration in photometric analyses. Linear calibrations had no less than 0.999 correlation coefficients. For TN and NO_3 analyses, standard curves

were run, along with one standard-check for every ten samples. If the calibration checks failed (error exceeded ±10%), samples were re-tested using a new standard curve.

Standards were created from stock solutions obtained from commercial chemical companies, as presented in Table 2-3. Standards for all phosphorus species and TN, TDN, and NO_3^- were premade at 1000 mg/L and diluted to desired concentrations. Standards for NO_2^- and NH_3/NH_4^+ were created by diluting proper masses of pure chemical into deionized water to achieve desired concentrations.

Table 2-3. Stock solution summary.

Analysis	Species	Manufacturer	Supplier	Concentration
TP, TDP, DRP	Potassium Dihydrogen Phosphate, dissolved	Ricca Chemical Company	Fisher Scientific	1000 mg/L as P
TN, TDN, NO_3^-	Potassium Nitrate, dissolved	Ricca Chemical Company	Fisher Scientific	1000 mg/L as N
NO_2^-	Sodium Nitrite, pure	Fisher Chemical	Fisher Scientific	-
NH_3/NH_4^+	Ammonium Chloride, pure	Acros Organics	Fisher Scientific	-

CHAPTER THREE: RESULTS AND DISCUSSION

3.1 Storm Event Characterization

Influent and effluent samples and rainfall data were collected for 24 storm events from June 2016 to May 2017. A summary of rainfall characteristics (precipitation depths, durations, intensities, and number of antecedent dry days) is presented in Appendix C, Table C-1. Antecedent dry days represent the number of days between storm events, monitored and non-monitored, that produce runoff; small, short storms that were not expected to have produced any runoff were not considered in this measure. Average and maximum rainfall intensities are reported for the entire duration and for the first 15, 30, and 60 minutes of the storm event.

On several instances, rainfall measurements taken at the Glenn Dale Fire Department were inaccurate or unavailable. Dates in which rain gauge errors occurred are denoted with * in Table C-1. Instances of rain gauge errors that were encountered during this project include the rain gauge clogging with debris (06/28/16, 07/04/16), the battery of the rain gauge dying (11/30/16), and the rainfall measurements not agreeing with local sources. This third instance was encountered for isolated thunderstorms (08/21/16, 02/25/17, 04/22/17) and wintry precipitation, including freezing rain (12/17/16, 02/09/17) and snowfalls (03/14/17). In the case of rain gauge errors, local weather reports, including Weather Channel and Weather Underground, were referenced for storm depths and durations, but rainfall intensities were unavailable.

Table 3-2 shows the distribution of monitored rainfall events based on depths and durations. The distribution of monitored events was compared to historical data for the state of Maryland (Kreeb 2003). The historical data is presented in parentheses. The smallest depth of rainfall for a single monitored event was 0.76 cm (0.30 in.) on February 9, 2017, and the largest

was 4.70 cm (1.85 in.) on June 21, 2016. As seen in the historical data, almost one-third of all storm events in Maryland fall under the shortest duration and smallest depth (0-2 hours and 0.0254-0.254 cm). Due to sampling constraints and storage in the SCM facilities, it was not possible to sample small storm events, creating bias towards larger and longer storms. Larger, longer duration storms dominate the distribution because they are more likely to produce significant runoff volumes that overcome the storage in the SCMs as to allow for effluent sampling. Storms greater than 1.28 cm (0.5 in.) make up 83% of the monitored events. Storms longer than 3 hours make up 80% of the monitored events, but, in several cases, short storms with very high rainfall intensities were sampled.

Table 3-1. Distribution of depths and durations of 24 monitored rainfall events compared to historical data for the state of Maryland, as shown in parentheses (Kreeb 2003). Shaded boxes represent depth-duration combinations that were recorded in this study.

Duration (hr)	Rainfall Depth in cm (in.)					Sum
	0.025-0.25 (0.01-0.10)	0.26-0.64 (0.10-0.25)	0.64-1.27 (0.25-0.50)	1.28-2.54 (0.50-1.00)	> 2.54 (> 1.00)	
0 – 1	0.00 (0.2857)	0.00 (0.0214)	0.04 (0.0167)	0.08 (0.0043)	0.00 (0.0008)	0.12 (0.3289)
1 – 2	0.00 (0.0164)	0.00 (0.0257)	0.00 (0.0221)	0.08 (0.0089)	0.00 (0.0025)	0.08 (0.0756)
2 – 3	0.00 (0.0085)	0.00 (0.0223)	0.00 (0.0198)	0.00 (0.0083)	0.00 (0.0038)	0.00 (0.0627)
3 – 6	0.00 (0.0099)	0.00 (0.0351)	0.13 (0.0475)	0.13 (0.0221)	0.17 (0.0087)	0.42 (0.1233)
6 – 12	0.00 (0.0058)	0.00 (0.0337)	0.00 (0.0629)	0.25 (0.0528)	0.13 (0.0266)	0.38 (0.1818)
12 – 24	0.00 (0.0024)	0.00 (0.0070)	0.00 (0.0397)	0.00 (0.0611)	0.00 (0.0515)	0.00 (0.1617)
> 24	0.00 0.0000	0.00 (0.0009)	0.00 (0.0043)	0.00 (0.0172)	0.00 (0.0435)	0.00 (0.0659)
Sum	0.00 (0.3287)	0.00 (0.1461)	0.17 (0.2130)	0.54 (0.1747)	0.29 (0.1374)	1.00 1.0000

3.2 SCM Characterization

3.2.1 Sampling Constraints

SCMs C and F were flagged as "backflowing SCMs". In these systems, the invert of the discharge pipe that connects the effluent monitoring well to the existing inlet is lower than the invert of the inlet. This is shown in Figure 3-1. As untreated runoff enters the existing inlet from the roadway, there is potential for backflowing into the effluent monitoring well. If this occurred before the effluent sampler was sealed off, the sample was compromised. Since the samplers fill at different rates every storm, there was no way of knowing when effluent samples were contaminated and when they were not. Therefore, rainfall data and field notes/observations for individual storm events were the main source of evidence in determining whether or not to expect backflowing in effluent samples for these SCMs. It was hypothesized that larger rainfall intensities (especially at the beginning of the storm event) would be more-likely to cause backflowing, as runoff would enter the existing inlet and backflow into the effluent monitoring well before treated runoff would discharge from the storage/filtration chambers. Figure 3-2 shows a photograph (taken following the storm event on January 3, 2017) of the effluent monitoring well of SCM F with leaves completely covering the effluent sampler.

In the SCM G, the water table is close to the ground surface. Depending on subsurface saturation conditions, the effluent monitoring well can become submerged. As groundwater from surrounding soils enters the monitoring well, it introduces sediment and provides the chance for contamination of effluent samples. This phenomenon was noted on occasions when effluent samplers were submerged upon sample collection. Therefore, effluent samples from SCM G were flagged as potentially compromised.

Figure 3-1. A photograph looking down into the existing inlet at the point of connection with discharge pipe of SCM F.

Figure 3-2. SCM F effluent monitoring well completely filled with leaves following an assumed backflowing event on January 3, 2017.

3.2.2 SCM Runoff Storage

Table 2-1 presents storage volumes and runoff depths for each of the SCMs. Storage volumes represent the total volume of water that can be stored in the SCMs at any given time. Runoff depths represent the total storage volume divided by the drainage area of the SCM.

All seven SCMs provide considerable water storage. The bioswale (SCM G) provides the most storage, with 60.9 m^3 (2,151 ft^3) available for incoming runoff. Storage volumes for the six underground systems range from 8.8 m^3 (311 ft^3) in SCM B to 26.1 m^3 (921 ft^3) in SCM F. Depths of direct runoff that can be stored by the underground SCMs range from 0.54 cm (0.21 in.) in SCM C to 0.86 cm (0.34 in.) in SCM F. SCM G has the capacity to store 0.37 cm (0.14 in.) of runoff from its contributing drainage area. SCM G treats a very large drainage area, so the maximum runoff depth that can be stored is lower than all other SCMs.

It is important to note that these calculations ignore temporal aspects of hydrologic storage. By assuming that the entire runoff volume is in the SCM at an instant, these calculations neglect active storage that functions over the duration of a storm, such as through infiltration (McCuen 2003). Therefore, these numbers underestimate the storage capacity of the SCMs.

Storage in SCMs is vital to design. McCuen (2003) suggests hydrologic storage compensation as one of the most important aspects to maintaining pre-development hydrologic conditions, as it reduces peak flows and keeps runoff at its source. This is especially true for small storm events. Kreeb (2003) found Maryland storms to be dominated by smaller, shorter rainfalls (Table 3-1). In this study, monitored storm events

were biased towards larger rainfall depths because smaller depths were not able to overcome the storage in the SCMs to produce effluent samples.

Based on field observations and simulation results, the SCMs are able to completely store storm events of approximately 1.3 cm (0.5 in.) or less. These depths are dependent on rainfall durations, intensities, and initial conditions within the SCMs. Storms with rainfall depths less than 1.3 cm (0.5 in.) account for 69% of storms in the state of Maryland (Kreeb 2003). Therefore, it is important to consider the hydrologic performance of the SCMs during small storm events that were not monitored. During these storms, runoff is stored in the SCMs and allowed to infiltrate into surrounding soils.

3.2.3 Drainage Area to Surface Area

Table 3-2 presents a summary of calculations of the ratios of contributing drainage areas (DAs) over facility surface areas (SAs) and percentages of SAs over DAs for the Camelot SCMs and other bioretention and sand filtration systems found in literature. Young et al. (1996) reported typical designs for sand filtration systems treating stormwater runoff in four regions of the United States. Davis (2007) monitored two bioretention cells treating parking lot runoff at the University of Maryland. Li and Davis (2009) monitored two bioretention cells treating parking lot runoff in College Park, Maryland, and Silver Spring, Maryland. Davis et al. (2012) monitored three bioretention cells treating parking lot runoff in Pennsylvania, Maryland, and North Carolina.

Percentages of facility surface areas to contributing drainage areas for the Camelot SCMs range from 0.86% for SCM D to 2.2% for SCM G. These values represent the amount of land surface area within a SCM's drainage area that is taken up

by the SCM facility. However, it is important to note that SCMs A-F are subsurface and their land requirement does not necessarily impact land availability on the surface.

The four sand filtration designs presented in Young et al. (1996) recommend percentages smaller than Camelot values, ranging from 0.41% in Austin, Texas, to 0.83% in Delaware. These sand filters have similar facility surface areas, but larger contributing drainage areas than the Camelot SCMs. Water quality improvements in these sand filters are similar to that of the Camelot SCMs, with excellent removal of particulate matter, moderate removal of phosphorus, and inconsistent nitrogen removal dominated by an export of nitrate (Young et al. 1996). However, the configurations of these sand filters present their own issues, ranging from minimum length-to-width requirements, structural design considerations, and extensive maintenance requirements.

Meanwhile, in the bioretention systems presented in Davis (2007), Li and Davis (2009), and Davis et al. (2012), percentages of facility surface areas to contributing drainage areas range from 2.2% (Davis 2007) to 6.6% (Davis et al. 2012). These values are larger than all Camelot SCMs, with the exception of SCM G and Davis (2007) being equal. With this, the bioretention systems performed better in terms of water quality improvements, primarily due to the ability of finer, more-chemically active media to remove dissolved nutrients. The design of these bioretention systems are most comparable to SCM G, where bowl storage and surface infiltration dominate water movement. Water storage on the surface limits land use, while, in SCMs A through F, which are completely subsurface, the land area above the SCMs are not impacted.

An advantage to HFM SCMs is their ability to treat large runoff volumes with small footprint systems. This is primarily due to high infiltration rates in the SCMs. This

reduces costs associated with land acquisition, excavation, and construction. Additionally, by distributing several HFM SCMs throughout an area to treat individual sub-watersheds, decentralized stormwater management is achieved. McCuen (2003) suggests that intelligent land use management must begin at the upper reaches of a watershed and that control of runoff at the source, not at the end of a pipe, provides optimal economic and environmental benefits.

Table 3-2. Summary of contributing area to facility surface area calculations.

SCM_1	**DA_2 ha (ac)**	**SA_3 m^2 (ft^2)**	**DA/SA (-)**	**SA/DA (%)**
A	0.25 (0.62)	21.7 (233)	116	0.86
B	0.15 (0.36)	18.0 (193)	81	1.2
C	0.19 (0.46)	27.9 (300)	67	1.5
D	0.24 (0.59)	22.3 (240)	107	0.93
E	0.28 (0.68)	29.7 (320)	93	1.1
F	0.30 (0.75)	55.7 (600)	54	1.8
G	1.67 (4.12)	372 (4000)	45	2.2
Austin, TX_4	0.4-12 (1-30)	41* (180**)	243	0.41
Washington, $D.C._4$	<4 (<10)	46* (200**)	218	0.46
Alexandria, VA_4	0.8-1.2 (2-3)	42* (183**)	238	0.42
$Delaware_4$	<2 (<5)	83* (360**)	121	0.83
College Park, MD_5	0.24 (0.59)	52.8 (568)	45	2.2
College Park, MD_6	0.28 (0.69)	181 (1950)	15	6.5
Silver Spring, MD_6	0.45 (1.11)	102 (1100)	44	2.3
Villanova, PA_7	1.3 (0.53)	149 (1600)	35	2.8
Silver Spring, MD_7	0.45 (0.18)	102 (1100)	18	5.6
Rocky Mount, NC_7	0.54 (0.22)	146 (1600)	15	6.6

(1) Stormwater Control Measure. (2) Contributing Drainage Area. (3) Facility Surface Area. (4) Young et al. 1996. (5) Davis 2007. (6) Li and Davis 2009. (7) Davis et al. 2012. (*) Values in m^2/ha. (**) Values in ft^2/ac.

3.2.4 HFM Characterization

SCMs A, B, C, D, and G contain HFM Y and SCMs E and F contain HFM X. The two HFM media are substantially different, as seen in Figure 3-3. Particles Size Distributions (PSDs) for the two HFMs are presented in Figure 3-4. HFM Y has larger particles, with a ten-percentile particle size, D_{10}, equal to 0.85 mm, while D_{10} for HFM X is 0.35 mm. Results of the LOI test show that HFM Y contain, on average, 1.49% organic matter (OM) and 0.14% carbonate, by mass, and Chesterfield samples 0.26% OM and 0% carbonate.

Figure 3-3. HFM X (left); HFM Y (right).

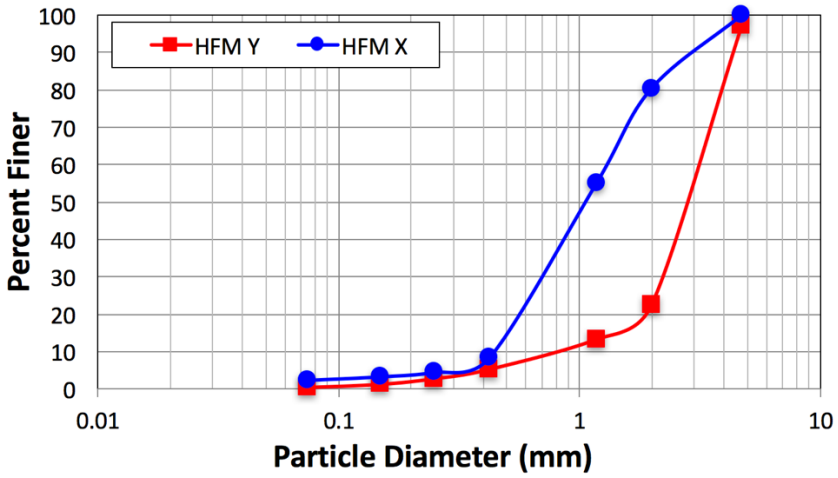

Figure 3-4. Sieve Analysis of HFMs X and Y.

3.3 First Flush Characterization

3.3.1 First Flush Concentrations

This study records water quality measurements in First Flush Concentrations (FFCs), as achieved by the first flush samplers described in Section 2.3. These are not the same as Event Mean Concentrations (EMCs). EMCs are flow-weighted average concentrations for an entire storm duration. FFCs are not representative of the entire storm event, as first flush predicts more polluted runoff in the early stages of a storm.

3.3.2 TSS First Flush

Influent TSS FFCs found in this study were compared to Maryland TSS EMCs found in peer reviewed literature to quantify the first flush in stormwater runoff in the Camelot subdivision. Davis (2007) is a study on two bioretention cells that manage stormwater runoff from a 0.24 ha (0.59 ac) section of an asphalt commuter parking lot on the University of Maryland campus. Li and Davis (2009) is a study on two bioretention cells, located in College Park (CP) and Silver Spring (SS), Maryland, United States. Cell CP treats 0.28 ha (0.69 ac) of 90% impervious land and Cell SS treats 0.45 ha (1.11 ac) of 90% impervious land. Li and Davis (2014) and Liu and Davis (2014) also studied Cell CP. The bioretention cells presented in these studies are larger than the HFM SCMs monitored in Camelot. Additionally, the bioretention cells account for larger percentages of the contributing drainage area as the HFM SCMs. Refer to Section 3.2.3 for more information.

Exceedance probability plots showing these comparisons are presented in Figure 3-5. Liu and Davis (2014) and Li and Davis (2014) do not present exceedance probability

plots and therefore are not included in Figure 3-29. It is clear that influent TSS FFCs are higher than influent TSS EMCs. Slopes of these lines vary, but, in general, follow similar distributions. With this, there is large variation between TSS concentration distributions for Camelot SCMs and previously studied bioretention cells. Therefore, the extent of first flush is not the same for all pairs of SCMs and previous studies. It is important to note that the bioretention systems in these studies are receiving runoff from parking lots, while the monitored SCMs are treating runoff from a residential neighborhood. This may account for the differences in stormwater composition.

Mean influent TSS FFCs can be compared to mean influent EMCs from these studies. All ratios are greater than 1.0, implying that a first flush is present. The average ratio between TSS FFCs for all SCMs and TSS EMCs for all referenced studies is 3.5.

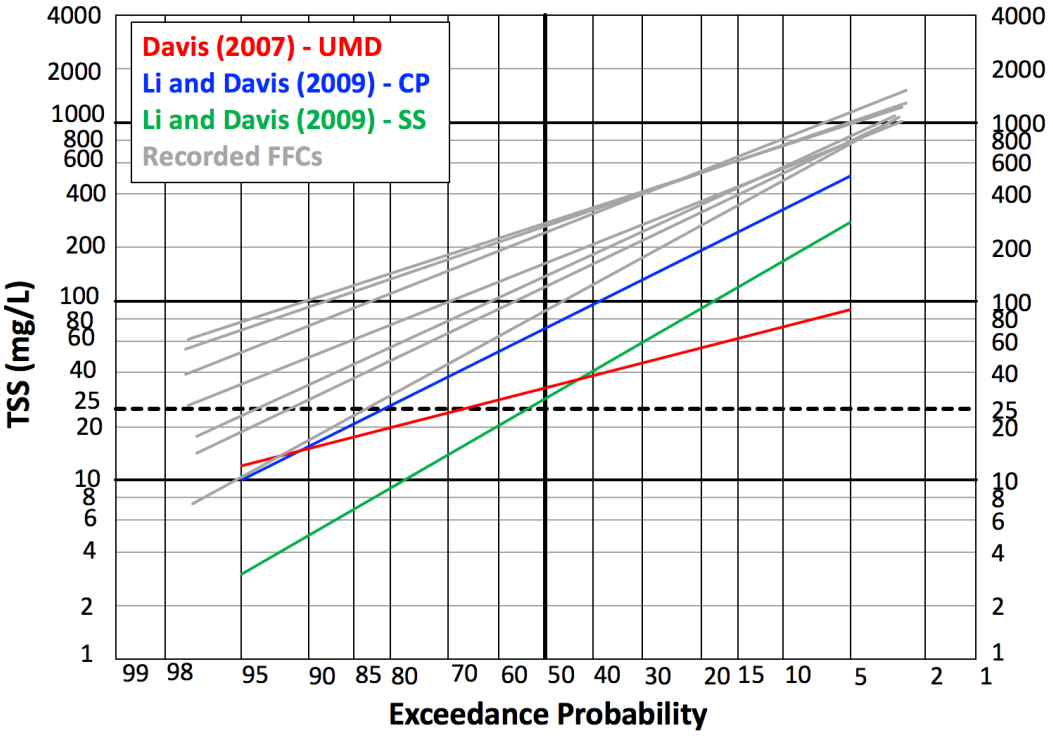

Figure 3-5. Influent TSS FFCs compared to previously published TSS EMCs. Grey lines represent recorded FFCs and colored lines represent previously published EMCs.

3.3.3 Phosphorus First Flush

Influent TP FFCs measured in the Camelot SCMs can be compared to TP EMCs from the same bioretention cells referenced above (Davis 2007, Li and Davis 2009, Li and Davis 2014, Liu and Davis 2014). The bioretention cells monitored in these studies will be referred to as UMD, CP, and SS, as described above. Exceedance probability plots showing this comparison are shown in Figure 3-6. Generally, TP FFCs in Camelot are larger than previously published TP EMCs. In all cases except SCM C and UMD, the ratios of median TP FFCs over TP EMCs are greater than 1.0. The average ratio among all SCMs and bioretention cells is 2.2. This is lower than the average of TSS values (3.5), indicating that TSS exhibits a larger first flush than TP. This makes sense, as first flush is most directly related to the mobilization of particulate matter. TSS is completely particulate-bound, while TP consists of dissolved and particulate species. Therefore, it is expected that TSS first flush is stronger than TP.

As is the case with TSS, there is large variation in influent TP concentration distributions among the Camelot SCMs and Maryland bioretention cells. The CP and SS bioretention cells have influent TP EMCs much lower than that of the UMD bioretention cell. Therefore, a much weaker first flush is seen between Camelot SCMs and the UMD bioretention cell than the first flush between Camelot SCMs and CP and SS bioretention cells. Variation between the SCMs is also present; specifically, influent TP FFCs of SCM E were found to be statistically lower than that of all other SCMs at α=5%. These factors must be considered when evaluating first flush.

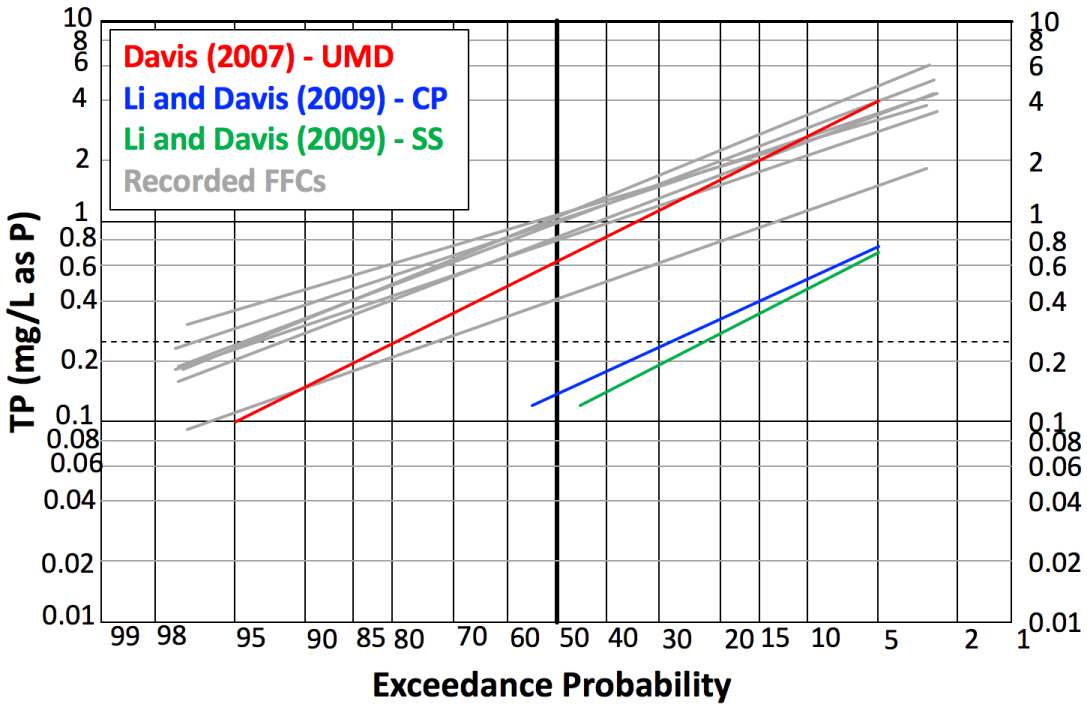

Figure 3-6. Influent TP FFCs compared to previously published TP EMCs. Grey lines represent recorded FFCs and colored lines represent previously published EMCs.

3.3.4 Nitrogen First Flush

Influent TN FFCs measured in the Camelot SCMs can be compared to TN EMCs from the CP and SS bioretention cells monitored in Li and Davis (2009), Li and Davis (2014), and Liu and Davis (2014); TN EMCs were not recorded in Davis (2007). Exceedance probability plots showing this comparison are shown in Figure 3-7. All Camelot TN FFCs are larger than previously published TN EMCs and all ratios of TN FFCs to EMCs are larger than 1.0. The average ratio among all Camelot SCMs and the CP and SS bioretention cells is 2.6. This implies that a TN first flush is present. This is lower than the average TSS first flush and higher than that of TP (3.5 and 2.2, respectively), indicating that TN exhibits a stronger first flush than TP, but a weaker first flush than TSS.

Variation in TN first flush among the SCMs and bioretention cells is much lower than that of TSS and TP. The seven TN FFC distributions of the Camelot SCMs, shown in grey, have similar medians. The two TN EMC distributions of the CP and SS bioretention cells also have similar medians. Therefore, it is expected that these ratios will be similar among the pairs of comparisons.

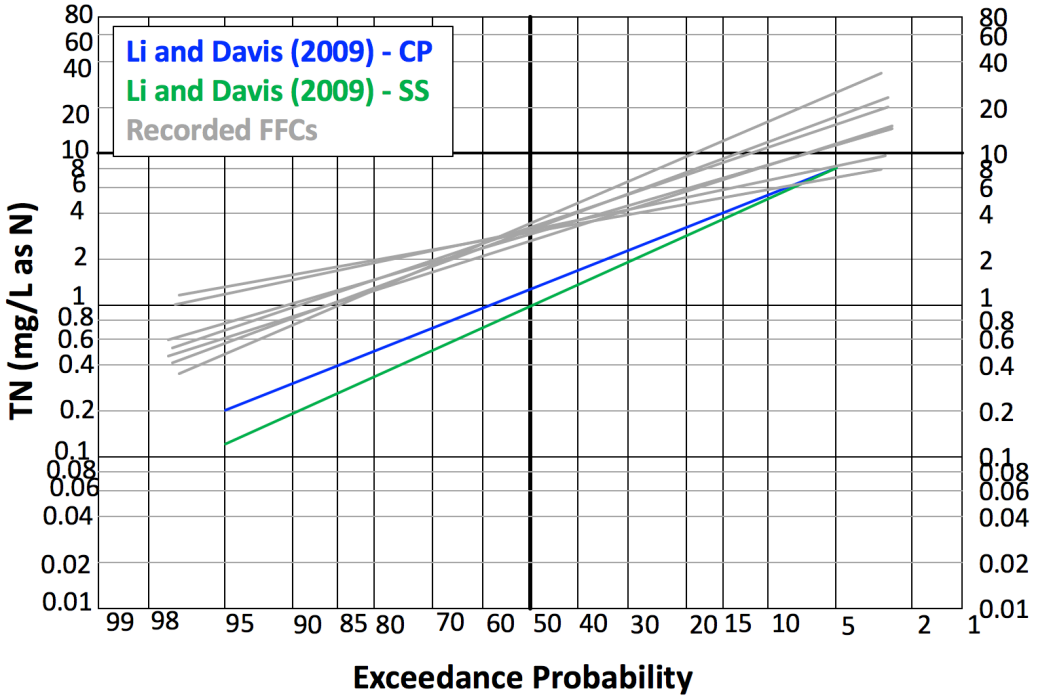

Figure 3-7. Influent TN FFCs compared to previously published TN EMCs.

3.3.5 First Flush Summary

TSS exhibits the largest first flush, followed by TN, and then TP. Median first flush ratios of recorded FFCs to local Maryland EMCs are 3.5 (TSS), 2.6 (TN), and 2.2 (TP). Previous studies (Lee et al. 2002, Hathaway et al. 2012) agree with these results, reporting TSS to exhibit the strongest first flush, followed by TN and then TP. Differences in the strength of first flush are common, as first flush is site-specific and highly dependent on individual species (Sansalone and Cristina 2004).

3.4 Total Suspended Solids

3.4.1 Overall Performance and Removal Mechanisms

Table 3-3 presents a summary of influent and effluent TSS First Flush Concentrations (FFCs) for all SCMs. The unweighted mean is the average of TSS FFCs and the weighted mean is the average of TSS FFCs normalized by individual storm sizes, as described in Section 2.5.2. Individual storm influent TSS FFCs range from 14 mg/L in SCM E to 2396 mg/L in SCM A. Individual storm effluent TSS FFCs range from <1 mg/L (detection limit) in SCMs A, B, and G to 806 mg/L in SCM C. High variability is found in influent and effluent TSS FFCs, in which standard deviations range from 185 mg/L in SCM B to 520 mg/L in SCM A and 8 mg/L in SCM A to 192 mg/L in SCM C, respectively. In many cases, the standard deviation is larger than the mean and median.

It is clear that influent TSS FFCs are larger than effluent TSS FFCs. One-tailed Mann-Whitney tests showed that all effluent data sets were significantly lower than corresponding influent data sets at α=5%. This decrease in influent-to-effluent TSS FFCs implies that all 7 SCMs are successful at removing TSS in stormwater runoff. TSS removal is driven by physical mechanisms, specifically, sedimentation and filtration. In the forebay and storage pipes, sedimentation removes larger, higher density particles via settling. Effective sedimentation occurs when the settling time of a particle is greater than the retention time of the particle in the control volume. In filtration, smaller particles are captured by HFM via sedimentation, interception, and diffusion transport mechanisms (Weber 2001). Since all SCMs incorporate sedimentation and filtration mechanisms into their configurations, it is expected that they all provide good TSS removal.

With this, differences in performance among the SCMs were evident. SCMs A, B,

D, and E all provide good TSS removal. All mean and median effluent TSS FFCs for these SCMs reach the Potomac River TSS water quality goal of 25 mg/L, as presented in Davis and McCuen (2005). Standard deviations of effluent TSS FFCs for SCMs A, B, and E (8, 14, and 13 mg/L, respectively) are lower than that of SCM D (43 mg/L). Since the goal of SCMs is to improve water quality for all storm events, low standard deviations in effluent concentrations are preferred. Therefore, SCMs A, B, and E are said to be providing the best TSS removal, followed closely by SCM D.

SCMs C, F, and G provide the poorest removal of TSS. In SCM F, the 25 mg/L water quality goal was reached for the median effluent TSS FFC but not the mean, and neither the mean or median reaches this goal in SCMs C and G. Standard deviations of effluent TSS FFCs for SCMs C, F, and G are very high, ranging from 110 mg/L to 192 mg/L. Large effluent TSS FFCs and standard deviations in effluent TSS FFCs for SCMs C, F, and G are attributed to the sampling constraints presented in Section 3.2.1.

Table 3-3. Summary of influent and effluent TSS FFCs for all monitored SCMs, with all values in mg/L. SCMs denoted with * represent those with effluent TSS data sets found to be statistically lower than corresponding influent TSS data sets at α=5%.

SCM	Influent (mg/L)				Effluent (mg/L)			
	Unweighted Mean	**Weighted Mean**	**Standard Deviation**	**Median (Min, Max)**	**Unweighted Mean**	**Weighted Mean**	**Standard Deviation**	**Median (Min, Max)**
A*	385	387	520	224 (42, 2396)	7*	7	8	7 (1, 31)
B*	264	266	185	203 (38, 810)	10*	10	14	4 (1, 60)
C*	221	222	305	82 (15, 1168)	108*	109	192	33 (2, 806)
D*	226	221	217	158 (29, 827)	25*	25	43	11 (3, 183)
E*	270	272	331	112 (14, 1479)	12*	12	13	9 (2, 54)
F*	366	368	317	293 (63, 1427)	111*	112	189	24 (4, 696)
G*	404	406	325	306 (65, 1408)	54	54	110	30 (1, 523)

The performance of these SCMs can be compared to other bioretention and sand filtration systems. Yu and Stanford (2006) monitored a Filterra® HFM system treating runoff from a 0.05 ha (0.12 ac) section of a parking lot in Falls Church, Virginia, for one year and found mean influent and effluent TSS EMCs of 29 mg/L and 5 mg/L, respectively. Barrett (2010) summarized performance measurements taken by the City of Austin, Texas, between 1985 and 1997 from 5 stormwater filtration facilities located in the Austin area, reporting average influent and effluent TSS EMCs of 198 and 15 mg/L, respectively. Urbonas (1999) summarized, after censoring outliers, the findings of sand filtration performance for stormwater treatment in four U.S. cities, namely, Alexandria, Virginia; Austin, Texas; Anchorage, Alaska; and Lakewood, Colorado, concluding with mean influent and effluent TSS concentrations of 160 mg/L and 16 mg/L, respectively.

All mean influent FFCs are larger than previously published EMCs. The influent TSS Event Mean Concentration (EMC) reported in Yu and Stanford (2006) is substantially lower than measured FFCs in Camelot (29 mg/L and 71 mg/L, respectively, versus a minimum 222 mg/L in SCM C). Barrett (2010) and Urbonas (1999) report mean influent TSS concentrations of 198 mg/L and 160 mg/L, which is more comparable to Camelot values, but still lower. It is important to consider that FFC measurements are not representative of the entire storm event, as first flush causes more polluted runoff in the early stages of a storm event. EMCs are more representative of an entire storm event. See Section 3.3.2 for a discussion on the TSS first flush.

Yu and Stanford (2006) report lower effluent TSS concentrations than all seven monitored SCMs. This may be due to the low influent concentrations, as removal

mechanisms for TSS are defined in terms of percent removals, so lower influent concentrations produce lower effluent concentrations (Benjamin and Lawler 2013). Barrett (2010) and Urbonas (1999) report mean effluent TSS concentrations higher than that of SCMs A, B, and E, but lower than SCMs C, D, F, and G. Thus, SCMs A, B, and E seem to be performing better than previously-studied sand filters, as effluent TSS concentrations are lower despite higher influent TSS concentrations.

Figure 3-8 presents influent TSS FFC exceedance probability plots for all SCMs. This plot shows that influent TSS FFCs are described by lognormal distributions, albeit with some deviation at the extremes. This agrees with other studies (Davis 2007, Li and Davis 2009) and is common for hydrologic and stormwater quality data (Van Buren et al. 1997). Correlation coefficients for the fits range from 0.944 (SCM D) to 0.981 (SCM F).

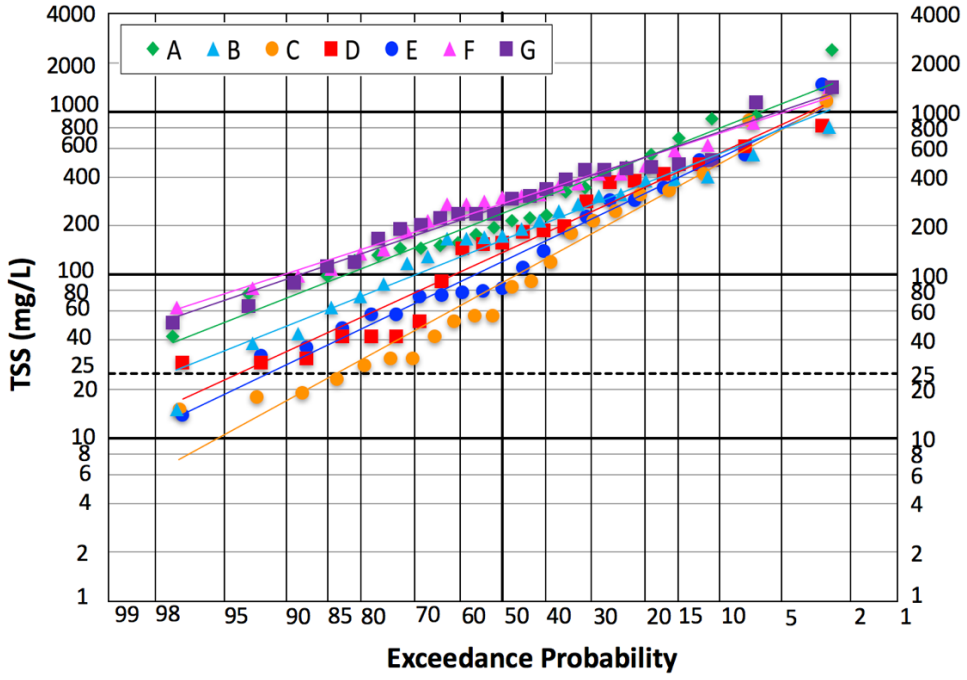

Figure 3-8. Exceedance probability plots of influent TSS FFCs for all seven SCMs.

Variation in influent TSS FFCs is primarily caused by rainfall characteristics. Irish et al. (1995) studied factors impacting pollutant runoff loads in Austin, Texas, and found influent TSS to primarily be impacted by rainfall volume and intensity, number of antecedent dry days, and previous storm intensity. Larger, more-intense rainfalls are expected to mobilize more sediment and generate higher influent TSS loads. More dry days allows for more sediment to build up on impervious surfaces and a more-intense previous storm will wash off more sediment, leaving the cleaner at the start of the dry period. These factors cause runoff to have varying characteristics.

Figure 3-9 presents influent and effluent samples for two storms: (a) April 6, 2017, and (b) May 13, 2017. These storms have significantly different rainfall distributions: (a) is characterized by high intensity thunderstorms totaling 3.63 cm (1.43 in) over 4 hours and (b) is characterized by low intensity rainfall totaling 1.91 cm (0.75 in) over 8 hours. There were 6 dry days prior to storm (a) after a low intensity rainfall on March 31, 2017 with an average rainfall intensity of 0.3 cm/hr (0.12 in/hr). There were 2 days prior to storm (b) after a high intensity rainfall on May 11, 2017 with an average rainfall intensity of 0.61 cm/hr. (0.24 in/hr.).

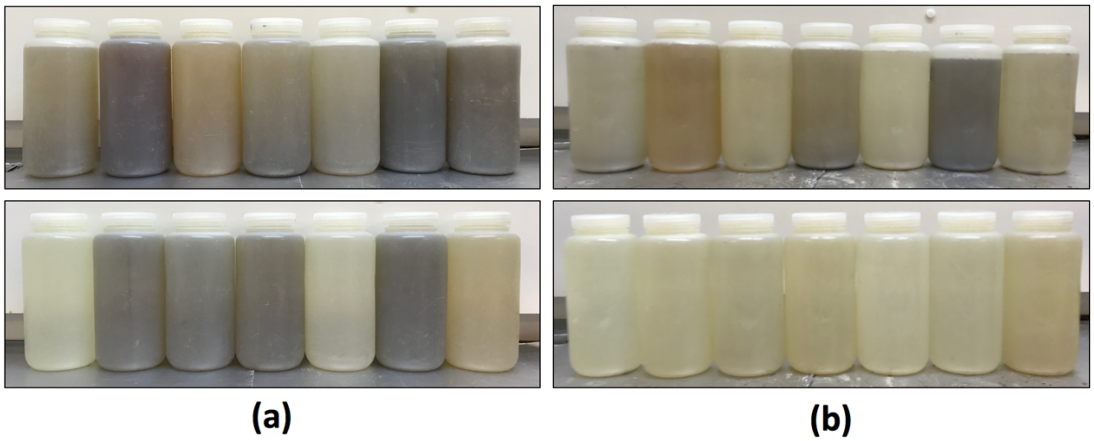

Figure 3-9. Photographs showing turbidity improvements between influent (top) and effluent (bottom) samples for SCMs A (far left) through SCM G (far right) for two storm events: (a) April 6, 2017, characterized by high intensity thunderstorms and (b) May 13, 2017, characterized by low intensity rain showers.

In comparing the influent samples for the two storms, it can be seen that influent samples for storm (a) are more turbid than those for storm (b). Median influent TSS FFCs for storms (a) and (b) are 248 mg/L and 77 mg/L, respectively. This implies that influent samples collected during high intensity storms with more antecedent dry days and lower rainfall intensities during the previous storm event are more polluted. Rainfall intensity was assumed to play the largest role in the difference between influent samples of the two storms. Vaze and Chiew (2002) found sediment accumulation on the road surface to occur relatively quickly after a rain event, but to slow down after a few days as redistribution occurs. This study also concludes that particle size distributions (PSDs) become finer as the number of dry days increases, as sediment is disintegrated by traffic and other factors (Vaze and Chiew 2002). Therefore, while number of antecedent dry days may not impact influent TSS masses, PSDs are impacted, so removals are predicted to be different. This will be addressed in the discussion of filtration theory.

Two-tailed Mann Whitney tests were performed to determine if influent TSS data

sets of the seven SCMs are significantly different among each other at α=5%. Of the 21 pairs of influent data sets, 7 were found to be significantly different and 14 were not found to be different. The influent data set of SCM B, which lies in the middle of the seven lines in Figure 3-1, was not found to be different than any other influent data sets. Meanwhile, the uppermost line in Figure 3-8, representing the influent TSS FFC distribution for SCM G, was found to be statistically larger than the three lowest lying data sets (SCMs C, D, and E). The lowest line in Figure 3-8 is the influent data set for SCM C; it is statistically lower than the three highest data sets (SCMs A, F, and G).

The variability in influent TSS FFC distributions among the SCMs is primarily due to watershed characteristics. It was found that influent TSS FFCs are not statistically different among SCMs A and B, which receive runoff from adjacent drainage areas. Meanwhile, both of these data sets were found to be statistically different than that of SCM C, which receives runoff from a drainage area on the opposite side of the neighborhood. Here, different vegetation and anthropogenic sources influence influent TSS levels. He et al. (2010) characterized urban stormwater runoff in Calgary, Canada, and concluded that suspended solids mainly originate from the watershed surface and the composition of solids on the surface is highly dependent on location and land cover / land use. TSS deposition has been found to be primarily due to human activities and traffic, as well as litter and abrasion of urban detritus (Sansalone and Kim 2008). Therefore, it is expected that pairs of adjacent SCMs, which treat runoff from similarly sized watersheds with identical land types, will have similar influent TSS characteristics. However, not much can be said about the variation in TSS composition throughout the neighborhood, as it is caused by several factors that were not measured.

A two-tailed Mann Whitney test was performed for influent TSS FFCs of SCMs B and G, which treat the smallest (0.15 ha, 0.36 ac) and largest (1.67 ha, 4.12 ac) drainage areas, respectively. It was found that the influent TSS FFCs of these two SCMs are not statistically different at α=5%, indicating that there is no apparent relationship between drainage area and influent TSS characteristics.

To further describe performance of the SCMs, exceedance probability plots were split up based on effluent TSS FFC distributions. Figures 3-10 and 3-11 present influent and effluent TSS FFC distributions for SCMs A, B, D, and E and SCMs C, F, and G, respectively. In both plots, it is clear that effluent distributions are lower than influent distributions.

Effluent TSS FFCs follow lognormal distributions, with correlation coefficients ranging from 0.912 for SCM A to 0.970 for SCM E. As is the case with influent distributions, the variation in effluent TSS FFCs is primarily due to rainfall characteristics. Figure 3-9 shows effluent samples taken from the same storm events as discussed previously for influent samples. As is the case with influent samples, effluent samples from storm (a), which is characterized by high intensity thunderstorms, are more turbid than that of storm (b), which is characterized by low intensity rainfall. Median effluent TSS FFCs for these two storms are 89 mg/L (storm a) and 2 mg/L (storm b). Therefore, it can be said that TSS removal is more successful during low-intensity storms. Several factors must be considered in this comparison, including differences in influent TSS FFCs between the storms, differences in retention times of runoff in the SCMs between the storms, and PSDs of influent runoff between the storms. This will be

addressed in further detail with the discussion on filtration theory.

Effluent TSS FFCs for SCMs A and B were found statistically to be lower than all other SCMs at α=5% with the exception of effluent TSS FFCs in SCM A being equal to that of SCM E. This indicates that SCMs A and B provide the lowest effluent TSS FFCs of monitored SCMs. In terms of the Potomac River water quality goal of 25 mg/L, both effluent distributions for SCMs A and B exceed this value only 6% of the time. Effluent TSS FFCs for SCMs A and B are statistically the same at α=5%. SCM A features filtration before storage and SCM B features storage before filtration. Therefore, in terms of effluent TSS FFCs, the order of filtration and storage does not seem to play a role in removal performance. However, the order does impact hydrologic performance and will be discussed in section 3.7.5.

SCMs D and E provide the next lowest effluent TSS FFCs. Exceedance probabilities of the 25 mg/L water quality goal for SCMs D and E are 28% and 16%, respectively. Pairs of effluent TSS FFCs for these SCMs were found statistically to be the same at α=5%. This makes sense, as they have the same configuration (HFM around pipe storage). The effluent TSS data set for SCM E is statistically lower than that of SCMs C, F, and G, but higher than that of SCM B. Thus, SCM E is performing better than SCMs C, F, and G, the same as SCM D and A, and worse than SCM B. For SCM D, effluent TSS FFCs are statistically higher than that of SCMs A and B and statistically the same as SCMs C, E, F, and G.

SCMs C, F, and G have the highest effluent TSS FFC distributions. Effluent data sets for SCMs C, F, and G are statistically higher than SCMs A, B, and E at α=5%. They

are all the same as that of SCM D at α=5%. The slopes of effluent TSS FFC distributions for SCMs C, F, and G are steeper than that of SCMs A, B, D, and E, indicating more variability in effluent FFCs for SCMs C, F, and G. As mentioned previously, lower effluent slopes are preferred, as SCMs should reach target values for most of the storm events. Exceedance probabilities of the 25 mg/L water quality goal for SCMs C, F, and G are 50%, 50%, and 42%, respectively. SCMs A, B, D, and E meet the 25 mg/L water quality goal more effectively than SCMs C, F, and G.

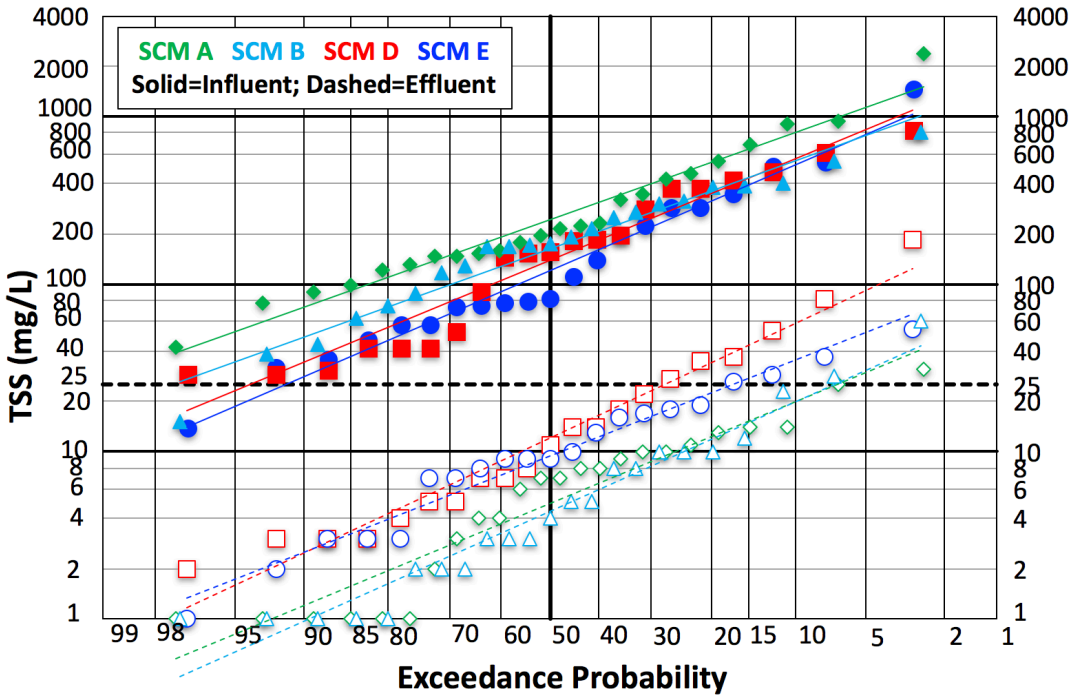

Figure 3-10. Exceedance probability plot of influent and effluent TSS FFCs for SCMs A, B, D, and E.

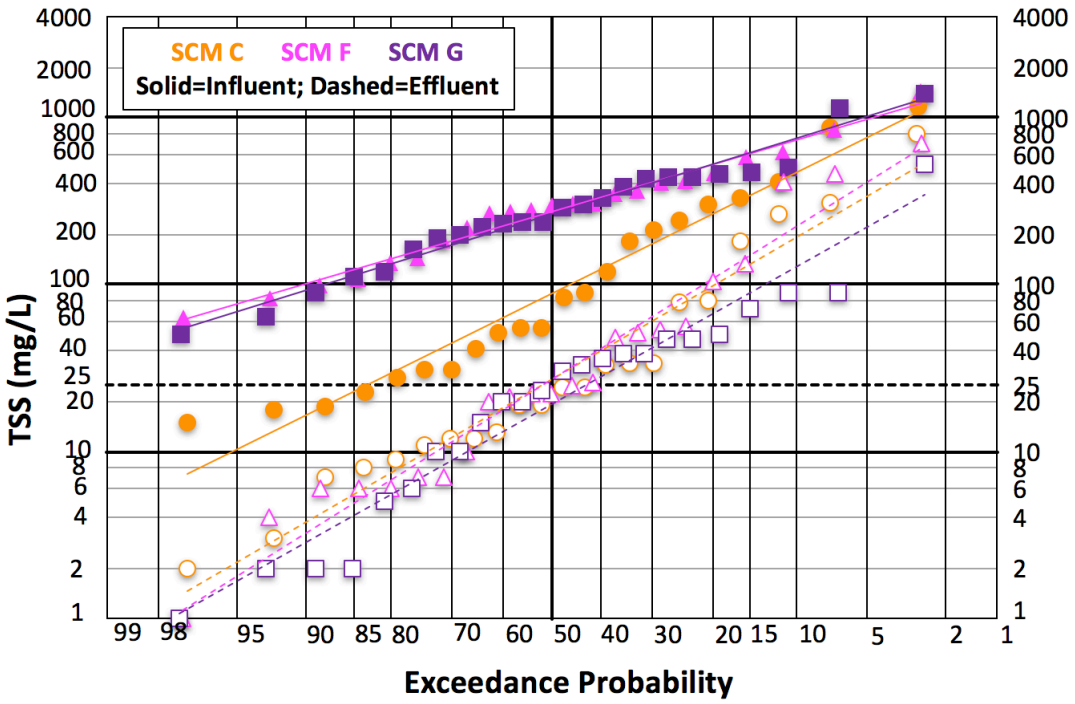

Figure 3-11. Exceedance probability plot of influent and effluent TSS FFCs for SCMs C, F, and G.

Weighted means presented in Table 3-3 show the effect of storm depth on influent and effluent TSS FFCs. In all SCMs but SCM D, the weighted mean influent TSS FFC is larger than the unweighted mean influent TSS FFC. This implies that larger storm events contribute higher TSS FFCs in influent runoff. This pattern is less apparent for effluent values. In SCMs A, B, D, E, and G, unweighted and weighted mean effluent TSS FFC are equal and in SCMs C and F, the weighted mean effluent TSS FFC is larger than the unweighted mean effluent TSS FFC. Thus, effluent TSS FFCs do not seem to change significantly among small and large storms.

To further explore this relationship, influent and effluent TSS FFCs were separated for small and large storm events. Based on a critical precipitation depth of 2.0

cm (0.8 in), 12 storm events were classified as small events (less than 2.0 cm) and 12 were classified as large events (more than 2.0 cm). Figure 3-12 presents exceedance probability distributions for influent and effluent TSS FFCs for all SCMs, separated between small and large events. As seen, the red lines, which represent larger storms, are higher than the blue lines (smaller events), implying that influent and effluent TSS FFCs are larger when the storm size is larger. Based on a one-tailed Mann Whitney test, it was found that both influent and effluent TSS FFCs for larger storms are significantly larger than that of the smaller storms at α=5%.

The difference between distributions for small and large storms is more significant in influent TSS FFCs than effluent TSS FFCs. Additionally, influent distributions are parallel, while effluent distributions diverge at higher TSS concentrations. At lower concentrations, effluent TSS FFCs are similar between small and large storm events. Diversion of the effluent TSS FFC distribution (red-dashed line) was dominated by large values on the right side of the exceedance probability plot. Therefore, it was hypothesized that the sampling constraints impacting SCMs C, F, and G were creating bias in effluent results, as sampling failures were more common in larger storm events.

Figure 3-13 presents exceedance probability distributions for influent and effluent TSS FFCs for SCMs A, B, D, and E, separated between small and large events. Data sets for SCMs C, F, and G were removed to reduce bias caused by sampling failures. Influent distributions follow the same trend, with large storms delivering significantly higher TSS FFCs to the SCMs than small storm events (α=5%) and parallel distributions between small and large events. This agrees with Vaze and Chiew (2003), who found that large

storms deliver higher TSS concentrations in runoff than small storms. This difference in TSS loads is attributed to the higher turbulence created by falling raindrops in larger storms and the higher shear stress imparted by larger surface runoff flows, as these factors are important in loosening surface particles and suspending them in water, making them available for washoff (Vaze and Chiew 2003).

However, effluent distributions of small and large events for SCMs A, B, D, and E are statistically the same at α=5% and follow more-parallel distributions than that of Figure 3-12. This implies that sampling constraints impacting effluent samples in SCMs C, F, and G did create bias. Therefore, it can be said that the SCMs are discharging identical effluent TSS levels despite larger inputs and higher flows.

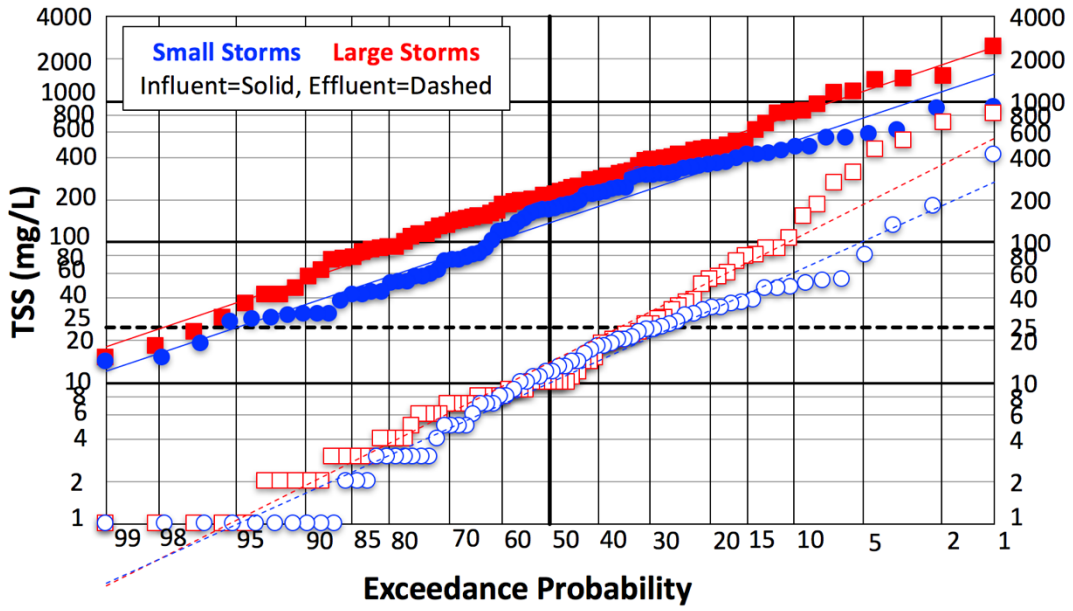

Figure 3-12. Exceedance probability plot of influent (solid) and effluent (dashed) TSS FFCs for all SCMs, split up between small (blue circles) and large (red squares) storm events. Small storms are those with precipitation depths below 2.0 cm and large storms are those with precipitation depths above 2.0 cm.

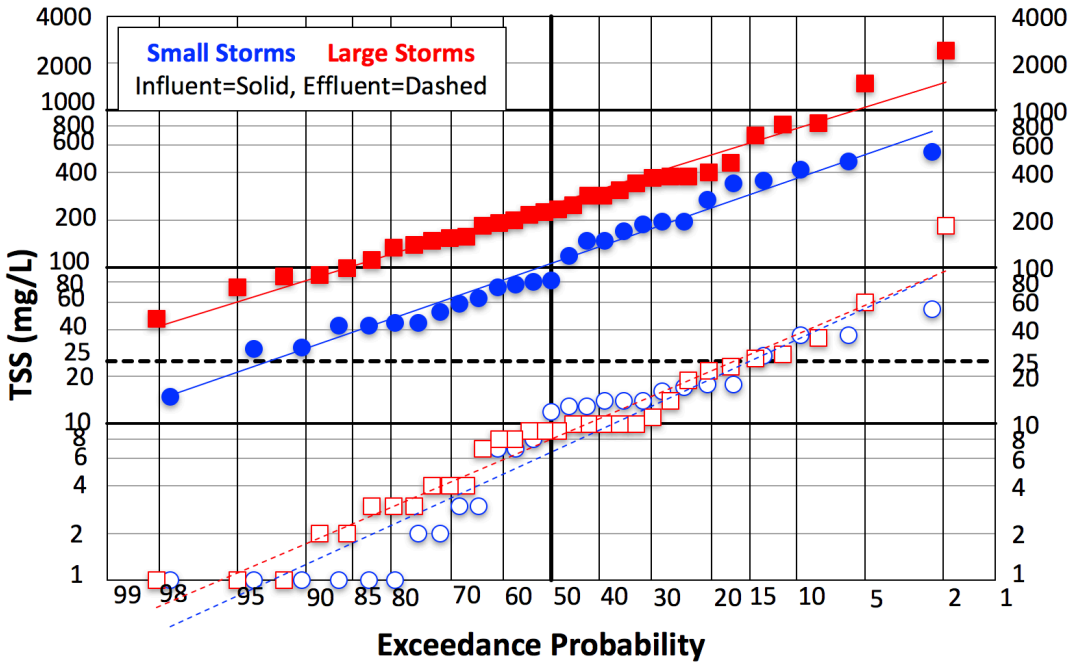

Figure 3-13. Exceedance probability plot of influent (solid) and effluent (dashed) TSS FFCs for SCMs A, B, D, and E, split up between small (blue circles) and large (red squares) storm events. Small storms are those with precipitation depths below 2.0 cm and large storms are those with precipitation depths above 2.0 cm.

3.4.2 Filtration Theory

Calculated TSS removals can be compared to conventional filtration theory, as presented in Yao et al. (1971):

$$\frac{C}{C_0} = exp\left[-\frac{3}{2}\frac{(1-\varepsilon)\alpha\eta}{d_c}L\right] \quad (3\text{-}1)$$

where C is the effluent concentration (mg/L); C_o is the influent concentration (mg/L); ε is the media porosity (dimensionless); α is the collision efficiency (dimensionless ratio of number of "sticks" over number of collisions); η is the transport/contact efficiency (dimensionless ratio of rate of contact over rate of approach); d_c is the collector (HFM)

particle diameter; and L is the length of the filter bed (m). This model assumes steady state conditions and a clean filter media.

Table 3-4 presents numerical values of parameters used in this comparison. ε is assumed to be 0.39; a value found by Rajagopalan et al. (1982) to be typical of packed filter beds. α is assumed to be 0.01; a value presented in Nakamoto et al. (2014) as a collision efficiency of particles in sand filters. d_c is estimated as the measured d_{10} of the two HFMs, as presented in Section 3.2.4 (0.85 mm for HFM Y and 0.35 mm for HFM X). L is assumed to be 0.46 m (18 in), per SCM design drawings provided by Prince George's County, Maryland, and presented in Appendix A. η is calculated based on sedimentation, diffusion, and interception mechanisms, with sedimentation and interception dominating η for larger particles and diffusion dominating η for smaller particles (Logan et al. 1995):

$$\eta = \left[\frac{(\rho_p - \rho_f)\, g\, {d_p}^2}{18\, \mu\, v}\right] + \left[0.9\left(\frac{K_B\, T}{\mu\, d_p\, d_c\, v}\right)^{2/3}\right] + \left[1.5\left(\frac{d_p}{d_c}\right)^2\right] \quad (3\text{-}2)$$

where ρ_p and ρ_f are the particle and fluid densities, respectively (kg/m^3); g is the gravitational constant, equal to 9.81 m/s^2; d_p is the incoming particle diameter (m); μ is the fluid viscosity (kg/m*s); v is the approach velocity of incoming particles (m/s); K_B is the Boltzmann Constant, equal to 1.38x10^{-23} m^2*kg/s^2*K; and T is the absolute temperature. ρ_p is assumed to be 2660 kg/m^3; a value typically used to represent sediments (Benjamin and Lawler 2013). ρ_f is the density of water, assumed as 1000 kg/m^3. μ is equal to 8.9x10^{-4} kg/m*s, which represents the viscosity of water. T is

assumed to be 298 K, which represents standard conditions. The approach velocity and incoming particle diameter were set as inputs to the model.

Table 3-4. Summary of input parameter values for filtration theory calculations.

Parameter	Value	Units
ε	0.40	-
α	0.01	-
d_c (Chesterfield)	3.5×10^{-4}	m
d_c (Rotondo)	8.5×10^{-4}	m
L	0.46	m
ρ_p	2660	kg/m^3
ρ_f	1000	kg/m^3
g	9.81	m/s^2
μ	8.9×10^{-4}	kg/m*s
K_B	1.38×10^{-23}	m^2*kg/s^2*K
T	298	K

Equation 3-1 shows increased removal efficiency as ε, α, η, and L increase. Conceptually, larger ε, α, and η mean more efficient filtration and larger L means a longer filter bed. Equation 3-1 also shows increased removal efficiency as d_c decreases; conceptually, finer HFMs with lower values of d_c are expected to filter influent solids more effectively.

Filtration theory curves for the two HFMs are presented in Figure 3-14. The x-axis represents the incoming particle diameters and the y-axis represents the percent removal efficiency; i.e., $100*(1 - C/C_0)$. The four colored curves in each plot represent the percent removal efficiency of particles at varying approach velocities. Filtration theory predicts that particles greater than 17 μm in diameter will completely be removed ($C/C_o<0.01$) for both HFMs at approach velocities as high as 254 cm/hr (100 in/hr).

However, colloids are only partially removed ($C/C_o>0$) and removal is dependent on velocities and HFM characteristics. At an approach velocity of 2.5 cm/hr (1.0 in/hr), HFM X exhibits more removal of 0.3 μm particles than HFM Y does (64% removal versus 50% removal, respectively). Therefore, at low flows and depending on influent PSDs, filtration theory predicts that HFM X will more-successfully filter incoming particles than HFM Y. Meanwhile, at very high approach velocities, the two HFM types are predicted to perform the same in terms of filtration. For incoming 1 μm particles at 254 cm/hr (100 in/hr), HFM X exhibits 4.8% removal and HFM Y exhibits 5.0% removal. Thus, at high approach velocities, the two HFMs are expected to perform the same, assuming that incoming PSDs are similar.

SCMs D and E have identical facility configurations (HFM around perforated pipe storage), but SCM D contains HFM Y and SCM E contains HFM X. Influent and effluent exceedance probability plots for these two SCMs were presented in Figure 3-10. As mentioned previously, influent TSS FFCs and effluent TSS FFCs for SCMs D and E were not found to be statistically different. These two systems seem to be working identically in terms of TSS removal, despite their varying media characteristics. Since HFM SCMs are designed to provide high infiltration rates, this agrees with filtration theory that media characteristics do not play a significant role in removal efficiencies at high flow rates.

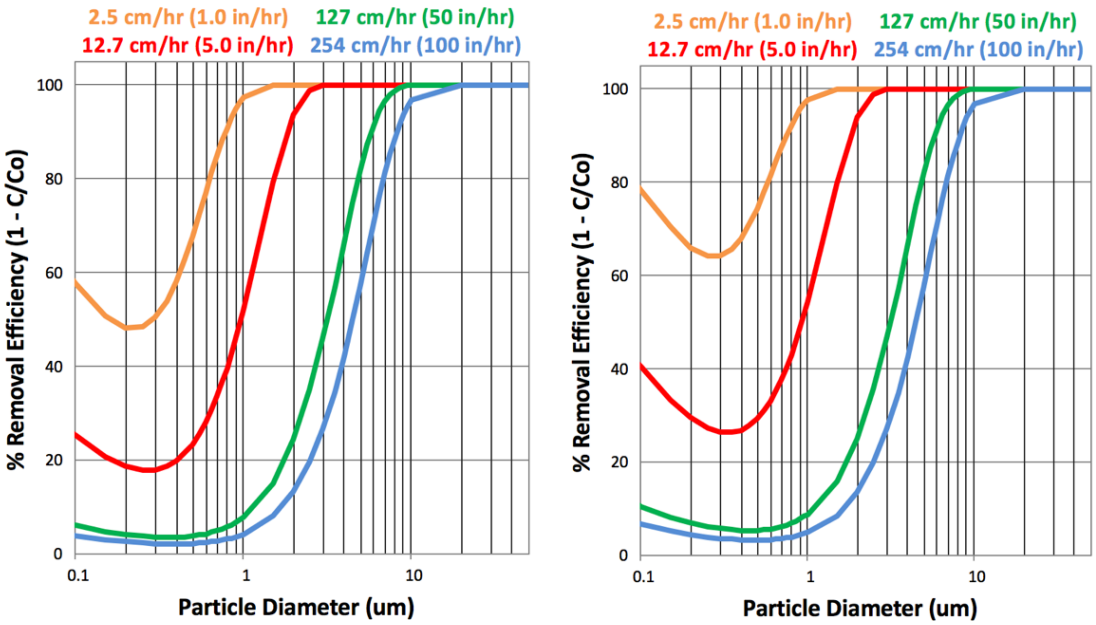

Figure 3-14. Filtration theory curves for HFM Y (left) and HFM X (right) under varying approach velocities, as calculated using equations 3-1 and 3-2. Values used in the development of these curves are presented in Table 3-2.

PSDs reported in literature are highly variable and it is generally accepted that PSDs of solids in stormwater runoff are site and storm specific. Selbig and Bannerman (2011) found that runoff from residential and urban areas are dominated by silt and clay particles less than 32 µm. Li et al. (2005) found 30-60% of particle mass in particles smaller than 50 µm. Meanwhile, Sartor and Boyd (1974) analyzed sediment from street surfaces and found about 6% of the total solids were less than 43 µm, 37% ranged from 43 to 246 µm, and 57% were greater than 246 µm. Sansalone et al. (1998) investigated runoff from a freeway and reported similar results: approximately 10% of the mass was less than 100 µm 25% to 60% of the solids were between 100 and 400 µm, and 40% to 70% of the solids were larger than 400 µm. Since both HFMs are performing identically in terms of TSS removal, it is assumed that the influent PSD of stormwater runoff in Camelot is dominated by particles larger than 17 µm and that the effluent PSD is dominated by particles smaller than 17 µm.

3.4.3 Load Reduction and Ultimate Fate

Table 3-5 presents annual input and output mass loads, net load reductions, and percent reductions for TSS in all SCMs. These values were calculated using the Simple Method, as presented in Section 2.5.5. This assumes no removal via volume reduction. The stormwater TSS behavior/fate in SCM D is diagrammed in Figure 3-15. To account for first flush, influent and effluent FFCs inputted into the Simple Method were divided by the average first flush ratio of TSS FFCs to Maryland EMCs (3.5), as presented in Section 3.3.2. Results for TSS mass loads that do not incorporate the first flush factor are included in Appendix C.

As seen, all SCMs provide significant reductions in TSS mass loads through the SCMs, implying significant removal. The input TSS mass loads into the SCMs range from 249 kg/ha-yr (221 lb/ac-yr) in SCM D to 577 kg/ha-yr (514 lb/ac-yr) in SCM A. Output TSS mass loads range from 10 kg/ha-yr (9 lb/ac-yr) in SCM A to 150 kg/ha-yr (134 lb/ac-yr) in SCM C. SCM A provides the best TSS load reduction (98%), as compared to SCM C, which only provides 51%. When drainage areas are taken into account, SCM G provides the largest TSS mass load reduction of 786 kg/yr (700 lb/yr) as compared to the lowest reduction of 29 kg/yr (26 lb/yr), documented in SCM C.

TSS mass loads can be compared to previous findings. Li and Davis (2009) report input and output TSS mass loads to Cell CP (see Section 3.3.2 for site description) of 1,190 and 37 kg/ha-yr (97% reduction). Liu and Davis (2014) monitored the same bioretention cell following retrofit and report input and output TSS mass loads of 1,090 and 47 kg/ha-yr (96% reduction). Influent TSS mass loads in the present study are lower

than previously-reported values. In all SCMs that did not experience effluent sampling constraints, output TSS mass loads are lower, as well. Percent reductions are similar in all cases, indicating similar removal performance. This may imply that the FFC:EMC ratio is an overestimate. It is also possible that this is due to watershed characteristics; the monitored study was performed in a residential area, while these studies monitored SCMs treating parking lot runoff. Parking lots account for more impervious area, which can lead to varying influent characteristics.

All SCMs are successful in removing TSS from stormwater runoff using mechanisms of sedimentation and filtration. SCM design, including system configurations and HFM types, are not significant factors in dictating TSS removal. The main reasons for varying results of TSS removal among the SCMs are sampling constraints and varying influent stormwater composition, especially uncertainty in PSDs. In general, HFM SCMs that incorporate sedimentation and filtration will perform well in terms of TSS removal.

Table 3-5. Load reductions of Total Suspended Solids for all SCMs. Influent and effluent mass loads incorporate the TSS first flush factor (3.5) to normalize FFCs to EMCs.

SCM		**A**	**B**	**C**	**D**	**E**	**F**	**G**
TSS	**L_{in} in kg/ha-yr (lb/ac-yr)**	577 (514)	353 (315)	308 (275)	249 (221)	356 (317)	468 (417)	542 (482)
	L_{out} in kg/ha-yr (lb/ac-yr)	10 (9)	15 (14)	150 (134)	28 (25)	17 (15)	131 (117)	70 (63)
	L_{red} in kg/ha-yr (lb/ac-yr)	566 (504)	338 (301)	158 (141)	220 (196)	339 (302)	337 (300)	471 (420)
	L_{red} in kg/yr (lb/yr)	142 (127)	49 (44)	29 (26)	53 (47)	93 (83)	102 (91)	786 (700)
	% Reduction	**98%**	**96%**	**51%**	**89%**	**95%**	**72%**	**87%**

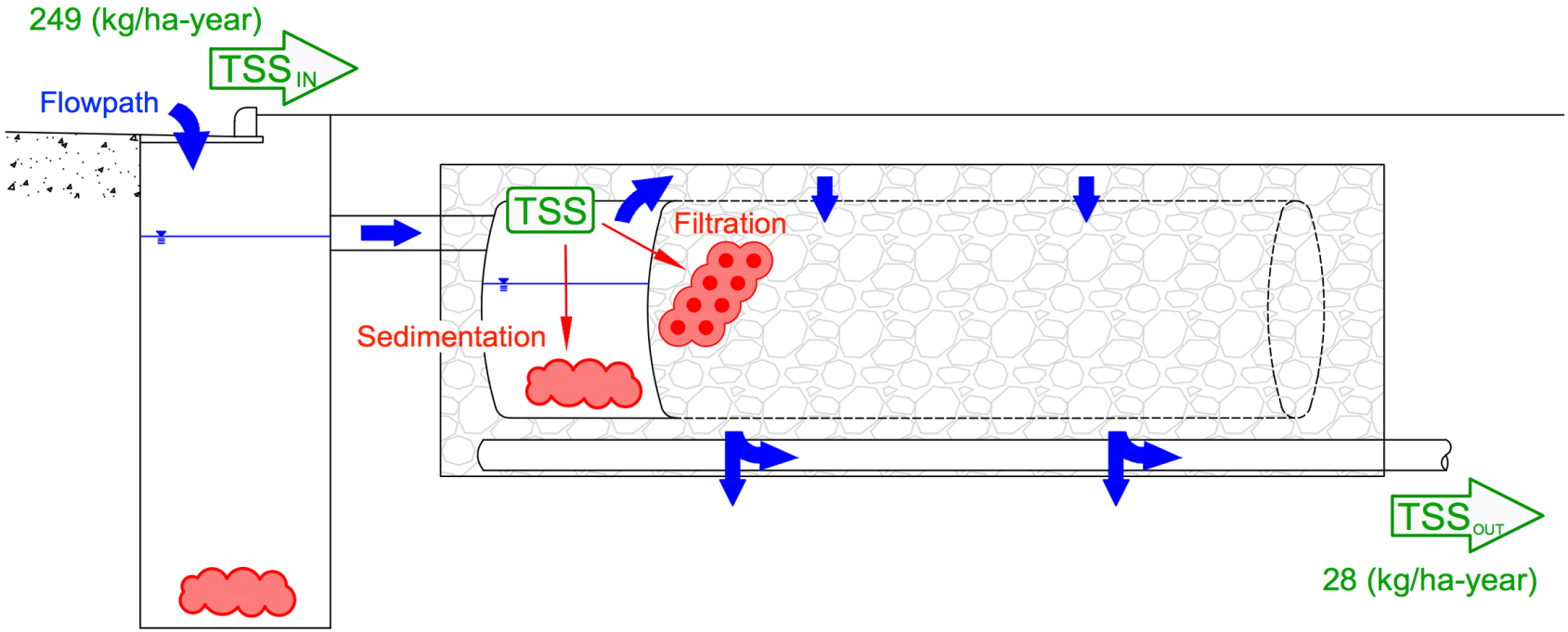

Figure 3-15. TSS behavior through SCM D. SCM D features storage before filtration. Legend: red=removal mechanism; blue=flowpath; green=input/output mass loads estimated with EMCs based on first flush ratios for individual species, in kg/ha-yr. Adapted from Li and Davis (2009).

3.4.4 Sediment Accumulation

To further assess TSS mass load reductions, results of the Simple Method calculations can be compared to HFM Y samples taken at SCM G throughout the duration of the project. A visual comparison of HFM samples taken at three stages of the project is presented in Figure 3-16. Sample (a) represents HFM Y at the time of installation; sample (b) represents HFM Y in cell one after one month of operation; and sample (c) represents HFM Y in cell one after 11 months.

Significant changes in HFM composition at the three stages of the project can be seen. At the time of installation, the media consisted of a mixture of coarse sand and fine peat particles. However, after one month of operation, the fine, peat particles had been washed out of the top 15 cm (6 in.) layer of HFM in cell one. It is possible that the peat accumulated deeper in the HFM matrix or was discharged out of the SCM with effluent runoff. Ten months into operation of the bioswale, the top layer of HFM in cell one had accumulated large amounts of sediment, as seen in sample (c). It is important to note that this accumulation of sediment is for the top 15 cm (6 in.) of HFM in cell one; sediment accumulation in deeper layers of HFM and in subsequent cells may not be as drastic as shown in Figure 3-16.

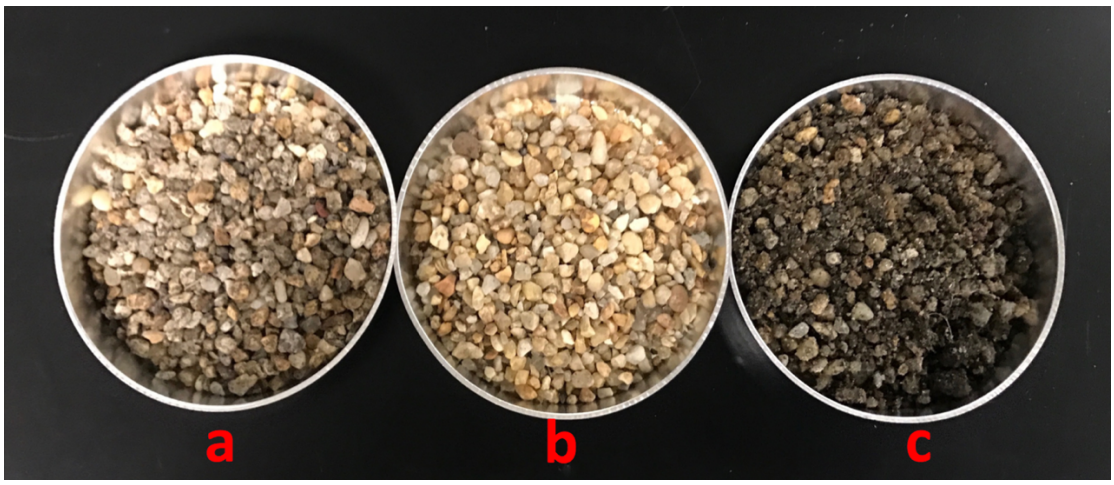

Figure 3-16. Comparison of HFM Y samples from different stages of the project: (a) at the time of installation; (b) one month into operation; and (c) 11 months into operation.

Sieve analysis of the three HFM Y samples are presented in Table 3-6. The first column presents the sample name: (a) represents HFM Y at the time of installation; (b) represents HFM Y at one month into operation of SCM G; (c) represents HFM Y eleven months into operation of SCM G; and subscripts represent the cell of SCM G. Cell one is the first to receive runoff and cell four is the most downstream cell in SCM G.

The second column in Table 3-6 presents sediment masses calculated for each 100 g HFM sample. Sediment represents anything that passes through a Number 8 sieve (2.38 mm opening). It can be seen that samples (b_1) and (b_2) have lower sediment masses than sample (a), but that the masses between the two cells after one month of operation are similar (15.1 and 14.8 g/100 g-HFM, respectively). This supports the argument that peat was washed out during the initial period following installation. Therefore, instead of using sample (a) as the control to measure sediment accumulation in (c) samples, the average of samples (b_1) and (b_2) are used to better represent the actual accumulation of sediment that is occurring in the SCM.

The third column in Table 3-6 presents sediment accumulation masses, normalized by subtracting sediment masses (column two) by the average of sediment masses in the clean HFM (b_1 and b_2). Finally, the fourth column translates sediment accumulation masses in the top layer (column three values) to the entire cell by multiplying by the volume of each cell times an assumed density of 2660 kg/m^3; a value typically used to represent sediment (Benjamin and Lawler 2013). All cells have the same volume, 6.0 m^3 (210 ft^3).

Table 3-6. Results of sediment accumulation sieve analysis for SCM G.

Sample	Sediment Mass (g/100 g-HFM)	Sediment Accumulation (g/100 g-HFM)	Sediment Accumulation (kg)
(a) Fresh HFM	17.6	-2.6	-417
(b_1) Cell One	15.1	-	-
(b_2) Cell Two	14.8	-	-
(c_1) Cell One	21.6	6.6	1062
(c_2) Cell Two	17.2	2.2	359
(c_3) Cell Three	16.8	1.8	299
(c_4) Cell Four	17.1	2.1	341

A clear decrease in sediment mass is observed from sample (a) to (b), totaling 1668 kg (417 kg per cell). Peat particles were washed out of the top layer of HFM Y in SCM G after one month of sampling. This value most likely an overestimate, as it assumes that sediment distribution in the cells are homogeneous. It is very likely that the peat fell deeper into the HFM matrix and were not completely washed out.

There is a large accumulation of sediment mass in SCM G between the first- to eleventh-month of sampling. The total accumulated sediment mass in all cells over the

ten months of sampling is 2061 kg. Majority of sediment accumulation occurs in first cell of SCM G. Cell one accumulated an estimated 1062 kg of sediment during the ten-month sampling period. Meanwhile, cells two through four only accumulated between 299 kg (cell three) and 359 kg (cell two). This is primarily due to the storage available in cell one. For storms producing runoff volumes less than the subsurface and bowl storage available in the first cell of the swale, there is no infiltration of runoff in the downstream cells. Since the majority of Maryland storm events have low precipitation depths (Kreeb 2003), it is assumed that cell one infiltrated the majority of runoff throughout the sampling period. This accounts for the larger sediment accumulation masses in cell one.

As compared to the TSS load reduction for SCM G found using the Simple Method (220 kg/yr), this value of accumulated sediment in SCM G is an overestimate. This calculation assumes that sediment accumulation and distribution is homogeneous throughout the cells in SCM G. Li and Davis (2008) found that majority of sediment buildup occurs in the top 10 cm of bioretention media. This pattern is similar to that observed in sand filters, where little TSS removal occurs deep within the filter (Barrett 2010). When this is taken into account and the depth of HFM that accumulates sediment is decreased from the total HFM depth (46 cm, 18 in.) to that found in Li and Davis (2008) (10 cm, 4 in.), the estimated sediment accumulation for SCM G is 451 kg. This value is much closer to that found using the Simple Method. This implies that the majority of sediment accumulation in SCM G occurs in the top layer of HFM. This may pose clogging-related problems and will be discussed further in Section 3.7.5.

3.5 Phosphorus

3.5.1 Overall Performance

Table 3-7 presents a summary of influent and effluent Total Phosphorus (TP) FFCs for all SCMs. The unweighted mean is the average of measured TP FFCs and the weighted mean is the average of TP FFCs normalized by individual storm sizes.

Individual storm influent TP FFCs range from 0.11 mg/L as P in SCM F to 5.21 mg/L as P in SCM C. Individual storm effluent TP FFCs range from <0.05 mg/L as P (detection limit) in SCMs A, E, and F to 2.59 mg/L as P in SCM C. Standard deviations are generally higher for influent TP FFCs than for effluent TP FFCs. Standard deviations of influent and effluent TP FFCs range from 0.50 mg/L as P in SCM E to 1.3 mg/L as P in SCM C and 0.08 mg/L as P in SCM E to 0.77 mg/L as P in SCM C, respectively.

SCMs A and E provide the lowest effluent TP FFCs, in which median effluent TP FFCs are 0.12 mg/L as P and 0.13 mg/L as P, respectively. SCMs B, D, F, and G provide the next-best TP removal, with median effluent TP FFCs ranging from 0.25 mg/L as P (SCM G) to 0.32 mg/L as P (SCM D). SCM C discharges a median TP FFC of 0.81 mg/L as P, which is the largest of all SCMs. Based on one-tailed Mann Whitney tests, effluent TP FFCs are statistically lower than influent TP FFCs in SCMs A, B, D, E, F, and G at α=5%. The difference between the influent and effluent TP FFCs for SCM C is not statistically significant. This indicates that SCMs A, B, D, E, F, and G are successfully removing TP in stormwater runoff, while SCM C is not. The main reason for higher effluent TP FFCs in SCM C is the sampling constraints described in Section 3.2.1.

TP removal is based on removal of both particulate and dissolved species.

Mechanisms of TP removal include filtration and sedimentation of particulate P and sorption of dissolved P (Liu and Davis 2014). P fate in SCMs is complex, as particulate and dissolved species have different removal mechanisms and efficiencies. In sand filtration systems, TP removal is primarily achieved via removal of particulate P (PP), while dissolved P is often found to pass through the filter untreated (Erickson et al. 2007). Therefore, since the SCMs perform similarly among each other in terms of TSS removal, it follows that their TP removals are also similar. This implies that majority of TP removal is through sedimentation and filtration of PP.

Table 3-7. Summary of influent and effluent TP FFCs for all monitored SCMs, with all values in mg/L as P. SCMs denoted with * represent those with effluent TP data sets found to be statistically lower than corresponding influent TP data sets at α=5%.

SCM	Influent (mg/L)				Effluent (mg/L)			
	Unweighted Mean	**Weighted Mean**	**Standard Deviation**	**Median (Min, Max)**	**Unweighted Mean**	**Weighted Mean**	**Standard Deviation**	**Median (Min, Max)**
A*	0.95	1.1	0.84	0.74 (0.28, 3.8)	0.13	0.15	0.11	0.12 (<0.05, 0.45)
B*	1.3	1.4	1.0	1.0 (0.19, 4.2)	0.30	0.34	0.15	0.28 (0.14, 0.82)
C	1.4	1.6	1.3	1.2 (0.26, 5.2)	0.87	0.97	0.77	0.81 (0.15, 2.6)
D*	1.3	1.0	0.90	1.1 (0.28, 4.1)	0.32	0.35	0.27	0.32 (0.09, 1.2)
E*	0.57	0.64	0.50	0.31 (0.12, 2.1)	0.13	0.15	0.08	0.13 (<0.05, 0.32)
F*	1.0	1.1	1.0	0.74 (0.11, 4.3)	0.49	0.55	0.48	0.29 (<0.05, 1.6)
G*	1.3	1.5	1.0	0.97 (0.35, 4.3)	0.34	0.38	0.41	0.25 (0.08, 1.8)

The same three studies on sand filtration systems as analyzed for TSS (Yu and Stanford 2006, Barrett 2010, Urbonas 1999) can be referenced to assess the performance of TP removal in the SCMs. See Section 3.4.1 for descriptions of the systems monitored in these studies. Mean influent and effluent TP concentrations for the three studies are: 0.23 mg/L as P and 0.09 mg/L as P (Yu and Stanford 2006); 0.22 mg/L as P and 0.08 mg/L as P (Barrett 2010); and 0.52 mg/L as P and 0.11 mg/L as P (Urbonas 1999).

In all SCMs, mean influent TP FFCs are larger than previously published EMCs. This is primarily attributed to the TP first flush described in Section 3.3.3. Additionally, all effluent TP FFCs for the SCMs are larger than EMCs from these studies. Despite larger mean influent TP FFCs (0.95 and 0.57 mg/L as P, respectively), SCMs A and E provide similar effluent TP FFCs to these studies (both 0.13 mg/L as P). This implies that the performance of SCMs A and E is comparable to previously studied sand filters. Meanwhile, all other SCMs discharge TP FFCs larger than previously published EMCs from these studies, indicating worse performance of TP removal.

Influent and effluent exceedance probability plots were produced for the same groups of SCMs as used for TSS. Figures 3-17 and 3-18 present plots for SCMs A, B, D, and E and SCMs C, F, and G, respectively. TP FFC distributions are shown to be lognormal, with correlation coefficients ranging from 0.875 (SCM E effluent) to 0.993 (SCM G influent).

All influent data sets follow distributions with parallel slopes. Two-tailed Mann Whitney tests were performed to determine if influent TP concentrations of the seven SCMs are significantly different among each other at α=5%. All SCMs but SCM E were found to have statistically similar influent TP FFCs. Influent TP FFCs for SCM E are

statistically lower than that of all other SCMs at α=5%. The difference between influent TP concentrations in SCM E and all other SCMs is credited to watershed characteristics. Sources of TP in urban watersheds include fertilizers, automobile exhaust, living and decaying plants, animal remains, and detergents (Liu and Davis 2014).

Davis and McCuen (2005) recommend a Potomac River TP water quality goal of 0.25 mg/L as P. This value was reached by mean and median effluent TP FFCs for SCMs A and E, the median only for SCM G, and neither the mean or median for SCMs B, C, D, and F. Exceedance probability distributions for SCMs A and E exceed this value only 18% and 15% of the time, respectively. All other SCMs exceed this value over 50% of the time: 65% (SCM B); 86% (C); 58% (D); 53% (F); 53% (G).

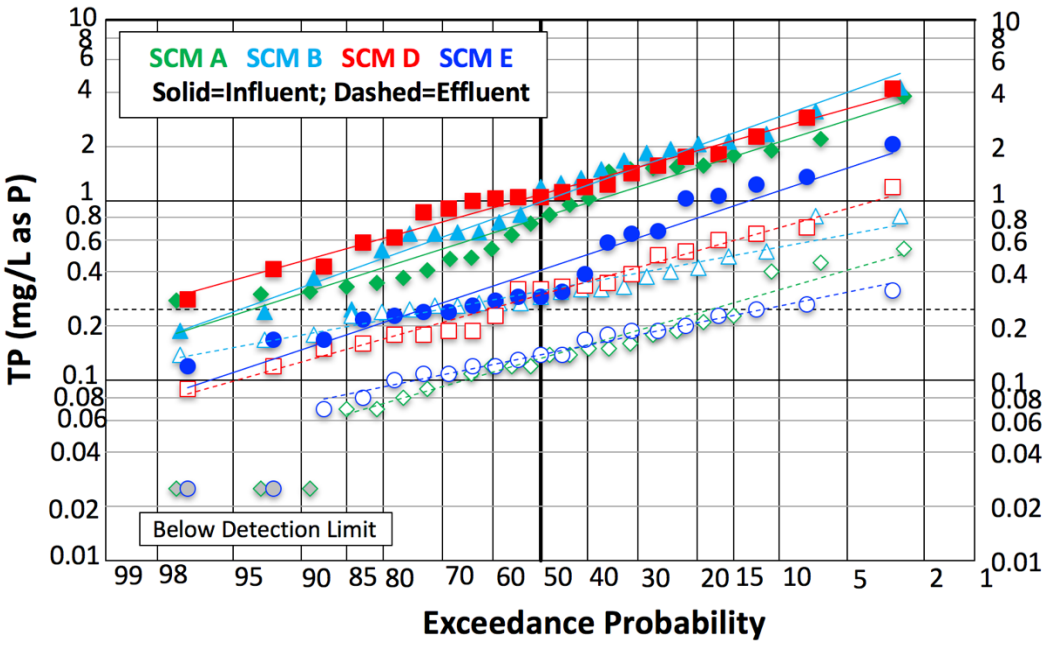

Figure 3-17. Exceedance probability plot of influent and effluent TP FFCs for SCMs A, B, D, and E.

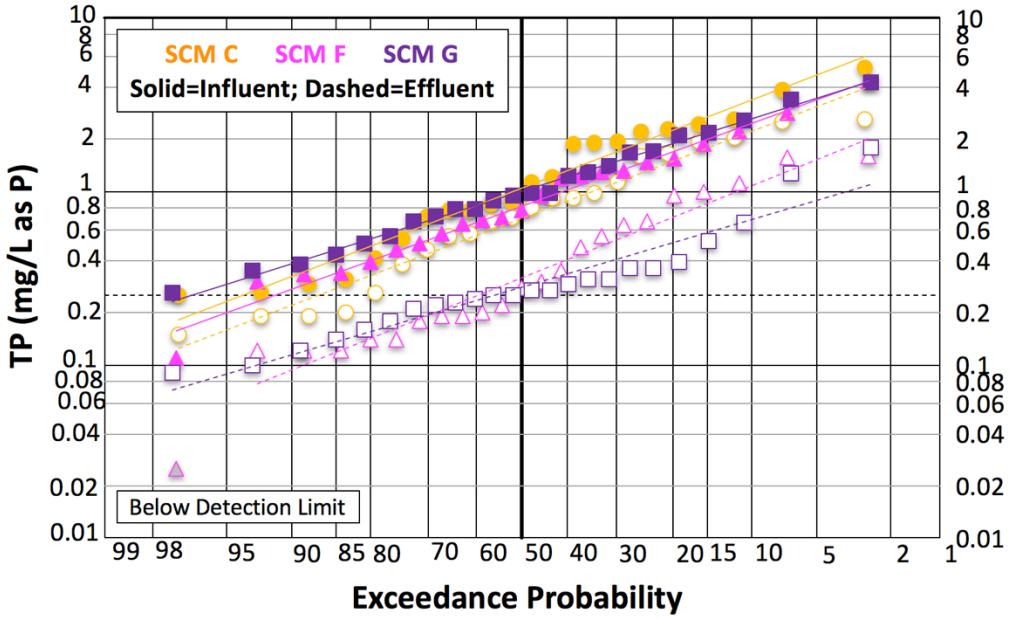

Figure 3-18. Exceedance probability plot of influent and effluent TP FFCs for SCMs C, F, and G.

3.5.2 Speciation and Removal Mechanisms

To fully understand removal of P in the SCMs, the fate of individual P species must be considered. TP is comprised of the following species: Particulate Phosphorus (PP), Dissolved Organic Phosphorus (DOP), and Dissolved Reactive Phosphorus (DRP).

3.5.2.1 Particulate Phosphorus

Figures 3-19 and 3-20 present exceedance probability plots of influent and effluent PP FFCs for SCMs A, B, D, and E and SCMs C, F, and G, respectively. All SCMs provide strong removal of PP, with median effluent concentrations ranging from <0.05 mg/L as P (detection limit) for SCMs A, B, and E to 0.18 mg/L as P for SCM C. In all SCMs, effluent PP FFCs are lower than influents at α=5%. See Table C-2 for a summary of PP FFCs. PP is successfully removed via sedimentation and filtration. These

two processes have been found to be effective at removing PP in bioretention facilities (Davis et al. 2006; Hsieh and Davis 2005; Davis 2007; Li and Davis 2009; Liu and Davis 2014).

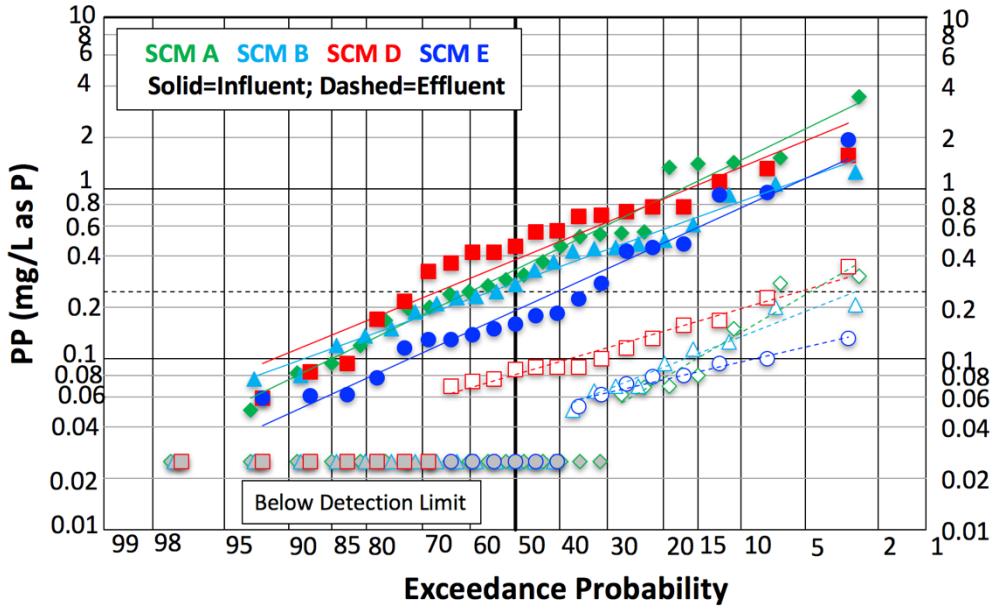

Figure 3-19. Exceedance probability plot of influent and effluent PP FFCs for SCMs A, B, D, and E.

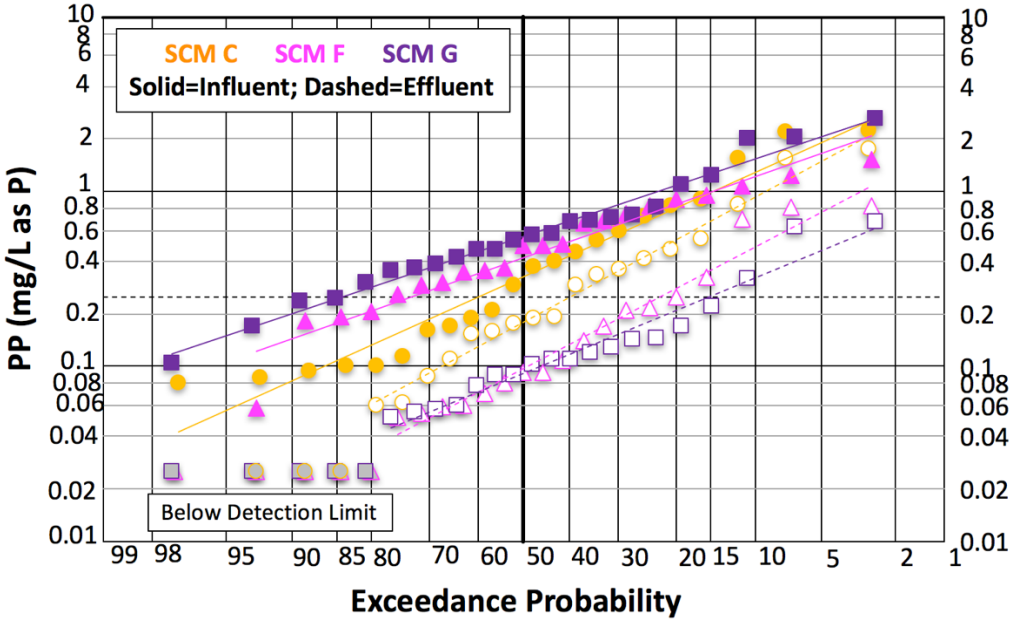

Figure 3-20. Exceedance probability plot of influent and effluent PP FFCs for SCMs C, F, and G.

On average, PP accounts for 49% of influent TP. The New York State Department of Environmental Conservation Stormwater Management Design Manual suggests that generally half of the phosphorus load in runoff from residential and commercial sites is particulate-bound (NYSDEC 2008). Since a large amount of influent TP is in particulate form, a relationship between influent PP and TSS can be expected, which is shown in Figure 3-21. The trend line shown and corresponding correlation coefficient have been forced through the origin to better reflect a realistic relationship. A strong correlation is noted, with a correlation coefficient of 0.58.

A less apparent trend was found for effluent PP. On average, PP accounts for 34% of effluent TP. Figure 3-22 presents a plot of effluent TSS and PP FFCs. Here, a weaker correlation between TSS and PP is noted with a correlation coefficient of 0.46. This trend line has also been forced through the origin. Clustering of low values limits the extent of correlation, but, in general, effluent PP FFCs increase with TSS FFCs.

The slopes of the trend lines represent an estimation of mass of PP per mass of TSS. Influent and effluent slopes show 1.6 mg-PP/g-TSS and 1.8 mg-PP/g-TSS, respectively. These slopes are very close in magnitude and may be indicative of similar proportions of PP-to-TSS in influent and effluent runoff. This implies that PP removal follows the same removal mechanisms as TSS. When both the influent and effluent data sets are plotted together, the trend line shows a slope of 1.6 mg-PP/g-TSS and a correlation coefficient of 0.64 (data not shown).

The effluent slope is larger than the influent. This implies that TSS is more-successfully removed in the SCMs than PP. In turn, this implies that some PP is

associated with fine particles that are not removed by the SCMs. A study by Vaze et al. (2003) on pollutant accumulation on urban road surfaces reported that majority of PP was associated with particles less than 50 µm. Based on filtration theory, particles greater than 17 µm are completely removed in the SCMs. However, fractions of PP associated with particles less than 17 µm are not predicted to be effectively removed by the HFM. Therefore, in effluent samples, PP is assumed to be associated with fine particles.

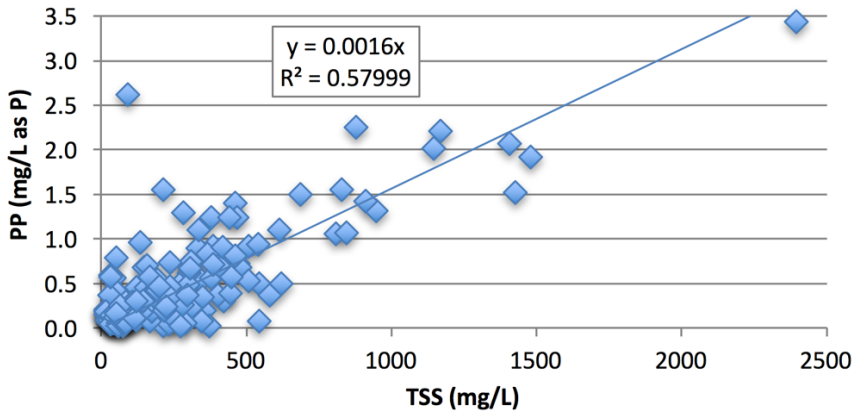

Figure 3-21. Relation between influent concentrations of Particulate Phosphorus (PP) and Total Suspended Solids (TSS). The x-axis represents TSS FFCs and the y-axis represents PP FFCs for influent samples.

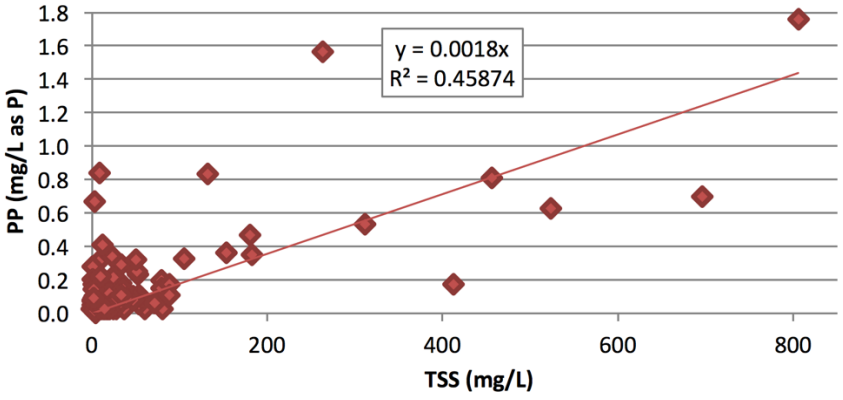

Figure 3-22. Relation between effluent concentrations of Particulate Phosphorus (PP) and Total Suspended Solids (TSS). The x-axis represents TSS FFCs and the y-axis represents PP FFCs for effluent samples.

3.5.2.2 Dissolved Organic Phosphorus

Figures 3-23 and 3-24 present exceedance probability plots of influent and effluent DOP FFCs for SCMs A, B, D, and E and SCMs C, F, and G, respectively. DOP has been found to be a significant part of the urban runoff load, primarily from pesticides, animal wastes, and organic matter decomposition (Yan et al. 2016). In all SCMs, influent DOP FFCs are larger than effluent DOP FFCs at α=5%. DOP FFCs were below the detection limit in 69% of effluent samples. Constant effluent concentrations suggest adsorption as the primary removal mechanism (Liu and Davis 2014). The slopes of effluent distributions for SCMs A, B, D, and E are flat, implying effective adsorption of DOP in these SCMs. Steeper slopes for SCMs C, F, and G are most likely due to sampling constraints.

Unweighted mean influent DOP FFCs range from 0.07 mg/L as P (SCM E) to 0.28 mg/L (SCM C). Unweighted mean effluent DOP FFCs are below the detection limit (0.05 mg/L as P) in SCMs A, B, D, and E. Liu and Davis (2014) report lower values of influent (0.030 mg/L as P) DOP EMCs and similar effluent DOP EMCs (0.028 mg/L as P). Export of DOP in Liu and Davis (2014) was accredited to biological transformation of accumulated PP within field bioretention systems.

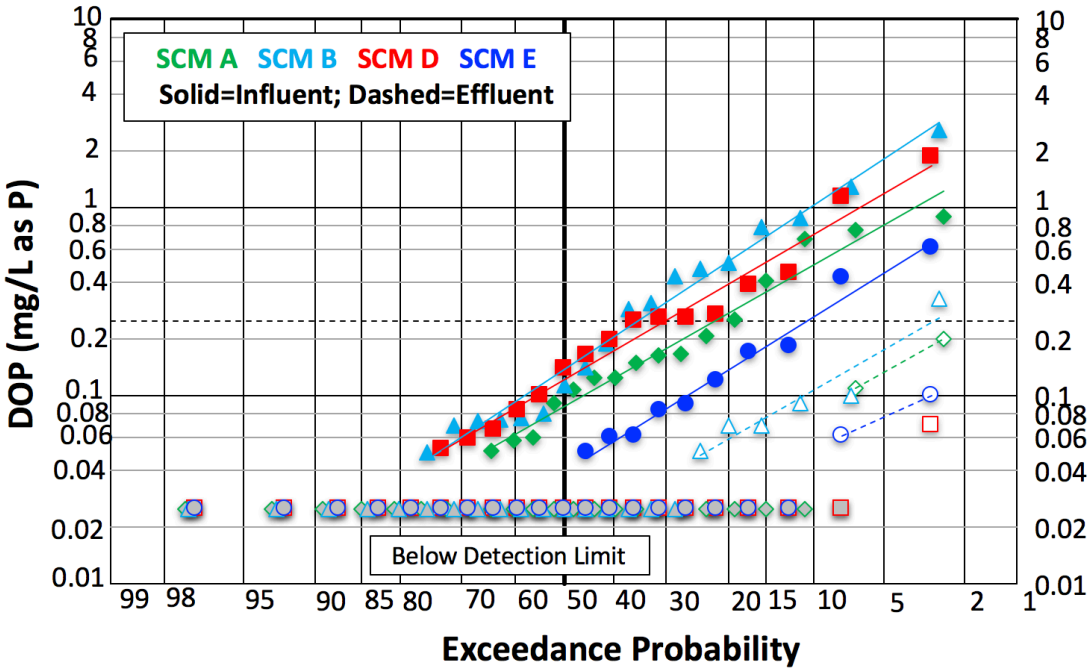

Figure 3-23. Exceedance probability plot of influent and effluent DOP FFCs for SCMs A, B, D, and E.

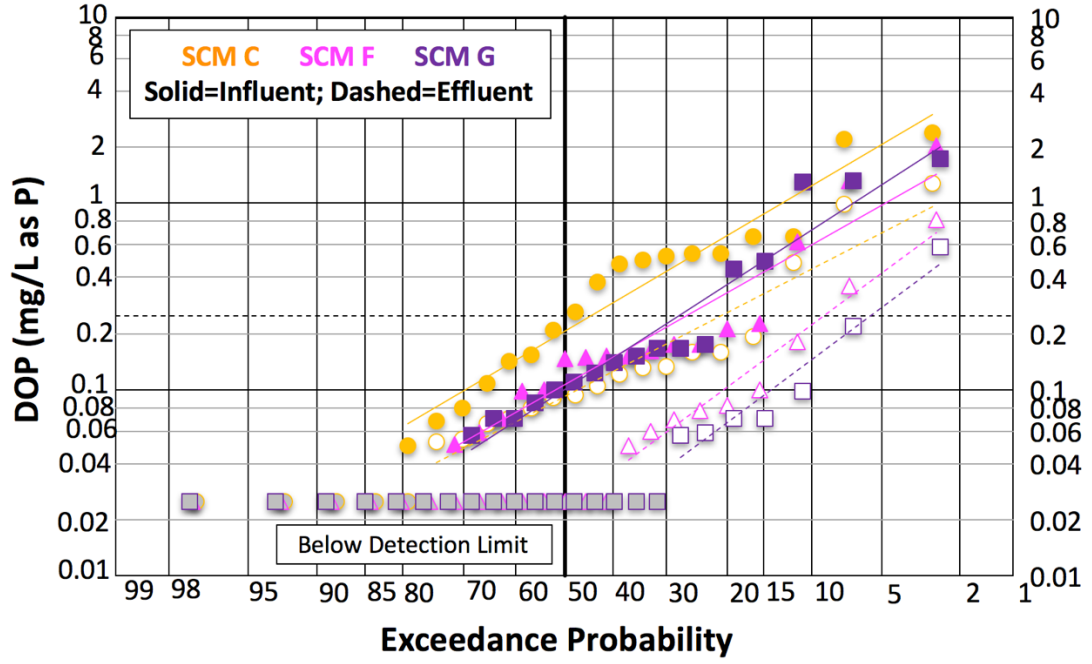

Figure 3-24. Exceedance probability plot of influent and effluent DOP FFCs for SCMs C, F, and G.

Erickson et al. (2013) reports very little removal of dissolved P (2.1%) from stormwater using sand filters and credits this to a low sorption capacity in the media. DOP FFCs can be split up between the first twelve storm events and the latter twelve storm events to determine whether or not a HFM adsorption capacity or leaching of captured P are dictating DOP removal. Figure 3-25 shows the results of this comparison for SCMs A, B, D, and E. SCMs C, F, and G were excluded from this analysis. In both cases, effluent DOP FFCs are lower than influent DOP FFCs at α=5% and effluent slopes are flat, indicating effective adsorption. Effluent DOP FFCs for the latter 12 storms are larger than effluent DOP FFCs for the first 12 storms. This may indicate that a sorption capacity is dictating DOP sorption in the SCMs. It may also indicate that captured P is leaching out of the SCMs in the form of DOP.

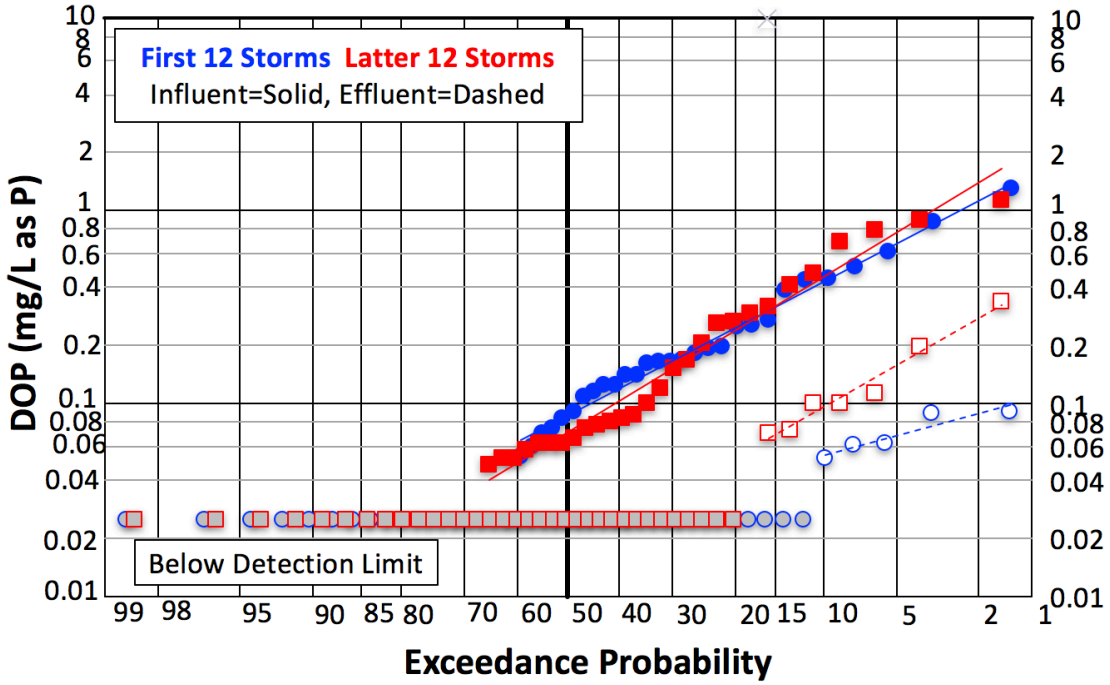

Figure 3-25. Exceedance probability plot of influent (solid) and effluent (dashed) DOP FFCs for SCMs A, B, D, and E, split up between the first twelve storm events (blue circles) and the latter twelve storm events (red squares).

3.5.2.3 Dissolved Reactive Phosphorus

Figures 3-26 and 3-27 present exceedance probability plots of influent and effluent DRP FFCs for SCMs A, B, D, and E and SCMs C, F, and G, respectively. DRP is of particular significance, as this species of phosphorus is the most bioavailable and therefore most connected to algal blooms and eutrophication (Hallegraeff 1993). Beretta and Sansalone (2011) found majority of TDP in stormwater runoff to be in the form of orthophosphates (DRP). SCMs A and D were the only two SCMs to provide statistically-lower effluent DRP FFCs than corresponding influents at α=5%.

Steep, parallel slopes are noted between pairs of influent and effluent DRP FFCs for all SCMs. This may indicate filtration and sedimentation to be playing a role in DRP removal. Arias et al. (2013) found TDP sorption in sand filtration systems to be dominated by sorption onto suspended solids. Thus, it is highly suspected that DRP sorption in the SCMs is achieved on influent and previously-accumulated sediment and not the HFM itself.

It is also possible that internal transformation and leaching of captured P is leading to poor DRP removal in the SCMs. Yan et al. (2016) found minimal DRP sorption from stormwater using sandy bioretention media. Ma et al. (2011) found similar results, reporting high DRP concentrations in effluent stormwater from a filter with a low adsorption capacity and attributing it to repartitioning/dissolution of captured PP.

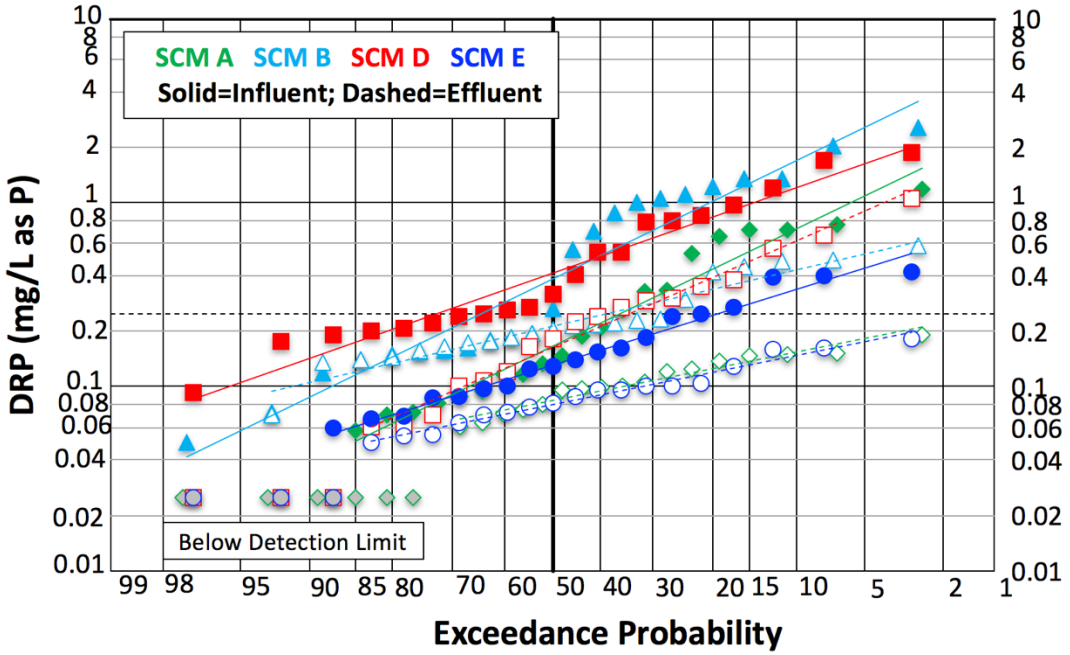

Figure 3-26. Exceedance probability plot of influent and effluent DRP FFCs for SCMs A, B, D, and E.

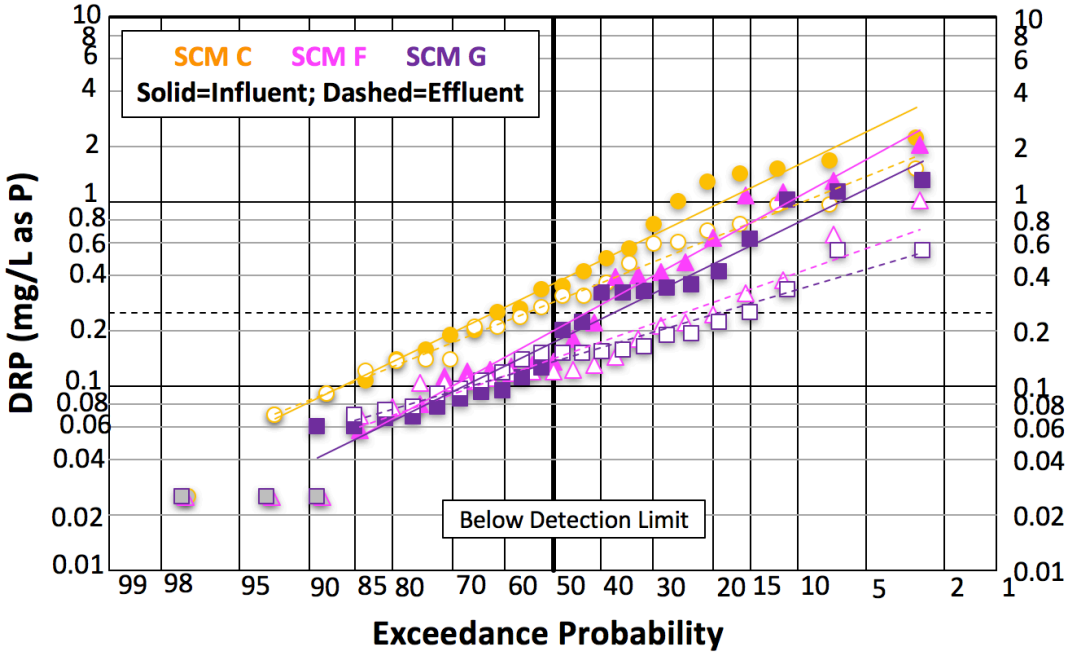

Figure 3-27. Exceedance probability plot of influent and effluent DRP FFCs for SCMs C, F, and G.

DRP FFCs were split up between the first twelve storm events and the latter twelve storm events to determine whether or not a HFM adsorption capacity of leaching of captured P are dictating DRP removal. Figure 3-28 shows the results of this comparison for SCMs A, B, D, and E. In both cases, effluent DRP FFCs are lower than corresponding influents at α=5%. Pairs of influent and effluent DRP FFCs are the same between the first and latter 12 storms and influent and effluent DRP FFCs are parallel for both cases. This may indicate adsorption of DRP to solids and subsequent removal via filtration and sedimentation as the primary removal mechanisms throughout the entire duration of the project. It may also indicate leaching of DRP from the SCMs.

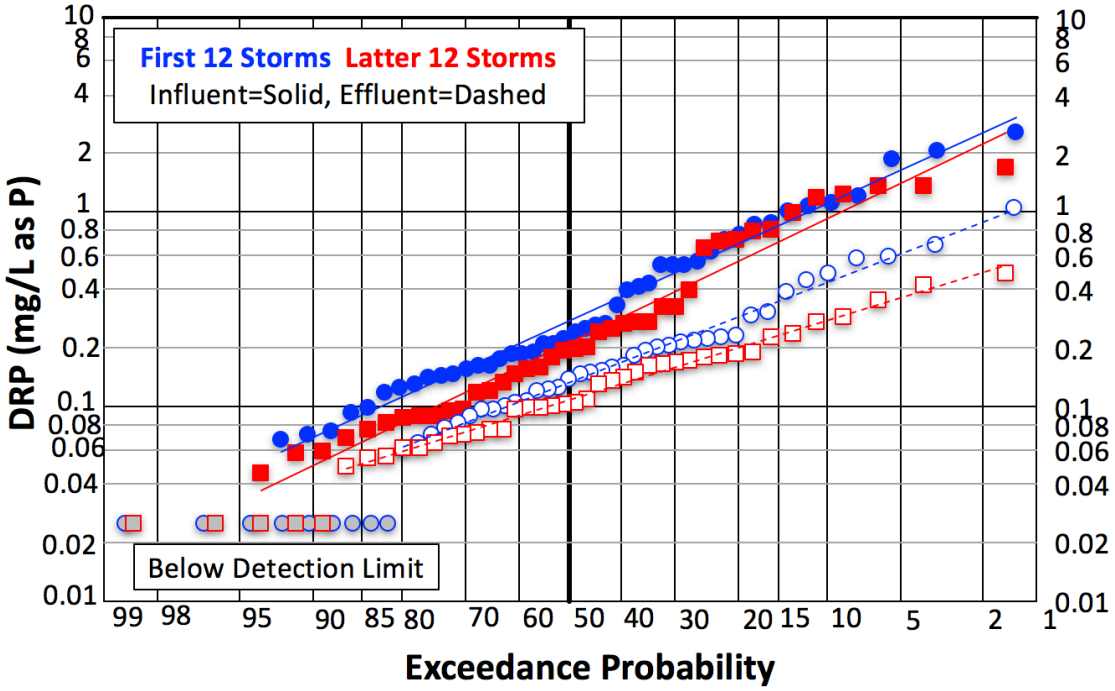

Figure 3-28. Exceedance probability plot of influent (solid) and effluent (dashed) DRP FFCs for SCMs A, B, D, and E, split up between the first twelve storm events (blue circles) and the latter twelve storm events (red squares).

3.5.3 Load Reduction and Ultimate Fate

Table 3-8 presents annual input and output mass loads, net load reductions, and percent reductions for various P species in all SCMs. These calculations assume no removal via volume reduction. The stormwater phosphorus behavior and fate in SCM D is diagrammed in Figure 3-29. These values were calculated using the Simple Method, as presented in Section 2.5.5. To account for first flush, influent and effluent FFCs inputted into the Simple Method were divided by the average first flush ratio of TP FFCs to Maryland EMCs (2.2), as presented in Section 3.3.3. Results for P mass loads that do not incorporate the first flush factor are included in Appendix C.

All of the SCMs successfully reduce TP loads from influent runoff. Input TP mass loads range from 1.3 kg/ha-yr (1.1 lb/ac-yr) in SCM E to 3.3 kg/ha-yr (2.9 lb/ac-yr) in SCM C. Output TP mass loads range from 0.33 kg/ha-yr (0.29 lb/ac-yr) in SCM E to 2.1 kg/ha-yr (1.9 lb/ac-yr) in SCM C. Li and Davis (2009) report input/output TP mass loads to Cells CP and SS (see Section 3.3.3 for site descriptions) of 3.6/0.7 and 0.9/0.4 kg/ha-yr, respectively. Liu and Davis (2014) report input/output TP loads to Cell CP as 2.7/1.2 kg/ha-yr, respectively (55% reduction). Calculated loads are comparable to these values.

TP load reductions are largest in SCMs A, B, and G, with values between 2.0 kg/ha-yr (1.9 lb/ac-yr) in SCM G and 2.2 kg/ha-yr (2.0 lb/ac-yr) in SCM B. Meanwhile SCM E only reduces input- to output-TP loads by 1.0 kg/ha-yr (0.85 lb/ac-yr). The low reduction witnessed in SCM E is most likely due to its low input mass load. SCMs A and E provide the best reduction in mass loads (83% and 75%, respectively). Meanwhile, SCMs C and F were only found to reduce TP loads by 35% and 53%, respectively. Low

reductions in SCMs C and F are probably due to sampling constraints; thus, these SCMs will not be considered in analysis.

TP entered the SCMs in the form of particulate P and dissolved P, each comprising approximately half of input TP mass loads in all SCMs. DRP accounted for more input TP than DOP in all SCMs.

PP mass load reductions are as high as 90% in SCM A. After excluding SCMs C and F, the lowest PP mass load reduction is 80% (SCM D). Strong PP reductions are credited to effective sedimentation and filtration mechanisms occurring within the SCMs. Reductions in dissolved P mass loads are also noted, but they are not as drastic as PP. DOP mass load reductions are as high as 84% (SCM D), with a median removal percentage of 75% (SCM A), while percent reductions of input DRP mass loads are lower, with a median removal percentage of 54% (SCM E). Reductions of DOP mass loads are larger than that of DRP due to lower input DOP mass loads. Mass load reductions of DOP and DRP are similar. Removal of DOP and DRP is most likely driven by sorption to captured sediment in the SCMs. It is also possible that internal transformation of previously-accumulated PP leads to eventual export of DOP and DRP.

In conclusion, all SCMs seem to be working similarly in terms of P removal. With the exception of SCMs that experienced sampling constraints, all SCMs provide substantial load reductions in all P species. This is primarily achieved via sedimentation and filtration of PP. Sorption of dissolved P species is also noted within the SCMs, but desorption/resuspension of accumulated P species limits the extent of TDP mass load reductions.

Table 3-8. Load reductions of phosphorus species for all SCMs. Influent and effluent mass loads incorporate the TP first flush factor (2.2) to normalize FFCs to EMCs.

SCM		A	B	C	D	E	F	G
TP	**L_{in} in kg/ha-yr. (lb/ac-yr.)**	2.6 (2.3)	3.0 (2.7)	3.3 (2.9)	1.9 (1.7)	1.3 (1.1)	2.2 (2.0)	2.9 (2.6)
	L_{out} in kg/ha-yr. (lb/ac-yr.)	0.44 (0.40)	0.81 (0.72)	2.1 (1.9)	0.61 (0.54)	0.33 (0.29)	1.0 (0.92)	0.82 (0.73)
	L_{red} in kg/ha-yr. (lb/ac-yr.)	2.1 (1.9)	2.2 (2.0)	1.1 (1.0)	1.3 (1.2)	1.0 (0.85)	1.2 (1.0)	2.1 (1.9)
	L_{red} in kg/yr. (lb/yr.)	0.54 (0.48)	0.32 (0.29)	0.21 (0.19)	0.32 (0.28)	0.26 (0.23)	0.36 (0.32)	3.5 (3.1)
	% Reduction	**83%**	**73%**	**35%**	**69%**	**75%**	**53%**	**72%**
PP	**L_{in} in kg/ha-yr. (lb/ac-yr.)**	1.4 (1.3)	0.86 (0.77)	1.3 (1.2)	0.85 (0.76)	0.76 (0.68)	1.1 (1.0)	1.7 (1.5)
	L_{out} in kg/ha-yr. (lb/ac-yr.)	0.14 (0.13)	0.13 (0.11)	0.80 (0.72)	0.17 (0.15)	0.10 (0.09)	0.40 (0.36)	0.32 (0.29)
	L_{red} in kg/ha-yr. (lb/ac-yr.)	1.3 (1.2)	0.73 (0.65)	0.50 (0.44)	0.68 (0.61)	0.66 (0.59)	0.68 (0.61)	1.4 (1.2)
	L_{red} in kg/yr. (lb/yr.)	0.33 (0.29)	0.11 (0.10)	0.09 (0.08)	0.16 (0.15)	0.18 (0.16)	0.21 (0.19)	2.3 (2.1)
	% Reduction	**90%**	**85%**	**38%**	**80%**	**87%**	**63%**	**81%**
DOP	**L_{in} in kg/ha-yr. (lb/ac-yr.)**	0.39 (0.35)	0.59 (0.53)	0.69 (0.61)	0.25 (0.23)	0.16 (0.14)	0.34 (0.3)	0.48 (0.43)
	L_{out} in kg/ha-yr. (lb/ac-yr.)	0.10 (0.09)	0.13 (0.12)	0.42 (0.37)	0.04 (0.04)	0.06 (0.05)	0.17 (0.15)	0.14 (0.12)
	L_{red} in kg/ha-yr. (lb/ac-yr.)	0.30 (0.26)	0.46 (0.41)	0.27 (0.24)	0.21 (0.19)	0.10 (0.09)	0.16 (0.15)	0.35 (0.31)
	L_{red} in kg/yr. (lb/yr.)	0.07 (0.07)	0.07 (0.06)	0.05 (0.04)	0.05 (0.05)	0.03 (0.02)	0.05 (0.04)	0.58 (0.52)
	% Reduction	**75%**	**77%**	**39%**	**84%**	**62%**	**49%**	**72%**
DRP	**L_{in} in kg/ha-yr. (lb/ac-yr.)**	0.75 (0.66)	1.6 (1.4)	1.3 (1.1)	0.83 (0.74)	0.36 (0.32)	0.79 (0.70)	0.74 (0.66)
	L_{out} in kg/ha-yr. (lb/ac-yr.)	0.21 (0.18)	0.55 (0.49)	0.91 (0.81)	0.40 (0.35)	0.17 (0.15)	0.46 (0.41)	0.36 (0.32)
	L_{red} in kg/ha-yr. (lb/ac-yr.)	0.54 (0.48)	1.0 (0.90)	0.36 (0.32)	0.43 (0.38)	0.19 (0.17)	0.33 (0.29)	0.38 (0.34)
	L_{red} in kg/yr. (lb/yr.)	0.14 (0.12)	0.15 (0.13)	0.07 (0.06)	0.10 (0.09)	0.05 (0.05)	0.10 (0.09)	0.63 (0.56)
	% Reduction	**72%**	**65%**	**28%**	**52%**	**54%**	**42%**	**51%**

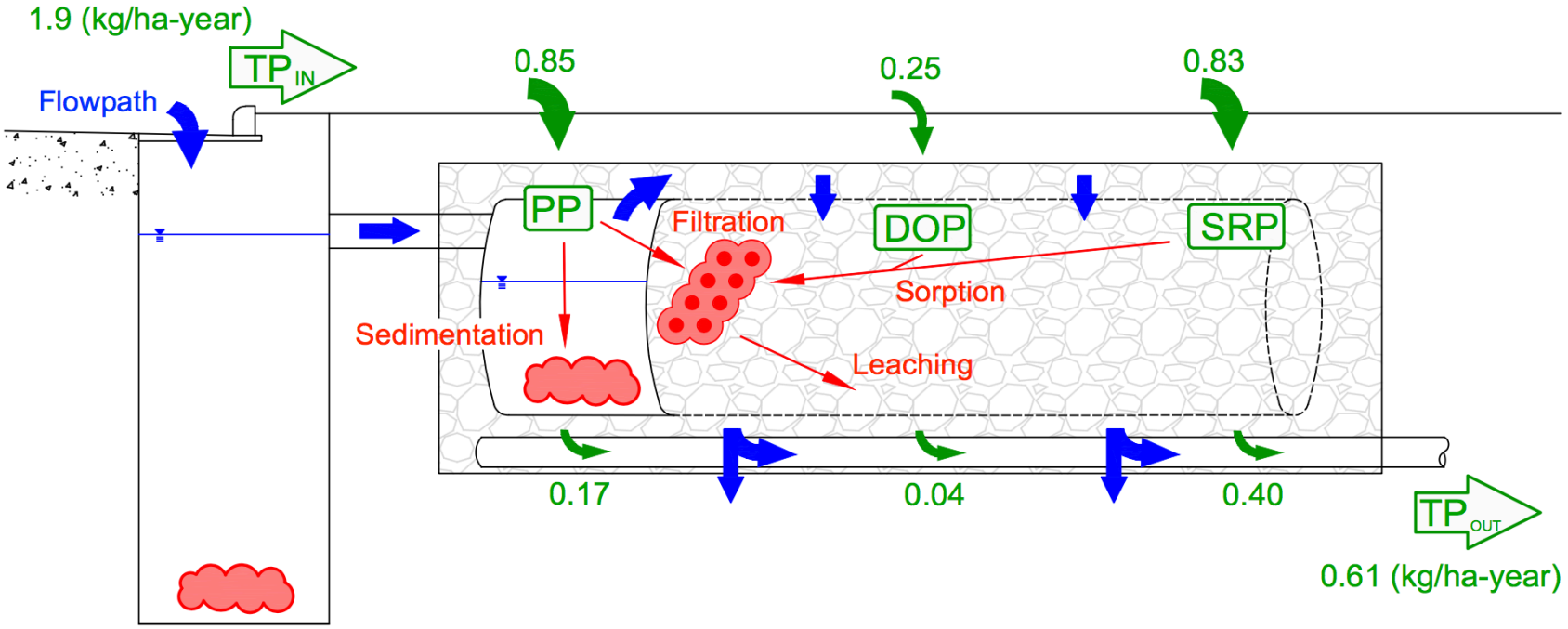

Figure 3-29. Phosphorus behavior through SCM D. SCM D features storage before filtration. Legend: red=removal mechanism; blue=flowpath; green=input/output mass loads estimated with EMCs based on first flush ratios for individual species, in kg/ha-yr. Adapted from Li and Davis (2009).

3.5 Nitrogen

3.5.1 Overall Performance

Table 3-9 presents a summary of influent and effluent Total Nitrogen (TN) FFCs for all seven SCMs. TN removal is inconsistent in the SCMs. In all cases, unweighted mean effluent TN FFCs are lower than that of influent TN FFCs, but, in SCMs B and G, median effluent TN FFCs are higher than corresponding influents.

Individual storm influent TN FFCs range from 0.71 mg/L as N in SCM A to 68 mg/L as N in SCM F. Individual storm effluent TN FFCs range from 0.32 mg/L as N in SCM A to 11.5 mg/L as N in SCM B. There is high variability in influent and effluent TN FFCs for all SCMs. Standard deviations of influent and effluent TN FFCs range from 2.1 mg/L as N in SCM C to 15 mg/L as N in SCM D and 0.93 mg/L as N in SCM A to 2.8 mg/L as N in SCM B, respectively. In several cases, standard deviations of influent TN FFCs are larger than corresponding means and medians. Standard deviations of effluent TN FFCs are also large, but, in all cases but SCM F, they are lower than mean and median effluent TN FFCs.

All weighted and unweighted influent mean TN FFCs are larger than corresponding medians; therefore, it can be said that mean calculations are biased by extreme events. Influent TN FFCs are as high as 68 mg/L as P, most likely due to washoff of fertilizers. That being said, the SCMs are expected to perform well for all storm events, making these extreme events important in assessment.

SCMs A and D provide the lowest effluent TN FFCs. SCMs C, E, and F provide

the next-lowest effluent TN FFCs. SCMs B and G also provide reductions in mean TN FFCs from influent to effluent, but mean effluent TN FFCs in these SCMs are larger than that of the other SCMs. It is important to consider the influent TN FFCs for each SCM; SCM D provides the second-lowest effluent TN FFC from the highest influent TN FFC, while SCMs A and E provide the lowest and third-lowest effluent TN FFCs from the second-lowest and lowest influent TN FFC, respectively. The largest difference in unweighted mean influent and effluent TN FFCs is seen in SCM A (3.5 mg/L as N to 1.1 mg/L). The lowest difference occurs in SCM G, where an influent mean TN FFC of 4.0 mg/L as N is treated to an effluent mean TN FFC of 3.9 mg/L as N.

Table 3-9. Summary of influent and effluent TN FFCs for all monitored SCMs, with all values in mg/L as N. SCMs denoted with * represent those with effluent TN data sets found to be statistically lower than corresponding influent TN data sets at α=5%.

SCM	Influent (mg/L)				Effluent (mg/L)			
	Unweighted Mean	**Weighted Mean**	**Standard Deviation**	**Median (Min, Max)**	**Unweighted Mean**	**Weighted Mean**	**Standard Deviation**	**Median (Min, Max)**
A*	3.5	3.3	3.4	2.3 (0.71, 16)	1.1	1.2	0.93	0.8 (0.32, 4.9)
B	5.7	3.4	9.9	2.7 (0.9, 49)	4.1	4.2	2.8	3.0 (0.97, 11.5)
C	3.7	3.6	2.1	3.6 (1.0, 8.9)	2.7	2.6	1.6	2.0 (0.71, 6.1)
D*	8.6	4.1	15	2.0 (0.62, 57)	1.9	1.6	1.6	1.2 (0.5, 6.5)
E*	3.2	3.0	1.7	2.8 (1.2, 7.1)	2.2	2.2	1.5	1.9 (0.73, 6.3)
F	6.5	3.6	14	3.1 (0.84, 68)	3.1	3.6	2.6	2.1 (0.97, 11)
G	4.0	4.0	3.4	3.4 (0.81, 13)	3.9	3.7	2.3	3.7 (0.34, 8.1)

Influent and effluent exceedance probability plots were produced for the same groups of SCMs as used for TSS and TP. Figures 3-30 and 3-31 present plots for SCMs A, B, D, and E and SCMs C, F and G, respectively. TN FFCs are shown to be lognormal, with correlation coefficients ranging from 0.873 (SCM D influent) to 0.92 (SCM E influent).

Two-tailed Mann Whitney tests were performed to determine if the influent TN data sets of the seven SCMs are significantly different among each other at α=5%. Influent TN FFCs were found statistically to be the same among all SCMs. The solid lines in Figures 3-30 and 3-31, which represent influent TN FFCs, follow very similar distributions. Influent TN FFC distributions for SCMs B, D, and F have steeper slopes than the other SCMs, indicating more variability in TN FFCs. Influent TN FFCs for SCMs B, D, and F also exhibit standard deviations much higher than that of the other SCMs. This is attributed primarily to extreme events; the three highest TN FFCs measured throughout the project (49, 57, and 68 mg/L as N) occurred in SCMs B, D, and F. These large inputs of TN into the SCMs are most likely due to application of fertilizers on lawns within the watersheds of SCMs B, D, and F, as each of these large TN inputs occurred during the spring and summer months.

One-tailed Mann Whitney tests were performed to determine if pairs of influent and effluent TN FFCs of the seven SCMs are significantly different at α=5%. Effluent TN FFCs are lower than corresponding influents in SCMs A, D, and E, but influent and effluent TN FFCs for SCMs B, C, F, and G were found statistically to be the same. The dashed-green line in Figure 3-31, which represents the distribution of effluent TN FFCs

for SCM A, is visually lower than all other influent and effluent distributions. Therefore, based on reaching effluent TN water quality goals, SCM A is performing the best of all monitored SCMs. SCMs D and E also provide good TN removal. However, it is important to compare the slopes of influent and effluent distributions for these SCMs. While the pair of influent and effluent TN FFC distributions for SCM E are parallel, there is an intersection between influent and effluent distributions for SCM D. This is due to the extreme events occurring in influent TN FFCs of SCM D. It can be said that SCM D is successful at removing large amounts of TN from influent runoff, but the same cannot be said for SCM E. SCMs C, F, and G provide no significant removal of TN. This could be due to the sampling constraints described in Section 3.2.1. Additionally, SCMs F and G are vegetated, which may contribute to the high effluent TN FFCs.

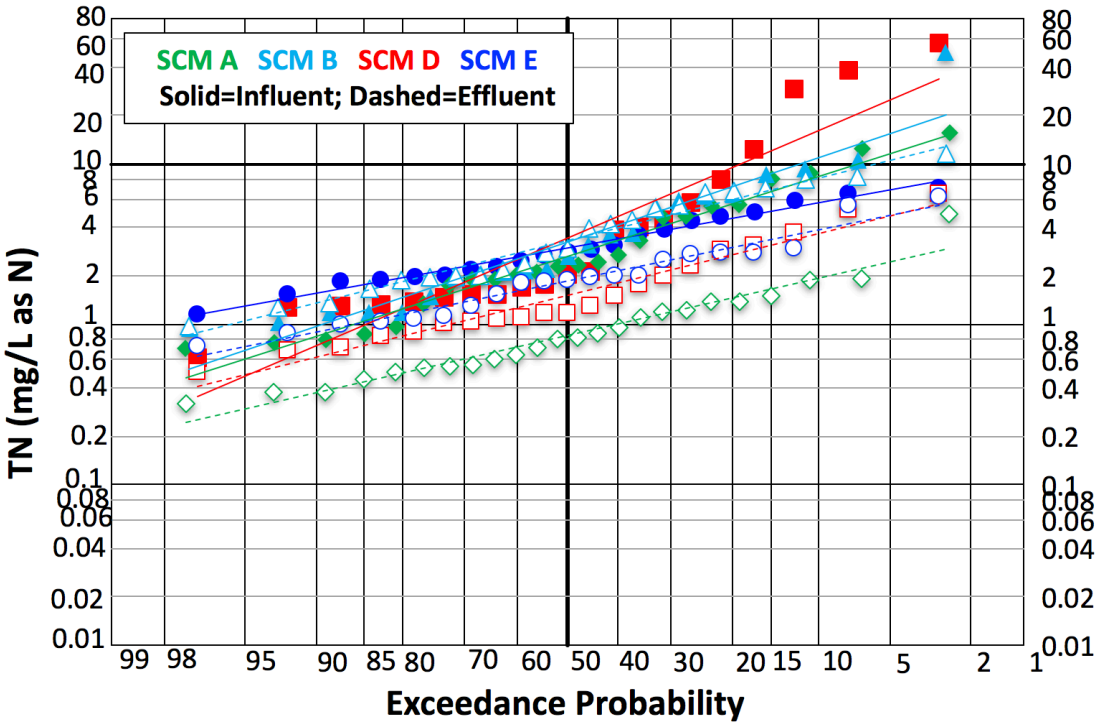

Figure 3-30. Exceedance probability plot of influent and effluent TN FFCs for SCMs A, B, D, and E.

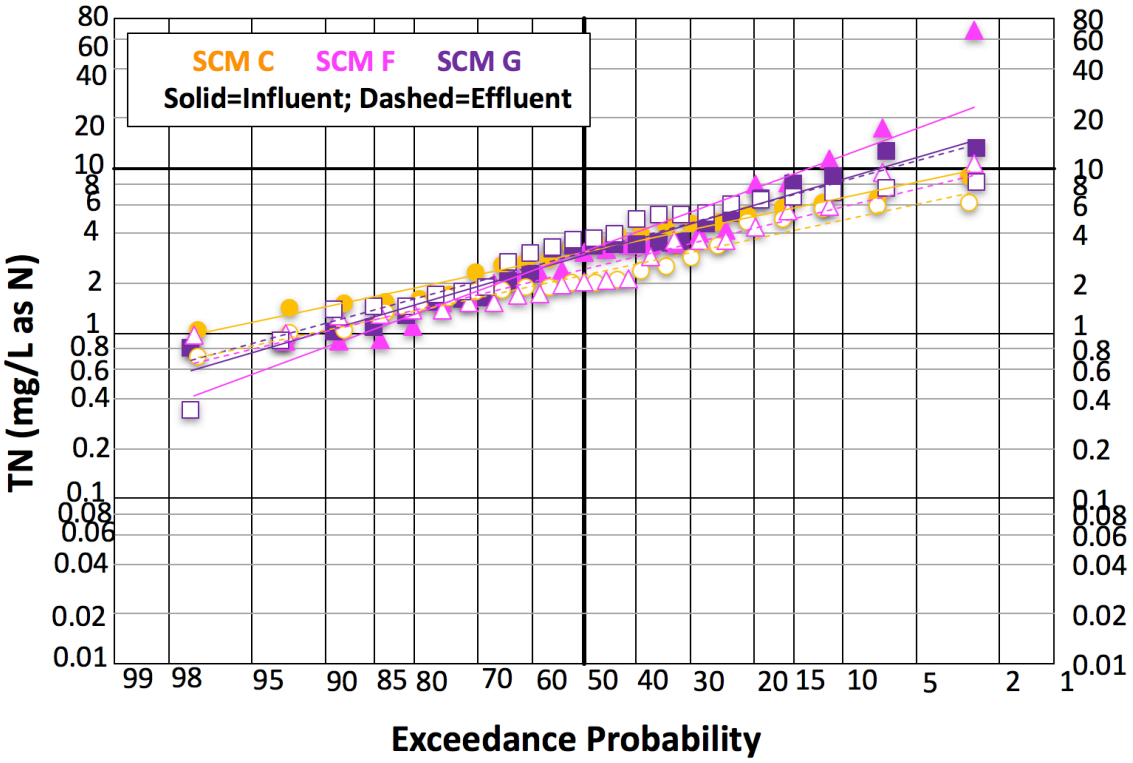

Figure 3-23. Exceedance probability plot of influent and effluent TN FFCs for SCMs C, F, and G.

Results of TN removal in the SCMs can be compared to other bioretention and sand filtration systems. The same three studies that were compared to TSS and TP results (Yu and Stanford 2006, Barrett 2010, Urbonas 1999) were referenced to assess TN removal in the Camelot SCMs.

Mean influent and effluent TN concentrations from Yu and Stanford (2006) and Barrett (2010) are 2.2 mg/L as N and 1.3 mg/L as N, 1.5 mg/L as N and 1.1 mg/L as N, respectively. Influent TN FFCs for all SCMs are larger than previously published EMCs from these studies. Collins et al. (2010) reported that average TN concentrations in stormwater for urban land uses are between 1.3 and 3.2 mg/L as N. Unweighted mean influent TN FFCs for all SCMs except SCM E are larger than this range. The mean

influent TN FFC for SCM E is 3.2 mg/L as N, equal to the upper-most value in this range. In all SCMs except SCM A, mean effluent TN FFCs are larger than effluent values from Yu and Stanford (2006) and Barrett (2010). Both influent and effluent TN FFCs for all SCMs are larger than EMCs reported in these studies.

Urbonas (1999) reports mean influent and effluent TN EMCs as 8.0 and 3.8 mg/L as N, respectively. Unweighted mean influent and effluent from SCM D are similar: 8.6 mg/L as N and 1.9 mg/L, respectively. In these two cases, influent and effluent TN concentrations are higher than that of other studies. High influent TN FFCs are due primarily to extreme events of high TN inputs, such as fertilizer application. There is high variability among influent and effluent TN concentrations for all SCMs and previously-reported values. This variability is due to the complexity of nitrogen behavior in bioretention and sand filtration systems, as nitrogen has a diverse speciation in runoff and its speciation and concentration varies with site and season (Taylor et al. 2005).

3.6.2 Speciation and Removal Mechanisms

TN consists of the following species: Particulate Nitrogen (PN); Nitrate (NO_3^-); Nitrite (NO_2^-); Ammonium (NH_4^+); and Dissolved Organic Nitrogen (DON). Nitrogen fate is complex and removal rates and pathways for various nitrogen species are highly variable (Davis et al. 2006). Treatment mechanisms for various nitrogen species in stormwater include sedimentation, filtration, adsorption, mineralization, and biological transformations (Li and Davis 2014). Previous studies have observed substantial reductions in TN through SCMs, attributing this primarily to the removal of PN and NH_4^+

(Davis et al. 2006, Hunt et al. 2012). SCMs have also been found to release NO_3^- and DON, mainly due to biological nitrification and denitrification processes and decomposition and transformation of previously-accumulated nitrogen (Li and Davis 2014).

3.6.2.1 Particulate Nitrogen

Figures 3-32 and 3-33 present exceedance probability plots of influent and effluent PN FFCs for SCMs A, B, D, and E and SCMs C, F, and G, respectively. PN FFCs for all SCMs but SCM F were found statistically to be lower than corresponding influent PN FFCs at α=5%. PN is successfully removed via filtration and sedimentation.

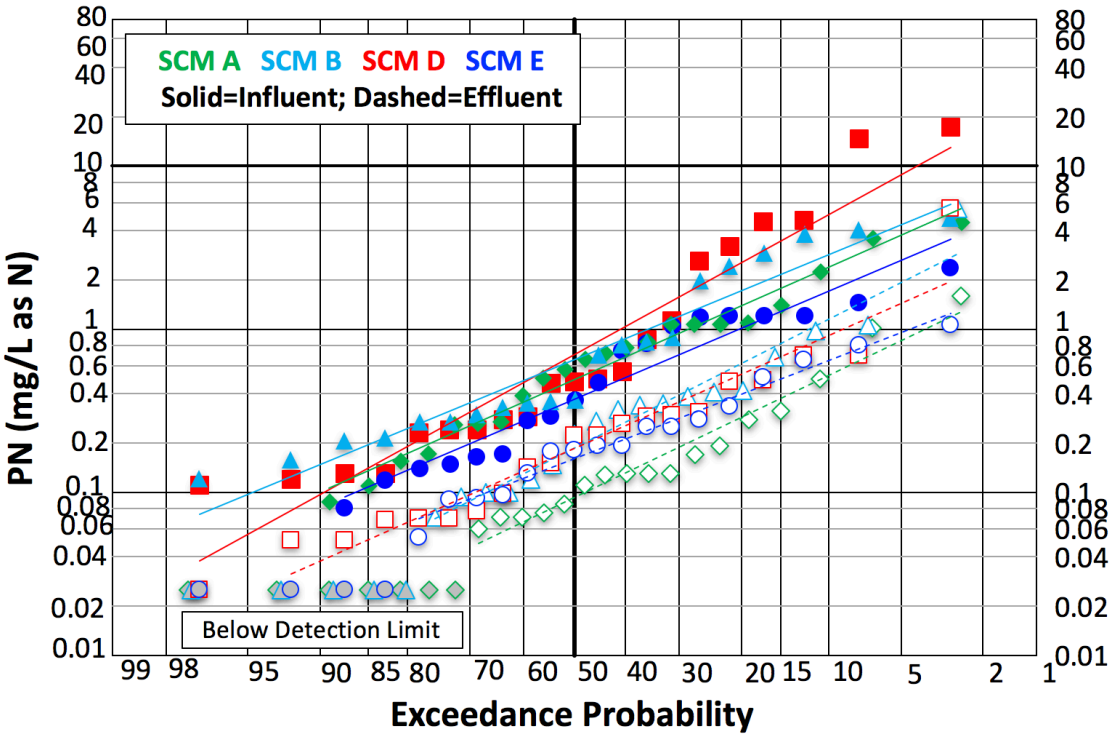

Figure 3-32. Exceedance probability plot of influent and effluent PN FFCs for SCMs A, B, D, and E.

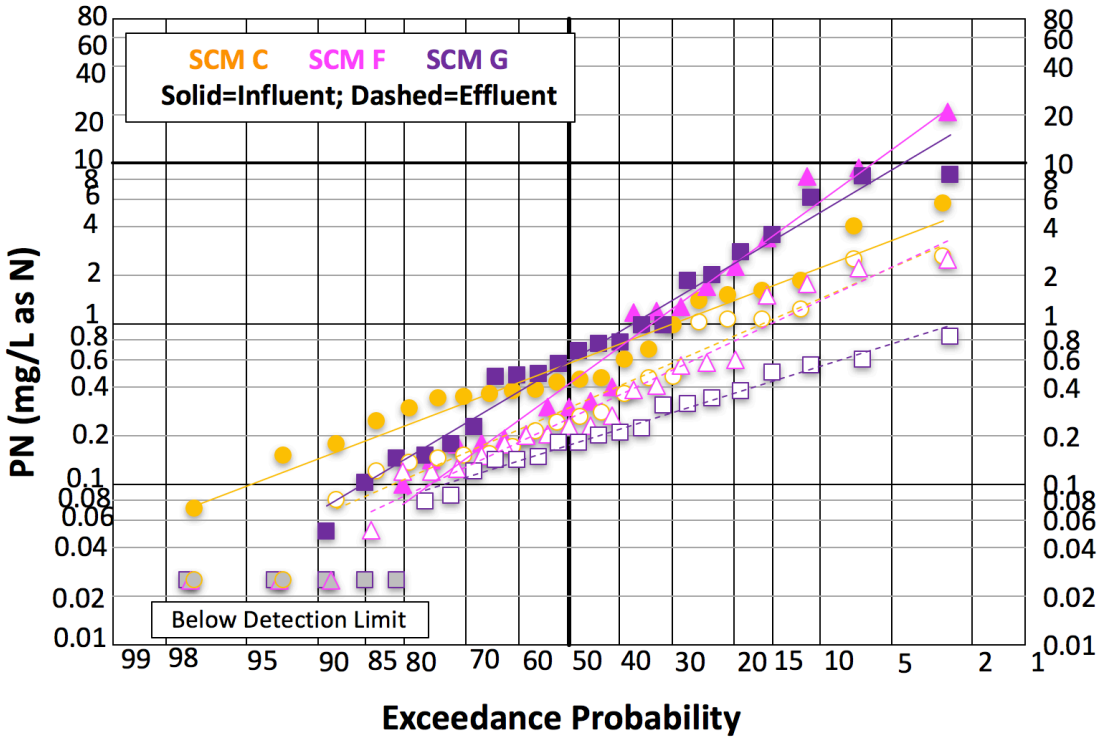

Figure 3-33. Exceedance probability plot of influent and effluent PN FFCs for SCMs C, F, and G.

Nitrogen is less particulate bound than phosphorus. On average, PN accounts for 24% of influent TN and 15% of effluent TN. This agrees with some studies and disagrees with others, as previous results on nitrogen composition in stormwater runoff vary significantly. Taylor et al. (2005) found particulate N to account for less than 20% of TN in residential runoff, while Li and Davis (2014) found parking lot TN to be dominated by Particulate Organic N (PON). It is generally accepted that PN is predominantly in organic form (Harris et al. 1996), but it cannot be assumed that all organic N is particulate.

Correlation plots between influent and effluent TSS and PN are presented in Figures 3-34 and 3-35, respectively. No correlation was found between TSS and PN, with correlation coefficients for influent and effluent relationships of -0.07 and -0.01, respectively. Influent and effluent trend lines have similar slopes: 0.0028 and 0.0034,

respectively. These slopes represent the mass of PN per mass of TSS. On average, influent samples have approximately 2.8 mg-PN/g-TSS and effluent samples have approximately 3.4 mg-PN/g-TSS. As is the case with phosphorus, the slopes are similar, but the effluent slope is larger. This implies that the proportion of PN per TSS is larger in effluent samples than in influent samples; thus, TSS is more successfully removed in the SCMs than PN. Vaze et al (2003) reported the majority of PN to be associated with particles less than 10 µm. Fractions of influent and effluent PN are assumed to be associated with fine particles that are not successfully removed in the SCMs.

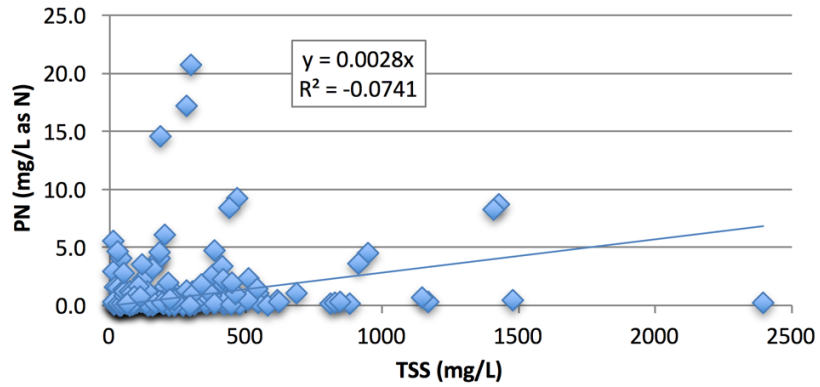

Figure 3-34. Relation between influent concentrations of Particulate Nitrogen (PN) and Total Suspended Solids (TSS). The x-axis represents TSS FFCs and the y-axis represents PN FFCs for influent samples.

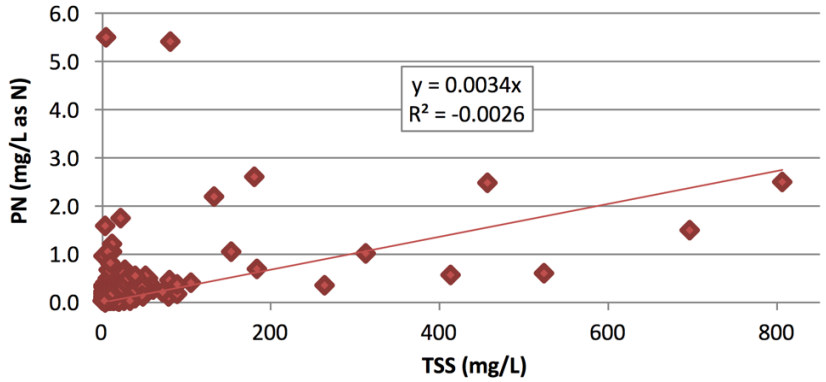

Figure 3-35. Relation between effluent concentrations of Particulate Nitrogen (PN) and Total Suspended Solids (TSS). The x-axis represents TSS FFCs and the y-axis represents PN FFCs for effluent samples.

3.6.2.2 Dissolved Organic Nitrogen

Figures 3-36 and 3-37 present exceedance probability plots of influent and effluent DON FFCs for SCMs A, B, D, and E and SCMs C, F, and G, respectively. DON is successfully removed in the SCMs. Effluent DON FFCs for all SCMs but SCM D were found statistically to be lower than corresponding influent DON FFCs at α=5%. In SCM D, influent/effluent DON FFCs are the same, most likely due to low influent DON FFCs. It is expected that DON removal is achieved via adsorption.

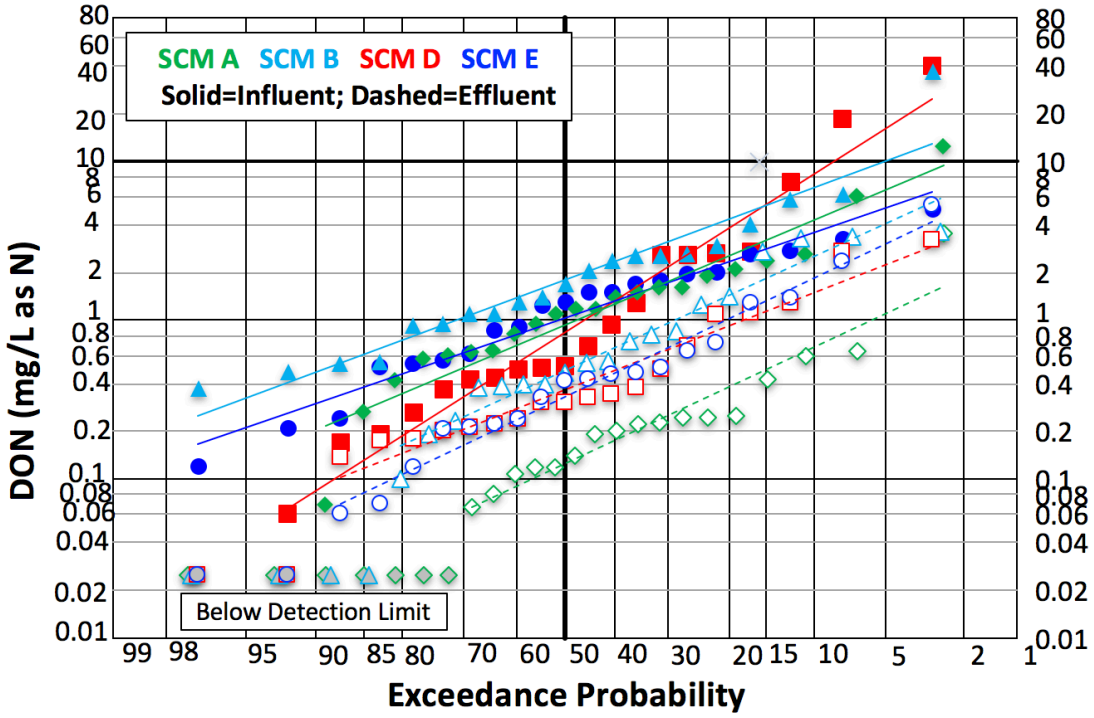

Figure 3-36. Exceedance probability plot of influent and effluent DON FFCs for SCMs A, B, D, and E.

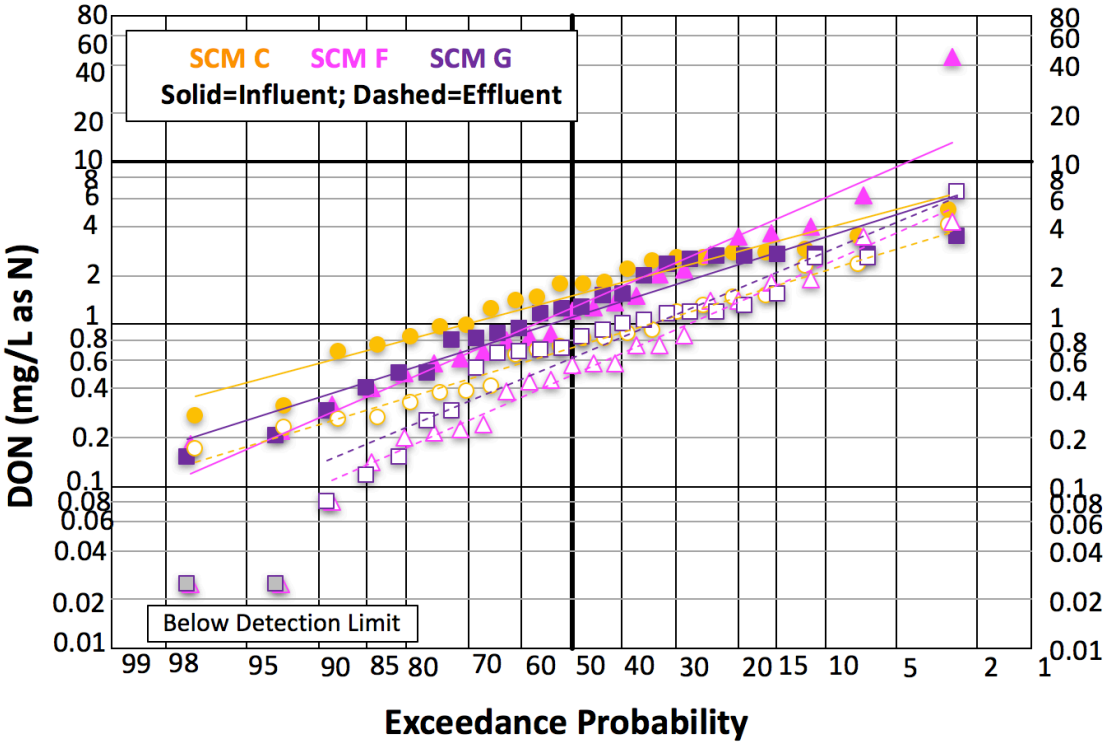

Figure 3-37. Exceedance probability plot of influent and effluent DON FFCs for SCMs C, F, and G.

On average, DON accounts for 45% of influent TN. In several cases, large inputs of DON, as high as 44 mg/L, were noted. Large inputs of DON are of particular importance; in particular, overload of DON may deplete oxygen levels and prevent nitrification, but may also enhance denitrification as a source of organic matter (Taylor et al. 2005). Low influent DON FFCs experience little- to no-removal, and there are many instances of DON export when influent DON FFCs are low.

Few studies have focused on DON in stormwater, but Li and Davis (2014) concluded that DON export is common for aerobic bioretention systems. Potential sources of DON export in the SCMs are captured PN, litter from vegetation, and organic matter accumulated in the SCM that has decomposed (Li and Davis 2014). Li and Davis

(2014) report relatively constant effluent DON concentrations from a bioretention cell, indicating sorption as the primary mechanism of DON removal during a storm event.

DON removal is also achieved during dry periods via mineralization. In the energy-releasing, multistep process of mineralization, organic nitrogen species, including both particulate and dissolved organic N, are biologically converted into NH_4^+ (Kadlec and Knight 1996). An example of a mineralization reaction is below; R-NH_2 represents an organic nitrogen species that is biologically converted into ammonium.

$$R - NH_2 + H_2O + H^+ \rightarrow ROH + NH_4^+ \quad (3\text{-}3)$$

3.6.2.3 Ammonium

Figures 3-38 and 3-39 present exceedance probability plots of influent and effluent NH_4^+ FFCs for SCMs A, B, D, and E and SCMs C, F, and G, respectively. NH_4^+ removal is highly variable among the SCMs. Based on a one-tailed Mann Whitney test, effluent NH_4^+ FFCs are lower than corresponding influents for SCMs A, E, and G at α=5%. In all other SCMs, influent and effluent NH_4^+ FFCs are the same at α=5%.

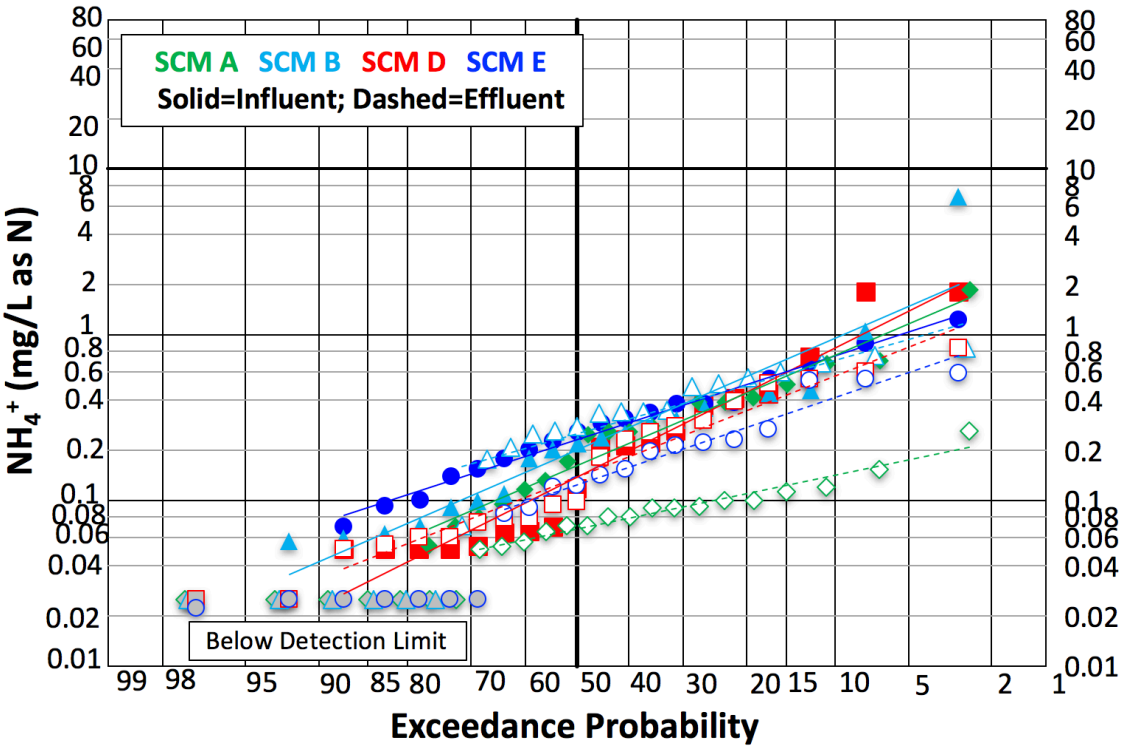

Figure 3-38. Exceedance probability plot of influent and effluent NH_4^+ FFCs for SCMs A, B, D, and E.

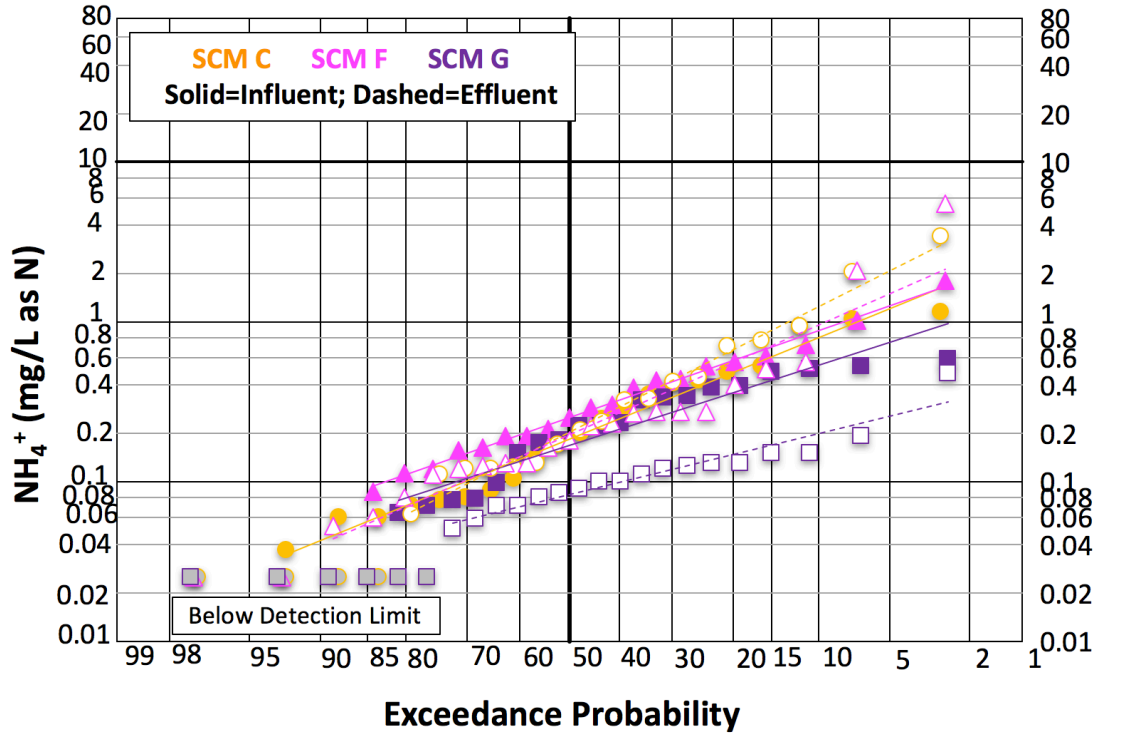

Figure 3-39. Exceedance probability plot of influent and effluent NH_4^+ FFCs for SCMs C, F, and G.

On average, NH_4^+ accounts for 10% of influent TDN (8% TN). Median influent NH_4^+ FFCs range from 0.12 mg/L as N in SCM D to 0.24 mg/L as N in SCM E. In general, influent NH_4^+ FFCs fell within this range, but, on several occasions, large inputs of NH_4^+ were observed. The maximum influent NH_4^+ FFC was 6.77 mg/L as N in SCM B on May 11, 2017. Larger inputs of NH_4^+ were observed in the last three months of sampling, most likely due to use of fertilizers in the spring months.

NH_4^+ removal has been observed in many other studies. Hunt et al. (2008) found NH_4^+ levels to be reduced to below the reporting limit (0.1 mg/L) by a bioretention cell, attributing removal to combined sorption-nitrification processes. Similar results were found by Li and Davis (2014) and Dietz and Clausen (2006). During storm events, adsorption of NH_4^+ onto negatively-charged soil particles, either in the HFM or in captured sediment, removes NH_4^+ from incoming runoff. Between events, nitrification transforms accumulated and mineralized NH_4^+ into NO_3^- via an aerobic oxidation process by autotrophic bacteria, most important being *Nitrosomonas* and *Nitrobacter* (Chen et al. 2006):

$$NH_4^+ + \frac{3}{2}O_2 \rightarrow 2H^+ + H_2O + NO_2^- \quad (3\text{-}4a)$$

$$NO_2^- + \frac{3}{2}O_2 \rightarrow NO_3^- \quad (3\text{-}4b)$$

3.6.2.4 Nitrite

Figures 3-40 and 3-41 present exceedance probability plots of influent and effluent NO_2^- FFCs for SCMs A, B, D, and E and SCMs C, F, and G, respectively. NO_2^- was rarely detected in the SCMs. Individual storm influent and effluent NO_2^- FFCs were

lower than the detection limit in 63% and 84% of samples, respectively. This is most likely due to the aerobic conditions on the roadway and in the SCMs. Li and Davis (2014) saw similar results, in which influent NO_2^- was completely oxidized and effluent NO_2^- concentrations were lower than the detection limit (0.01 mg/L) nearly all of the monitored period. Oxidation of NO_2^- into NO_3^- during nitrification is a fast process and oxidation of NH_4^+ is usually the rate limiting step in the conversion of NH_4^+ to NO_3^- (Chen et al. 2006).

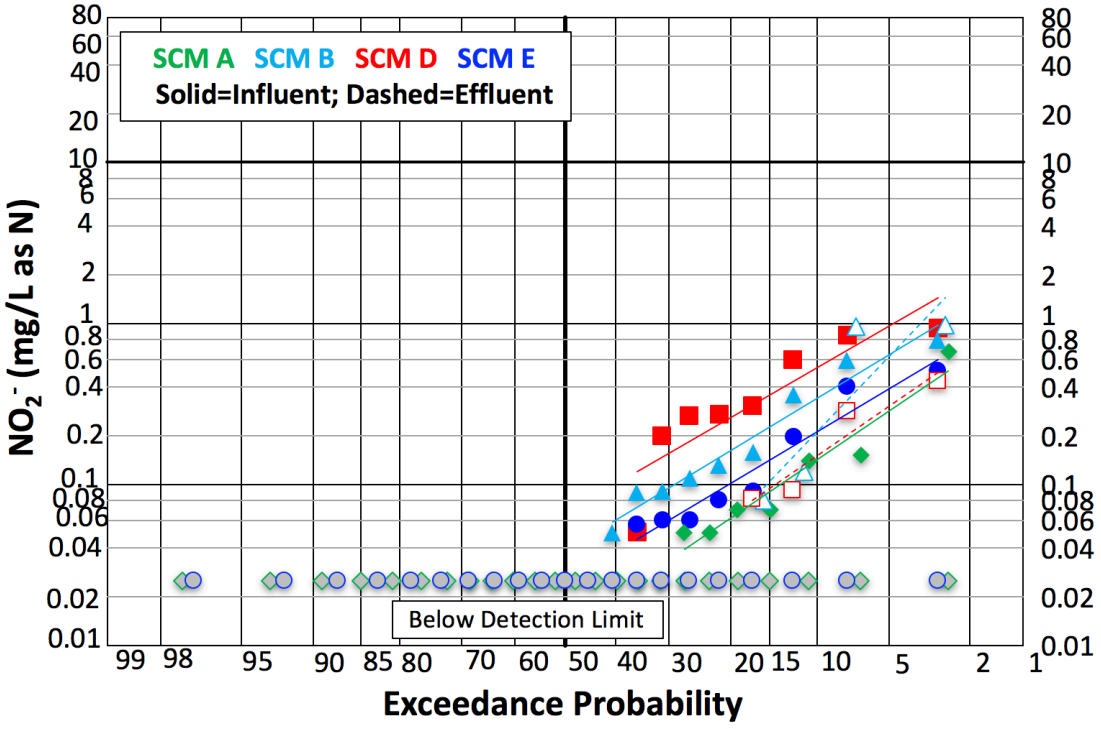

Figure 3-40. Exceedance probability plot of influent and effluent NO_2^- FFCs for SCMs A, B, D, and E.

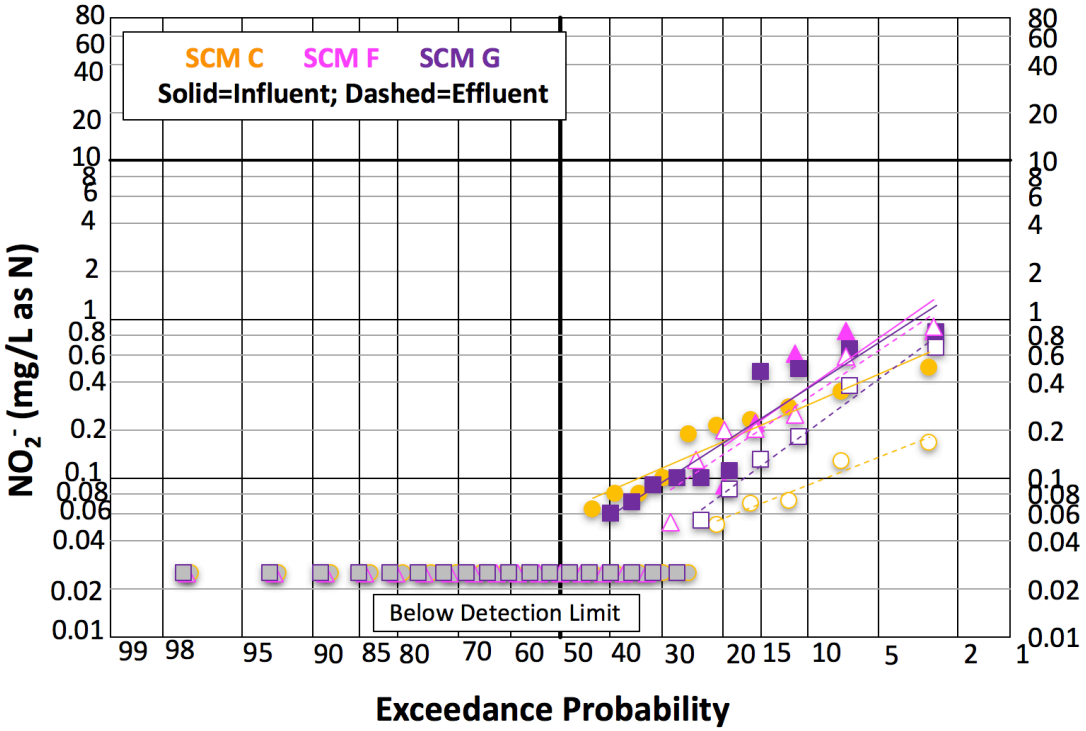

Figure 3-41. Exceedance probability plot of influent and effluent NO_2^- FFCs for SCMs C, F, and G.

3.6.2.5 Nitrate

Figures 3-42 and 3-43 present exceedance probability plots of influent and effluent NO_3^- FFCs for SCMs A, B, D, and E and SCMs C, F, and G, respectively. NO_3^- removal is unsuccessful in the SCMs, and, in many cases, NO_3^- export was noted. In SCMs A, C, D, and E, there is no statistical difference between influent and effluent NO_3^- FFCs at α=5%. In SCMs B, F, and G, effluent NO_3^- FFCs were found to be statistically larger than influent NO_3^- FFCs at α=5%.

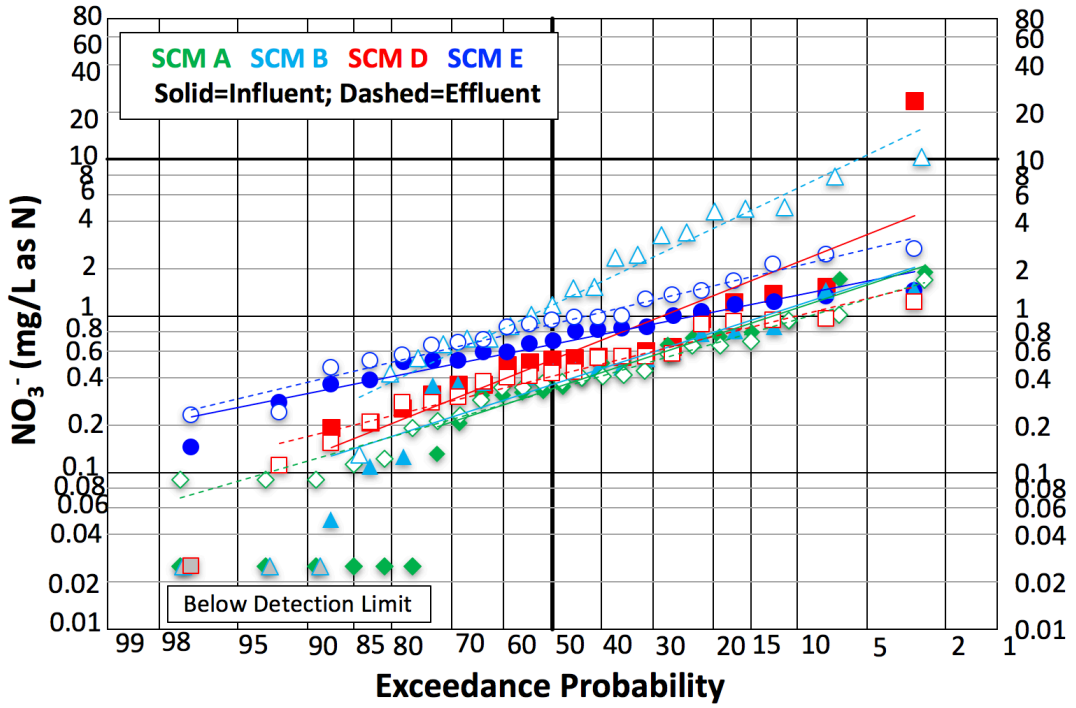

Figure 3-42. Exceedance probability plot of influent and effluent NO_3^- FFCs for SCMs A, B, D, and E.

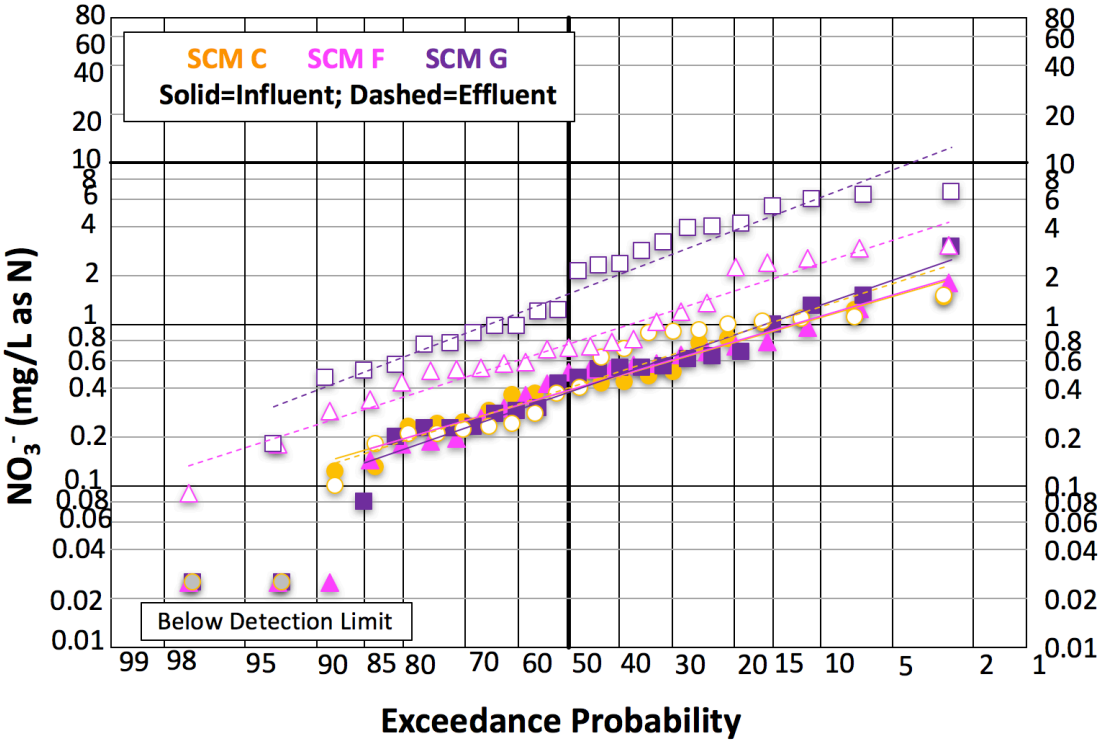

Figure 3-43. Exceedance probability plot of influent and effluent NO_3^- FFCs for SCMs C, F, and G.

Poor NO_3^- removal is attributed to internal assimilation/release processes and from direct transformation of runoff nitrogen; specifically, the conversion of captured DON, NH_4^+, and NO_2^- into NO_3^- between storm events. Similar results have been found in other studies (Kim et al. 2003, Hsieh and Davis 2005, Zinger et al. 2013), concluding that NO_3^- is highly mobile and it will generally wash straight through an aerobic sand filter and/or bioretention cell. Lucas and Greenway (2011) suggest that NO_3^- can be removed in SCMs with low hydraulic conductivities, but that removal will be minimal under high flows due to highly aerobic conditions. In anaerobic conditions, denitrification transforms NO_3^- into nitrogen gas (Kim et al. 2003). SCMs are generally thought to provide an aerobic substrate, organic matter, and microorganisms for mineralization and nitrification to occur, but traditional SCM design often does not incorporate denitrification into its treatment regime (Brown et al. 2013). Therefore, this lack of NO_3^- removal witnessed in the SCMs can be attributed to a release of NO_3^- through mineralization and nitrification.

To further characterize nitrification in the SCMs, NO_3^- FFCs can be separated between storms with less and more antecedent dry days. During dry periods, the SCMs are completely aerobic, allowing nitrification to occur. Therefore, it was predicted that longer antecedent dry periods would create higher influent and effluent NO_3^- FFCs. Influent and effluent NO_3^- FFCs were separated between storms with 7 of fewer dry days and those with 8 or more dry days.

Figure 3-44 presents the results of this comparison for all SCMs. No relationship is seen between influent and effluent NO_3^- FFCs for storms with less- and more-

antecedent dry days. Based on a one-tailed Mann Whitney test, pairs of influent NO_3^- FFCs and effluent NO_3^- FFCs for storms with less- and more-dry days are not significantly different at α=5%. This implies no impact of antecedent dry days on influent and effluent NO_3^- FFCs.

However, when this comparison is performed for the three SCMs in which NO_3^- export was observed (SCMs B, F, and G), results are different. This is shown in Figure 3-45. Based on a one-tailed Mann Whitney test, effluent NO_3^- FFCs of storms with more dry days are significantly larger than effluent NO_3^- FFCs of storms with less dry days at α=5%. Manka et al. (2016) also saw a direct correlation between number of antecedent dry days and effluent NO_3^- concentrations in bioretention. There is no statistical difference between influent NO_3^- FFCs of the two storm types for SCMs B, F, and G. In characterizing stormwater runoff in Austin, Texas, Irish et al. (1995) reported no correlation between number of antecedent dry days and influent NO_3^- concentrations.

Results of this comparison indicate nitrification is the dominant mechanism of NO_3^- export in SCMs B, F, and G. The same cannot be said for SCMs A, C, D, and E. Reasons for differences in the fate of N species within the SCMs include influent runoff composition and SCM designs; particularly, SCMs F and G incorporate vegetation into their designs. Several studies (Davis et al. 2006, Bratieres et al. 2008, Lucas and Greenway 2008) have suggested that more NO_3^- is exported from systems that do not incorporate plants than those that do incorporate plants. This study concludes the opposite, as SCMs F and G were found to export NO_3^-.

NO_3^- is often a pollutant of concern since it is readily formed under aerobic

conditions via nitrification (Davis and McCuen 2005). For this reason, a Potomac River NO_3^- water quality goal of 0.50 mg/L as N is presented in Davis and McCuen (2005). This value is exceeded by effluent NO_3^- FFCs of SCMs A, C, and D only 30%, 40%, and 40% of the time, respectively. In the case of SCMs B, E, F, and G, this value is exceeded 65%, 80%, 70%, and 80% of the time. Therefore, based on effluent NO_3^- FFCs and assuming that mineralization and nitrification are the primary mechanisms of N transformations, it can be said that SCMs A, C, and D are more effective at removing N from incoming stormwater runoff than SCMs B, E, F, and G.

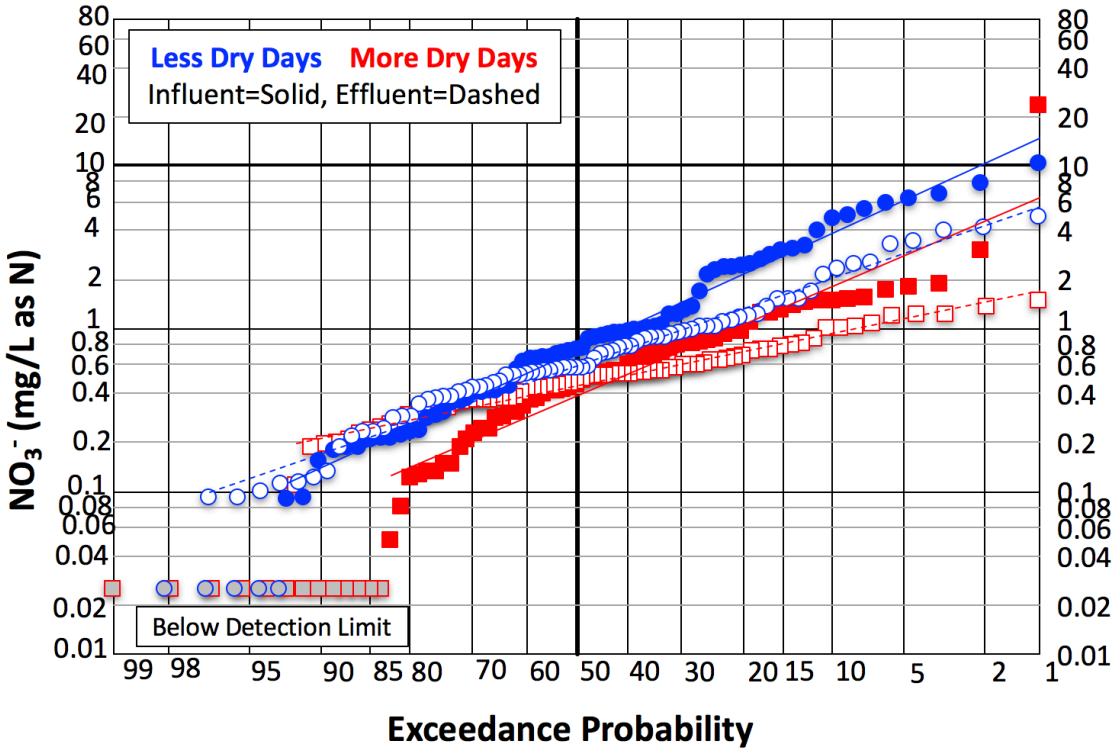

Figure 3-44. Exceedance probability plot of influent (solid) and effluent (dashed) NO_3^- FFCs for all SCMs, split up between storms with less than seven antecedent dry days (blue circles) and storms with more than eight antecedent dry days (red squares).

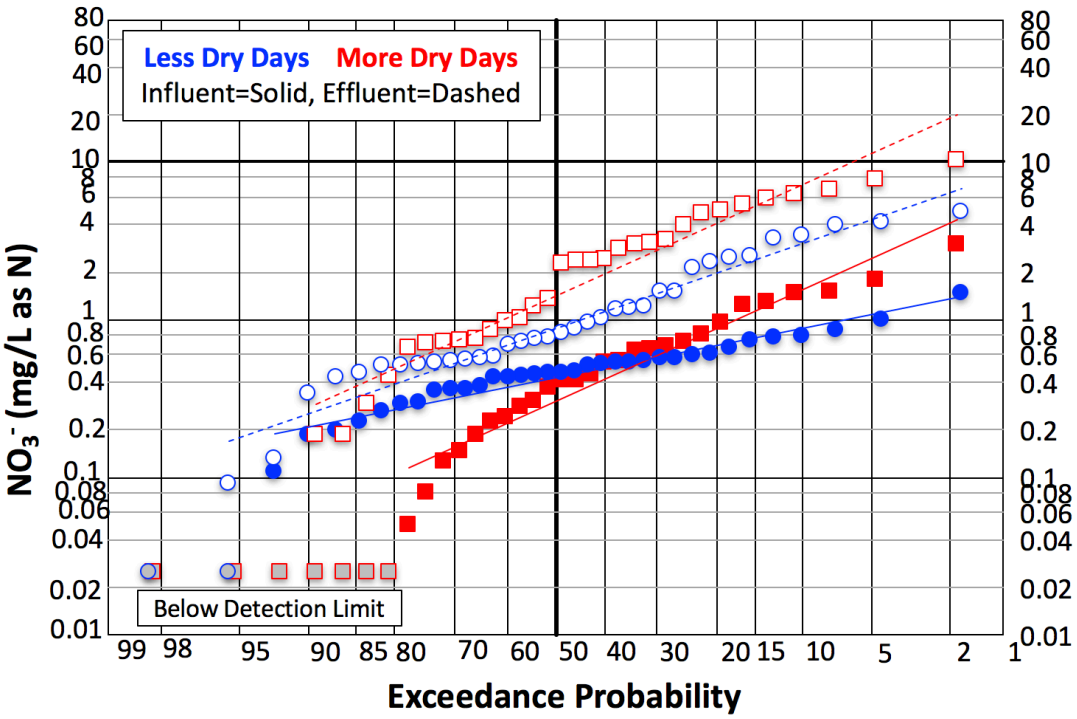

Figure 3-45. Exceedance probability plot of influent (solid) and effluent (dashed) NO_3^- FFCs for SCMs B, F, and G, split up between storms with less than seven antecedent dry days (blue circles) and storms with more than eight antecedent dry days (red squares).

3.6.3 Load Reduction and Ultimate Fate

Table 3-10 presents annual input and output mass loads, net load reductions, and percent reductions for various N species in all SCMs. The stormwater nitrogen behavior and fate in SCM X is diagrammed in Figure 3-46. These calculations assume no removal via volume reduction. To account for first flush, FFCs inputted into the Simple Method were multiplied by the average first flush ratio of TN FFCs to Maryland EMCs (2.6), as presented in section 3.3.4. Results for N mass loads that do not incorporate the first flush factor are included in Appendix C.

Input TN mass load ranges from 5.7 kg/ha-yr (5.1 lb/ac-yr) in SCM E to 10.1 kg/ha-yr (9.0 lb/ac-yr) in SCM F. Output TN mass loads range from 2.3 kg/ha-yr (2.1 lb/ac-yr) in SCM A to 7.6 kg/ha-yr (6.8 lb/ac-yr) in SCM B. TN load reduction is largest

in SCM D (7.4 kg/ha-yr, 74%), while SCM G performed the worst, only reducing input- to output-TN loads by 7.2 kg/ha-yr (7%). In comparing SCMs D and E, a larger percent TN mass load reduction is seen in HFM Y (SCM D, 74%) than in HFM X (SCM E, 33%). This is most likely due to enhanced microbial activity associated with the higher organic matter in HFM Y.

Input PN mass loads are successfully reduced in all SCMs. Median input and output PN mass loads are 1.8 kg/ha-yr (1.6 lb/ac-yr) (SCMs B and C) and 0.55 kg/ha-yr (0.49 lb/ac-yr) (SCM D), respectively. Percent reductions in PN range from 41% (SCM C) to 88% (SCM G). Sampling constraints limit the observed performance in SCM C. In all other SCMs, PN reductions are greater than 50%, indicating strong removal. Removal of PN is achieved via filtration and sedimentation.

Release/export of NO_3^- via mineralization and nitrification is the main reason for poor removal of dissolved N. In many SCMs, a similar pattern is noted among dissolved N mass reductions that incorporates substantial mass reductions in DON, NH_4^+, and NO_2^-, but release of NO_3^-. Large inputs of DON and NH_4^+ were noted in the spring months towards the end of sampling, which could account for these reductions. It is possible that these species were still undergoing transformations at the end of sampling and were released from the SCMs following the sampling period. Export of NO_3^- mass was noted in SCMs B, E, F, and G, reaching as high as 420% (SCM B). In SCMs A and C, NO_3^- mass load reductions are insignificant (2% and 0%, respectively). SCM D provides a NO_3^- mass reduction of 66%, indicating that mineralization and nitrification may not be the only transformations SCM D. It is possible that denitrification is occurring in SCM D.

Export of NH_4^+ is noted in SCMs C and G, most likely caused by sampling constraints.

All in all, SCMs A and D are significantly reducing TN levels, while all other SCMs are providing minimal- to moderate-TN reductions. This implies that SCM configuration plays a significant role in N removals. Filtration and sedimentation are successful in removing PN from input runoff, but internal transformations of TDN species and accumulated PN, especially through mineralization and nitrification, lead to eventual release of NO_3^-. Brown et al. (2013) predict that the dynamics of effluent nitrogen loads from sand filters will mimic, although dampened, those of influent loads. This is the case with many of the SCMs, as reductions in TN mass loads were also associated with eventual re-release of TDN species.

Table 3-10. Load reductions of Nitrogen Species for all SCMs. Influent and effluent mass loads incorporate the TN first flush factor (2.6) to normalize FFCs to EMCs.

SCM		A	B	C	D	E	F	G
TN	**L_{in} in kg/ha-yr (lb/ac-yr)**	7.3 (6.5)	9.0 (8.1)	7.1 (6.4)	10.0 (8.9)	5.7 (5.1)	10.1 (9.0)	7.7 (6.9)
	L_{out} in kg/ha-yr (lb/ac-yr)	2.3 (2.1)	7.6 (6.8)	5.2 (4.6)	2.6 (2.3)	3.8 (3.4)	5.4 (4.8)	7.2 (6.4)
	L_{red} in kg/ha-yr (lb/ac-yr)	4.9 (4.4)	1.4 (1.3)	2.0 (1.8)	7.4 (6.6)	1.9 (1.7)	4.6 (4.1)	0.57 (0.50)
	L_{red} in kg/yr (lb/yr)	1.2 (1.1)	0.21 (0.19)	0.37 (0.33)	1.8 (1.6)	0.52 (0.46)	1.4 (1.3)	0.95 (0.84)
	% Reduction	**68%**	**16%**	**28%**	**74%**	**33%**	**46%**	**7%**
PN	**L_{in} in kg/ha-yr (lb/ac-yr)**	1.6 (1.5)	1.8 (1.6)	1.8 (1.6)	2.7 (2.4)	1.1 (1.0)	3.0 (2.7)	3.3 (3.0)
	L_{out} in kg/ha-yr (lb/ac-yr)	0.44 (0.40)	0.86 (0.76)	1.1 (0.95)	0.55 (0.49)	0.38 (0.34)	1.0 (0.89)	0.41 (0.36)
	L_{red} in kg/ha-yr (lb/ac-yr)	1.2 (1.1)	0.96 (0.86)	0.75 (0.67)	2.2 (2.0)	0.70 (0.62)	2.0 (1.8)	2.9 (2.6)
	L_{red} in kg/yr (lb/yr)	0.30 (0.27)	0.14 (0.12)	0.14 (0.12)	0.52 (0.47)	0.19 (0.17)	0.62 (0.55)	4.9 (4.4)
	% Reduction	**73%**	**53%**	**41%**	**80%**	**65%**	**67%**	**88%**

Table 3-10 (continued). Load reductions of N Species for all SCMs. Influent and effluent loads incorporate the TN first flush factor (2.6) to normalize FFCs to EMCs.

SCM		A	B	C	D	E	F	G
DON	L_{in} in kg/ha-yr (lb/ac-yr)	4.0 (3.5)	5.4 (4.8)	3.6 (3.2)	4.5 (4.0)	2.6 (2.3)	5.3 (4.7)	2.7 (2.4)
	L_{out} in kg/ha-yr (lb/ac-yr)	0.90 (0.80)	1.9 (1.7)	1.8 (1.6)	0.92 (0.82)	1.5 (1.3)	1.4 (1.2)	2.2 (1.9)
	L_{red} in kg/ha-yr (lb/ac-yr)	3.1 (2.7)	3.5 (3.1)	1.7 (1.5)	3.6 (3.2)	1.1 (1.0)	3.9 (3.5)	0.57 (0.51)
	L_{red} in kg/yr (lb/yr)	0.77 (0.69)	0.52 (0.46)	0.32 (0.29)	0.85 (0.76)	0.31 (0.28)	1.2 (1.1)	0.95 (0.85)
	% Reduction	**77%**	**65%**	**48%**	**80%**	**44%**	**74%**	**21%**
NH_4^+	L_{in} in kg/ha-yr (lb/ac-yr)	0.66 (0.58)	0.79 (0.71)	0.64 (0.57)	0.41 (0.37)	0.62 (0.56)	0.64 (0.57)	0.46 (0.41)
	L_{out} in kg/ha-yr (lb/ac-yr)	0.15 (0.13)	0.54 (0.48)	1.2 (1.1)	0.33 (0.3)	0.29 (0.26)	1.1 (1.0)	0.19 (0.17)
	L_{red} in kg/ha-yr (lb/ac-yr)	0.51 (0.46)	0.26 (0.23)	-0.59 (-0.53)	0.08 (0.07)	0.34 (0.3)	-0.49 (-0.44)	0.27 (0.24)
	L_{red} in kg/yr (lb/yr)	0.13 (0.11)	0.04 (0.03)	-0.11 (-0.1)	0.02 (0.02)	0.09 (0.08)	-0.15 (-0.13)	0.45 (0.4)
	% Reduction	**78%**	**32%**	**-93%**	**19%**	**54%**	**-77%**	**59%**
NO_2^-	L_{in} in kg/ha-yr (lb/ac-yr)	0.16 (0.15)	0.22 (0.2)	0.19 (0.17)	0.26 (0.23)	0.16 (0.14)	0.22 (0.2)	0.27 (0.24)
	L_{out} in kg/ha-yr (lb/ac-yr)	0.05 (0.04)	0.25 (0.22)	0.08 (0.07)	0.07 (0.06)	0.04 (0.04)	0.19 (0.17)	0.19 (0.17)
	L_{red} in kg/ha-yr (lb/ac-yr)	0.11 (0.10)	-0.02 (-0.02)	0.11 (0.1)	0.19 (0.17)	0.12 (0.1)	0.04 (0.03)	0.08 (0.07)
	L_{red} in kg/yr (lb/yr)	0.03 (0.03)	0 (0)	0.02 (0.02)	0.04 (0.04)	0.03 (0.03)	0.01 (0.01)	0.13 (0.12)
	% Reduction	**70%**	**-11%**	**57%**	**73%**	**74%**	**17%**	**30%**
NO_3^-	L_{in} in kg/ha-yr (lb/ac-yr)	0.83 (0.74)	0.78 (0.70)	0.93 (0.83)	2.1 (1.9)	1.2 (1.1)	0.87 (0.78)	0.93 (0.83)
	L_{out} in kg/ha-yr (lb/ac-yr)	0.81 (0.72)	4.1 (3.6)	0.94 (0.83)	0.72 (0.64)	1.6 (1.4)	1.8 (1.6)	4.2 (3.8)
	L_{red} in kg/ha-yr (lb/ac-yr)	0.02 (0.02)	-3.3 (-2.9)	0.01 (0)	1.4 (1.2)	-0.39 (-0.34)	-0.89 (-0.80)	-3.3 (-2.9)
	L_{red} in kg/yr (lb/yr)	0 (0)	-0.48 (-0.43)	0 (0)	0.33 (0.30)	-0.11 (-0.09)	-0.27 (-0.24)	-5.5 (-4.9)
	% Reduction	**2%**	**-420%**	**0%**	**66%**	**-31%**	**-103%**	**-354%**

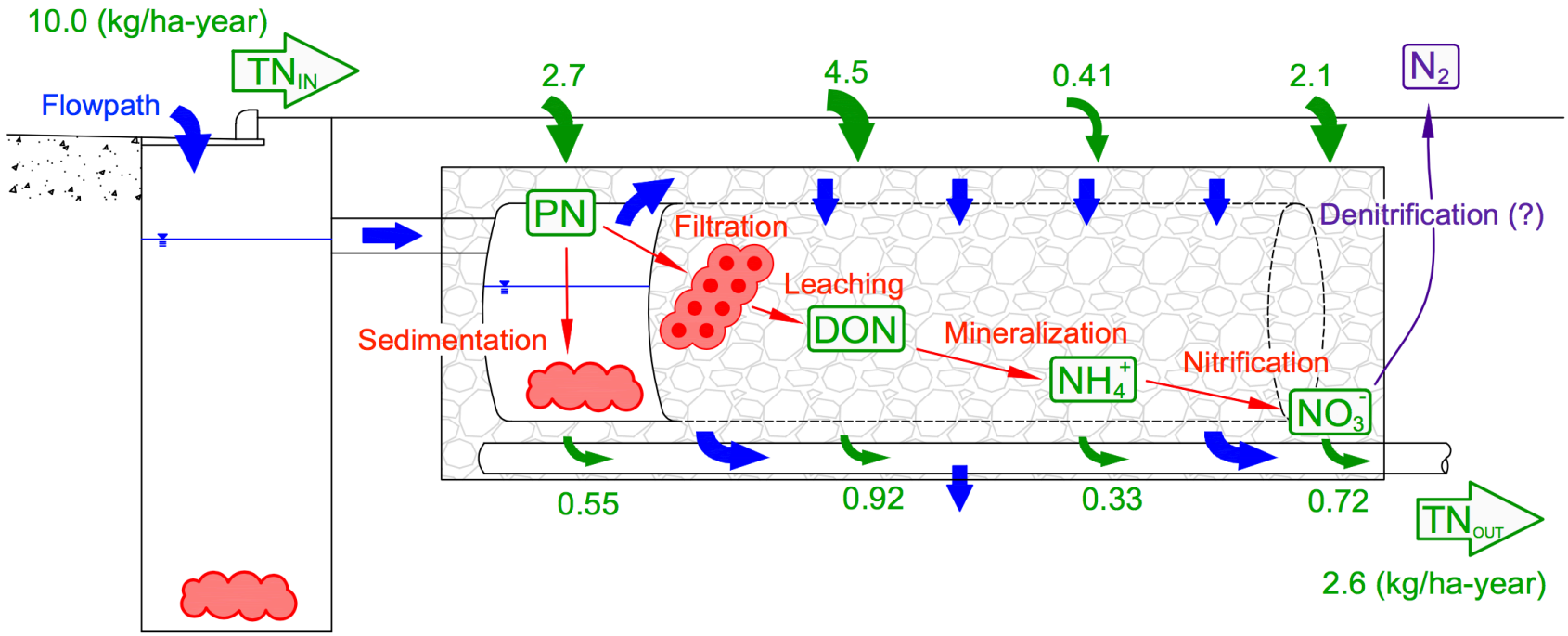

Figure 3-46. Nitrogen behavior through SCM D. SCM D features storage before filtration. Legend: red=removal mechanism; purple=possible removal mechanism, as NO_3^- was not noted in any other SCMs; blue=flowpath; green=input/output mass loads estimated with EMCs based on first flush ratios for individual species, in kg/ha-yr. Adapted from Li and Davis (2009).

3.7 Optimal SCM Design

3.7.1 HFM Selection

HFM characteristics do not play a significant role in removal of TSS and particulate-bound nitrogen and phosphorous. Based on filtration theory and water quality results, the varying grain sizes of the HFMs do not impact particulate removal at high flow rates. These results imply that any sandy HFM that has characteristics similar to HFM X and HFM Y will provide effective particulate removal in SCMs.

HFM characteristics were, however, found to impact the removal of dissolved nutrients; specifically, nitrogen. In comparing SCMs D and E, which have identical configurations, mass load reductions of total nitrogen were higher in the HFM X, primarily caused by a higher NO_3^- export in SCM E, which features HFM X. It is hypothesized that the larger fractions of organic matter in the HFM Y of SCM D were more successful at fostering microbial growth for retention/removal of nitrogen.

In terms of phosphorus removal, differences in organic content did not seem to play a significant role between HFM X and HFM Y. There was no notable difference in phosphorus sorption between the two HFM types. It is probable that sorption was taking place on influent and accumulated sediment in the SCMs, implying that the HFMs did not provide many sorption sites to incoming runoff. Barrett et al. (2013) also found no significant impact of small amounts of organic matter in sand filters on phosphorus removal.

3.7.2 Inclusion of Vegetation

Results of this study show that inclusion of vegetation does not significantly impact SCM performance of TSS and TP removal. However, larger exports of NO_3^- were noted in the vegetated SCMs. It is important to note that the two vegetated SCMs (SCMs F and G) both experienced sampling constraints, which may be the primary reasoning for these results. Barrett et al. (2013) concluded that vegetated sand filters demonstrate a substantial removal of nutrients (59-79% of TN and 77-94% of TP), while nonvegetated sand filters will more-than-often export NO_3^-. This was not the case in the HFM SCMs, as more NO_3^- was noted in vegetated SCMs.

Increased NO_3^- export in the vegetated SCMs may be due to increased microbial activity in the vegetated SCMs. Several studies (Anderson et al. 1993, Schnoor et al. 1995) have found vegetation to increase microbial activity in soils, especially nitrifying and denitrifying species. Since the SCMs are assumed to be highly-aerobic, it is possible that vegetation increased the amount of nitrifying bacteria, but had no impact on denitrifiers because environmental conditions were not optimal for survival of these species. Increased NO_3^- export may also be from the decomposition of dead plant roots, which Hatt et al. (2008) found to be a considerable factor in nutrient cycling in bioretention cells.

Figure 3-47 presents a photograph of SCM F, taken at the end of sampling on May 19, 2017. A visual evaluation shows the trees to be healthy, indicating that they are uptaking nutrients from the HFM and playing a role in nutrient cycling in the SCMs. Although water quality results do not show this, it is recommended that vegetation be

incorporated into HFM SCM design, as to improve nutrient cycling and microbial growth within the systems.

Figure 3-47. Photograph, taken on May 19, 2017, showing the trees in SCM F 11 months into operation of the system.

3.7.3 Forebay Design

Forebays are incorporated into the SCMs to provide storage and pretreatment. In order to maximize storage, the depths and diameters of forebays can be increased, as space permits. This will also increase the retention time of runoff in the forebays, improving pretreatment via sedimentation and sorption of dissolved nutrients to suspended solids in the runoff. Forebays should be designed to drain quickly following a rainfall event. This will maximize available storage for upcoming storms and limit the presence of mosquitos in the forebays.

3.7.4 Initial Flushing

Yu and Stanford (2007) recommend that sand filters be washed upon installation to stabilize the HFM and flush out any fine media particles. No initial flushing of sediment was noted in effluent samples of the SCMs. However, as larger organic fractions are incorporated into HFM mixtures, this may become more of a concern, as fine sediment is more likely to be flushed.

3.7.5 Clogging Concerns

Sand filters are generally considered to have greater maintenance requirements than many other types of stormwater treatment facilities, primarily due to accumulation of sediment in the filters (Barrett 2010). As solids accumulate in a filter bed, pore size decreases, in turn decreasing hydraulic conductivity. Urbonas (1999) states that initial flow-through rates in sand filtration systems are generally very high, but, as the fine sediment accumulates on the surface, flow-through rates diminish. Typically, sand filters have been found to begin experiencing clogging problems within three to five years of operation (NVPDC 1992). However, due to the large ratios of contributing drainage areas to facility surface areas, as presented in Section 3.2.3, HFM SCMs are expected to experience clogging before three years.

During the first year of operation of the SCMs, clogging was only assumed to be occurring in SCM A. After eight months of operation, in March 2017, runoff began pooling in the roadway at the curb inlet of SCM A during rainfall-runoff events. Figure 3-48 shows this phenomenon, with the forebay completely filled with water following the rainfall-runoff event on March 31, 2017. Based on field observations, no other SCMs

experienced this occurrence. In all other SCMs, and up until March 2017 in SCM A, water depths in the forebay never exceeded the connector pipe.

SCM A features filtration before storage. Thus, the pooling of runoff in the roadway at the entrance to SCM A may be due to clogging of the HFM matrix. Since runoff travels directly from the forebay into the HFM matrix, it is suspected that the HFM matrix was overwhelmed with sediment, leading to earlier-than-expected clogging. In all other SCMs, runoff enters storage pipes prior to infiltrating the HFM. This allows for settling of particles, in turn reducing loads on the HFM matrices. Thus, it is assumed that HFM SCMs with storage prior to filtration experience less clogging. The forebays are able to provide sedimentation, but in designing for optimal runoff mitigation, it is recommended to incorporate additional subsurface storage prior to filtration in the SCMs.

Figure 3-48. A photograph, taken on March 31, 2017, showing pooling of runoff in the roadway at the forebay of SCM A.

3.7.6 Optimal SCM Configuration

Table 3-11 presents a summary of TSS, TP, and TN mass load reductions in all SCMs. SCM configuration was not found to substantially impact removal of TSS or phosphorus species in stormwater runoff. With the exception of SCMs in which sampling constraints limited data reliability (SCMs C, F, and G), all SCMs provide >89% TSS mass load reductions and >69% TP mass load reductions. Primary mechanisms of TSS and TP removal are sedimentation, filtration, and sorption on suspended solids; thus, any configuration that incorporates storage pipes and HFM matrices are expected to perform similarly in TSS and TP removal. Storage pipes should come before HFM matrices, as to reduce loads on the HFM matrices and extend the lifetime of the SCMs.

Nitrogen mass load reductions were less consistent among the SCMs. SCM D provides the best TN mass reduction (74%). However, SCM E only reduced influent TN mass loads by 33%, despite its identical configuration to SCM D. This indicates that HFM selection is a more important consideration in optimal SCM design for nitrogen removal than SCM configuration. SCM A also performs well in terms of nitrogen removal (68% TN mass reduction), but, due to clogging concerns, this design is not recommended.

The configuration of SCM D, HFM around perforated pipe storage, is recommended for future SCM design. Figure 3-49 presents a schematic of this configuration. SCM D provides TSS, TP, and TN mass reductions of 89%, 69%, and 74%, respectively. By placing the storage pipes within the HFM matrix, instead of having two separate treatment chambers for storage and filtration, this configuration saves space without comprising water quality improvements. This design only accounts for 0.93% of

its contributing drainage area, making it a cost- and space-efficient alternative for decentralized stormwater management.

Table 3-11. Summary of percent mass load reductions of TSS, TP, and TN for SCM D.

SCM	A	B	C	D	E	F	G
% TSS Mass Load Reduction	98%	96%	51%	89%	95%	72%	87%
% TP Mass Load Reduction	83%	73%	35%	69%	75%	53%	72%
% TN Mass Load Reduction	68%	16%	28%	74%	33%	46%	7%

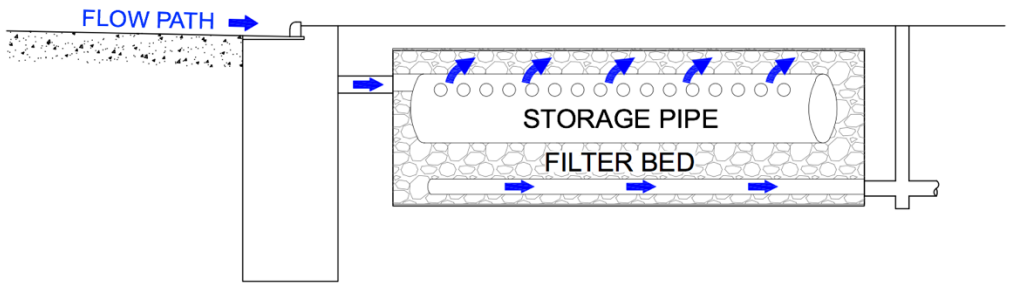

Figure 3-49. Schematic of SCM D: HFM around perforated pipe storage.

CHAPTER FOUR: CONCLUSIONS AND RECOMMENDATIONS

4.1 Conclusions

Seven full-scale SCMs with HFM were evaluated from June 2016 to May 2016, during which 24 storm events were monitored and influent and effluent first flush samples were analyzed for TSS, nitrogen, and phosphorus species.

Overall, the SCMs all provide substantial reductions in TSS mass loads, with a median reduction of 338 kg/ha-yr. (96% of influent TSS). This is achieved via sedimentation and filtration. Since a large portion of phosphorus is particulate-bound, the SCMs also perform well in TP mass load reductions. The median TP mass load reduction was 1.3 kg/ha-yr. (69% of influent TP), comprised of approximately half each of particulate P and dissolved P. Adsorption of dissolved P is noted, with higher removals for DOP than DRP, but desorption of previously-accumulated PP, DOP, and DRP limits the extent of TDP mass load reductions. It is likely that sorption is occurring on sediment and not the HFM itself. Nitrogen removal is less consistent, with a median TN mass load reduction of 2.0 kg/ha-yr. (28% of influent TN). This is most likely due to an export of NO_3^- via mineralization and nitrification of previously accumulated PN, DON, and NH_4^+.

TSS exhibited the strongest first flush, followed by TP, and then TN. Median first flush ratios of recorded FFCs to local Maryland EMCs are 3.5 (TSS); 2.6 (TN); and 2.2 (TP). First flush is significantly impacted by the initial rainfall intensity of a storm event. First flush was more apparent in influent samples than in effluent samples, indicating successful treatment of first flush stormwater runoff using HFM.

HFM SCMs are a cost-efficient approach to decentralized stormwater management in space-limited areas. HFM SCMs can account for as little as 0.86% of their contributing drainage areas and provide storage and treatment of large volumes of stormwater runoff. HFM SCMs should be designed with sedimentation before filtration, as this will reduce the sediment load on the HFM and extend SCM lifetime. HFM grain size and organic content did not significantly impact TSS or P removal, but higher organic content was associated with higher N retention.

4.2 Recommendations for future HFM SCM design

The seven monitored HFM SCMs in Camelot have proven to provide excellent removal of TSS, moderately good removal of phosphorus, and moderate removal of nitrogen. Nitrogen and phosphorus removal is achieved primarily through sedimentation and filtration of particulate species. Therefore, optimization and advancement of the removal of dissolved nitrogen and phosphorus is the primary means of improving HFM SCM design.

Sorption of dissolved phosphorus was noted in several of the SCMs, but it is highly suspected that sorption was taking place on sediment and not the HFM itself. The two studied HFMs have low organic contents, which limits the amount of sorption sites available to incoming runoff. Therefore, improving the sorption capacity of the HFM is a necessity. Media mixtures with high amorphous aluminum contents have high P sorption potential (Shang et al. 1990, Elliott et al. 2002, Lucas and Greenway 2011, O'Neill and Davis 2012, Yan et al. 2016). Sorption of dissolved phosphorus is also dependent on solid/water contact time. There is a trade-off between hydraulic conductivity and

phosphorus removal; usually higher phosphorus removal is observed with longer contact time (Ayoub et al. 2001). Thus, balancing hydraulic conductivity and contact time for phosphorus sorption will promote better removal of dissolved phosphorus in HFM SCMs.

Yan et al. (2016) suggests two promising amendments for increased phosphorus removal in HFM mixtures: water treatment residual (WTR) and alum. HFM modified with WTR and alum have demonstrated significantly higher sorption capacities compared to unmodified HFM and it is expected that these amendments to HFM mixtures can promote high infiltration of runoff without comprising phosphorus removal. Erickson et al. (2013) found steel wool to be another alternative for increasing sorption of dissolved phosphorus without impacting infiltration rates and/or retention times.

In this study, poor net nitrogen removal is attributed primarily to production of NO_3^- via mineralization and nitrification. Previously-accumulated nitrogen may contribute to leached NO_3^-. Consequently, removal of accumulated sediment in the SCMs may prevent the eventual export of nitrogen in effluent flow.

Due to their expected aerobic conditions, the SCMs were not found to remove NO_3^- via denitrification. An effective method for NO_3^- removal is to promote anoxic conditions via an internal water storage zone (IWS). A laboratory study by Peterson et al. (2015) shows that a 19-hour average retention time in anoxic conditions can result in 82% NO_3^- removal. Storage pipes can be redesigned to incorporate an IWS; particularly, by implementing an upturned elbow to the discharge pipe. This will improve denitrification by providing anoxic conditions in the volume of the treatment chamber below the upturned elbow.

Khorsha and Davis (2017) found the use of clinoptilolite zeolite to improve NH_4^+ sorption in bioretention media. However, as is the case with phosphorus, there is a trade-off between hydraulic conductivities and sorption kinetics; higher NH_4^+ is associated with lower hydraulic conductivities. Therefore, adjustments to HFM characteristics that incorporate longer contact times between runoff and the HFM will most likely improve nitrogen removal.

In addition to SCM design modifications, actions taken at the watershed level can also be implemented to improve effluent water quality from SCMs. Selbig (2016) suggests that influent TP and TN mass loads can be reduced by 84% and 74%, respectively, with an active leaf removal program. It also concludes that nearly 60% of annual phosphorus load comes from leaf litter in the fall. By implementing a street sweeping program, either in the fall or year-round, influent nutrient loads can be minimized. This will reduce accumulation of particulate species within the SCMs, which may also extend the lifetime of the SCMs.

4.3 Recommendations for Future Research

HFM SCMs are a promising technology for stormwater management in urban watersheds. They provide cost-effective, small-footprint facilities that provide good water quality improvements for TSS, P, and some N species. However, little research has been done on this technology and there are several research gaps, creating a need for further research on HFM SCMs. The follow research options are recommended to succeed this project:

1. More measurements within the SCMs should be taken in order to more fully understand the mechanisms of treatment that may be taking place. These measurements may consist of particle size distributions, pH, oxidation/reduction potential, and dissolved oxygen concentrations. It may also be useful to characterize microbial populations within the SCMs using 16S rRNA sequencing as to further understand the microbial transformations taking place in the SCMs. Particularly, it would be beneficial to target *Nitrosomonas* and *Nitrobacter*, for this will help explain the extent of nitrification occurring in the SCMs.
2. Influent and effluent samples should be taken over the entire duration of a storm, as to fully characterize first flush. Although this sampling protocol was unique in that it provided first flush samples, the use of automated samplers that collect influent and effluent samples throughout the entire duration of the storms will provide information on the exact timing of samples and the extent of first flush. This will also be much more costly.
3. Inflow and outflow measurements should be taken to improve mass load calculations. In this study, mass load calculations were estimated based on the precipitation depth, which is highly empirical. By logging flow measurements and incorporating them into mass load calculations, a more realistic representation of pollutant accumulation in the SCMs can be achieved. Despite higher costs, this will also allow for a clearer understanding of the available storage in the SCMs.
4. Anoxic conditions can also be achieved via Real Time Control (RTC). RTC systems are cloud-based platforms that predict and optimize storage/retention in stormwater infrastructure for flood control and water quality improvement

(OptiRTC n.d.). By permitting continuous responses to individual storm events and changing land uses, RTC evolves traditional SCMs from static to intelligent and adaptive. A RTC valve installed at the effluent pipe of HFM SCMs will provide the opportunity for longer durations and larger volumes of saturated anoxic conditions during dry periods. This will increase NO_3^- removal via denitrification in the SCMs.

APPENDIX A: SITE INFORMATION

A.1 Additional Site Information/Photos

A.1.1 Neighborhood Map

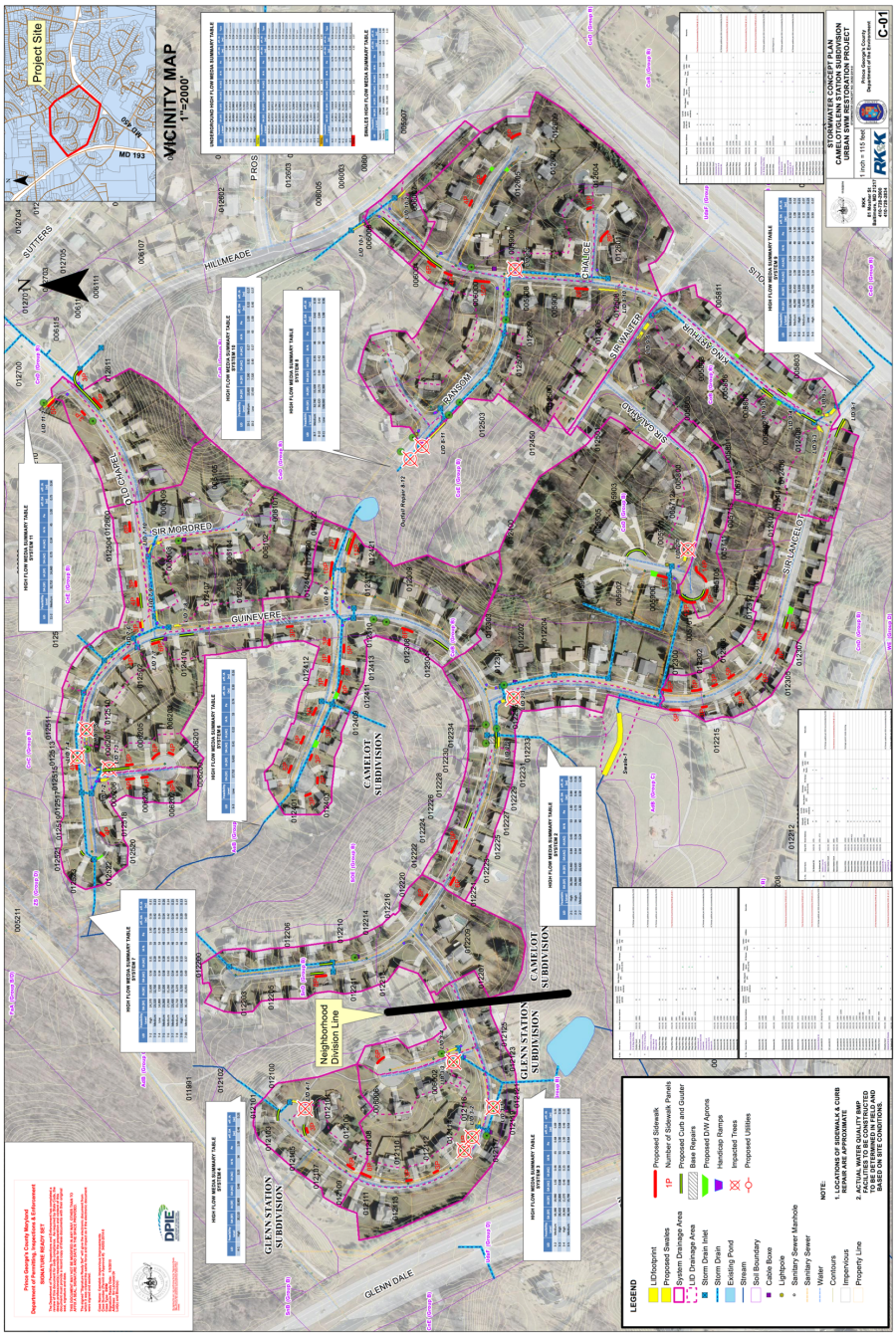

Figure A-1. Neighborhood map of Camelot subdivision.

A.1.2 SCM A

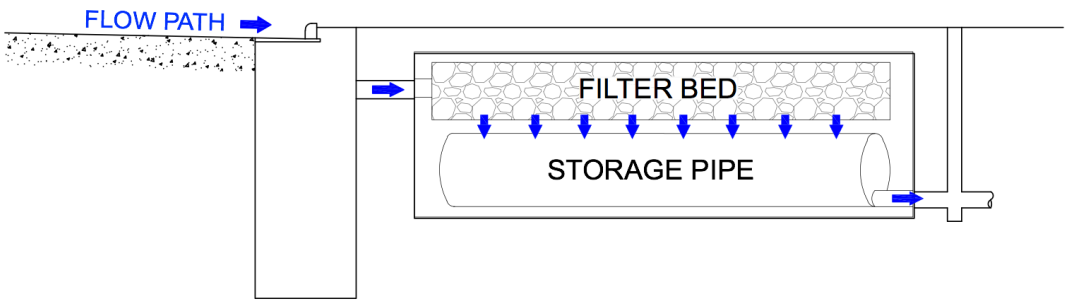

Figure A-2. Schematic of SCM A; filtering before storage.

Figure A-3. SCM A site photograph (taken March 25, 2016).

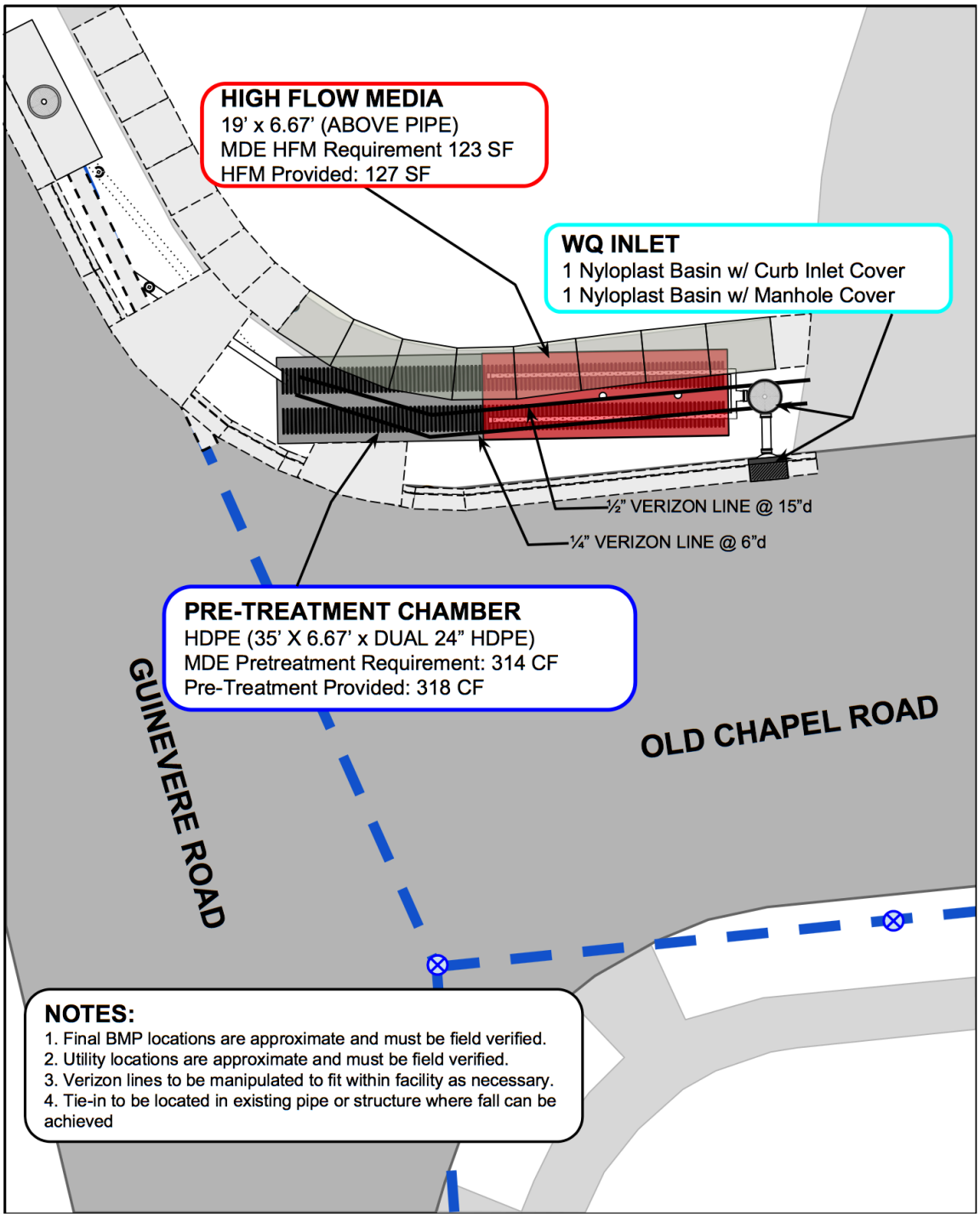

Figure A-4. Aerial plan of SCM A.

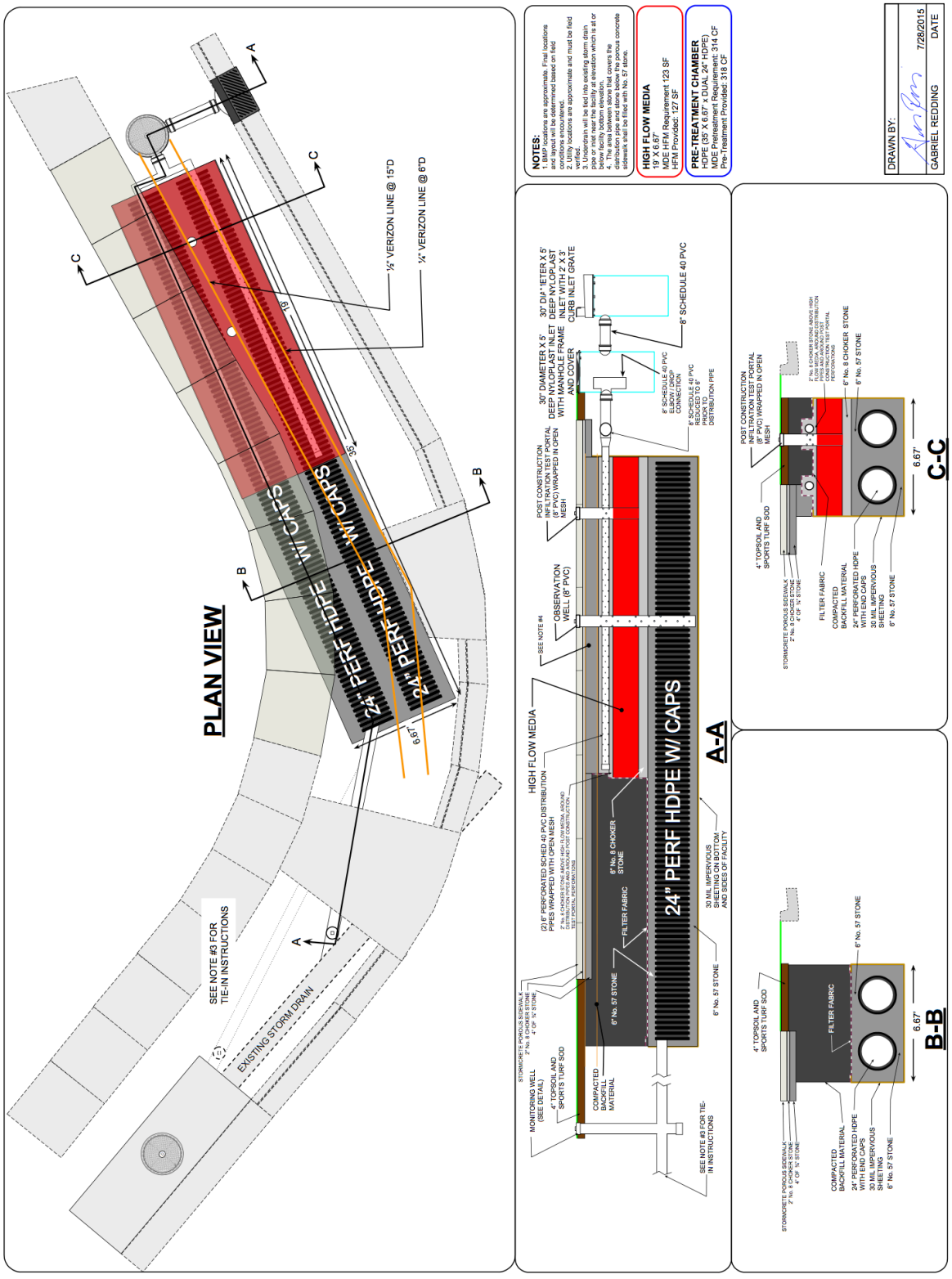

Figure A-5. Cross section plan of SCM A.

A.1.3 SCM B

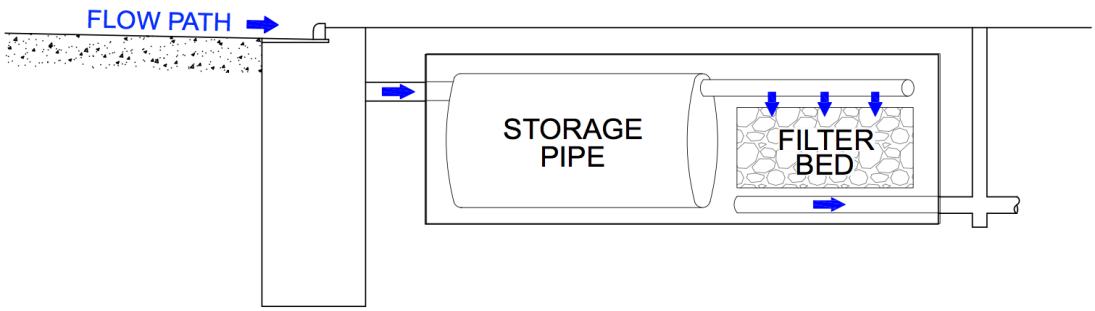

Figure A-5. Schematic of SCM B: storage before filtration.

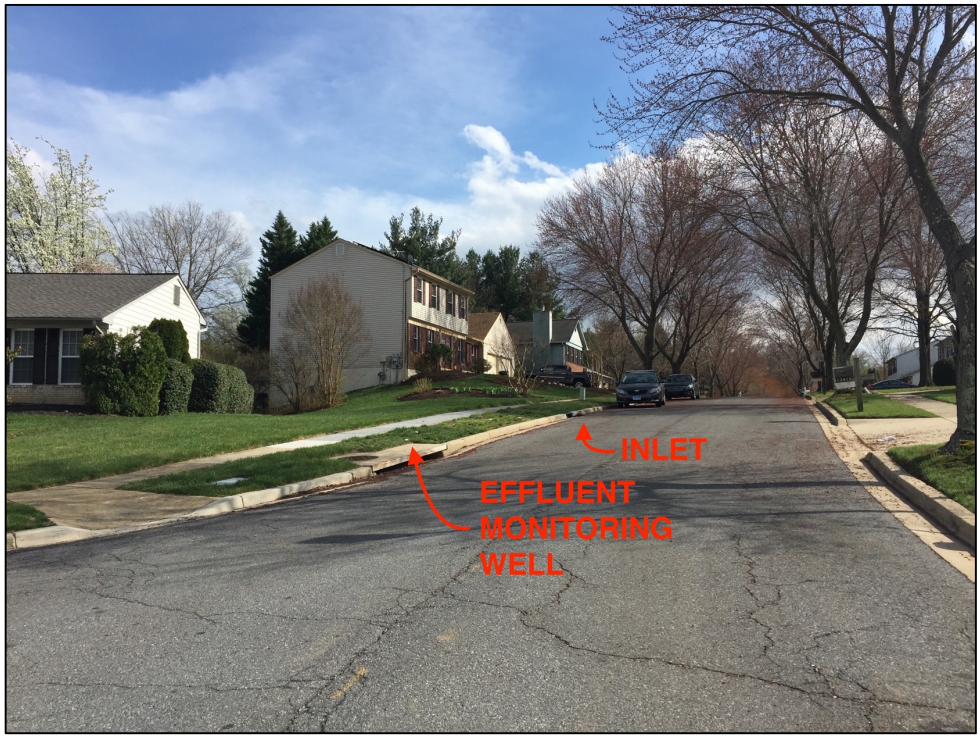

Figure A-6. SCM B site photograph (taken March 25, 2016).

Figure A-7. SCM B treatment chamber during construction (taken April 25, 2015).

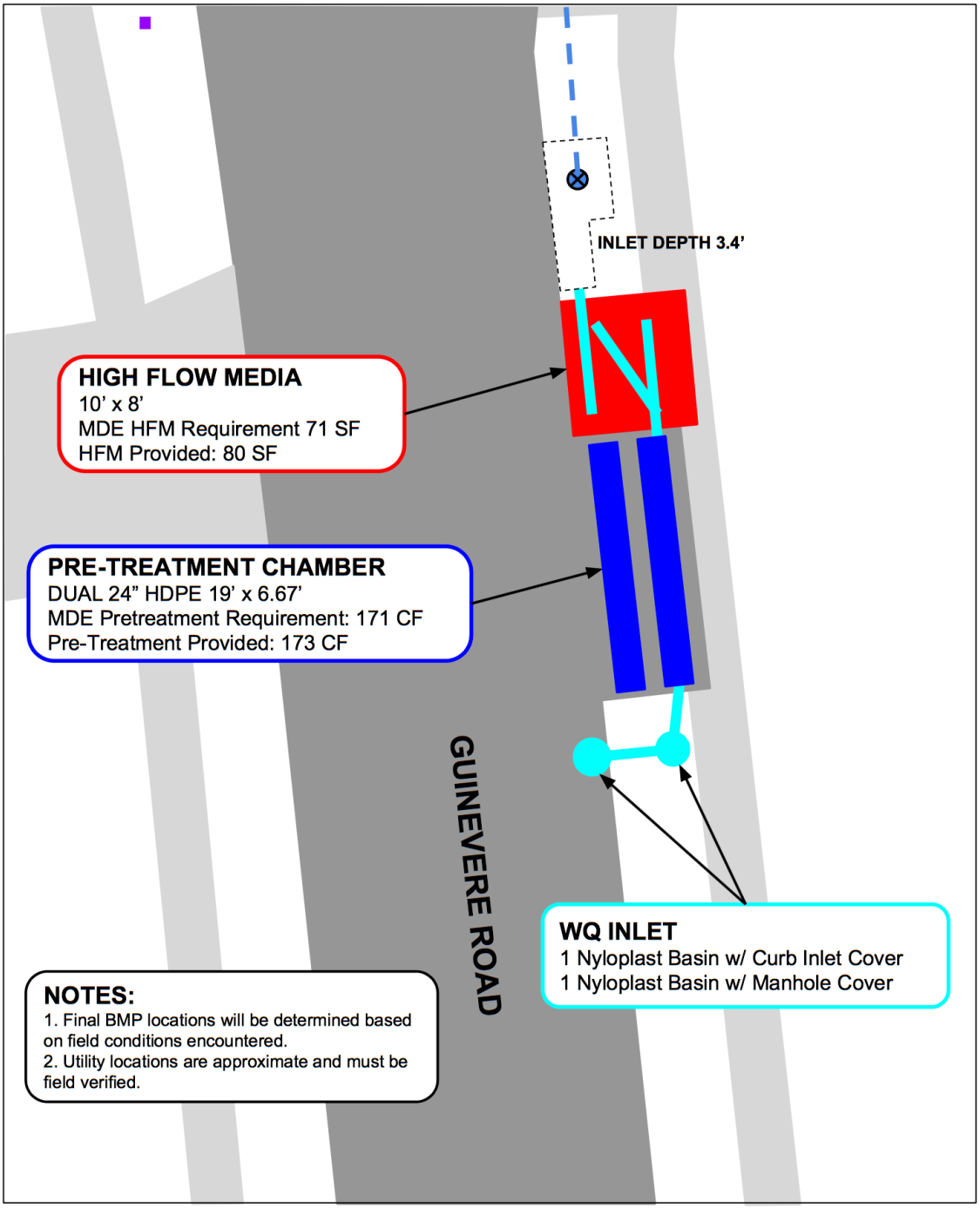

Figure A-8. Aerial plan of SCM B.

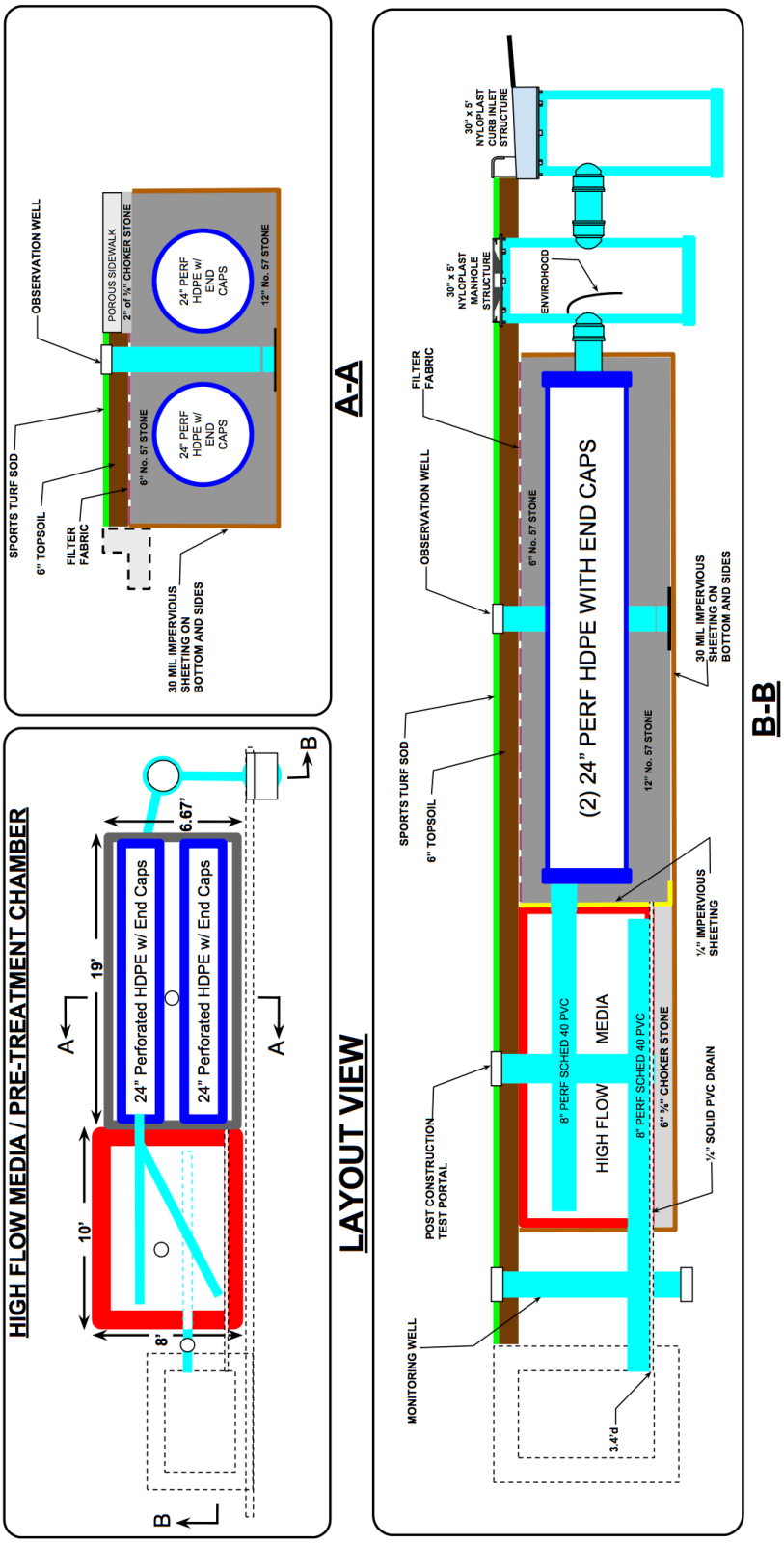

Figure A-9. Cross section plan of SCM B.

A.1.4 SCM C

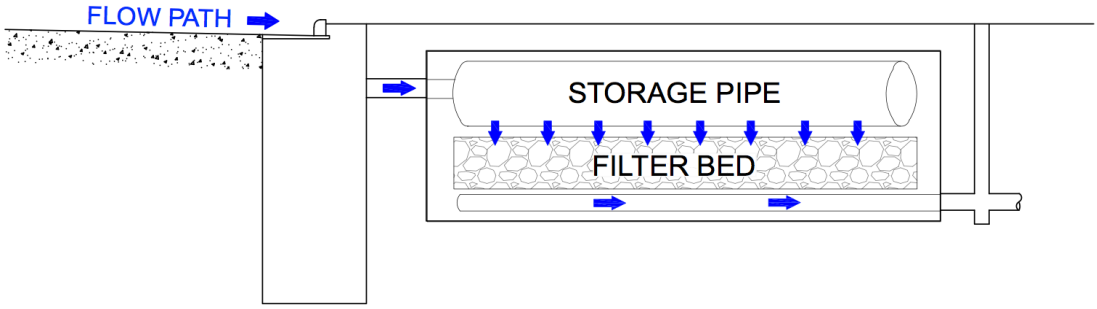

Figure A-10. Schematic of SCM C: storage above filtration.

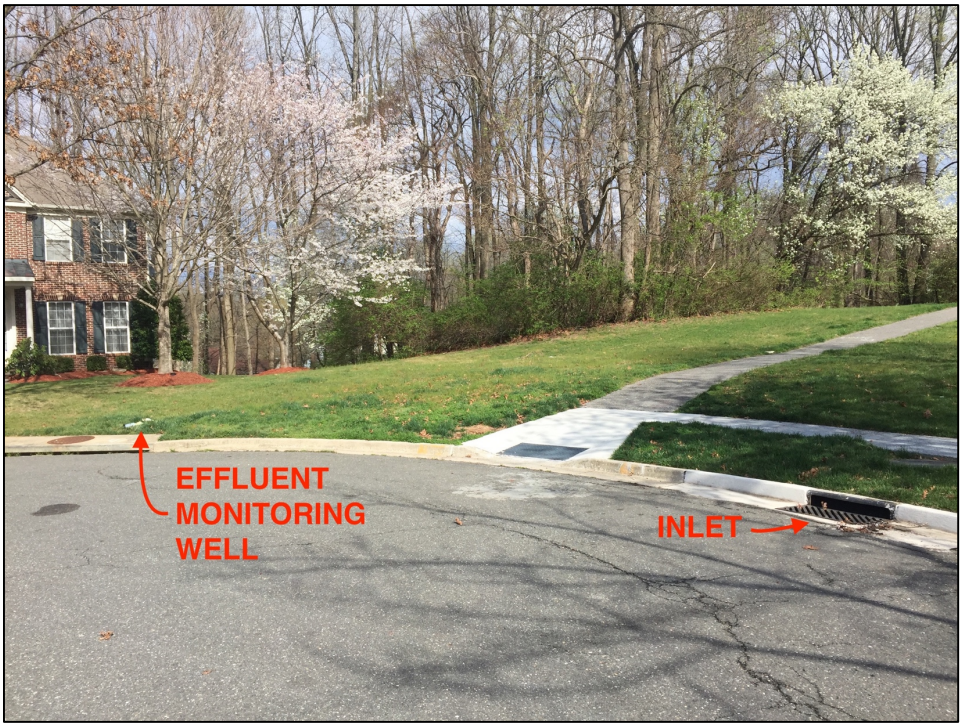

Figure A-11. SCM C site photograph (taken March 25, 2016).

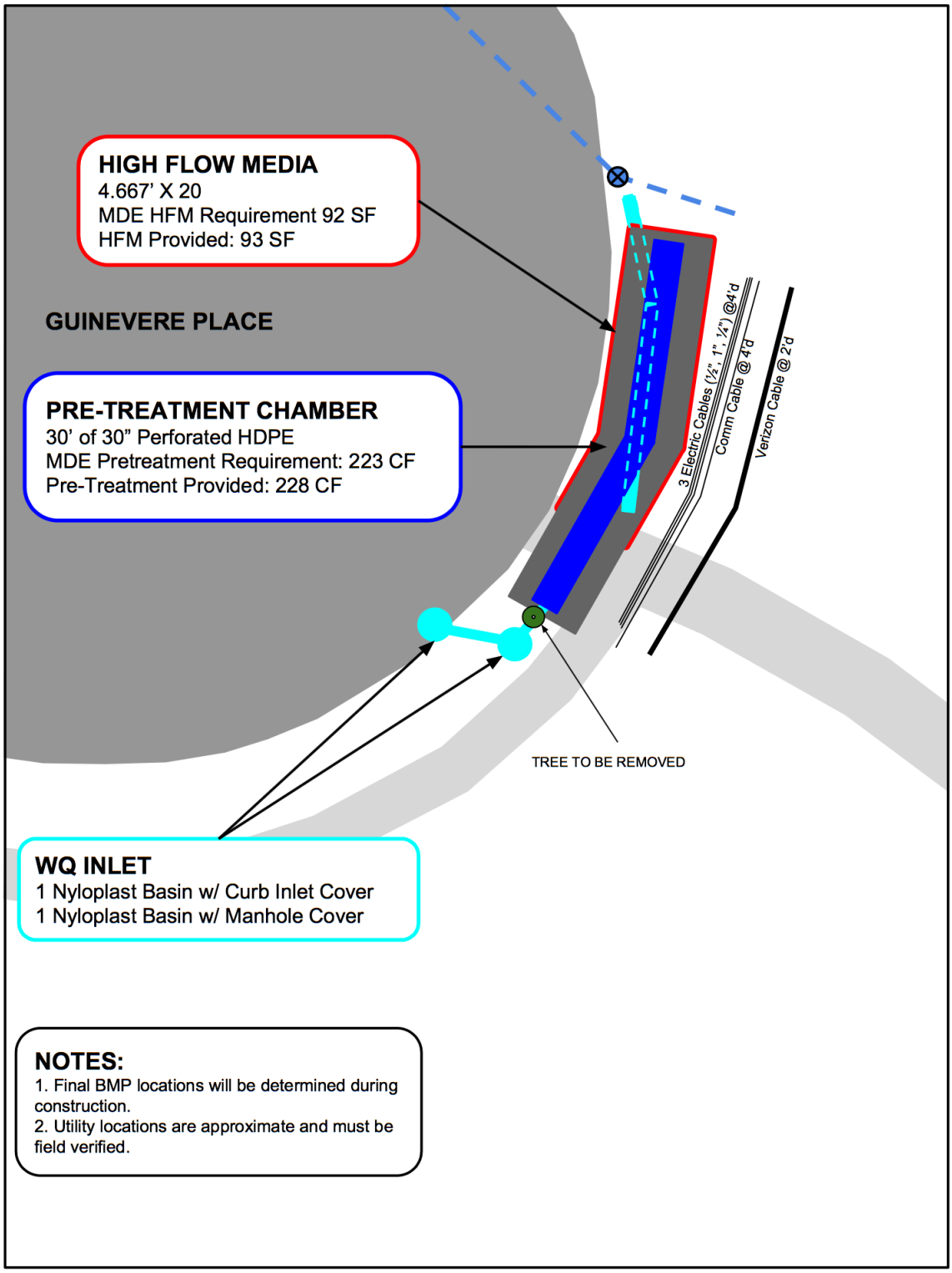

Figure A-12. Aerial plan of SCM C.

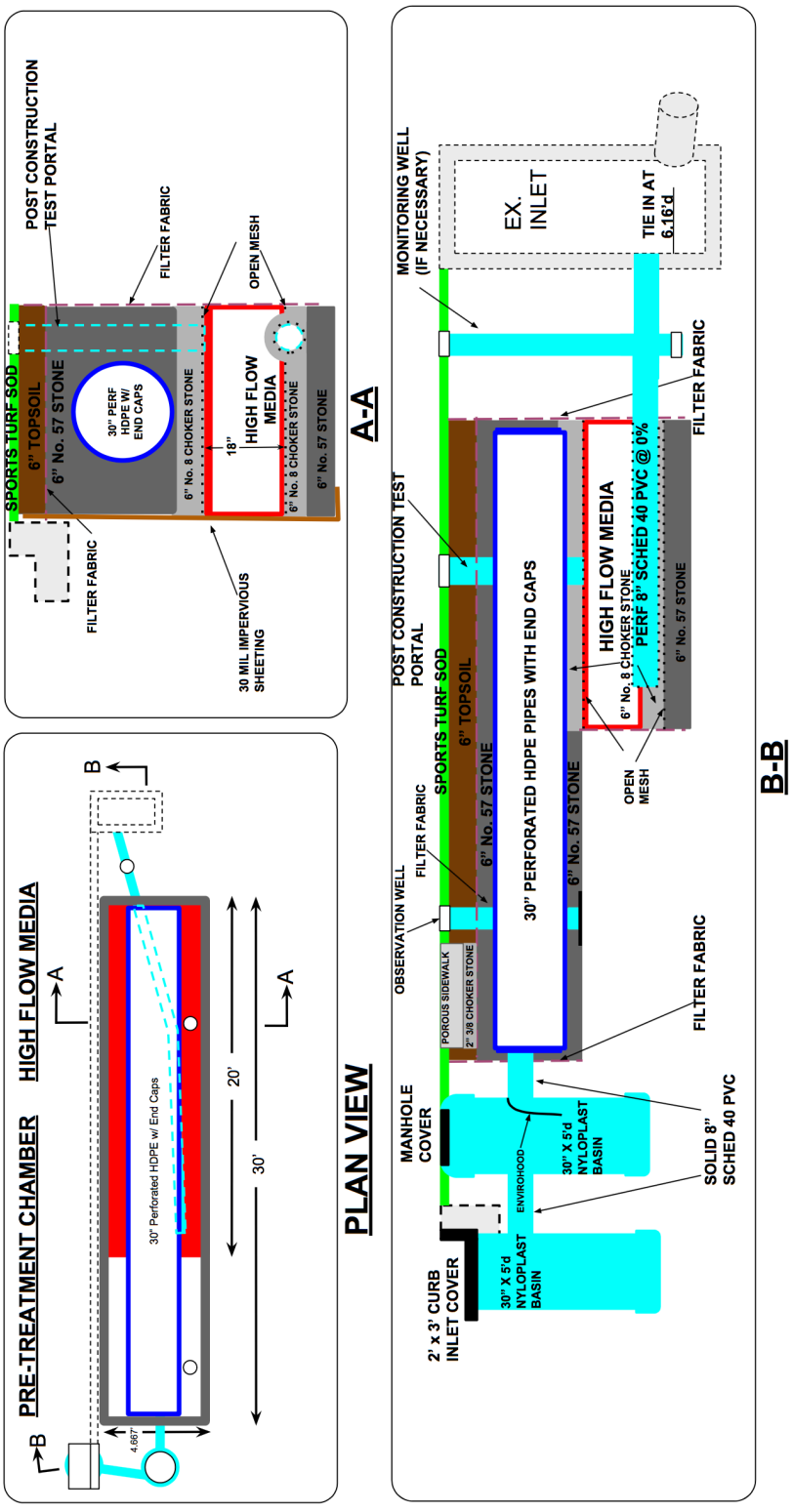

Figure A-13. Cross section plan of SCM C.

A.1.5 SCM D

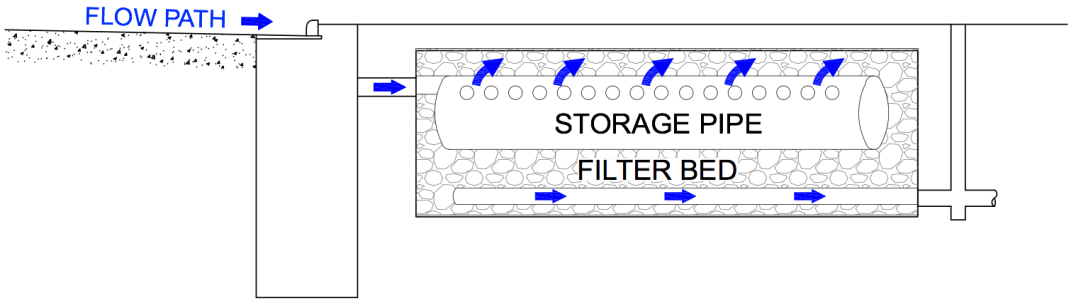

Figure A-14. Schematic of SCM D: HFM around storage.

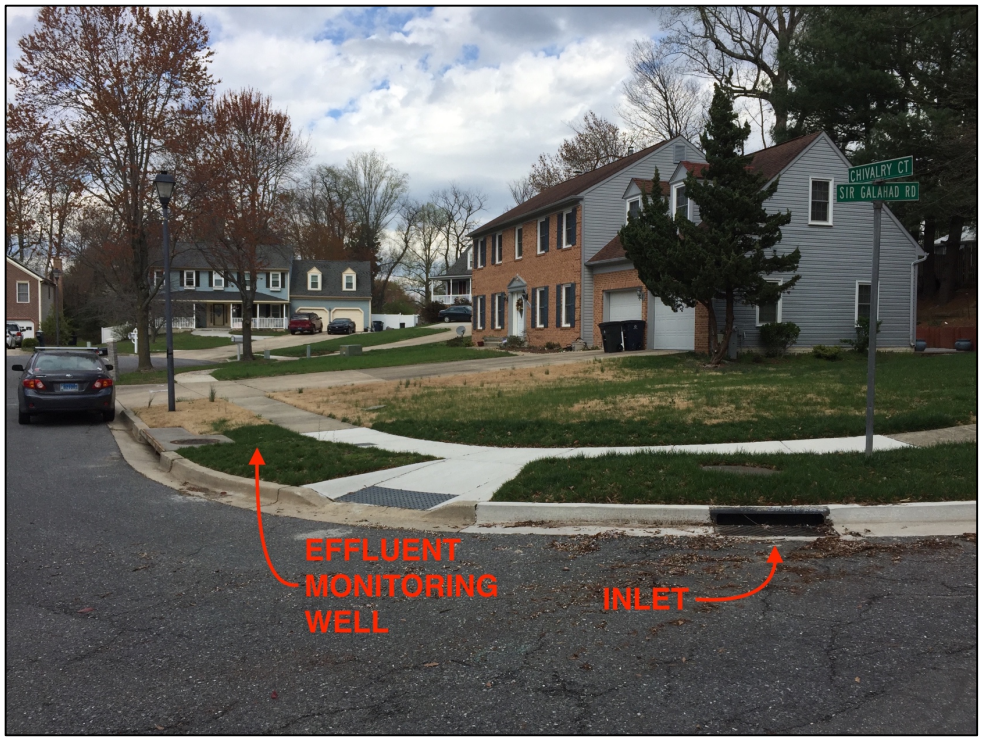

Figure A-15. SCM D site photograph (taken March 25, 2016).

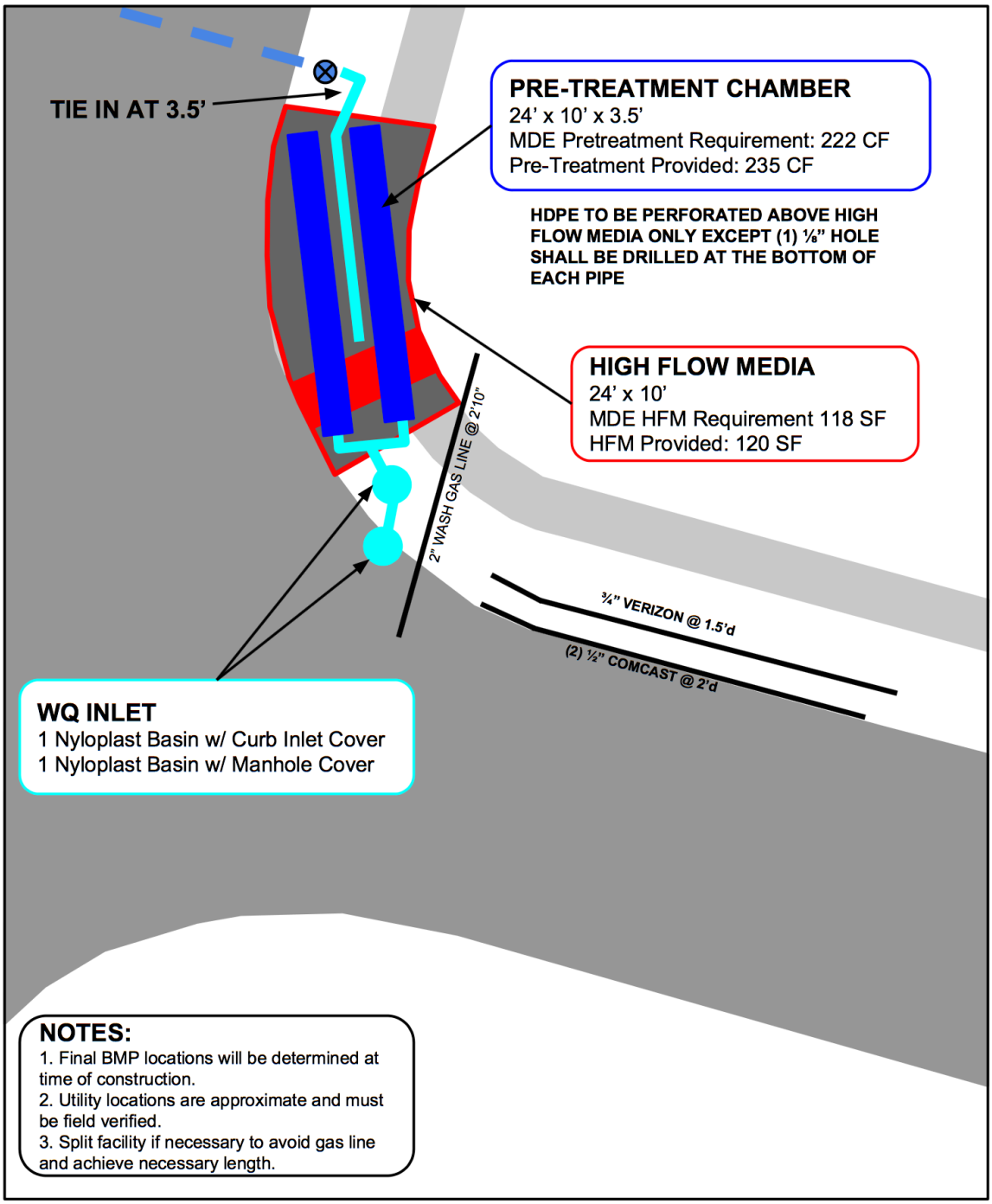

Figure A-16. Aerial plan of SCM D.

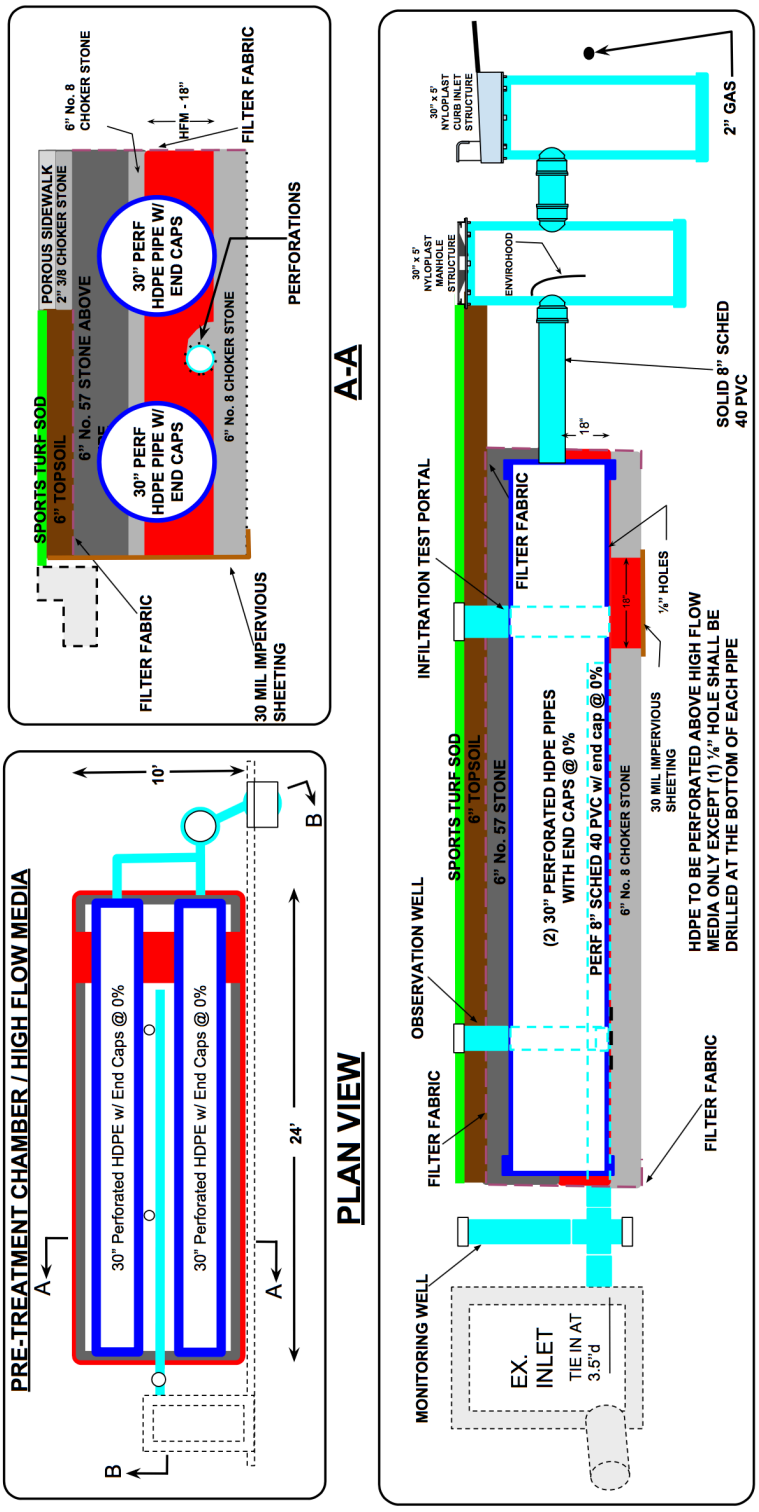

Figure A-17. Cross section plan of SCM D.

A.1.6 SCM E

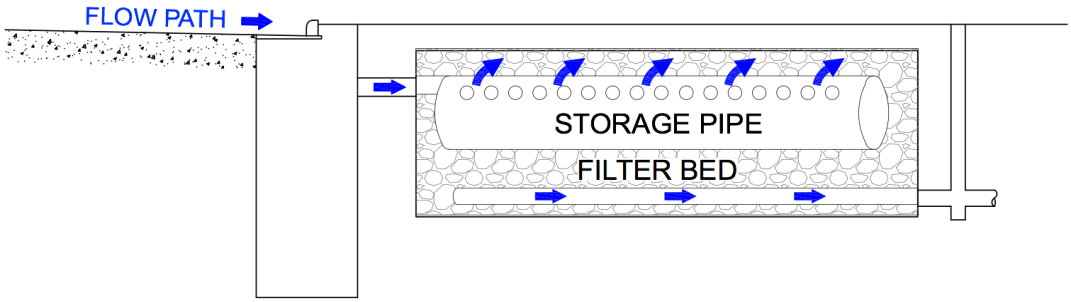

Figure A-18. Schematic of SCM E: HFM around storage.

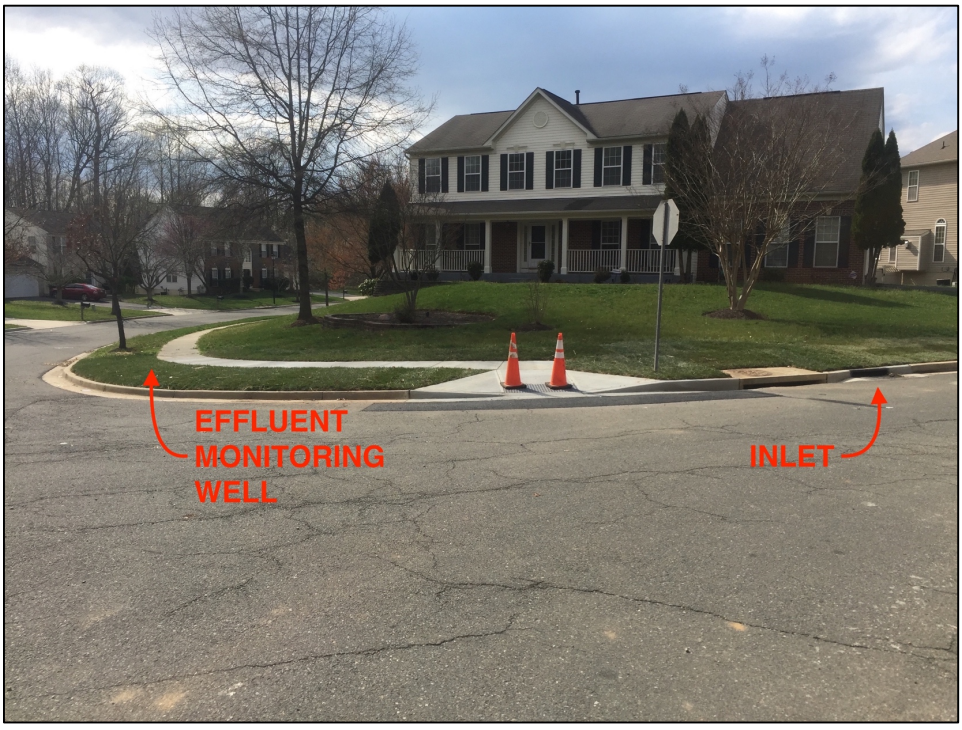

Figure A-19. SCM E site photograph (taken March 25, 2016).

Figure A-20. SCM E treatment chamber during construction (taken December 6, 2015).

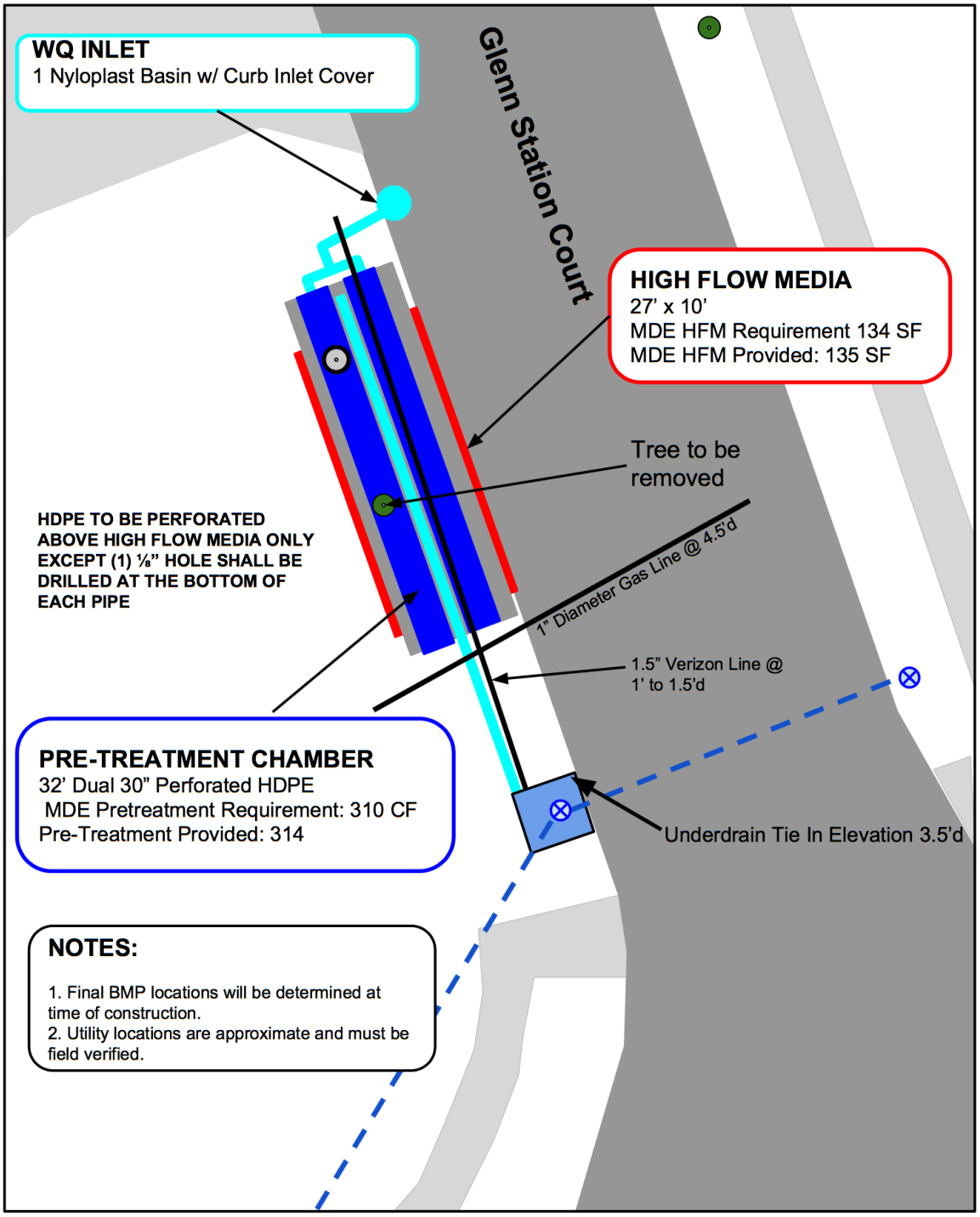

Figure A-21. Aerial plan of SCM E.

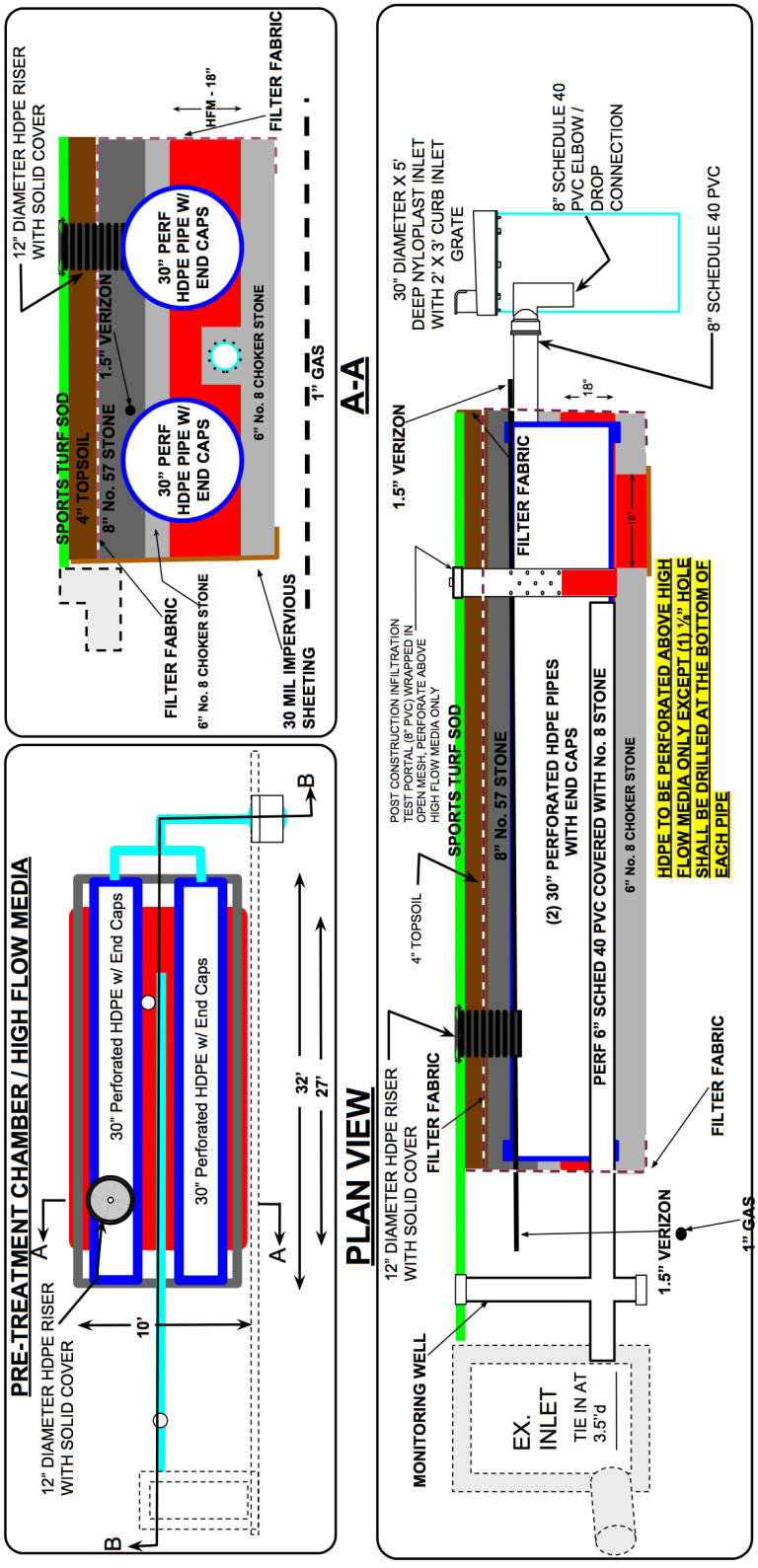

Figure A-22. Cross section plan of SCM E.

A.1.7 SCM F

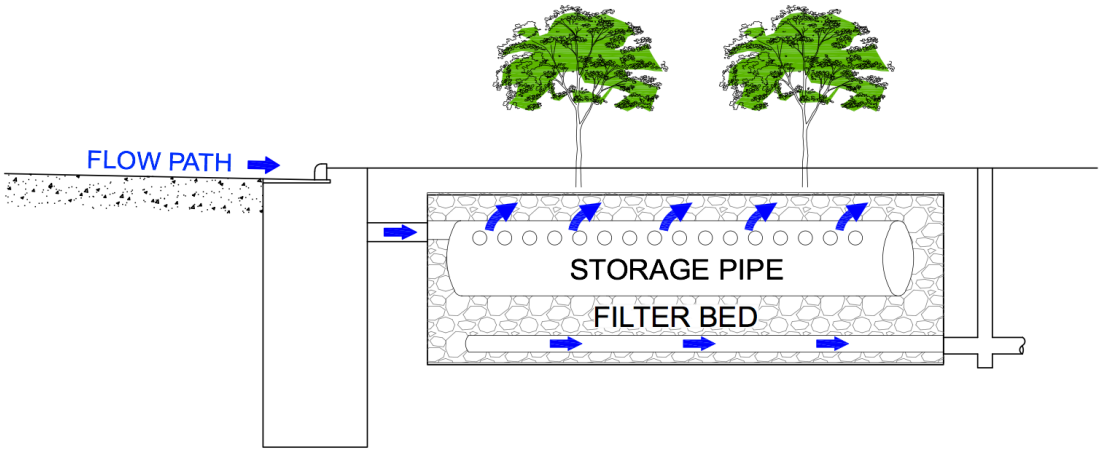

Figure A-23. Schematic of SCM F: tree box.

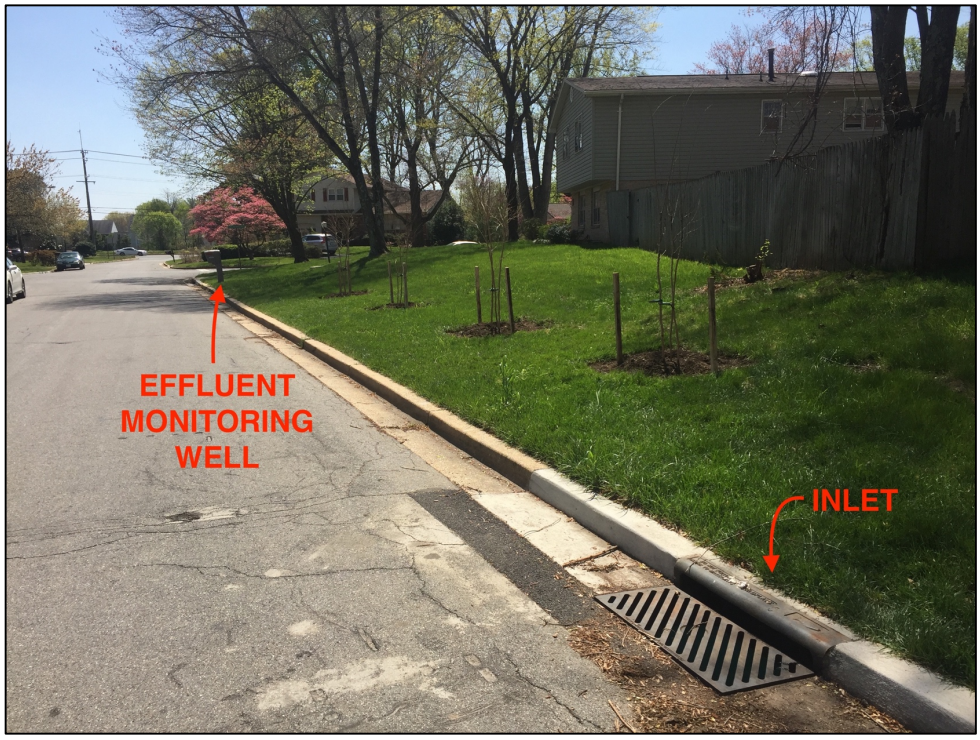

Figure A-24. SCM F site photograph (taken March 25, 2016).

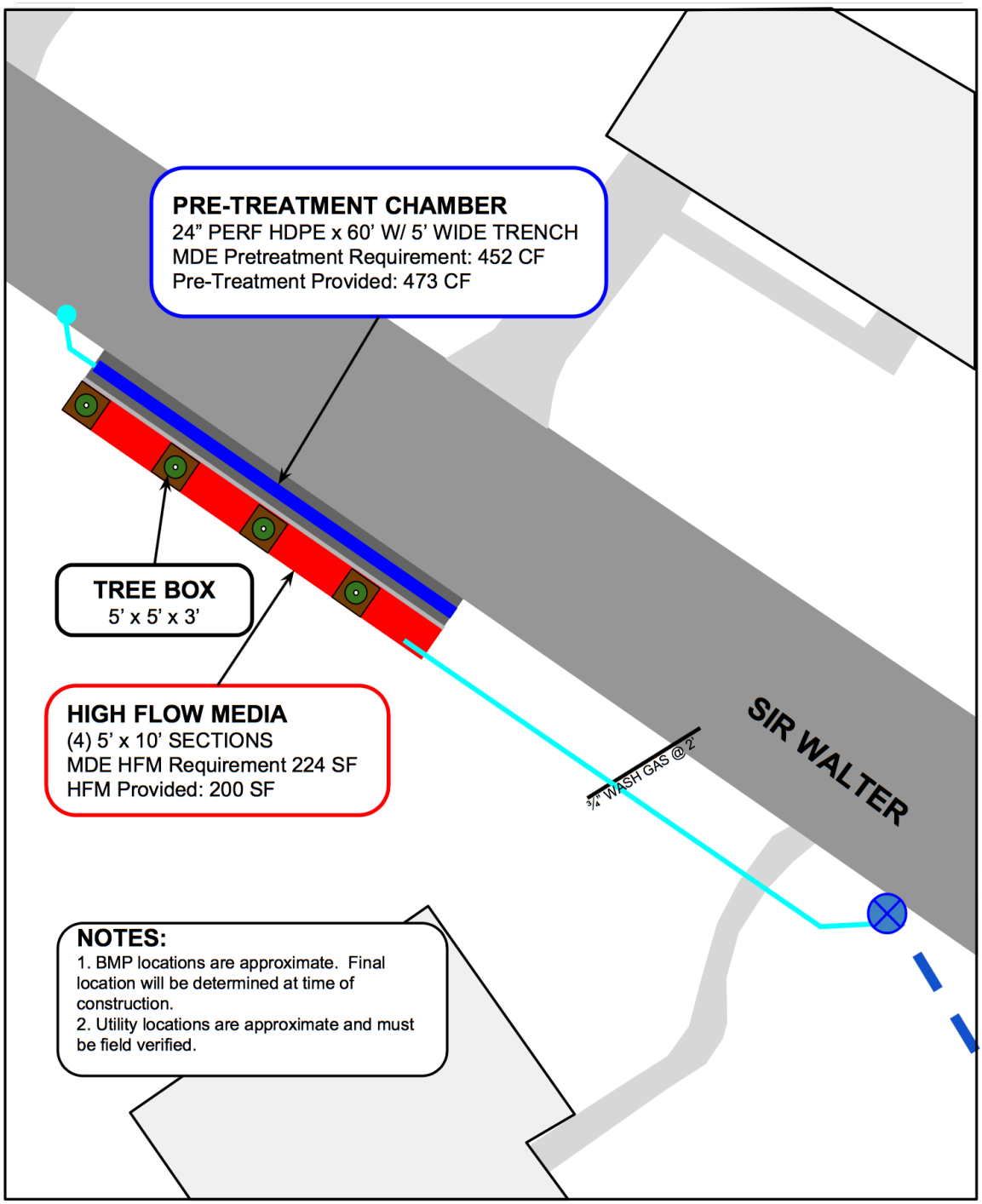

Figure A-25. Aerial plan of SCM F.

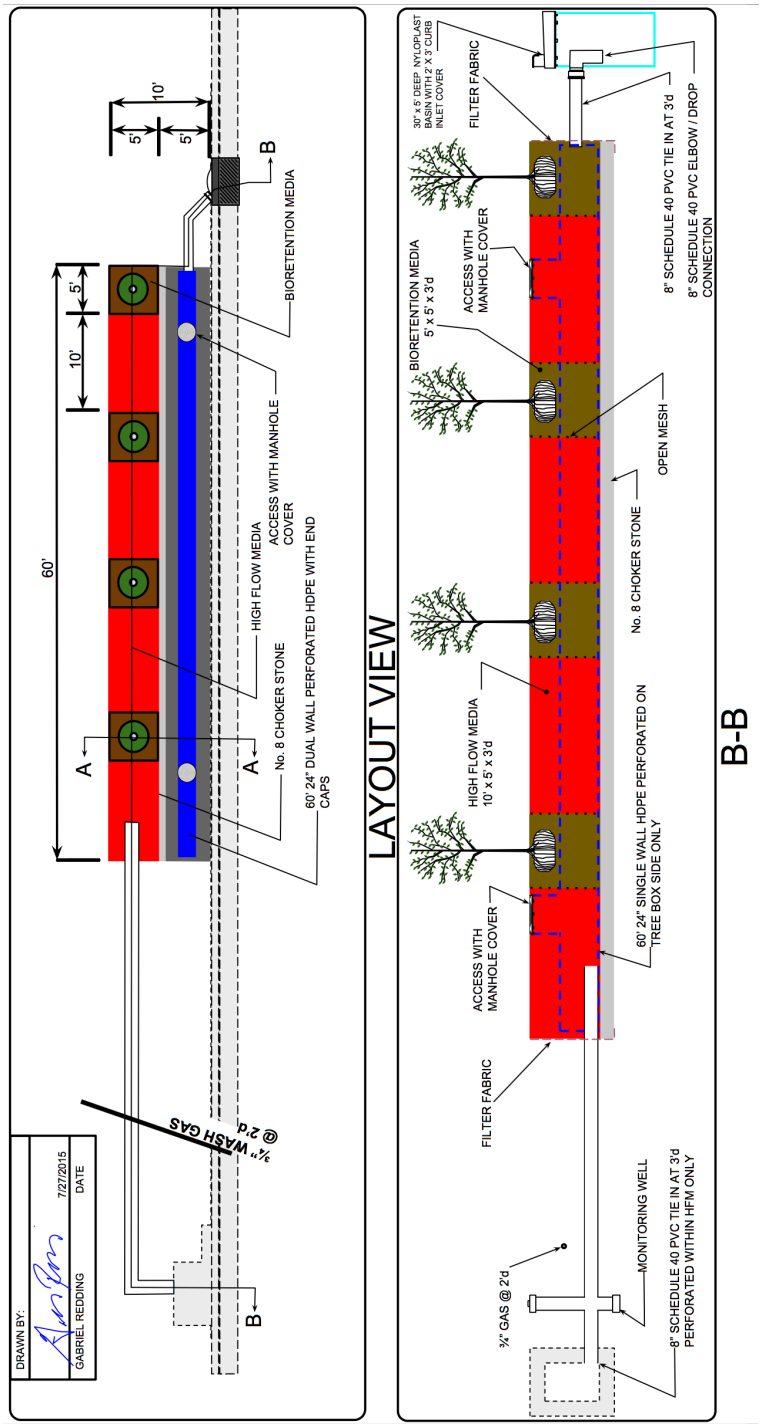

Figure A-26. Cross section plan of SCM F.

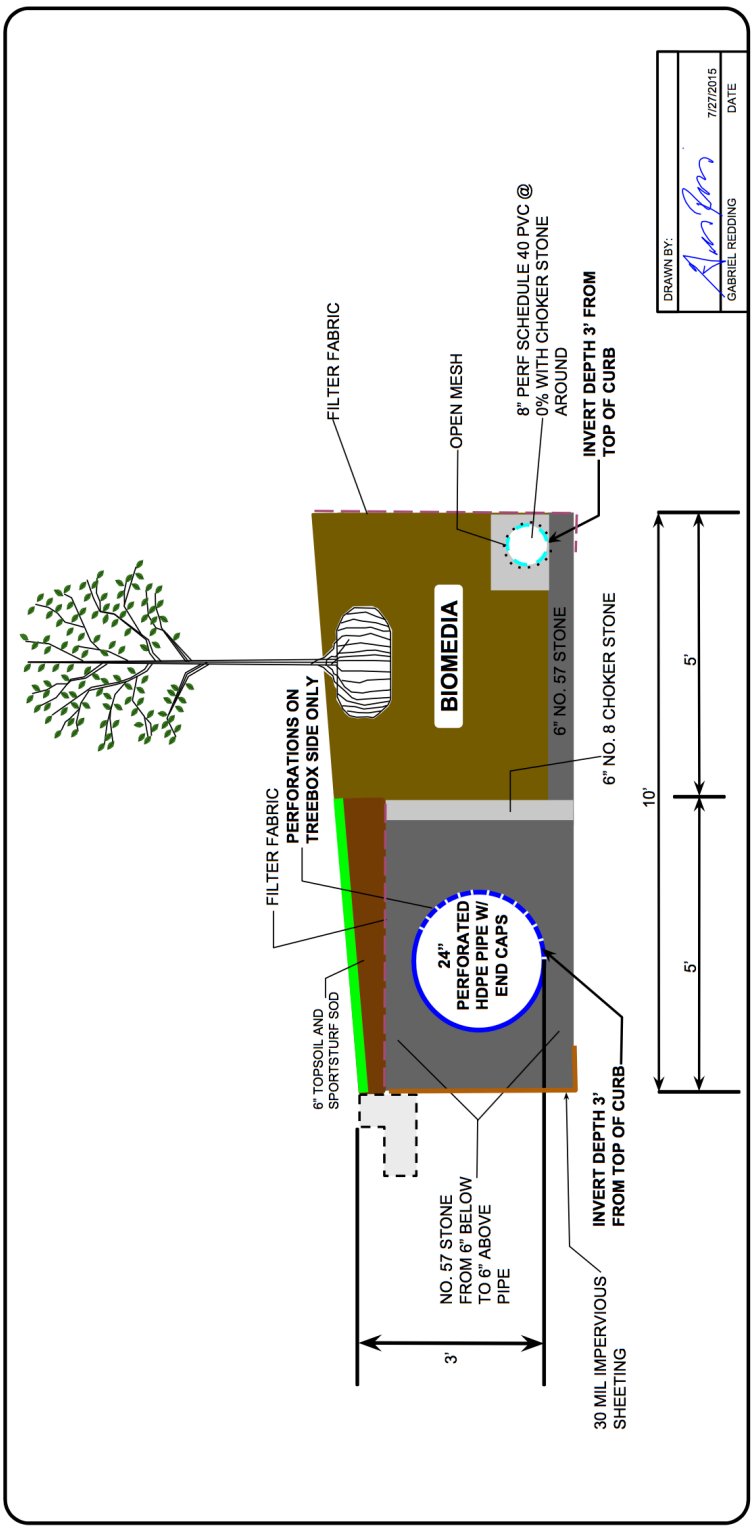

Figure A-27. Cross section plan of SCM F.

A.1.8 SCM G

Figure A-28. SCM G site photograph (taken March 25, 2016).

Figure A-29. SCM G influent/outfall (taken March 25, 2016).

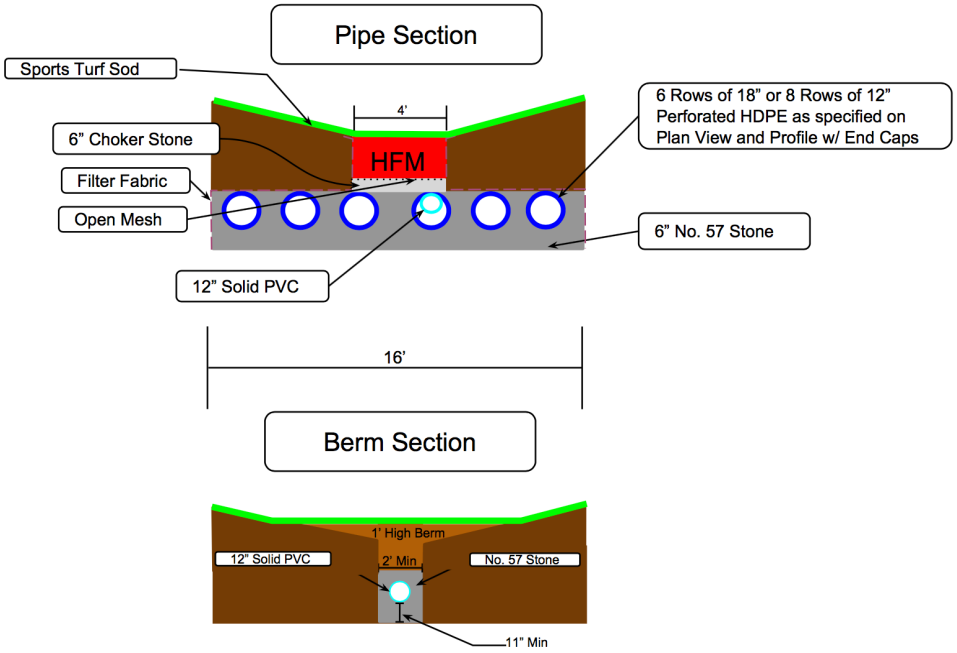

Figure A-30. Cross section (lateral) plan of SCM G.

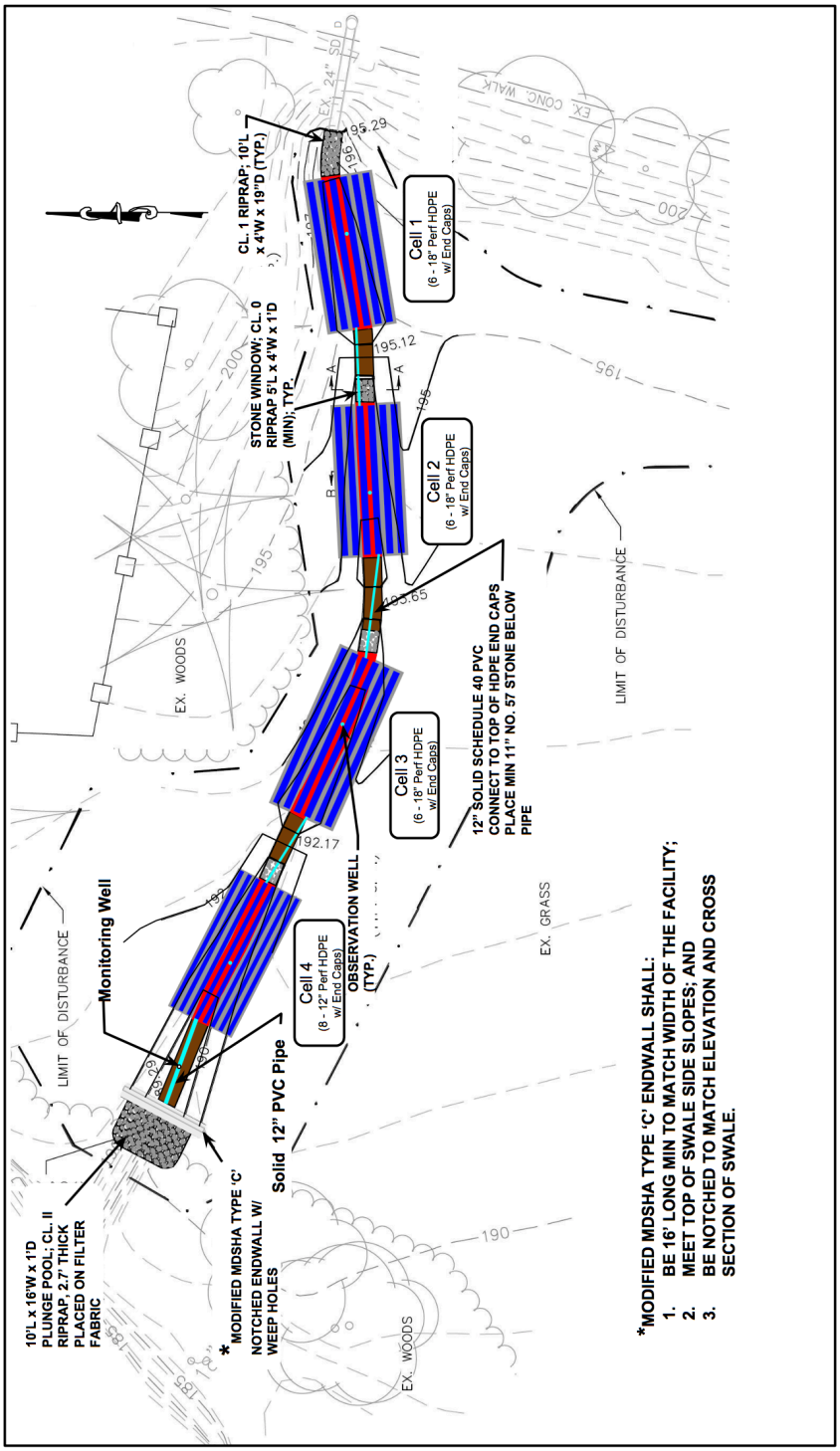

Figure A-31. Aerial plan of SCM G.

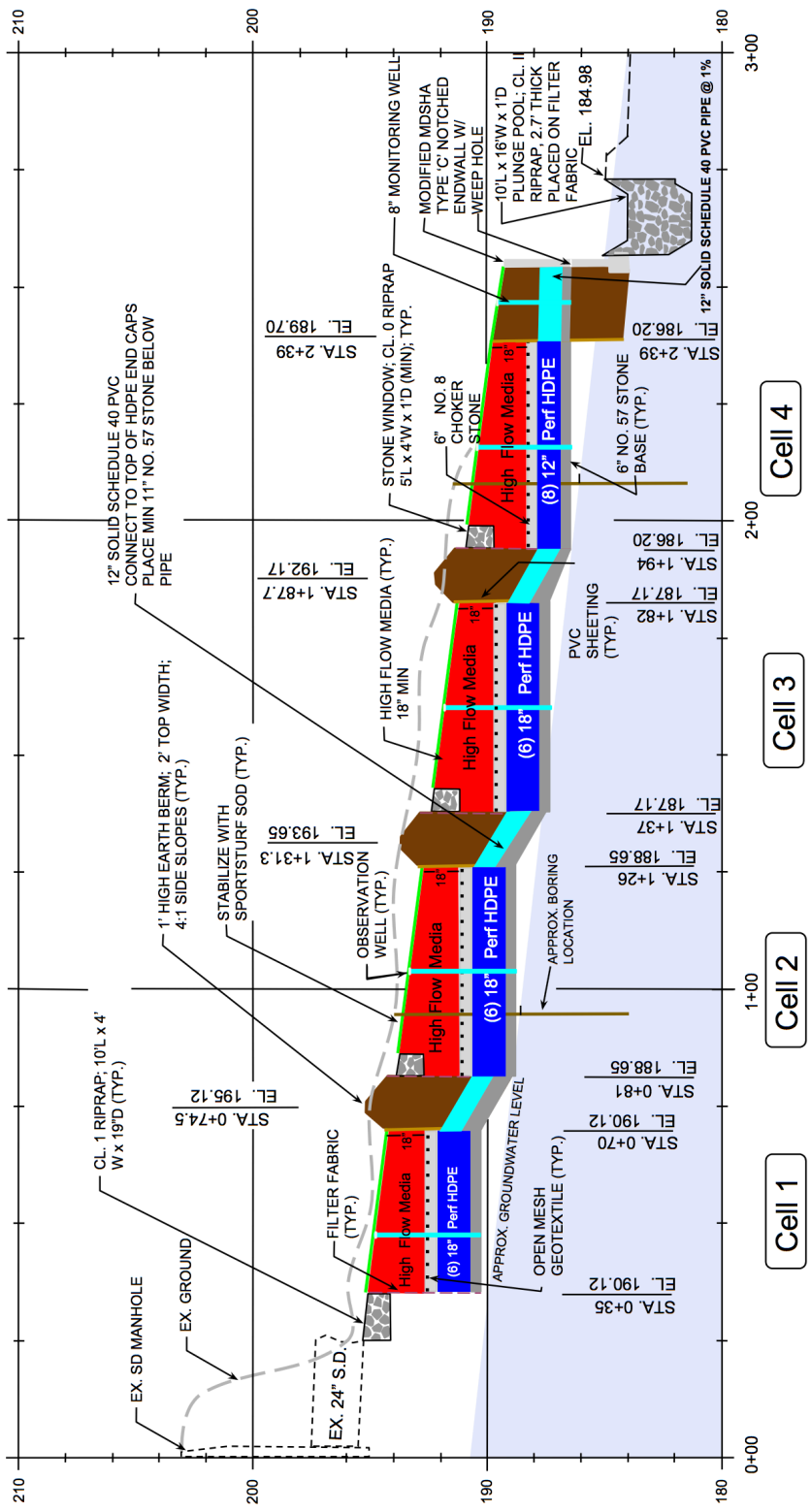

Figure A-32. Cross section plan of SCM G.

A.2 Sampling Photos

Figure A-33. Runoff entering forebay of SCM D during storm event on January 23, 2017.

Figure A-34. Effluent sampler installed in effluent monitoring well prior to storm event.

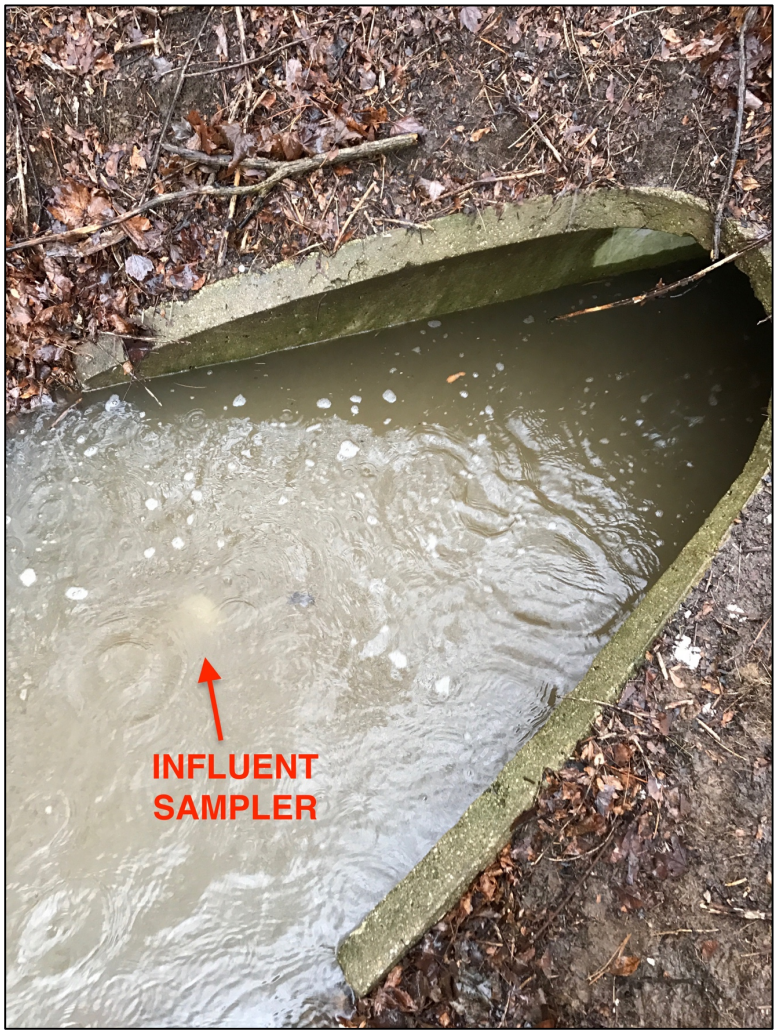

Figure A-35. Influent sampler of SCM G during dry period. **Figure A-36.** SCM G influent sampling (taken 01/23/2017).

Figure A-37. SCM G influent during storm event on May 5, 2016.

Figure A-38. Cell one of SCM G is saturated during storm event on May 5, 2016.

Figure A-39. Cells one and two of SCM G are saturated during storm event on January 23, 2017.

Figure A-40. Overflow berm connecting cells one and two in SCM G (January 23, 2017).

Figure A-41. SCM G effluent outfall (taken during storm event on January 23, 2017).

APPENDIX B: SIMULATION MODEL

B.1 Introduction

Simulation modeling is an effective means by which treatment processes in stormwater systems can be mathematically quantified and evaluated. Using simulation models, reasonable estimates can be made where measured data are not available, allowing complex processes to be characterized and predicted in a manner that is similar to the real world functioning of these physical processes. Therefore, a simulation model was developed to provide a numerical tool of replicating the movement of runoff through SCM D based on rainfall, watershed, and facility characteristics.

As described in chapter 1, first flush has several definitions. It is a function of rainfall volume, duration, and intensity; pollutant accumulation from antecedent dry days, vehicle discharges, and anthropogenic influences; and SCM facility characteristics. Understanding and quantifying first flush is necessary in predicting environmental impacts to receiving waters and in designing efficient treatment systems (Davis and McCuen 2005), but the quantification of first flush is complex, inconsistent, and highly debated. This model aims to improve the understanding of first flush and how first flush relates to optimal SCM design.

B.2 Model Formulation

This model simulates rainfall events that would be expected in the Baltimore-Washington area and monitors the movement of water from the roadway surface

through the SCM facilities. A flowchart schematic of the water quantity model is presented in Figure B-1. It is based on the configuration of SCM D. The blue terms represent a point of water balance and the red terms represent inputs/outputs to the water quantity balances, in terms of volumes. It can also be explained in terms of flowrates. First, a rainfall event is simulated to produce rainfall hyetographs and runoff hydrographs. Then, runoff enters the forebay via a curb inlet. The volume that remains in the facility (i.e., does not infiltrate out of the bottom of the forebay) enters one-of-two storage pipes within the treatment chamber. The storage pipes are perforated at the top, so, once the storage pipes are filled, runoff disperses into the HFM matrix and infiltrates downward. Filtered runoff can either enter the effluent collector pipe and discharge into the existing storm drain network or infiltrate to surrounding soils. A full list of inputs is provided in Table B-1.

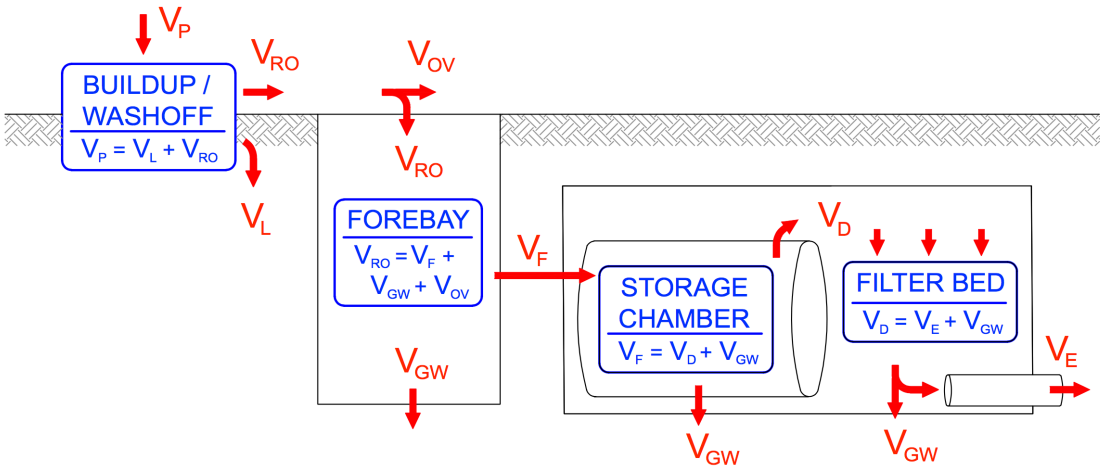

Figure B-1. Flowchart schematic of water quantity model. Subscripts: P=precipitation, L=rainfall losses, RO=runoff, F=facility, GW=groundwater, OV=overflow, D=discharge.

Table B-1. Summary of inputs to simulation model.

Variable	Units
Drainage area	ac
Curve Number	-
Depth of rainfall	in.
Duration of rainfall	hr
Time of concentration	min
Peak Rate Factor	-
Bottom area of forebay	ft^2
Maximum depth of water in the forebay	ft
Diameter of holes in floor of forebay	in.
Number of drainage holes in floor of forebay	-
Infiltration rate from forebay and gravel box	in./hr
Depth forebay floor to connector pipe invert	ft
Diameter of connector pipe	in.
Height of layer 1 of gravel box	ft
Height of layer 2 of gravel box	ft
Height of layer 3 of gravel box	ft
Length of gravel box and surface storage area	ft
Width of gravel box and surface storage area	ft
Void space fraction in gravel box: layer 1	-
Void space fraction in gravel box: layer 2	-
Void space fraction in gravel box: layer 3	-
Infiltration rate: layer 1 to layer 2	in./hr
Infiltration rate: layer 2 to layer 3	in./hr
Diameter of chamber pipe	ft
Length of chamber pipe	ft
Number of holes in top of the chamber	-
Diameter of holes in the top of the chamber	in.
Invert elevation of holes in top of the chamber	ft
Height of the chamber hole above datum	in.
Diameter of chamber drainage hole	in.
Number of holes in the outlet pipe	-
Diameter of holes in the outlet pipe	in.

B.2.1 Rainfall/Runoff Generation

The rainfall generation component of this model simulates one-minute precipitation depths to synthesize rainfall hyetographs. A rainfall hyetograph is developed using the NRCS Type II Rainfall Distribution. However, since the ordinates for this distribution are for a 24-hour storm event, a modified model, presented in equation (3-1), is used to standardize the hyetograph for a given rainfall depth and duration.

$$y = \begin{cases} c_1\, e^{c_2 t}\, t^{c_3} & for\ 0 \le t < t_{c_1} \\ c_8 + c_4\left(t - t_{c_1}\right) & for\ t_{c_1} \le t < t_{c_2} \\ c_9 + c_5 e^{c_6\left(t - t_{c_2}\right)}\left(t - t_{c_2}\right)^{c_7} & for\ t_{c_2} \le t < t_{c_3} \end{cases} \qquad \text{(B-1)}$$

The time scales of the functions of equation (B-1) were compressed from 24-hours to the duration that was randomly generated in the program based on observed rainfall depths and durations for the Baltimore-Washington area. This maintains the center-loaded characteristics of the intensity-duration-frequency curves that is the dominant profile of storms in the Middle Atlantic region. Random uniform variates, U(0,1), are used to generate depths (P) and durations (D). Using the standardized rainfall distribution, y is calculated for each minute of the storm (from t=0 to t=D minutes) and multiplied by P to obtain a minute-by-minute distribution of precipitation depths, P(t). The sum of all ordinates in this matrix is the total precipitation depth for the storm event.

Next, the NRCS method is employed to separate precipitation into the initial abstraction, losses, and precipitation excesses (runoff). Initial abstraction is all of the losses that occur before runoff begins. Losses include water retained in surface

depressions and water intercepted by vegetation, evaporation, and infiltration. Using the CN values presented in chapter 2, a matrix of runoff depths, Q(t), can be generated based on P(t) using equation (B-2). The runoff depth, Q, is a function of cumulative precipitation, land cover / land use, and antecedent moisture conditions (NRCS 1986).

$$Q = \frac{(P-I_a)^2}{P-I_a+S} \quad \text{(B-2a)}$$

$$I_a = 0.2 * S \quad \text{(B-2b)}$$

$$S = \frac{1000}{CN} - \gamma \quad \text{(B-2c)}$$

$$\gamma = 10 + 0.00256 * (98 - CN)^{5/3} * \sqrt{24 - D} \quad \text{(B-2d)}$$

where Q is the depth of runoff over a drainage area (in.); P is the matrix of precipitation values (in.); S is the maximum potential retention of water by site soil (in.); I_a is the initial abstraction (in.); and D is the storm duration (hrs.). γ presents McCuen's adjustment to S that corrects for storm events less than 24 hours in duration. Note that when D=24 hours or CN=98, γ is 10 (which is the standard model).

A unit hydrograph is then developed to normalize the runoff matrix into a discharge hydrograph of one area-inch of direct runoff that results from one area-inch of rainfall excess. Before developing the unit hydrograph, times of concentration must be estimated to be used as inputs. Times of concentration represent the travel time of runoff from the hydraulically-most distant point in the watershed to the facility inlet. The NRCS Lag Equation, presented in equation (B-3), is used to estimate times of concentration for each of the SCM facilities.

$$t_c = 0.00526 * (L^{0.8}) * \left[\frac{1000}{CN} - 9\right]^{0.7} / \sqrt{s} \quad \text{(B-3)}$$

where L is the length of the longest flowpath (feet); CN is the curve number (dimensionless); and s is the flowpath slope (feet per foot). Lengths and slopes were estimated in AutoCAD by scaling the large neighborhood map (Figure A-1) and delineating watersheds and flowpaths based on contours and topographic info.

Since the NRCS unit hydrograph can be fitted exactly by a gamma distribution, this type of distribution was used in the model. The gamma distribution has two parameters: a shape and a scale parameter. These were fitted using the time of concentration, which was converted to a time-to-peak, and the peak flow rate factor. Equation (B-4) presents the calculation for the peak discharge of the unit hydrograph.

$$q_p = k * \frac{A*Q}{t_p} \quad \text{(B-4)}$$

where q_p is a matrix of peak rates ($ft^3/s.$); k is the peak rate factor (dimensionless); A is the watershed area ($mi.^2$); Q is the runoff depth (in.); and t_p is the time to peak (hrs.). The peak rate factor is assumed to be 484; a standard value for the Maryland region (McCuen and Bondelid 1983). The time to peak is calculated as two-thirds of the time of concentration (i.e., $t_p=(2/3)*t_c$).

Finally, the precipitation excess hyetograph, Q(t), is convolved with a unit hydrograph to obtain a vector of direct runoff, DRO(t). Convolution is a process of linear superpositioning: a forcing function (precipitation excess) is multiplied, translated, and added to a response function (unit hydrograph) to derive a runoff hydrograph (McCuen 2005). The DRO(t) vector acts as the input to the SCM facilities on one-minute time intervals.

B.2.2 Facility Model: Forebay

Runoff enters a curb inlet (forebay) from the roadway. The characteristics of the forebay are presented in section 2.1.1. Inputs for the forebay include height, bottom surface area, height from the bottom to the connector pipe, maximum water level, characteristics of drainage holes in the bottom, and initial storage volume, as to provide a representation of antecedent dry days. Drainage holes on the bottom surface of the forebay release runoff into the surrounding soils. The movement of runoff in the forebay is modeled using a stage-storage-discharge relationship, where weir and orificial flow dictate effluent discharge. There is one influent and three effluent terms in the water balance:

$$V_{RO} = V_{OV} + V_{GW} + V_F \quad \text{(B-9)}$$

where V is the volume (or flowrate); RO is the direct runoff vector, DRO(t); OV is the overflow; GW represents the volume of water that infiltrates to surrounding soils; and F represents the volume that remains in the facility via the connector pipe. V_{GW} was calculated as orificial flow, as the drainage holes are at a datum of zero. V_F is calculated as weir flow for a depth between the invert and top of the connector pipe and orificial flow for depths larger than the invert plus the diameter of the connector pipe. In the case of large RO volumes, the forebay may become overwhelmed and a volume will bypass the facility.

A weir is an unsubmerged outlet and an orifice is a submerged outlet (McCuen 2004). Weir flow is calculated using equation (B-10) and orificial flow is calculated using equation (B-11).

$$Q(t)_F = C_w * L * h^{1.5} \quad \text{(B-10)}$$

where $Q(t)_F$ is the effluent flowrate out of the discharge pipe (ft^3/s); Cw is the weir coefficient, assumed to be 3.0; L is the weir length (ft), calculated as the wetted circumference of the discharge pipe for a given depth; and h is the depth of runoff in the forebay (ft). The flowrates are converted to one-minute volumes, as to correspond with the influent DRO(t) matrix.

$$Q(t)_F = C_d * A * \sqrt{2 * g * h} \quad \text{(B-11)}$$

where $Q(t)_F$ is the effluent flowrate out of the discharge pipe (ft^3/s); C_d is the discharge coefficient, assumed to be 0.6; A is the area of the orifice (ft^2); g is the gravitational constant, assumed to be 32.1 ft/s^2; and h is the depth of water in the forebay (ft).

Large storm events can overwhelm SCM facilities, and, once the storage capacity is reached, runoff will bypass these systems and continue as runoff on the roadway. The inlets are on-grade, meaning that the bypass volume will continue down-grade as surface runoff until the next inlet is reached. In this model, V_{OV} never actually enters the facility. The GW volume is considered to have left the system. The F volume acts as the input into the next facility component: the storage chamber.

B.2.3 Facility Model: Storage Chamber

From the forebay connector pipe, runoff splits and enters two horizontally-laying cylindrical storage pipes. Input characteristics of the storage pipes include length and diameter of the pipes and the number, diameter, and invert elevations of drainage holes. The chamber is perforated and surrounded by a filter bed. There is one drainage hole at the bottom of each pipe and several holes at the top of the chamber. The configuration of the drainage holes was unknown; therefore, the size, number, and

location of drainage holes was set as an input and a rationality/sensitivity analysis was performed. Again, a stage-storage-discharge relationship was used to simulate discharge out of the storage chambers. There is one influent term and two effluent terms in this water balance:

$$V_F = V_D + V_{GW} \quad \text{(B-12)}$$

where V is the volume (or flowrate); F is the matrix of one-minute effluent volumes from the forebay; D is the volume that exits the storage pipes via the top holes; and GW is the volume that infiltrates out of the bottom drainage hole. V_{GW} is calculated as orificial flow based on the depth of water in the storage chamber. V_D is calculated as weir flow for a depth between the invert and top of the discharge pipe and orificial flow for depths larger than the invert plus the diameter of the discharge pipe. In the case that the storage chamber is completely filled, a universal datum is used to input the orificial depth as the depth of the drainage holes to the water surface in the forebay.

B.2.4 Facility Model: Filtration Chamber

Discharge from the top drainage holes in the chambers disperses over the filter bed in the treatment chamber and infiltrates through the HFM matrix. The filter bed is comprised of three layers: two gravel layers with a HFM layer between the two. Input variables are depth, porosity, and infiltration rate of each of the three layers, length and width of the filter bed, and diameter and number of drainage holes in the effluent pipe. The flow balance through the filter bed is modeled using one input term and two outflow terms:

$$V_D = V_E + V_{GW} \quad \text{(B-13)}$$

where V is the volume; D is the matrix of one-minute volumes from the storage pipes; E is the volume that enters the outlet pipe at the bottom of the filter bed; and GW is the volume that drains to surrounding soils. The bottom of the chamber is pervious, so effluent that does not enter the outlet pipe infiltrates to surrounding soils. This flow balance assumes no accumulation or storage of water in the filter bed. Filtration is modeled using inputted infiltration rates and pore volumes that are calculated using inputted lengths and widths of the treatment chamber and porosities of each of the three media layers.

B.3 Sensitivity Analyses

Sensitivity analysis is an important tool in model simulation because it allows for an understanding of the impacts of individual parameters on system performance. Therefore, sensitivity analyses were performed on selected input parameters to assess the impact of these parameters on SCM performance.

B.3.1 Drainage Area

Davis and McCuen (2005) suggest Drainage Area (DA) as probably the single most important watershed characteristic for hydrologic design because it reflects the volume of water that can be generated from a rainfall event. When DA is increased from 0.24 ha (0.6 ac) to 0.41 ha (1.0 ac), the volume of rainfall for a simulated 1.9-cm (0.75-in) storm event increases from 1633 ft^3 to 2722 ft^3. The volume of runoff for the two simulated storms are 460 and 766 ft^3, respectively. The volumes of rainfall and

runoff both increase with DA. This impacts SCM performance. In the simulation with a DA of 0.24 ha (0.6 ac), there was no overflow from the forebay. However, in the simulation with a DA of 0.41 ha (1.0 ac), 47 ft^3 of runoff overflowed and bypassed the system. Thus, SCMs must be designed for individual DAs and expected rainfall characteristics. This will ensure adequate storage of runoff in respective microwatersheds.

B.3.2 Curve Number

Curve Number (CN) affects the volume of runoff that can be generated from a rainfall event. CN is a measure of imperviousness, Hydrologic Soil Group, and land cover / land use, as presented in Section 2.1.9. CN values for the monitored SCMs range from 87-89; values typical for a residential area. For a 1.0 in. storm event over 10 hours, changing CN from 87 to 89 did not impact the rainfall volume, but it increased the runoff volume from 3267 ft^3 to 3299 ft^3. System performance was not impacted by this increase in influent runoff volume. This comparison only represents slight changes in CN; if CN were reduced to 30, its minimum value that represents a highly-pervious area, the volume of runoff would decrease substantially. For this reason, CN should be taken into account during SCM design to ensure that systems are able to mitigate runoff volumes from their DAs.

B.3.3 Depth of Rainfall

The depth of rainfall also plays a vital role in SCM design. When the depth of rainfall is increased from 0.25 in to 1.5 in, the simulated volume of rainfall increases

from 535 ft^3 to 3212 ft^3. Runoff volumes increase from 23 ft^3 to 1781 ft^3. The SCMs must be able to storage and mitigate these runoff volumes. In the simulated 0.25 in. storm, only 5.5 ft^3 of effluent flow was generated, while, in the 1.5 in. event, 1059 ft^3 of effluent flow was generated. The larger-storm also produced overflow, while the smaller storm did not. Kreeb (2003) concluded that the majority of Maryland storms have small rainfall depths, but, in the case of large rainfall depths, SCMs are expected to perform. Thus, consideration of the local design storm depth is a must in proper SCM design.

B.3.4 Duration of Rainfall

When the duration of rainfall for a 1.5 in. storm event is increased from 6 hr to 7 hr, volumes of rainfall and runoff do not change, but the timing of runoff does change. It takes 110 min until the start of runoff for the 6-hr event and 130 min for the 7-hr event. The duration of runoff is longer in the 7-hr event, as well: 315 min vs. 275 min for the 6-hr event. This also has implications to first flush. The 7-hr simulated event reaches 0.20 in. of runoff after 82 min, while the 6-hr simulated event only takes 72 min to do so. Rainfall intensities are lower for the simulated 7-hr storm. It is important to remember that this model assumes a NRCS Type II storm distribution for all events. Both simulations show overflow from the SCMs, most likely due to the sampling shortcomings that will be presented in Section B.4. That being said, consideration of rainfall duration is important to proper design, as it represents the time frame of incoming runoff. Temporal changes in storage, such as an active storage through infiltration, can be optimized for various storm durations.

B.3.5 Sizing of Forebay

The forebay provides storage to incoming runoff. Increasing the depth and bottom area of the forebay was found to increase the storage capacity of the SCM. For a storm of 0.25 in., an increase in the bottom area of the forebay from 5 ft^2 to 10 ft^2 increased the amount of runoff stored in the forebay from 17 ft^3 to 23 ft^3. Increasing the depth of the forebay provides similar results: when the depth of the forebay increases from 5.5 ft to 6 ft, the amount of runoff stored in the forebay increases from 23 to 24 ft^2. Therefore, a deeper and wider forebay is preferred, as it will allow for more available storage to incoming runoff. However, this comes with space limitations and excavation costs and a balance of space and costs is necessary for optimal design.

B.3.6 Drainage Holes in Forebay

The drainage holes in the bottom of the forebay provide infiltration of stored water to surrounding soils. However, the sizing of the holes does play a significant role in their performance. It was found that the infiltration rate underneath the forebay dictates flow out of the bottom of the forebay. When the total area of drainage holes is increased, either by increasing the number of holes or increasing the diameter of the holes, there was no difference in the volume of water that infiltrates out of the forebay.

B.3.7 Height of Connector Pipe Invert

The height of the connector pipe invert impacts the flow of runoff from the forebay to the treatment chamber. Increasing the height of the connector pipe invert

(with respect to the bottom of the forebay) increases the amount of runoff that infiltrates out of the bottom of the forebay. Additionally, when the forebay and treatment chamber are saturated and the connector pipe acts as an orifice, the height of the connector pipe invert also impacts the hydraulic head. Simulation results show that a higher connector pipe invert will create higher effluent flows out of the treatment chamber.

B.3.8 Size of Treatment Chamber

The length, width, and height of the treatment chamber dictates the amount of storage available for runoff. Therefore, increasing the length and/or diameter of the chamber creates more storage and less overflow, as does increases in the length, width, and height of the gravel box. However, as is the case with the forebay, increasing the size of the treatment chamber comes with increased space allocations and construction costs.

B.3.9 Media Characteristics

Simulation results show that media with higher porosities provide more storage of runoff in the gravel box. The infiltration rate was not found to impact the hydrologic performance of the SCMs. For a simulated storm event of 1.5 in., there was no difference in outflow hydrographs between simulations with infiltration rates of 2.5 in./hr, 10 in./hr, and 100 in./hr. This produces large uncertainty in the model, as infiltration rate is often thought to be the limiting factor in the flow of water through a media.

B.4 Model Shortcomings

While simulation is a powerful tool, it is important to keep in mind that the simulated data are not real; they are projected values obtained from a model (McCuen 2003). This model was powerful in providing numerical representations of runoff flow through the SCMs, but it also presents several shortcomings that should be taken into account.

This model assumes a NRCS Type II storm distribution for all simulated storms. Individual storm events in the real world do not necessarily follow this distribution, although the Washington-Baltimore Intensity-Duration-Frequency curve says that they do follow this distribution over the long term. Therefore, rainfall intensities simulated in the model may not represent the true distribution of rainfall events that the SCMs are experiencing in the real world.

The forebay overflow also presents a constraint of the model. In the real world, the forebay of SCM D was never observed to leave weir flow. In the model, the forebays reached orificial flow for many storm events. Thus, the overflow observed in simulated events is most likely dictated by the lack of knowledge on infiltration rates.

The model assumes that drainage holes in the storage chamber are all located at a constant height above the bottom of the pipe. Based on field observations in the monitoring well of SCM D, the storage pipes seemed to have perforations all around their circumference. Thus, the dispersion of runoff out of the storage pipes was most likely different than what is shown in the model.

In the algorithm of this simulation, the effluent collector pipe comes before infiltration to surrounding soils. In the real world, these two occur at the same time,

depending on where the effluent collector pipe is located within the gravel box. Thus, the amount of runoff that infiltrates out of the gravel box may be underestimated.

B.5 Model Results and Discussion

A sample output file for a simulated storm event is presented at the end of the appendix. The model shows that from a hydrologic perspective the HFM SCMs are successful at reducing the adverse impacts of urban stormwater runoff. The hydrologic philosophy of smart growth, as presented in McCuen (2003), incorporates three primary metrics: hydrologic storage compensation; stream channel preservation; and travel time maintenance. The SCMs achieve proper hydrologic storage compensation and travel time maintenance for the majority of simulated storms. Stream channel preservation is not directly achieved by the SCMs, but, it can be said that the increased storage and travel time of runoff will have positive impacts to stream health downstream.

B.5.1 Hydrologic Storage Compensation

In achieving smart growth, McCuen (2003) recommends that a significant amount of water be kept at its source in attempt to maintain natural hydrologic processes. This is especially important at the microwatershed level. When storage in a microwatershed is sufficient, it has been found to reduce peak discharge both from the microwatershed and from the larger watershed that drains into a first-order stream (McCuen 2003).

Despite their small footprints, the SCMs were found to provide adequate storage for most simulation storm events. For an event with a rainfall depth of 0.25 in. and a duration of 2 hr, 23.1 ft^3 of direct runoff is generated. The SCM discharges 5.5 ft^3 out of the effluent pipe; 0.4 ft^3 infiltrates out of the forebay; and 17.1 ft^3 is completely stored in the SCM. For a 0.75 in., 10-hr simulated storm, 795 ft^3 of direct runoff is generated: 44 ft^3 of which is overflow, most likely due to model shortcomings; 8 ft^3 infiltrates out of the bottom of the foreaby; 49 ft^3 infiltrates out of the gravel box, and 670 ft^3 is discharged out of the effluent pipe. Note that these values represent volumes of runoff; not rainfall. Additional storage is available on the surface via the initial abstraction.

B.5.2 Travel Time Maintenance

McCuen (2003) suggests that, although a connection between storage and travel time are obvious, travel time maintenance is, in itself, a very important parameter in hydrologic smart growth. One way to reduce travel time is to reduce peak flow. Hunt et al. (2008) suggest peak flow mitigation as one of the most important aspects of SCM design.

Figure B-2 presents a comparison of runoff and outflow hydrographs for a simulated rainfall event of 1.0 in. and 10 hr. A clear decrease in peak flow is noted, with influent and effluent peak flows of 34.3 ft^3/min and 5.8 ft^3/min, respectively. There is a 14-min lag time between influent and effluent peak flows for this storm.

The steep jump/start to outflow discharge at 48 minutes is most likely due to the dead storage volume in the SCM being achieved. The decline in outflow discharge

at 115 minutes is assumed to be due to the height of runoff in the storage pipe decreasing to below the invert of the top drainage holes. This causes flow out of the storage pipes to solely be occurring through the bottom drainage hole.

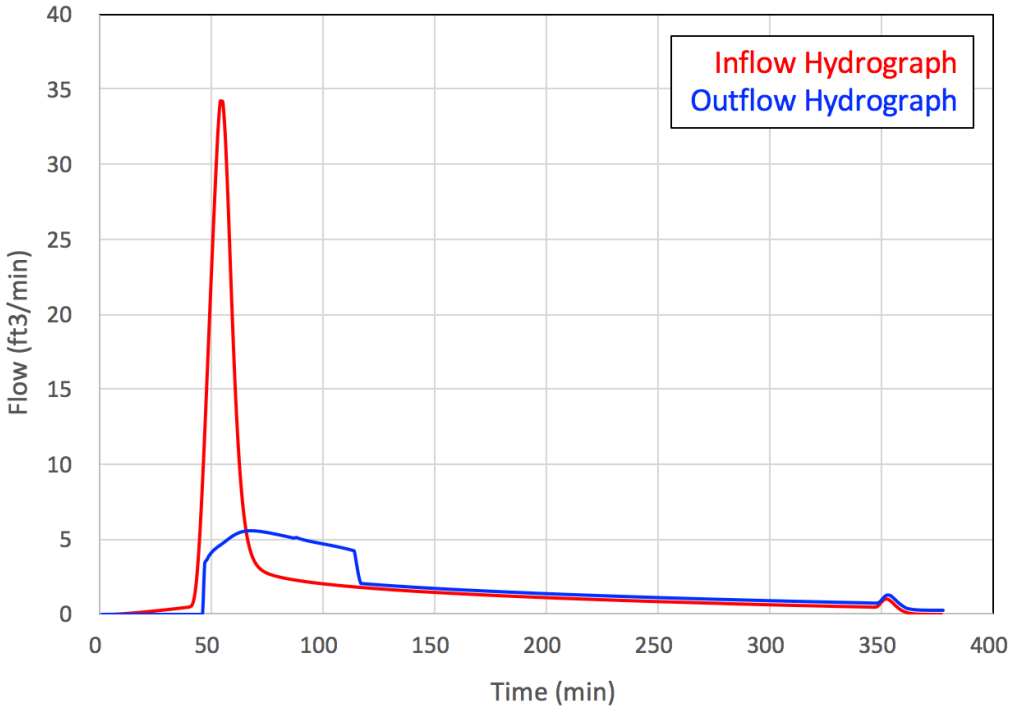

Figure B-2. Comparison of influent and effluent hydrographs for a 2.5 cm (1.0 in.) storm over 10 hours.

B.6 Conclusion

Based on simulation results, the SCMs are successful at mitigating stormwater runoff in the Camelot subdivision. Although overflow was noted in some simulated events and results of the model were not completely consistent with field observations, the SCMs were found to provide adequate storage and peak flow mitigation for the majority of storm events in the state of Maryland. By placing HFM SCMs in the upper reaches of a watershed, travel times will be reduced throughout the entire watershed and more water will be kept at the source. These systems will be promote more natural

hydrologic processes in an urbanized area, and will be associated with a healthier Chesapeake Bay watershed for years to come.

The results of this simulation model also show that the design of these SCMs plays a crucial role in their performance. Optimal SCM design incorporates a balance of runoff storage and space limitations. By increasing the surface area and depth of the SCMs, more runoff can be stored, but construction costs will increase. Water exchange between the SCMs and surrounding soils should be maximized, as to promote groundwater recharge. This can be achieved by increasing the number and/or size of drainage holes in the bottom of the storage components to the SCMs. Local design storms should be used to design SCMs, as these systems perform very differently under different storm events. Although the model does not show infiltration rate to play a substantial role in water movement, this parameter must be considered in media selection, as it dictates the extent of active storage that is available in the SCMs through infiltration.

```
Version 17.06

Richard H. McCuen
Department of Civil Engineering
University of Maryland
College Park, MD  20742-3021

rhmccuen@eng.umd.edu    or    (301) 405-1949

------------------------------------------------------------
LISTING OF INPUT DATA

      .60 = drainage area (ac)
      87. = curve number
     .750 = depth (in.) of rainfall
      8.0 = duration (hr) of rainfall
      9.0 = time of concentration (min)
     484. = the peak rate factor
      10. = bottom area (ft^2) of the forebay
      5.5 = maximum depth (ft) of water in the forebay
     6.00 = diameter (in.) of holes in floor of forebay
        4 = number of drainage holes in floor of forebay
     5.00 = infiltration rate (in/hr) from forebay & gravel box
     3.00 = depth (ft) forebay floor to connector pipe invert
       8. = diameter (in.) of connector pipe
       .5 = height (ft) of layer 1 of the gravel box
      1.5 = height (ft) of layer 2 of the gravel box
      1.0 = height (ft) of layer 3 of the gravel box
      24. = length (ft) of gravel box & surface storage area
      10. = width (ft) of gravel box & surface storage area
      .42 = void space fraction in gravel box: layer 1
      .40 = void space fraction in gravel box: layer 2
      .42 = void space fraction in gravel box: layer 3
   100.00 = infilt. rate (in./hr): layer 1 to layer 2
   100.00 = infilt. rate (in./hr): layer 2 to layer 3
      2.5 = diameter (ft) of chamber pipe
      24. = length (ft) of chamber pipe
      192 = number of holes in the top of the chamber
     1.00 = diameter (in.) of holes in top of chamber
     1.50 = invert elevation(ft) of holes in top of chamber
     2.00 = height (in.) of chamber drainage hole above datum
      1.0 = diameter (in.) of chamber drainage hole
       10 = number of holes in the outlet pipe
      1.0 = diameter (in.) of holes in the outlet pipe

RAINFALL EXCESS HYETOGRAPH (ft^3/min)


RUNOFF HYDROGRAPH INTO FOREBAY (ft^3/min)
```

```
    .000    .000    .001    .002    .005    .010    .018    .029    .
073    .273
    .809   1.832   3.408   5.518   8.075  10.959  14.047  17.154
19.782  21.286
  21.358  20.148  18.065  15.565  13.020  10.677   8.662   7.014
5.715   4.721
   3.977   3.428   3.026   2.734   2.521   2.365   2.248   2.158
2.088   2.032
   1.985   1.945   1.910   1.879   1.850   1.824   1.799   1.776
1.755   1.734
   1.714   1.695   1.676   1.658   1.641   1.625   1.608   1.593
1.578   1.563
   1.548   1.534   1.521   1.507   1.494   1.481   1.469   1.456
1.444   1.433
   1.421   1.410   1.398   1.387   1.377   1.366   1.355   1.345
1.335   1.325
   1.315   1.305   1.296   1.286   1.277   1.268   1.259   1.250
1.241   1.232
   1.224   1.215   1.206   1.198   1.190   1.182   1.174   1.166
1.158   1.150
   1.142   1.134   1.127   1.119   1.112   1.104   1.097   1.089
1.082   1.075
   1.068   1.061   1.054   1.047   1.040   1.033   1.027   1.020
1.013   1.007
   1.000    .994    .987    .981    .974    .968    .962    .956    .
949    .943
    .937    .931    .925    .919    .913    .907    .901    .896    .
890    .884
    .878    .873    .867    .862    .856    .850    .845    .840    .
834    .829
    .823    .818    .813    .808    .802    .797    .792    .787    .
782    .777
    .772    .767    .762    .757    .752    .747    .742    .737    .
732    .727
    .723    .718    .713    .708    .704    .699    .694    .690    .
685    .681
    .676    .672    .667    .663    .658    .654    .650    .645    .
641    .636
    .632    .628    .624    .619    .615    .611    .607    .603    .
599    .594
    .590    .586    .582    .578    .574    .570    .566    .562    .
558    .554
    .551    .547    .543    .539    .535    .531    .528    .524    .
520    .516
    .513    .509    .505    .502    .498    .494    .491    .487    .
484    .480
    .477    .473    .470    .466    .463    .459    .456    .452    .
449    .446
    .442    .439    .435    .432    .429    .425    .422    .419    .
416    .412
```

```
    .409    .406    .403    .400    .410    .483    .599    .698    .
739    .718
    .649    .553    .450    .351    .266    .196    .141    .099    .
069    .047
    .031    .021    .014    .009    .006    .004    .002    .001    .
001    .001
    .000    .000    .000    .000

 ___________________________________________________________________
 SUMMARY OF EVENT DEPTHS AND VOLUMES
       .0375000 = total volume (ac-ft) of rainfall
       .7500000 = total depth (in.) of rainfall
       .2111527 = total depth (in.) of rainfall excess
       .2111527 = total depth (in.) of direct runoff
       .9999999 = total depth (in.) of unit hydrograph
   1633.5000000 = total volume (ft^3) of rainfall
    459.8906000 = total volume (ft^3) of direct runoff
       .0000000 = volume (ft^3) of forebay overflow
      7.8348620 = volume (ft^3) of infiltration from forebay
     26.5252300 = volume (ft^3) of recharge from gravel box
    401.8575000 = volume (ft^3) of outflow through pipe

 The following are in inches, ft^3, and minutes
    .0356411     77.6  241. = max 1-min rainfall; time of maximum
    .0159643     34.8   17. = max 1-min rainfall excess; time of
maximum
    .0098064     21.4   21. = max 1-min DRO; time of maximum
    .0022946      5.0   27. = max 1-min BMP outflow; time of maximum
 NOTE: Rainfall excess begins at time t = 0.
       Times for the Pe, DRO, and outflow are measured from
           the start of the rainfall excess

  The following are water storages remaining at end of storm
     23.6717200 = volume (ft^3) in forebay
       .0000000 = volume (ft^3) in chamber
       .0000000 = volume (ft^3) in box: layer 1
       .0000000 = volume (ft^3) in box: layer 2
       .0000000 = volume (ft^3) in box: layer 3
     23.6717200 = total volume (ft^3) remaining in storages


 OUTFLOW HYDROGRAPH (ft^3/min)
   .0000   .0000   .0000   .0000   .0000   .0000   .0000   .0000   .
0000   .0000
   .0000   .0000   .0000   .0000   .0000   .9493  3.4214  3.6909
4.0171  4.2409
  4.4134  4.5475  4.6595  4.7480  4.8234  4.8802  4.9977  4.9958
4.9953  4.9938
  4.9901  4.9835  4.9739  4.9614  4.9463  4.9288  4.9091  4.8877
4.8645  4.8399
```

```
  4.8140  4.7869  4.7586  4.7292  4.6987  4.6669  4.6339  4.5995
4.5635  4.5255
  4.4851  4.4414  3.8687  2.9799  2.0803  2.0636  2.0475  2.0318
2.0166  2.0018
  1.9873  1.9733  1.9595  1.9461  1.9330  1.9202  1.9077  1.8954
1.8833  1.8715
  1.8599  1.8485  1.8373  1.8263  1.8155  1.8049  1.7944  1.7841
1.7740  1.7640
  1.7541  1.7444  1.7348  1.7254  1.7161  1.7069  1.6978  1.6888
1.6799  1.6712
  1.6625  1.6539  1.6455  1.6371  1.6288  1.6206  1.6125  1.6045
1.5966  1.5887
  1.5809  1.5732  1.5656  1.5580  1.5505  1.5431  1.5357  1.5285
1.5212  1.5141
  1.5070  1.4999  1.4929  1.4860  1.4791  1.4723  1.4656  1.4589
1.4522  1.4456
  1.4391  1.4326  1.4261  1.4197  1.4133  1.4070  1.4008  1.3945
1.3884  1.3822
  1.3761  1.3701  1.3641  1.3581  1.3522  1.3463  1.3405  1.3346
1.3289  1.3231
  1.3174  1.3118  1.3061  1.3006  1.2950  1.2895  1.2840  1.2785
1.2731  1.2677
  1.2624  1.2570  1.2518  1.2465  1.2413  1.2361  1.2309  1.2258
1.2207  1.1045
   .7661   .7611   .7561   .7511   .7462   .7413   .7364   .7315   .
7267   .7219
   .7171   .7124   .7076   .7029   .6983   .6936   .6890   .6844   .
6798   .6753
   .6707   .6662   .6618   .6573   .6529   .6485   .6441   .6397   .
6354   .6310
   .6267   .6225   .6182   .6140   .6098   .6056   .6014   .5973   .
5931   .5890
   .5849   .5809   .5768   .5728   .5688   .5648   .5608   .5569   .
5530   .5490
   .5451   .5413   .5374   .5336   .5298   .5260   .5222   .5184   .
5147   .5110
   .5073   .5036   .4999   .4962   .4926   .4890   .4854   .4818   .
4782   .4747
   .4711   .4676   .4641   .4606   .4572   .4537   .4503   .4468   .
4434   .4401
   .4367   .4333   .4300   .4267   .4233   .4200   .4168   .4135   .
4102   .4070
   .4038   .4006   .3974   .3942   .4041   .4776   .5940   .6922   .
7335   .7123
   .6433   .5476   .4441   .3460   .2605   .1660   .1168   .0855   .
0599   .0421
   .0292   .0200   .0135   .0090   .0058   .0036   .0021   .0011   .
0004   .0001
   .0000   .0000   .0000   .0000
```

```
 2.5000 = diameter (ft) of chamber
 1.2108 = maximum depth of water in chamber

TIME PARAMETERS
 225 = no. of minutes to start of runoff
 480 = storm duration (min)
 255 = duration (min) of rainfall excess
  30 = duration (min) of unit hydrograph
 284 = duration (min) of direct runoff hydrograph//

WATER BALANCE
  459.89 = volume (ft^3) of direct runoff into forebay
     .00 = volume (ft^3) of forebay overflow
    7.83 = volume (ft^3) of infiltration from forebay
   26.53 = volume (ft^3) of recharge from gravel box
  401.86 = volume (ft^3) of outflow through pipe
   23.67 = volume (ft^3) reamining in the system
     .00 = water balance (ft^3)

FIRST FLUSH TIMES
  20 = time (min) at which inflow depth = 0.05 in.
  28 = time (min) at which inflow depth = 0.10 in.
 215 = time (min) at which inflow depth = 0.20 in.
```

APPENDIX C: ADDITIONAL DATA

Table C-1. Rainfall Data. Legend: P=precipitation depth; D=rainfall duration; ADD=antecedent dry days; i=rainfall intensity; avg=average; max=maximum; 1=initial 15 minutes of rainfall event; 2=initial 30 minutes of rainfall event; 3=initial 1 hour of rainfall event. Dates denoted with * represent rainfall events in which a rain gauge error occurred. In these cases, local rainfall data was referenced for precipitation depths and durations.

Date	**P in cm. (in.)**	**D in hrs.**	**ADD**	**$i_{avg,D}$ in cm/hr (in/hr)**	**$i_{max,D}$ in cm/hr (in/hr)**	**$i_{avg,1}$ in cm/hr (in/hr)**	**$i_{max,1}$ in cm/hr (in/hr)**	**$i_{avg,2}$ in cm/hr (in/hr)**	**$i_{max,2}$ in cm/hr (in/hr)**	**$i_{avg,3}$ in cm/hr (in/hr)**	**$i_{max,3}$ in cm/hr (in/hr)**
06/21/16	4.70 (1.85)	9.5	4	0.48 (0.19)	1.32 (0.52)	0.11 (0.04)	0.11 (0.04)	0.71 (0.28)	1.32 (0.52)	0.91 (0.36)	1.32 (0.52)
06/28/16*	1.14 (0.45)	4.0	5	Rain Gauge Error	Rain Gauge Error	Rain Gauge Error	Rain Gauge Error	Rain Gauge Error	Rain Gauge Error	Rain Gauge Error	Rain Gauge Error
07/04/16*	2.21 (0.87)	9.0	6	Rain Gauge Error	Rain Gauge Error	Rain Gauge Error	Rain Gauge Error	Rain Gauge Error	Rain Gauge Error	Rain Gauge Error	Rain Gauge Error
07/16/16	0.97 (0.38)	1.5	8	0.56 (0.22)	2.95 (1.16)	0.20 (0.08)	0.20 (0.08)	1.63 (0.64)	2.95 (1.16)	0.91 (0.36)	2.95 (1.16)
07/28/16	2.39 (0.94)	12.0	9	0.41 (0.16)	1.93 (0.76)	0.30 (0.12)	0.30 (0.12)	0.20 (0.08)	0.30 (0.12)	0.11 (0.04)	0.30 (0.12)
08/15/16	2.29 (0.90)	7.0	18	0.11 (0.04)	1.12 (0.44)	0.11 (0.04)	0.11 (0.04)	0.11 (0.04)	0.11 (0.04)	0.11 (0.04)	0.20 (0.08)
08/17/16	1.93 (0.76)	2.0	2	0.30 (0.12)	2.54 (1.00)	2.54 (1.00)	2.54 (1.00)	2.03 (0.80)	2.54 (1.00)	1.52 (0.60)	2.54 (1.00)
08/21/16*	1.50 (0.59)	1.5	5	Rain Gauge Error	Rain Gauge Error	Rain Gauge Error	Rain Gauge Error	Rain Gauge Error	Rain Gauge Error	Rain Gauge Error	Rain Gauge Error

09/19/16	2.21 (0.87)	0.8	18	1.02 (0.40)	2.64 (1.04)	0.11 (0.04)	0.11 (0.04)	0.30 (0.12)	0.41 (0.16)	0.30 (0.12)	0.41 (0.16)
09/29/16	3.81 (1.50)	7.0	3	0.20 (0.08)	0.61 (0.24)	0.11 (0.04)	0.11 (0.04)	0.11 (0.04)	0.11 (0.04)	0.11 (0.04)	0.11 (0.04)
11/30/16*	1.80 (0.71)	6.0	40	Rain Gauge Error	Rain Gauge Error	Rain Gauge Error	Rain Gauge Error	Rain Gauge Error	Rain Gauge Error	Rain Gauge Error	Rain Gauge Error
12/06/16	2.01 (0.79)	8.5	7	0.30 (0.12)	0.91 (0.36)	0.30 (0.12)	0.30 (0.12)	0.30 (0.12)	0.30 (0.12)	0.30 (0.12)	0.30 (0.12)
12/17/16*	0.97 (0.38)	4.5	5	Rain Gauge Error	Rain Gauge Error	Rain Gauge Error	Rain Gauge Error	Rain Gauge Error	Rain Gauge Error	Rain Gauge Error	Rain Gauge Error
01/03/17	1.93 (0.76)	5.5	1	0.30 (0.12)	1.83 (0.72)	0.30 (0.12)	0.30 (0.12)	0.30 (0.12)	0.30 (0.12)	0.30 (0.12)	0.30 (0.12)
01/23/17	2.08 (0.82)	10.5	20	0.30 (0.12)	1.22 (0.48)	0.30 (0.12)	0.30 (0.12)	0.30 (0.12)	0.30 (0.12)	0.30 (0.12)	0.30 (0.12)
02/09/17*	0.76 (0.30)	4.0	17	Rain Gauge Error	Rain Gauge Error	Rain Gauge Error	Rain Gauge Error	Rain Gauge Error	Rain Gauge Error	Rain Gauge Error	Rain Gauge Error
02/25/17*	2.57 (1.01)	5.5	16	Rain Gauge Error	Rain Gauge Error	Rain Gauge Error	Rain Gauge Error	Rain Gauge Error	Rain Gauge Error	Rain Gauge Error	Rain Gauge Error
03/14/17*	3.45 (1.36)	8.5	14	Rain Gauge Error	Rain Gauge Error	Rain Gauge Error	Rain Gauge Error	Rain Gauge Error	Rain Gauge Error	Rain Gauge Error	Rain Gauge Error
03/31/17	3.02 (1.19)	6.5	12	0.30 (0.12)	1.83 (0.72)	0.30 (0.12)	0.30 (0.12)	0.30 (0.12)	0.30 (0.12)	0.30 (0.12)	0.61 (0.24)

04/06/17	3.63 (1.43)	4.0	6	0.91 (0.36)	7.01 (2.76)	0.30 (0.12)	0.61 (0.24)	0.30 (0.12)	0.91 (0.36)	0.30 (0.12)	0.91 (0.36)
04/22/17*	1.42 (0.56)	2.5	16	Rain Gauge Error	Rain Gauge Error	Rain Gauge Error	Rain Gauge Error	Rain Gauge Error	Rain Gauge Error	Rain Gauge Error	Rain Gauge Error
05/05/17	3.73 (1.47)	5.1	13	0.61 (0.24)	2.74 (1.08)	0.30 (0.12)	0.30 (0.12)	0.30 (0.12)	0.61 (0.24)	0.30 (0.12)	0.91 (0.36)
05/11/17	1.45 (0.57)	5.5	6	0.61 (0.24)	0.61 (0.24)	0.30 (0.12)	0.30 (0.12)	0.30 (0.12)	0.30 (0.12)	0.30 (0.12)	0.30 (0.12)
05/13/17	1.91 (0.75)	8.2	2	0.30 (0.12)	0.91 (0.36)	0.30 (0.12)	0.61 (0.24)	0.30 (0.12)	0.61 (0.24)	0.30 (0.12)	0.61 (0.24)

Table C-2. Summary of influent and effluent PP FFCs for all monitored SCMs, with all values in mg/L as P. SCMs denoted with * represent those with effluent PP data sets found to be statistically lower than corresponding influent PP data sets at α=5%.

SCM	Influent				Effluent			
	Unweighted Mean	Weighted Mean	Standard Deviation	Median (Min, Max)	Unweighted Mean	Weighted Mean	Standard Deviation	Median (Min, Max)
A*	0.60	0.66	0.76	0.29 (<0.05,3.4)	0.06	0.04	0.08	<0.05 (<0.05,0.31)
B*	0.38	0.43	0.32	0.27 (<0.05,1.3)	0.06	0.07	0.06	<0.05 (<0.05,0.21)
C	0.54	0.65	0.64	0.29 (<0.05,2.3)	0.36	0.38	0.47	0.18 (<0.05,1.76)
D*	0.54	0.48	0.41	0.46 (<0.05,1.6)	0.10	0.09	0.08	0.09 (<0.05,0.35)
E*	0.31	0.39	0.44	0.16 (<0.05,1.9)	0.05	0.05	0.04	<0.05 (<0.05,0.15)
F*	0.55	0.56	0.39	0.49 (<0.05,1.5)	0.19	0.22	0.25	0.09 (<0.05,0.83)
G*	0.74	0.88	0.64	0.55 (0.11,2.6)	0.15	0.15	0.17	0.10 (<0.05,0.67)

Table C-3. Summary of influent and effluent TDP FFCs for all monitored SCMs, with all values in mg/L as P. SCMs denoted with * represent those with effluent TDP data sets found to be statistically lower than corresponding influent TDP data sets at α=5%.

SCM	Influent				Effluent			
	Unweighted Mean	Weighted Mean	Standard Deviation	Median (Min, Max)	Unweighted Mean	Weighted Mean	Standard Deviation	Median (Min, Max)
A*	0.35	0.40	0.36	0.28 (<0.05,1.33)	0.10	0.12	0.08	0.10 (<0.05,0.39)
B*	0.87	0.97	1.02	0.43 (0.09,3.87)	0.24	0.27	0.13	0.22 (0.12,0.62)
C	0.84	0.94	1.12	0.48 (0.06,4.62)	0.53	0.59	0.67	0.37 (0.12,2.5)
D*	0.77	0.56	0.71	0.58 (0.12,2.83)	0.24	0.27	0.26	0.19 (0.05,1.06)
E*	0.22	0.25	0.26	0.16 (<0.05,1.00)	0.09	0.10	0.06	0.10 (<0.05,0.23)
F*	0.52	0.58	0.79	0.27 (<0.05,3.35)	0.29	0.33	0.35	0.17 (<0.05,1.39)
G*	0.53	0.60	0.74	0.19 (0.08,3.05)	0.20	0.22	0.24	0.17 (<0.05,1.12)

Table C-4. Summary of influent and effluent SRP FFCs for all monitored SCMs, with all values in mg/L as P. SCMs denoted with * represent those with effluent SRP data sets found to be statistically lower than corresponding influent SRP data sets at α=5%.

SCM	Influent				Effluent			
	Unweighted Mean	Weighted Mean	Standard Deviation	Median (Min, Max)	Unweighted Mean	Weighted Mean	Standard Deviation	Median (Min, Max)
A*	0.29	0.27	0.31	0.14 (<0.05,1.2)	0.08	0.09	0.05	0.09 (<0.05,0.19)
B	0.68	0.74	0.69	0.27 (0.05,2.6)	0.25	0.25	0.14	0.20 (<0.05,0.59)
C	0.61	0.62	0.61	0.35 (<0.05,2.2)	0.42	0.42	0.37	0.29 (<0.05,1.5)
D*	0.58	0.45	0.51	0.32 (0.09,1.9)	0.25	0.24	0.25	0.18 (<0.05,1.1)
E	0.19	0.17	0.15	0.13 (<0.05,0.62)	0.09	0.08	0.04	0.08 (<0.05,0.18)
F	0.41	0.45	0.52	0.14 (<0.05,2.0)	0.20	0.25	0.23	0.12 (<0.05,1.0)
G	0.31	0.37	0.36	0.16 (<0.05,1.3)	0.17	0.18	0.14	0.15 (<0.05,0.54)

Table C-5. Summary of influent and effluent DOP FFCs for all monitored SCMs, with all values in mg/L as P. SCMs denoted with * represent those with effluent DOP data sets found to be statistically lower than corresponding influent DOP data sets at α=5%.

SCM	Influent				Effluent			
	Unweighted Mean	Weighted Mean	Standard Deviation	Median (Min, Max)	Unweighted Mean	Weighted Mean	Standard Deviation	Median (Min, Max)
A*	0.11	0.12	0.16	0.06 (<0.05,0.68)	<0.05	<0.05	0.04	<0.05 (<0.05,0.2)
B*	0.21	0.24	0.33	0.08 (<0.05,1.3)	<0.05	<0.05	0.02	<0.05 (<0.05,0.1)
C*	0.28	0.31	0.54	0.15 (<0.05,2.4)	0.16	0.18	0.34	0.09 (<0.05,1.3)
D*	0.19	0.11	0.25	0.10 (<0.05,1.1)	<0.05	<0.05	0.01	0.05 (<0.05,0.09)
E*	0.07	0.08	0.14	<0.05 (<0.05,0.61)	<0.05	<0.05	0.02	<0.05 (<0.05,0.10)
F*	0.13	0.14	0.28	0.09 (<0.05,1.3)	0.08	0.08	0.19	<0.05 (<0.05,0.82)
G*	0.20	0.22	0.45	0.08 (<0.05,1.7)	0.05	0.05	0.12	<0.05 (<0.05,0.58)

Table C-6. Summary of influent and effluent PN FFCs for all monitored SCMs, with all values in mg/L as N. SCMs denoted with * represent those with effluent PN data sets found to be statistically lower than corresponding influent PN data sets at α=5%.

SCM	Influent				Effluent			
	Unweighted Mean	Weighted Mean	Standard Deviation	Median (Min, Max)	Unweighted Mean	Weighted Mean	Standard Deviation	Median (Min, Max)
A*	0.91	0.76	1.1	0.61 (<0.05,4.5)	0.22	0.25	0.36	0.10 (<0.05,1.6)
B*	1.1	0.79	1.4	0.36 (<0.05,4.8)	0.51	0.51	1.1	0.23 (<0.05,5.5)
C*	0.97	0.88	1.3	0.43 (<0.05,5.6)	0.58	0.49	0.73	0.25 (<0.05,2.6)
D*	2.5	0.85	4.7	0.47 (0.11,17.2)	0.48	0.40	1.2	0.22 (<0.05,5.4)
E*	0.62	0.55	0.62	0.33 (<0.05,2.4)	0.26	0.25	0.28	0.18 (<0.05,1.1)
F	2.0	1.0	4.5	0.3 (<0.05,20.7)	0.54	0.70	0.72	0.23 (<0.05,2.5)
G*	1.6	1.5	2.5	0.62 (<0.05,8.4)	0.23	0.24	0.21	0.18 (<0.05,0.82)

Table C-7. Summary of influent and effluent TDN FFCs for all monitored SCMs, with all values in mg/L as N. SCMs denoted with * represent those with effluent TDN data sets found to be statistically lower than corresponding influent TDN data sets at α=5%.

SCM	Influent				Effluent			
	Unweighted Mean	Weighted Mean	Standard Deviation	Median (Min, Max)	Unweighted Mean	Weighted Mean	Standard Deviation	Median (Min, Max)
A*	2.6	2.6	3.0	1.9 (0.51,14.6)	0.85	0.98	0.74	0.66 (0.25,3.9)
B	4.5	2.6	9.1	2.0 (0.73,45.2)	3.6	3.7	2.8	2.7 (0.70,11.4)
C	2.8	2.7	1.5	2.7 (0.96,6.1)	2.1	2.1	1.3	1.7 (0.43,5.5)
D*	6.1	3.2	10.5	1.6 (0.49,42.0)	1.4	1.2	1.1	0.97 (0.47,4.5)
E*	2.6	2.5	1.4	2.2 (0.85,5.9)	2.0	2.0	1.5	1.5 (0.70,5.9)
F	4.5	2.6	9.5	1.9 (0.64,46.9)	2.6	2.9	2.3	1.6 (0.46,8.8)
G*	2.5	2.4	1.5	2.0 (0.52,5.9)	3.7	3.5	2.3	3.3 (0.33,8.0)

Table C-8. Summary of influent and effluent NO_3^- FFCs for all monitored SCMs, with all values in mg/L as N. SCMs denoted with * represent those with effluent NO_3^- data sets found to be statistically higher than corresponding influent NO_3^- data sets at α=5%.

SCM	Influent				Effluent			
	Unweighted Mean	Weighted Mean	Standard Deviation	Median (Min, Max)	Unweighted Mean	Weighted Mean	Standard Deviation	Median (Min, Max)
A	0.48	0.42	0.49	0.34 (<0.05,1.9)	0.45	0.40	0.37	0.37 (0.09,1.7)
B*	0.46	0.44	0.40	0.41 (<0.05,1.5)	2.3	2.5	2.7	1.3 (<0.05,10.3)
C	0.50	0.41	0.38	0.42 (<0.05,1.5)	0.55	0.51	0.43	0.38 (<0.05,1.5)
D	1.7	1.6	5.0	0.52 (<0.05,23.4)	0.50	0.48	0.32	0.43 (<0.05,1.2)
E	0.75	0.72	0.35	0.68 (0.15,1.5)	1.1	0.91	0.69	0.93 (0.23,2.7)
F*	0.50	0.51	0.42	0.45 (<0.05,1.8)	1.1	1.1	0.91	0.72 (0.09,3.1)
G*	0.59	0.52	0.63	0.49 (<0.05,3.0)	2.4	2.0	2.1	1.7 (<0.05,6.6)

Table C-9. Summary of influent and effluent NO_2^- FFCs for all monitored SCMs, with all values in mg/L as N. SCMs denoted with * represent those with effluent NO_2^- data sets found to be statistically lower than corresponding influent NO_2^- data sets at α=5%.

SCM	Influent				Effluent			
	Unweighted Mean	**Weighted Mean**	**Standard Deviation**	**Median (Min, Max)**	**Unweighted Mean**	**Weighted Mean**	**Standard Deviation**	**Median (Min, Max)**
A	<0.05	<0.05	<0.05	<0.05 (<0.05,0.15)	<0.05	<0.05	0	<0.05 (<0.05,<0.05)
B	0.10	0.11	0.20	<0.05 (<0.05,0.78)	0.14	0.15	0.29	<0.05 (<0.05,0.97)
C	0.09	0.10	0.13	<0.05 (<0.05,0.49)	<0.05	0.05	0.04	<0.05 (<0.05,0.17)
D	0.18	0.19	0.28	<0.05 (<0.05,0.94)	0.05	0.05	0.11	<0.05 (<0.05,0.44)
E*	0.09	0.10	0.14	<0.05 (<0.05,0.51)	<0.05	<0.05	0	<0.05 (<0.05,<0.05)
F	0.13	0.14	0.27	<0.05 (<0.05,0.84)	0.11	0.12	0.23	<0.05 (<0.05,0.90)
G	0.15	0.16	0.24	<0.05 (<0.05,0.83)	0.10	0.11	0.15	<0.05 (<0.05,0.66)

Table C-10. Summary of influent and effluent NH_4^+ FFCs for all monitored SCMs, with all values in mg/L as N. SCMs denoted with * represent those with effluent NH_4^+ data sets found to be statistically lower than corresponding influent NH_4^+ data sets at α=5%.

SCM	Influent				Effluent			
	Unweighted Mean	**Weighted Mean**	**Standard Deviation**	**Median (Min, Max)**	**Unweighted Mean**	**Weighted Mean**	**Standard Deviation**	**Median (Min, Max)**
A*	0.29	0.32	0.39	0.21 (<0.05,1.9)	0.07	0.06	0.05	0.07 (<0.05,0.26)
B	0.51	0.19	1.4	0.20 (<0.05,6.8)	0.30	0.25	0.26	0.26 (<0.05,0.83)
C	0.30	0.30	0.33	0.18 (<0.05,1.1)	0.49	0.58	0.80	0.19 (<0.05,3.4)
D	0.33	0.18	0.52	0.12 (<0.05,1.8)	0.23	0.18	0.23	0.1 (<0.05,0.83)
E*	0.32	0.30	0.29	0.24 (<0.05,1.2)	0.17	0.16	0.17	0.12 (<0.05,0.59)
F	0.37	0.29	0.40	0.25 (<0.05,1.8)	0.51	0.79	1.2	0.18 (<0.05,5.5)
G*	0.23	0.23	0.18	0.20 (<0.05,0.58)	0.10	0.10	0.09	0.09 (<0.05,0.48)

Table C-11. Summary of influent and effluent DON FFCs for all monitored SCMs, with all values in mg/L as N. SCMs denoted with * represent those with effluent DON data sets found to be statistically lower than corresponding influent DON data sets at α=5%.

SCM	Influent				Effluent			
	Unweighted Mean	**Weighted Mean**	**Standard Deviation**	**Median (Min, Max)**	**Unweighted Mean**	**Weighted Mean**	**Standard Deviation**	**Median (Min, Max)**
A*	1.8	1.8	2.6	1.1 (<0.05,12.5)	0.31	0.51	0.70	0.13 (<0.05,3.5)
B*	3.4	1.9	7.5	1.4 (0.22,36.9)	0.95	0.80	1.1	0.47 (<0.05,3.6)
C*	1.8	1.9	1.1	1.8 (0.27,5.1)	1.0	0.94	0.92	0.77 (0.17,4.1)
D	3.9	1.2	9.1	0.51 (<0.05,39.6)	0.65	0.52	0.85	0.31 (<0.05,3.2)
E*	1.4	1.4	1.2	1.3 (0.12,5.0)	0.73	0.92	1.2	0.41 (<0.05,5.2)
F*	3.5	1.6	9.0	1.2 (0.18,44.3)	0.90	0.88	1.1	0.56 (<0.05,4.3)
G*	1.5	1.5	1.0	1.3 (0.15,3.5)	1.1	1.3	1.4	0.77 (<0.05,6.6)

Table C-12. Load reductions of Total Suspended Solids for SCMs A through G based on FFCs. No first flush factor was used for influent and effluent calculations.

SCM		A	B	C	D	E	F	G
TSS	**L_{in} in kg/ha-yr (lb/ac-yr)**	2018	1236	1079	870	1244	1637	1895
	L_{out} in kg/ha-yr (lb/ac-yr)	36	53	525	98	58	458	247
	L_{red} in kg/ha-yr (lb/ac-yr)	1982	1183	554	772	1186	1179	1649
	L_{red} in kg/yr (lb/yr)	498	172	103	184	327	358	2750
	% Reduction	**98%**	**96%**	**51%**	**89%**	**95%**	**72%**	**87%**

Table C-13. Load reductions of Phosphorus species for SCMs A through G based on FFCs. No first flush factor was used for influent and effluent calculations.

SCM		A	B	C	D	E	F	G
TN	**L_{in} in kg/ha-yr (lb/ac-yr)**	2.6 (2.3)	3.0 (2.7)	3.3 (2.9)	1.9 (1.7)	1.3 (1.1)	2.2 (2.0)	2.9 (2.6)
	L_{out} in kg/ha-yr (lb/ac-yr)	0.44 (0.40)	0.81 (0.72)	2.1 (1.9)	0.61 (0.54)	0.33 (0.29)	1.0 (0.92)	0.82 (0.73)
	L_{red} in kg/ha-yr (lb/ac-yr)	2.1 (1.9)	2.2 (2.0)	1.1 (1.0)	1.3 (1.2)	1.0 (0.85)	1.2 (1.0)	2.1 (1.9)
	L_{red} in kg/yr (lb/yr)	0.54 (0.48)	0.32 (0.29)	0.21 (0.19)	0.32 (0.28)	0.26 (0.23)	0.36 (0.32)	3.5 (3.1)
	% Red	**83%**	**73%**	**35%**	**69%**	**75%**	**53%**	**72%**
PN	**L_{in} in kg/ha-yr (lb/ac-yr)**	1.4 (1.3)	0.86 (0.77)	1.3 (1.2)	0.85 (0.76)	0.76 (0.68)	1.1 (1.0)	1.7 (1.5)
	L_{out} in kg/ha-yr (lb/ac-yr)	0.14 (0.13)	0.13 (0.11)	0.80 (0.72)	0.17 (0.15)	0.10 (0.09)	0.40 (0.36)	0.32 (0.29)
	L_{red} in kg/ha-yr (lb/ac-yr)	1.3 (1.2)	0.73 (0.65)	0.50 (0.44)	0.68 (0.61)	0.66 (0.59)	0.68 (0.61)	1.4 (1.2)
	L_{red} in kg/yr (lb/yr)	0.33 (0.29)	0.11 (0.10)	0.09 (0.08)	0.16 (0.15)	0.18 (0.16)	0.21 (0.19)	2.3 (2.1)
	% Red	**90%**	**85%**	**38%**	**80%**	**87%**	**63%**	**81%**

Table C-13 (continued). Load reductions of Phosphorus species for SCMs A through G based on FFCs. No first flush factor was used for influent and effluent calculations.

SCM		A	B	C	D	E	F	G
NO3	L_{in} in kg/ha-yr (lb/ac-yr)	0.83 (0.74)	0.78 (0.70)	0.93 (0.83)	2.1 (1.9)	1.2 (1.1)	0.87 (0.78)	0.93 (0.83)
	L_{out} in kg/ha-yr (lb/ac-yr)	0.81 (0.72)	4.1 (3.6)	0.94 (0.83)	0.72 (0.64)	1.6 (1.4)	1.8 (1.6)	4.2 (3.8)
	L_{red} in kg/ha-yr (lb/ac-yr)	0.02 (0.02)	-3.3 (-2.9)	0.01 (0)	1.4 (1.2)	-0.39 (-0.34)	-0.89 (-0.80)	-3.3 (-2.9)
	L_{red} in kg/yr (lb/yr)	0 (0)	-0.48 (-0.43)	0 (0)	0.33 (0.30)	-0.11 (-0.09)	-0.27 (-0.24)	-5.5 (-4.9)
	% Red	**2%**	**-420%**	**0%**	**66%**	**-31%**	**-103%**	**-354%**
NO2	L_{in} in kg/ha-yr (lb/ac-yr)	0.16 (0.15)	0.22 (0.2)	0.19 (0.17)	0.26 (0.23)	0.16 (0.14)	0.22 (0.2)	0.27 (0.24)
	L_{out} in kg/ha-yr (lb/ac-yr)	0.05 (0.04)	0.25 (0.22)	0.08 (0.07)	0.07 (0.06)	0.04 (0.04)	0.19 (0.17)	0.19 (0.17)
	L_{red} in kg/ha-yr (lb/ac-yr)	0.11 (0.10)	-0.02 (-0.02)	0.11 (0.1)	0.19 (0.17)	0.12 (0.1)	0.04 (0.03)	0.08 (0.07)
	L_{red} in kg/yr (lb/yr)	0.03 (0.03)	0 (0)	0.02 (0.02)	0.04 (0.04)	0.03 (0.03)	0.01 (0.01)	0.13 (0.12)
	% Red	**70%**	**-11%**	**57%**	**73%**	**74%**	**17%**	**30%**
NH4	L_{in} in kg/ha-yr (lb/ac-yr)	0.66 (0.58)	0.79 (0.71)	0.64 (0.57)	0.41 (0.37)	0.62 (0.56)	0.64 (0.57)	0.46 (0.41)
	L_{out} in kg/ha-yr (lb/ac-yr)	0.15 (0.13)	0.54 (0.48)	1.2 (1.1)	0.33 (0.3)	0.29 (0.26)	1.1 (1.0)	0.19 (0.17)
	L_{red} in kg/ha-yr (lb/ac-yr)	0.51 (0.46)	0.26 (0.23)	-0.59 (-0.53)	0.08 (0.07)	0.34 (0.3)	-0.49 (-0.44)	0.27 (0.24)
	L_{red} in kg/yr (lb/yr)	0.13 (0.11)	0.04 (0.03)	-0.11 (-0.1)	0.02 (0.02)	0.09 (0.08)	-0.15 (-0.13)	0.45 (0.4)
	% Red	**78%**	**32%**	**-93%**	**19%**	**54%**	**-77%**	**59%**
DON	L_{in} in kg/ha-yr (lb/ac-yr)	4.0 (3.5)	5.4 (4.8)	3.6 (3.2)	4.5 (4.0)	2.6 (2.3)	5.3 (4.7)	2.7 (2.4)
	L_{out} in kg/ha-yr (lb/ac-yr)	0.90 (0.80)	1.9 (1.7)	1.8 (1.6)	0.92 (0.82)	1.5 (1.3)	1.4 (1.2)	2.2 (1.9)
	L_{red} in kg/ha-yr (lb/ac-yr)	3.1 (2.7)	3.5 (3.1)	1.7 (1.5)	3.6 (3.2)	1.1 (1.0)	3.9 (3.5)	0.57 (0.51)
	L_{red} in kg/yr (lb/yr)	0.77 (0.69)	0.52 (0.46)	0.32 (0.29)	0.85 (0.76)	0.31 (0.28)	1.2 (1.1)	0.95 (0.85)
	% Red	**77%**	**65%**	**48%**	**80%**	**44%**	**74%**	**21%**

Table C-14. Load reductions of Phosphorus species for SCMs A through G based on FFCs. No first flush factor was used for influent and effluent calculations.

SCM		A	B	C	D	E	F	G
TP	L_{in} in kg/ha-yr (lb/ac-yr)	2.6 (2.3)	3.0 (2.7)	3.3 (2.9)	1.9 (1.7)	1.3 (1.1)	2.2 (2.0)	2.9 (2.6)
	L_{out} in kg/ha-yr (lb/ac-yr)	0.44 (0.40)	0.81 (0.72)	2.1 (1.9)	0.61 (0.54)	0.33 (0.29)	1.0 (0.92)	0.82 (0.73)
	L_{red} in kg/ha-yr (lb/ac-yr)	2.1 (1.9)	2.2 (2.0)	1.1 (1.0)	1.3 (1.2)	1.0 (0.85)	1.2 (1.0)	2.1 (1.9)
	L_{red} in kg/yr (lb/yr)	0.54 (0.48)	0.32 (0.29)	0.21 (0.19)	0.32 (0.28)	0.26 (0.23)	0.36 (0.32)	3.5 (3.1)
	% Red	**83%**	**73%**	**35%**	**69%**	**75%**	**53%**	**72%**
PP	L_{in} in kg/ha-yr (lb/ac-yr)	1.4 (1.3)	0.86 (0.77)	1.3 (1.2)	0.85 (0.76)	0.76 (0.68)	1.1 (1.0)	1.7 (1.5)
	L_{out} in kg/ha-yr (lb/ac-yr)	0.14 (0.13)	0.13 (0.11)	0.80 (0.72)	0.17 (0.15)	0.10 (0.09)	0.40 (0.36)	0.32 (0.29)
	L_{red} in kg/ha-yr (lb/ac-yr)	1.3 (1.2)	0.73 (0.65)	0.50 (0.44)	0.68 (0.61)	0.66 (0.59)	0.68 (0.61)	1.4 (1.2)
	L_{red} in kg/yr (lb/yr)	0.33 (0.29)	0.11 (0.10)	0.09 (0.08)	0.16 (0.15)	0.18 (0.16)	0.21 (0.19)	2.3 (2.1)
	% Red	**90%**	**85%**	**38%**	**80%**	**87%**	**63%**	**81%**
SRP	L_{in} in kg/ha-yr (lb/ac-yr)	0.75 (0.66)	1.6 (1.4)	1.3 (1.1)	0.83 (0.74)	0.36 (0.32)	0.79 (0.70)	0.74 (0.66)
	L_{out} in kg/ha-yr (lb/ac-yr)	0.21 (0.18)	0.55 (0.49)	0.91 (0.81)	0.40 (0.35)	0.17 (0.15)	0.46 (0.41)	0.36 (0.32)
	L_{red} in kg/ha-yr (lb/ac-yr)	0.54 (0.48)	1.0 (0.90)	0.36 (0.32)	0.43 (0.38)	0.19 (0.17)	0.33 (0.29)	0.38 (0.34)
	L_{red} in kg/yr (lb/yr)	0.14 (0.12)	0.15 (0.13)	0.07 (0.06)	0.10 (0.09)	0.05 (0.05)	0.10 (0.09)	0.63 (0.56)
	% Red	**72%**	**65%**	**28%**	**52%**	**54%**	**42%**	**51%**
DOP	L_{in} in kg/ha-yr (lb/ac-yr)	0.39 (0.35)	0.59 (0.53)	0.69 (0.61)	0.25 (0.23)	0.16 (0.14)	0.34 (0.3)	0.48 (0.43)
	L_{out} in kg/ha-yr (lb/ac-yr)	0.10 (0.09)	0.13 (0.12)	0.42 (0.37)	0.04 (0.04)	0.06 (0.05)	0.17 (0.15)	0.14 (0.12)
	L_{red} in kg/ha-yr (lb/ac-yr)	0.30 (0.26)	0.46 (0.41)	0.27 (0.24)	0.21 (0.19)	0.10 (0.09)	0.16 (0.15)	0.35 (0.31)
	L_{red} in kg/yr (lb/yr)	0.07 (0.07)	0.07 (0.06)	0.05 (0.04)	0.05 (0.05)	0.03 (0.02)	0.05 (0.04)	0.58 (0.52)
	% Red	**75%**	**77%**	**39%**	**84%**	**62%**	**49%**	**72%**

Table C-15. Water Quality Data. All values in mg/L. Values denoted with * represent quality assurance / quality control measurements.

Event	Species	SCM A		SCM B		SCM C		SCM D		SCM E		SCM F		SCM G	
		In	Out	In	Out	In	Out	In	Out	In	Out	In	Out	In	Out
06/21/2016	TSS	686	10	810	10	1168	312	827	14	1479	26	845	22	1147	50
	TP	1.54	0.08	1.32	0.42	2.43	1.64	1.79	0.33	2.06	0.17	1.31	1.60	2.18	0.52
	PP	1.50	<0.05	1.06	0.21	2.21	0.54	1.55	0.16	1.92	0.13	1.07	0.21	2.02	0.32
	TDP	<0.05	0.05	0.25	0.21	0.22	1.11	0.24	0.17	0.14	<0.05	0.24	1.39	0.16	0.20
	SRP	<0.05	<0.05	0.18	0.16	0.20	0.95	0.18	0.12	0.10	<0.05	0.14	1.03	0.09	0.15
	DOP	<0.05	<0.05	0.07	0.05	<0.05	0.16	0.06	<0.05	<0.05	<0.05	0.10	0.36	0.07	<0.05
	TN	2.04	4.86	1.93	7.05	1.70	4.86	1.54	2.93	3.91	6.25	2.02	10.54	3.39	6.34
	PN	1.07	1.01	0.16	1.05	0.34	1.01	0.24	0.30	0.47	0.33	0.30	1.75	0.68	0.34
	TDN	0.97	3.85	1.78	6.00	1.36	3.85	1.30	2.63	3.45	5.92	1.72	8.79	2.71	6.00
	NO3	<0.05	0.21	0.47	3.28	0.25	<0.05	0.19	0.91	0.36	0.47	0.43	0.82	0.23	4.15
	NO2	<0.05	<0.05	<0.05	0.97	0.19	<0.05	0.30	0.09	0.51	<0.05	<0.05	0.58	0.47	0.66
	NH4	0.12	0.11	0.31	0.34	0.25	3.44	0.12	0.54	0.89	0.19	0.60	5.49	0.53	0.15
	DON	0.88	3.55	0.96	1.41	0.68	0.43	0.69	1.09	1.69	5.24	0.67	1.91	1.49	1.05
06/28/2016	TSS	178	3	167	5	308	11	615	5	14	3	348	7	386	5
	TP	0.54	<0.05	0.53	0.27	0.78	0.19	1.22	0.12	0.26	0.12	0.39	0.12	0.79	0.12
	PP	0.52	<0.05	0.45	0.07	0.72	0.06	1.10	0.07	0.18	<0.05	0.35	<0.05	0.71	<0.05
	TDP	<0.05	<0.05	0.09	0.20	0.06	0.14	0.12	0.05	0.08	0.07	<0.05	0.08	0.08	0.08
	SRP	<0.05	<0.05	0.07	0.20	<0.05	0.14	0.09	<0.05	0.07	0.07	<0.05	0.08	0.06	0.07
	DOP	<0.05	<0.05	<0.05	<0.05	<0.05	<0.05	<0.05	<0.05	<0.05	<0.05	<0.05	<0.05	<0.05	<0.05
	TN	1.35	0.53	1.49	1.28	1.42	1.89	1.53	2.00	1.55	1.79	0.84	1.54	1.58	3.98
	PN	0.27	0.07	0.30	0.09	0.45	0.21	0.46	0.29	0.29	0.25	0.20	0.23	0.18	0.18
	TDN	1.08	0.46	1.19	1.19	0.97	1.67	1.07	1.71	1.26	1.54	0.64	1.31	1.41	3.80

	NO3	0.35	0.11	0.45	0.43	0.37	1.10	0.32	0.88	0.52	0.85	0.20	0.57	0.54	2.12
	NO2	<0.05	<0.05	<0.05	0.96	0.21	<0.05	0.27	0.08	0.41	<0.05	<0.05	0.90	0.49	0.38
	NH4	0.08	0.09	0.24	0.33	0.08	0.23	0.22	0.26	0.09	0.21	0.11	0.27	0.17	0.11
	DON	0.66	0.28	0.47	<0.05	0.31	0.36	0.26	0.49	0.24	0.46	0.32	<0.05	0.21	1.20
07/04 /2016	TSS	151	6	129	3	121	2	91	8	36	2	63	7	166	3
	TP	0.30	<0.05	0.66	0.26	0.84	0.20	0.62	0.09	0.29	<0.05	0.34	0.14	0.72	0.09
	PP	0.29	<0.05	0.45	<0.05	0.45	<0.05	0.22	<0.05	0.14	<0.05	0.18	0.07	0.58	<0.05
	TDP	<0.05	<0.05	0.20	0.22	0.39	0.17	0.40	0.06	0.15	<0.05	0.16	0.07	0.14	0.08
	SRP	<0.05	<0.05	0.16	0.22	0.25	0.14	0.24	0.06	0.14	<0.05	0.12	0.11	0.11	0.08
	DOP	<0.05	<0.05	<0.05	<0.05	0.14	<0.05	0.16	<0.05	<0.05	<0.05	<0.05	<0.05	<0.05	<0.05
	TN	0.80	0.46	2.19	2.34	3.93	1.87	2.13	1.11	1.91	1.00	2.13	1.55	3.41	1.45
	PN	0.16	0.08	0.21	<0.05	0.38	0.14	0.13	0.07	<0.05	0.10	0.19	0.05	0.14	<0.05
	TDN	0.64	0.37	1.98	2.30	3.55	1.73	2.00	1.04	1.87	0.90	1.94	1.50	3.26	1.46
	NO3	<0.05	0.12	0.77	0.53	1.02	0.70	0.63	0.38	0.81	0.56	0.56	0.77	0.53	0.87
	NO2	<0.05	<0.05	<0.05	<0.05	0.28	0.13	<0.05	<0.05	<0.05	<0.05	<0.05	<0.05	<0.05	<0.05
	NH4	0.05	0.05	0.10	0.50	0.06	0.21	0.07	0.28	0.14	0.12	0.16	0.27	0.10	<0.05
	DON	0.59	0.21	1.09	1.28	2.19	0.70	1.28	0.38	0.92	0.22	1.22	0.46	2.62	0.56
07/16 /2016	TSS	146	14	170	12	331	24	52	14*	30*	16	101*	26*	235	47
	TP	0.74	0.07	0.83*	0.38*	1.89	0.46	1.57	5.70	0.29*	0.20*	0.78	0.67	0.89	0.14
	PP	0.46	0.07	0.43	0.13	0.90	0.34	0.78	2.97	<0.05	0.07	0.19	0.22	0.74	0.10
	TDP	0.28	<0.05	0.41*	0.26*	0.99	0.12	0.78	2.73	0.24*	0.12*	0.59	0.45	0.15	<0.05
	SRP	0.12	<0.05	0.27*	0.21*	0.33	<0.05	0.53	0.76	0.16*	0.08*	0.42	0.38	<0.05	<0.05
	DOP	0.17	<0.05	0.14	<0.05	0.66	0.10	0.25	1.97	0.08	<0.05	0.17	0.08	0.12	<0.05
	TN	1.89	0.37	2.13*	6.70*	3.98	1.99	4.02	2.32	2.49*	5.47*	3.24	9.39	3.54	7.02
	PN	0.66	<0.05	0.35	0.32	0.39	0.45	1.12	0.31	0.15	0.05	0.30	0.60	0.49	0.32
	TDN	1.23	0.40	1.78*	6.38*	3.60	1.53	2.90	2.01	2.34*	5.41*	2.94	8.79	3.05	6.70
	NO3	<0.05	0.09	<0.05*	4.96*	0.42	<0.05	<0.05	0.21	0.69*	2.46*	<0.05	2.42	<0.05	5.89

	NO2	<0.05	<0.05	0.09*	<0.05*	0.35	<0.05	<0.05	0.44	<0.05*	<0.05*	<0.05	<0.05	<0.05	0.08
	NH4	<0.05	0.06	0.25*	0.67*	0.35	0.06	0.21	0.08	0.39*	0.59*	0.72	2.07	0.38	<0.05
	DON	1.18	0.25	1.41	0.73	2.47	1.44	2.67	1.29	1.23	2.34	2.20	4.27	2.64	0.70
07/28/2016	TSS	2396	2	192	4	91	7	153	7	47	3	183	4	477	6
	TP	3.77	0.18	1.84	0.31	1.21	0.67	1.19	0.15	0.28	0.14	0.70	0.19	0.79*	0.16
	PP	3.43	<0.05	0.27	0.10	0.08	0.16	0.46	0.08	0.12	<0.05	0.34	0.05	0.68	0.06
	TDP	0.33	0.13	1.57	0.22	1.12	0.51	0.73	0.07	0.16	0.09	0.35	0.14	0.11*	0.11
	SRP	0.21	0.14	1.06	0.20	0.75	0.46	0.53*	<0.05*	0.13	0.08	0.18	0.12	0.07	0.07
	DOP	0.12	<0.05	0.51	<0.05	0.38	0.05	0.20	<0.05	<0.05	<0.05	0.17	<0.05	<0.05	<0.05
	TN	2.29	0.96	3.60	5.47	4.41	3.38	3.85	0.89	1.97	1.89	3.49	3.66	0.81*	6.64*
	PN	0.26	<0.05	0.37	0.38	0.30	0.24	0.23	0.07	0.12	<0.05	0.40	0.20	0.05	0.08
	TDN	2.02	0.93	3.24	5.09	4.11	3.14	3.62	0.82	1.85	1.85	3.10	3.46	0.76*	6.57*
	NO3	<0.05	0.69	<0.05	4.68	0.80	0.91	<0.05	0.40	0.81	1.28	<0.05	2.97	0.28*	6.58*
	NO2	<0.05	<0.05	0.78*	<0.05	0.49	<0.05	0.94	<0.05	<0.05	<0.05	0.84*	<0.05	<0.05	<0.05
	NH4	0.50	<0.05	0.06	0.48*	0.09	0.70*	0.06	0.08	0.18	0.15	0.21	0.27	0.06	0.06
	DON	1.54	0.23	2.39	<0.05	2.73	1.49	2.61	0.36	0.85	0.44	2.04	0.23	0.44	<0.05
08/15/2016	TSS	461	11*	380	8	215	263	146	35	226	8	313*	56	194	39
	TP	1.77	0.15	2.20	0.27	3.89	1.94	2.27	1.19	1.23	0.27	1.54	0.35	1.23	0.31
	PP	1.40	<0.05	1.25	0.11	1.55	1.57	0.68	0.13	0.22	0.10	0.75	0.09	0.42	0.13
	TDP	0.37	0.11	0.95	0.16	2.33	0.37	1.59	1.06	1.00	0.17	0.79	0.26	0.81	0.18
	SRP	0.33	0.12	0.88	0.15	1.67	0.31	1.20	1.05	0.39	0.10	0.64	0.25	0.63	0.19
	DOP	<0.05	<0.05	0.07	<0.05	0.66	0.07	0.39	<0.05	0.61	0.06	0.15	<0.05	0.18	<0.05
	TN	2.44	1.39	2.67	11.51	3.29	2.38	2.04	0.72	2.22	2.74	4.00	5.49	3.35	8.11
	PN	0.50	0.28	0.27	0.15	0.35	0.36	0.49	0.07	0.17	0.09	0.18	0.39	0.23	0.09
	TDN	1.94	1.11	2.40	11.36	2.94	2.01	1.55	0.65	2.05	2.65	3.83	5.10	3.13	8.03
	NO3	0.33	0.94	0.13	10.25	0.12	0.89	0.21	0.15	0.15	2.13	0.15	3.08	0.22	1.20
	NO2	<0.05	<0.05	0.16	<0.05	<0.05	0.07	0.84	0.28	0.06	<0.05	0.83	0.05	0.83	0.13

	NH4	0.41	0.15	0.06	0.54	0.08	0.33	0.06	<0.05	0.07	0.27	0.15	0.56	0.08	0.08
	DON	1.17	<0.05	2.05	0.54	2.74	0.72	0.44	0.17	1.78	0.23	2.69	1.41	1.99	6.61
08/17/2016	TSS	421	<1*	559*	<1*	879	9	473	3	345	54	581	6	445	47
	TP	0.41	0.12	0.65	0.25	2.63	1.13	1.03	0.39	0.31	0.13	0.50	0.12	0.55	0.27
	PP	0.31	<0.05	0.49	<0.05	2.25	0.84	0.73	0.10	0.08	0.05	0.37	0.09	0.39	0.08
	TDP	0.10	0.10	0.16	0.20	0.37	0.30	0.31	0.29	0.23	0.07	0.13	<0.05	0.16	0.19
	SRP	0.07	0.10	0.14	0.19	0.35	0.27	0.26	0.29	0.18	0.06	0.11	<0.05	0.12	0.19
	DOP	<0.05	<0.05	<0.05	<0.05	<0.05	<0.05	<0.05	<0.05	<0.05	<0.05	<0.05	<0.05	<0.05	<0.05
	TN	0.87	1.51	0.94	2.15	1.49	2.50	1.37	1.07	4.43	1.52	1.52	0.99	1.07	1.44
	PN	0.09	0.32	0.21	0.23	0.18	0.15	0.47	0.26	0.27	0.50	<0.05	0.18	0.10	0.15
	TDN	0.78	1.20	0.73	1.93	1.32	2.35	0.90	0.81	4.16	1.02	1.48	0.81	0.97	1.29
	NO3	0.33	1.02	0.37	1.52	0.29	0.78	0.37	0.55	1.00	0.87	0.52	0.52	0.43	0.96
	NO2	<0.05	<0.05	<0.05	<0.05*	0.08	0.09	<0.05	<0.05	<0.05	<0.05	<0.05	<0.05	<0.05	<0.05
	NH4	<0.05	<0.05	<0.05	<0.05	0.10	0.42	<0.05	0.10	0.39	<0.05	0.09	0.05	<0.05	<0.05
	DON	0.41	0.12	0.34	0.39	0.84	1.06	0.48	0.14	2.73	0.11	0.84	0.22	0.51	0.31
08/21/2016	TSS	159	8*	303	3	72	-	419	11	241*	-	366	21	306	30
	TP	0.94	0.14	1.91	0.26	0.68	-	1.05	0.49	0.94	-	2.20	0.22	0.94	0.18
	PP	0.25	<0.05	0.62	<0.05	<0.05	-	0.78	0.09	0.17	-	0.83	0.05	0.67	0.05
	TDP	0.69	0.12	1.30	0.24	0.63	-	0.27	0.41	0.78	-	1.36	0.16	0.27	0.13
	SRP	0.53	0.10	1.11	0.22	0.56	-	0.22	0.38	0.62	-	1.13	0.12	0.20	0.10
	DOP	0.16	<0.05	0.19	<0.05	0.08	-	0.05	<0.05	0.16	-	0.23	<0.05	0.07	<0.05
	TN	1.74	0.81	2.09	1.88	2.00	-	1.33	1.02	1.18	-	3.10	1.72	2.25	3.05
	PN	<0.05	<0.05	0.80	<0.05	<0.05	-	0.28	0.05	0.13	-	1.17	0.12	0.97	0.49
	TDN	1.73	0.79	1.28	1.87	2.01	-	1.05	0.97	1.05	-	1.94	1.60	1.28	2.56
	NO3	<0.05	0.64	0.11	1.49	0.37	-	0.49	0.57	0.63	-	0.19	1.18	0.30	2.31
	NO2	<0.05	<0.05	<0.05	<0.05	<0.05	-	<0.05	<0.05	<0.05	-	<0.05	<0.05	0.11	<0.05*
	NH4	0.09	0.07	0.06	0.26	<0.05	-	0.05	0.05	0.13	-	0.38	0.16	0.08*	0.12

	DON	1.63	0.08	1.12	0.12	1.55	-	0.50	0.34	0.28	-	1.37	0.25	0.79	0.13
09/19/2016	TSS	343	<1	401	10*	245	80	184	4	288*	9	305	105	507	523
	TP	1.51	0.16	4.24	0.33	2.94	0.91	1.41	0.32	1.06	0.23	1.22	0.55	2.87	1.26
	PP	0.54	<0.05	0.37	<0.05	0.62	0.19	0.42	<0.05	0.45	0.06	0.66	0.32	1.44	0.63
	TDP	0.96	0.14	3.86	0.30	2.32	0.72	0.99	0.34	0.61	0.17	0.56	0.23	1.43	0.63
	SRP	0.71	0.15	2.57	0.48	1.42	0.58	0.85	0.30	0.42	0.16	0.40	0.21	1.13	0.54
	DOP	0.25	<0.05	1.30	<0.05	0.90	0.13	0.14	<0.05	0.18	<0.05	0.16	<0.05	0.30	0.09
	TN	5.59	0.54	10.56	8.36	4.63	2.87	29.36*	1.04	3.61	3.80	4.20	2.89	5.25	5.16
	PN	0.84	<0.05	2.43	<0.05	0.59	0.46	4.58	0.08	0.08	0.18	1.18	0.41	0.47	0.60
	TDN	4.75	0.52	8.13	8.35	4.04	2.41	24.78*	0.96	3.53	3.62	3.02	2.48	4.78	4.56
	NO3	1.70	0.37	1.46	7.79	1.09	1.04	23.41*	0.55	1.45	2.65	1.25	2.27	1.29	2.83
	NO2	<0.05	<0.05	0.59	<0.05	0.06	<0.05	0.59	<0.05	0.20	<0.05	0.60	<0.05	0.65	0.05
	NH4	0.39	<0.05	0.29	0.83	1.14	0.45	0.41	0.09	0.38	0.53	0.29	0.13	0.33	0.48
	DON	2.67	0.12	6.37	<0.05	1.75	0.91	0.36	0.31	1.50	0.43	1.48	0.09	2.51	1.25
09/29/2016	TSS	99	4	311	10	56	33	198	22	288	3*	143	54	238*	20
	TP	0.48	0.14	1.67	0.32	1.94	0.70	0.58	0.34	0.24	0.19	0.46	0.30	0.98	0.22
	PP	0.20	<0.05	0.23	<0.05	0.40	0.18	0.33	0.09	0.06	0.08	0.30	0.11	0.47	0.12
	TDP	0.28	0.16	1.44	0.32	1.54	0.52	0.25	0.25	0.17	0.11	0.16	0.19	0.52	0.10
	SRP	0.19	0.12	1.01	0.23	1.00	0.36	0.21	0.23	0.13	0.10	0.13	0.14	0.35	0.11
	DOP	0.09	<0.05	0.44	0.09	0.54	0.16	<0.05	<0.05	<0.05	<0.05	<0.05	<0.05	0.17	<0.05
	TN	0.76	0.55	1.03	2.98	1.55	1.78	0.62	0.69	1.88	1.31	0.91	3.66	1.01	2.65
	PN	0.26	0.13	0.05	0.10	0.24	0.14	0.13	0.10	0.16	0.28	0.06	0.27	<0.05	<0.05
	TDN	0.51	0.43	0.98	2.88	1.30	1.64	0.49	0.60	1.72	1.03	0.88	3.39	1.01	2.64
	NO3	0.21	0.44	<0.05	2.46	<0.05	1.09	0.25	0.54	1.35	1.03	0.57	2.53	<0.05	<0.05
	NO2	<0.05	<0.05	<0.05	<0.05	<0.05	0.17	<0.05	<0.05	<0.05	<0.05	<0.05	0.20	<0.05	<0.05
	NH4	<0.05	<0.05	<0.05	0.18	<0.05	0.12	<0.05	0.07	0.15	<0.05	<0.05	0.27	<0.05	<0.05
	DON	0.27	<0.05	0.94	0.25	1.29	0.27	0.21	<0.05	0.21	<0.05	0.27	0.39	0.99	2.60

11/30/2016	TSS	545	31	166	5	20*	34	29	81	57	10	273	413	238	3*
	TP	0.35	0.23	0.75	0.52	2.23	2.59	1.04	0.70	0.22	0.11	0.65	0.28	3.40	1.79
	PP	0.08	0.06	0.08	<0.05	0.19	0.09	0.37	<0.05	0.06	<0.05	<0.05	0.17	0.35	0.67
	TDP	0.27	0.16	0.67	0.51	2.04	2.50	0.68	0.69	0.16	0.09	0.61	0.11	3.05	1.12
	SRP	0.15	0.15	0.56	0.45	1.50	1.52	0.41	0.67	0.15	0.09	0.47	0.11	1.31	0.54
	DOP	0.12	<0.05	0.11	0.06	0.54	0.99	0.27	<0.05	<0.05	<0.05	0.15	<0.05	1.74	0.58
	TN	3.35	0.38	3.71	6.56	5.17	1.79	5.71	6.44	2.69	2.00	0.90	4.42	1.54	0.34
	PN	1.07	0.13	0.69	5.51	1.61	0.28	4.66	5.42	0.81	0.80	0.18	0.57	0.47	<0.05
	TDN	2.28	0.25	3.01	1.06	3.56	1.51	1.05	1.02	1.88	1.20	0.72	3.85	1.06	0.33
	NO3	0.31	0.23	0.41	0.86	<0.05	0.18	0.95	0.93	1.23	1.00	0.30	0.18	0.24	0.18
	NO2	<0.05	<0.05	0.06*	<0.05	<0.05	<0.05	<0.05	<0.05	0.09	<0.05	<0.05	0.13	<0.05	<0.05
	NH4	<0.05	<0.05	<0.05	<0.05	0.07	<0.05	<0.05	<0.05	<0.05	<0.05	<0.05	0.08	<0.05	<0.05
	DON	1.90	<0.05	2.54	0.19	3.47	1.30	0.06	<0.05	0.53	0.21	0.40	3.46	0.81	0.15
12/06/2016	TSS	44*	8	117	1*	31	34	31	18	83	18	135	132	90	10
	TP	1.43	0.45	3.13	0.82	5.21	2.54	2.88	0.60	0.39	0.32	4.32	1.57	4.26	0.36
	PP	0.56	0.31	0.21	0.20	0.59	0.29	0.57	<0.05	0.13	0.09	0.96	0.83	2.62	<0.05
	TDP	0.87	0.15	2.92	0.62	4.62	2.24	2.32	0.59	0.26	0.22	3.35	0.74	1.65	0.34
	SRP	0.76	0.11	2.04	0.59	2.22	0.96	1.87	0.57	0.25	0.18	2.04	0.67	0.33	0.34
	DOP	0.11	<0.05	0.87	<0.05	2.40	1.29	0.44	<0.05	<0.05	<0.05	1.31	0.07	1.32	<0.05
	TN	0.71	0.32	1.18	5.29	1.58	1.64	1.46	0.50	2.31	1.03	0.91	3.67	1.27	3.65
	PN	<0.05	<0.05	0.27	<0.05	0.15	0.17	0.12	<0.05	0.37	<0.05	0.14	2.20	0.75	0.82
	TDN	0.68	0.30	0.92	5.27	1.43	1.48	1.34	0.47	1.94	1.02	0.77	1.46	0.52	2.83
	NO3	0.51	0.19	0.44	4.83	0.23	0.24	1.22	0.28	1.06	0.93	0.26	0.58	0.36	1.22
	NO2	0.15	<0.05	<0.05	<0.05	<0.05	<0.05	0.05	<0.05	<0.05	<0.05	<0.05	<0.05	<0.05	<0.05
	NH4	<0.05	<0.05	0.07	<0.05	0.18	<0.05	0.05	<0.05	0.36*	<0.05	<0.05	<0.05	<0.05	0.08
	DON	<0.05	0.12	0.36	0.39	0.97	1.19	<0.05	0.18	0.51	0.06	0.50	0.85	0.17	1.54
	TSS	224	4	38	3	31	12*	39*	7	57	7	83	20	65	2

12/17/2016	TP	0.28	0.07	0.24	0.23	1.90	0.91	1.11	0.19	0.12	0.07	0.11	1.00	0.35	0.27
	PP	0.17	<0.05	0.08	0.07	0.09	0.06	0.09	<0.05	<0.05	<0.05	0.06	<0.05	0.25	0.14
	TDP	0.11	0.07	0.16	0.16	1.80	0.85	1.02	0.19	0.10	0.05	0.05	0.95	0.10	0.13
	SRP	0.09	0.07	0.15	0.14	1.28	0.76	0.98	0.18	0.09	0.05	0.06	0.13	0.09	0.12
	DOP	<0.05	<0.05	<0.05	<0.05	0.52	0.09	<0.05	<0.05	<0.05	<0.05	<0.05	0.82	<0.05	<0.05
	TN	1.92	1.88	2.11	2.01	2.67	2.09	1.29	1.16	2.04	1.95	1.64	1.71	0.90	0.89
	PN	1.09	1.59	0.84	0.41	1.51	1.05	0.55	0.48	1.20	1.06	0.10	0.12	0.15	0.14
	TDN	0.83	0.29	1.28	1.59	1.16	1.04	0.74	0.68	0.85	0.90	1.53	1.59	0.75	0.75
	NO3	0.72	0.29	0.59	1.16	0.37	0.37	0.55	0.41	0.59	0.37	0.78	0.70	0.52	0.51
	NO2	0.05	<0.05	<0.05	<0.05	<0.05	<0.05	<0.05	<0.05	<0.05	<0.05	<0.05	<0.05	<0.05	<0.05
	NH4	0.07	<0.05	0.09	<0.05	<0.05	<0.05	<0.05	0.06	0.10	<0.05	0.12	0.11	0.07	<0.05
	DON	<0.05	<0.05	0.55	0.40	0.74	0.65	0.17	0.20	0.12	0.50	0.58	0.74	0.15	0.25
01/03/2017	TSS	356*	7	63	<1	28	19	42	3	74	17	217	20*	295	23
	TP	0.33	0.09	0.37	0.215*	0.53	0.98	0.41	0.16	0.17*	0.08	0.33	0.20	0.50	0.23
	PP	0.20	<0.05	0.14	<0.05	0.11	0.19	0.06	<0.05	0.06	<0.05	0.20	0.06	0.37	0.06
	TDP	0.12	0.08	0.24	0.20	0.41	0.79	0.35	0.12	0.11	0.06	0.13*	0.14	0.13	0.18
	SRP	0.08	0.07	0.16	0.18	0.26	0.60	0.27	0.11	0.07	0.05	0.08	0.11	0.08	0.15
	DOP	<0.05	<0.05	0.08	<0.05	0.15	0.19	0.08	<0.05	<0.05	<0.05	0.05	<0.05	0.06	<0.05
	TN	2.13	0.71	3.10	2.00	2.79	1.32	1.69	0.85	2.84	1.83	2.40	1.29	1.64	1.78
	PN	0.17	0.07	0.33	0.10	0.43	0.26	0.11	0.15	<0.05	0.19	<0.05	0.15	<0.05	0.31
	TDN	1.96	0.64	2.77	1.90	2.36	1.07	1.58	0.70*	2.83	1.64	2.36	1.15	1.63	1.47
	NO3	0.65	0.38	0.85	1.01	0.43	0.23	0.60	0.28	0.67*	0.97	0.67	0.54	0.61*	0.75
	NO2	0.07	<0.05	0.09	<0.05	0.08	<0.05	<0.05	<0.05	<0.05	<0.05	<0.05	<0.05	<0.05	<0.05
	NH4	0.13	<0.05	0.11	<0.05	0.06	<0.05	0.05	0.06	0.20	<0.05	0.19	0.06	0.15	0.07
	DON	1.11	0.25	1.70	0.86	1.79	0.81	0.93	0.38	1.94	0.64	1.51	0.56	0.87	0.66
01/23/2017	TSS	147	14	270	2	18	79	42	37	195	7*	270*	6	462	20
	TP	0.47	0.15	0.66	0.29*	0.26	0.55	0.43	0.18	0.58	0.12	0.57	0.12	0.97	0.25

	PP	0.37	<0.05	0.47	0.07	0.09	0.15	0.17	0.09	0.47	<0.05	0.49	<0.05	0.81	<0.05
	TDP	0.10	0.11*	0.19	0.22	0.17	0.40	0.26	0.09	0.11	0.11	0.08	0.10	0.15	0.21
	SRP	0.06	0.10	0.12	0.18	0.11	0.31	0.19	0.06	0.05	0.07	<0.05	0.07	0.07	0.15
	DOP	<0.05	<0.05	0.07	<0.05	0.07	0.09	0.07	<0.05	0.06	<0.05	<0.05	<0.05	0.08	0.06
	TN	0.96*	0.50	1.18	1.36	1.03	0.71	1.26	1.17	1.16	0.88	1.09	0.97	3.23	1.39
	PN	0.11	<0.05	0.07	0.33	0.07	0.12	0.24	0.22	0.14	0.13	<0.05	<0.05	0.98	0.22
	TDN	0.85	0.45	1.11	1.03	0.96	0.59	1.02	0.96	1.03	0.75	1.08*	0.94	2.25	1.17
	NO3	0.50	0.42	0.37	0.71	0.47	0.21	0.36	0.44	0.39	0.64	0.45	0.72	0.72	0.97
	NO2	<0.05	<0.05	<0.05	<0.05	<0.05	<0.05	<0.05	<0.05	<0.05	<0.05	<0.05	<0.05	0.07	<0.05
	NH4	0.25	0.10	0.18	0.25	0.20	0.12	0.21	0.30	<0.05	0.12	0.43	0.23	0.22	0.12
	DON	0.07	<0.05	0.54	0.40	0.27	0.26	0.43	0.21	0.62	<0.05	0.18	<0.05	1.24	0.08
02/09/2017	TSS	122	25	-	-	-	-	-	-	-	-	-	-	223	36
	TP	0.64	0.11	-	-	-	-	-	-	-	-	-	-	0.38	0.31
	PP	0.09	<0.05	-	-	-	-	-	-	-	-	-	-	0.24	0.14
	TDP	0.54	0.09	-	-	-	-	-	-	-	-	-	-	0.14	0.16
	SRP	0.13	0.06	-	-	-	-	-	-	-	-	-	-	0.09	0.16
	DOP	0.41	<0.05	-	-	-	-	-	-	-	-	-	-	<0.05	<0.05
	TN	4.58	1.23	-	-	-	-	-	-	-	-	-	-	6.47	5.20
	PN	2.24	0.13	-	-	-	-	-	-	-	-	-	-	0.56	0.20
	TDN	3.24*	1.10	-	-	-	-	-	-	-	-	-	-	5.91	5.00
	NO3	1.88	0.35*	-	-	-	-	-	-	-	-	-	-	3.00	3.99
	NO2	<0.05	<0.05	-	-	-	-	-	-	-	-	-	-	<0.05	<0.05
	NH4	0.26	0.10	-	-	-	-	-	-	-	-	-	-	0.22	0.13
	DON	0.63	0.60	-	-	-	-	-	-	-	-	-	-	2.67	0.83
02/25/2017	TSS	947	7	386	8	415	806	-	-	508	29	1427	456	1408	89
	TP	1.49	0.11	1.19	0.24	1.13	2.05	-	-	1.03	0.19	2.81	1.11	2.56	0.39
	PP	1.32	<0.05	0.92	<0.05	0.83	1.76	-	-	0.92	0.08	1.52	0.81	2.07	0.17

	TDP	0.17	0.07	0.27	0.22	0.29	0.29	-	-	0.11	0.11	1.30	0.30	0.49	0.22
	SRP	0.12	0.06	0.20	0.17	0.19	0.24	-	-	0.09*	0.10	1.08	0.22	0.32	0.16
	DOP	0.05	<0.05	0.08	<0.05	0.11	0.05	-	-	<0.05	<0.05	0.21	0.08	0.17	0.06
	TN	8.14	1.39	8.57	4.46	4.53	6.05	-	-	4.76	2.76	17.29*	5.86	12.64	4.89
	PN	4.51	0.49	4.77	0.67	1.85	2.49	-	-	2.37	0.19	8.72	2.48	8.26	0.18
	TDN	3.62	0.90	3.80*	3.79	2.67	3.56	-	-	2.38	2.56	8.57	3.37	4.39	4.71
	NO3	0.92	0.65	0.80	0.66	0.76	0.88	-	-	0.59	0.98	1.80	1.03	1.49*	3.19
	NO2	<0.05	<0.05	<0.05	<0.05	<0.05	<0.05*	-	-	<0.05	<0.05	<0.05	<0.05	0.06	<0.05
	NH4	0.29	0.07	0.41	0.35	0.41*	0.32	-	-	0.26	0.23	0.44	0.50	0.48	0.19
	DON	2.36	0.14	2.54	2.72	1.45	2.31	-	-	1.49	1.30	6.28	1.80	2.36	1.29
03/14/2017	TSS	214	1	74	1	15	8	29	5	78*	9	281	6*	113	15
	TP	0.31	<0.05	0.19	0.14	0.41*	0.15	0.28	0.18	0.17	<0.05	0.30	<0.05	0.43	0.08
	PP	<0.05	<0.05	<0.05	<0.05	0.21	<0.05	0.09	<0.05	0.15	<0.05	0.26	<0.05	0.11	<0.05
	TDP	0.29	<0.05	0.12	0.12	0.20	0.15	0.20	0.17	<0.05	<0.05	<0.05	<0.05	0.32	<0.05
	SRP	0.09	<0.05	0.18	0.16	0.16	0.12	0.20	0.17	<0.05	<0.05	0.08	<0.05	0.32*	<0.05
	DOP	0.06	<0.05	<0.05	<0.05	<0.05	<0.05	<0.05	<0.05	<0.05	<0.05	<0.05	<0.05	<0.05	<0.05
	TN	2.69	0.64	1.18	2.78	8.85	1.04	1.77	1.49	2.94	1.12	2.31	1.28	2.03	3.31
	PN	0.57	0.06	0.12	0.12	5.56	0.15	0.29	0.05	1.18	0.18	1.27	0.23	0.76	0.12
	TDN	2.12	0.58	1.06	2.66	3.29	0.89	1.48	1.43	1.76	0.93	1.04	1.05	1.28	3.19*
	NO3	0.79	0.40	0.41	2.37	0.43	0.28	0.54	0.96	0.84	0.67	0.18	0.73	0.55*	2.37
	NO2	<0.05	<0.05	<0.05	<0.05	<0.05	<0.05	<0.05	<0.05	<0.05	<0.05	<0.05	<0.05	<0.05	<0.05
	NH4	0.67	0.08	0.22	0.21	1.03	0.17	0.37	0.18	0.31	0.14	0.19	0.13	0.39	0.10
	DON	0.60	<0.05	0.37	<0.05	1.77	0.38	0.51	0.24	0.56	0.07	0.62	0.14	0.29	0.67
03/31/2017	TSS	132	10	214*	28	42	19*	378	3	139	9	412	26	440	72
	TP	1.57	0.12	2.05	0.40	0.31	0.26	0.90	0.35	0.34	0.11	0.94	0.19	1.68	0.24
	PP	0.24	<0.05	0.23	0.05	0.16	0.06	0.56	0.09	0.18	<0.05	0.68	0.06	1.24	0.06
	TDP	1.33	0.10	1.82	0.35	0.15	0.20	0.35	0.27	0.16	0.10	0.25	0.13	0.44	0.17

	SRP	0.65	0.08	1.35	0.28	0.09	0.14	0.25	0.24	0.10	0.10	0.22	0.12	0.34	0.15
	DOP	0.68	<0.05	0.47	0.07	0.05	0.05	0.10	<0.05	0.06	<0.05	<0.05	<0.05	0.10	<0.05
	TN	15.64	1.19	9.39	3.97	3.59	5.54*	12.37	3.70	7.06	2.53	8.15	2.11	13.06	3.69
	PN	1.06	0.07	1.99	0.42	0.45	<0.05	2.60	0.22	1.20	0.65	3.42	<0.05	8.43	0.21
	TDN	14.58	1.12	7.40	3.55	3.14	5.54	9.77	3.48	5.86	1.88	4.73	2.07	4.63	3.48
	NO3	0.13	0.35	0.53	<0.05	0.24*	0.62	1.37	0.30	0.28	0.24	0.64	0.44	0.67	0.76*
	NO2	0.14	<0.05	0.13	0.12	<0.05	0.05	0.20	<0.05	0.06	<0.05*	0.09*	<0.05	0.10	<0.05
	NH4	1.86	0.09	0.46	0.04	0.29*	0.76	0.73	0.39	0.54*	0.22	0.56	0.18	0.34	0.10
	DON	12.45	0.64	6.28	3.34	2.56	4.10	7.47	2.74	4.98	1.38	3.44	1.40	3.52	2.57
04/06/2017	TSS	232	9*	248	60	23	153	373	183	112	19*	621	696	449	89
	TP	0.83	0.40	1.48	0.49	0.72	0.57*	0.86	0.65	0.67	0.25	1.89	0.94	1.71	0.36
	PP	0.05	<0.05	0.12	<0.05	0.17	0.36	<0.05	0.35	0.28	<0.05	0.50	0.70	0.57	0.11
	TDP	0.77	0.39	1.37	0.49	0.55	0.21	0.83	0.30	0.39	0.23	1.39	0.24	1.14	0.25
	SRP	0.71	0.19	1.35	0.42	0.55	0.09	0.80*	0.27	0.27	0.13*	1.31	0.18	1.03	0.25
	DOP	0.06	0.20	<0.05	0.07	<0.05	0.12	<0.05	<0.05	0.12	0.10	0.07	0.06	0.11	<0.05
	TN	2.61	0.61	4.61	0.97	6.49	1.49	4.51	1.77	3.58	0.73	5.10	1.96	5.51	1.88
	PN	0.39	0.19	0.88	0.27	0.36	1.06	0.86	0.69	0.73	0.03	0.33	1.50	1.98	0.38
	TDN	2.22	0.42	3.73	0.70	6.13	0.43	3.65*	1.08	2.85*	0.70	4.77	0.46	3.53	1.50
	NO3	0.31	0.09*	0.36	0.13	0.50	0.10	0.55	0.11	0.52	0.23	0.54	0.09	0.46	0.46
	NO2	<0.05	<0.05*	<0.05	<0.05	<0.05	<0.05	<0.05	<0.05	<0.05	<0.05	0.05	<0.05	<0.05	<0.05
	NH4	0.26	0.08	0.36	<0.05	0.53*	0.11	0.44	0.23*	0.29	0.09	0.53	0.12	0.32	0.07
	DON	1.60	0.20	2.96	0.47	5.05	0.17	2.61	0.69	1.99	0.33	3.65	0.20	2.70	0.92
04/22/2017	TSS	911	1	173	1	182	180	284	53	-	-	418	51	336*	39
	TP	1.89	0.21	0.65	0.17	0.87	0.81	4.14	0.32*	-	-	1.18	0.48	1.29*	0.25
	PP	1.42	0.08	0.19	<0.05	0.53	0.47	1.30	0.23	-	-	0.91	0.25	1.10	0.09
	TDP	0.47	0.14	0.46	0.13	0.34	0.34	2.83	0.09	-	-	0.28	0.22	0.19	0.16
	SRP	0.26	0.10	0.15	<0.05	0.14	0.21	1.70*	0.07	-	-	0.13	0.12	0.06	0.09

	DOP	0.21	<0.05	0.31	0.10	0.21	0.13	1.13	<0.05	-	-	0.15	0.10	0.14	0.07
	TN	5.40	0.87	5.40	1.96	6.05	4.62	37.90	1.29*	-	-	3.42	2.06	3.35	6.01
	PN	3.61	0.11	3.81	0.97	4.06	2.61	17.23	0.47	-	-	2.27	0.55	1.83	0.55
	TDN	1.79	0.76	1.59	0.99	1.99	2.01	20.67	0.82	-	-	1.15	1.51	1.52	5.46
	NO3	<0.05	0.41	<0.05	<0.05	0.13	0.22	0.50	<0.05	-	-	<0.05	0.29	0.08	5.32
	NO2	<0.05	<0.05	<0.05*	<0.05	<0.05	<0.05	<0.05	<0.05	-	-	<0.05	0.25	<0.05	<0.05
	NH4	0.28	0.26	0.20	0.07*	0.43	0.93	1.80	0.50	-	-	0.25	0.40	0.23	0.09
	DON	1.41	<0.05	1.29	0.82	1.38	0.81	18.32	0.22	-	-	0.80	0.57	1.16	<0.05
05/05/2017	TSS	90	1	88	23	85	12	158	2*	75	1	108	10	201	10
	TP	2.19	0.54	2.34*	0.82	1.26	1.60	1.75	0.52*	0.65	0.18	1.30	0.64	1.39	0.66
	PP	0.12	0.28	0.33	<0.05	0.29	0.41	0.70	0.17	0.16	<0.05	0.29	0.14	0.47	0.22
	TDP	2.08	0.26	2.01	0.82	0.96	1.18	1.05	0.35	0.48	0.16	1.02	0.51	0.92	0.44
	SRP	1.18	0.15	1.22	0.48	0.49	0.70*	0.79	0.35	0.40	0.16	0.39	0.32	0.42	0.22*
	DOP	0.90	0.11	0.79	0.33	0.47	0.48	0.26	<0.05	0.09	<0.05	0.62	0.18	0.49	0.22
	TN	8.67	0.82	5.86	4.20	6.47	5.82	7.94	3.11	6.61	2.97	7.90	2.10	8.88	7.46
	PN	0.71	0.13	0.36	0.07	0.97	1.21	3.18	0.14	1.21	<0.05	1.69	<0.05	6.12	0.14
	TDN	7.96	0.69	5.50	4.13	5.50	4.61	4.76	2.97	5.40	2.96	6.21	2.06	2.76	7.32
	NO3	0.52	0.09*	0.05	<0.05	1.46	0.21*	1.53	1.21	0.86	1.66	0.95	1.34	0.63	6.29
	NO2	0.67	<0.05	0.36	0.08	0.23	<0.05	0.27*	<0.05*	0.06	<0.05	0.22	<0.05	0.10	0.18
	NH4	0.70	0.12	1.05	0.74	0.93*	2.06	0.26	0.59	1.23	0.52	1.01*	0.22	0.50	0.15
	DON	6.07	0.43	4.04	3.26	2.88	2.29	2.70	1.12	3.25	0.73	4.03	0.45	1.53	0.70
05/11/2017	TSS	195	13	44*	1	52	24	-	-	542	37	468	48	120	33*
	TP	1.02	0.19	1.24	0.27	0.78	0.38	-	-	1.35	0.14	1.46	0.18	0.67	0.29
	PP	0.54	0.15	0.25	<0.05	0.10	0.11	-	-	0.94	<0.05	1.24	0.08	0.30	0.11
	TDP	0.48	<0.05	0.99	0.25	0.68	0.28	-	-	0.40	0.10	0.22	0.10*	0.37	0.18
	SRP	0.33	<0.05	0.70	0.23	0.42	0.21	-	-	0.24	0.10	0.12	0.11	0.22	0.14
	DOP	0.15	<0.05	0.29	<0.05	0.26	0.07	-	-	0.17	<0.05	0.10	<0.05	0.15	<0.05

	TN	4.71	1.91	49.24	8.04	5.72	1.99	-	-	5.92	1.99	11.27	1.38	7.90	5.31
	PN	1.40	<0.05	4.04	0.35	1.37	0.08	-	-	1.46	0.09	9.28	0.12	3.53	<0.05
	TDN	3.31*	1.88	45.20	7.69	4.35	1.91	-	-	4.46	1.90	1.99	1.26	4.37	5.28
	NO3	0.74	1.68	1.47	3.42	1.21	1.51	-	-	1.18	1.34	0.36	0.51	1.00	3.94
	NO2	0.07	<0.05	0.11	<0.05	0.10	<0.05	-	-	0.08	<0.05	<0.05	<0.05	0.09	<0.05
	NH4	0.39	0.07	6.77	0.60	0.48	0.12	-	-	0.61	<0.05	0.30	0.13	0.58	0.13
	DON	2.11	0.08	36.85	3.62	2.56	0.23	-	-	2.60	0.46	1.28	0.57	2.69	1.16
05/13/2017	TSS	77	1	15	2	56	3	187	27	80	13*	299	1	51	2
	TP	0.37	0.12	0.25	0.18	0.25	0.19	1.00	0.19	0.23	0.10	0.68	0.14	0.26	0.21
	PP	0.27	0.07	0.15	<0.05	0.10	<0.05	0.42	0.07	0.13	<0.05	0.49	<0.05	0.17	0.09
	TDP	0.09	<0.05	0.10	0.16	0.15	0.15	0.58	0.12	0.11	0.09	0.20	0.10	0.09	0.12
	SRP	0.08	<0.05	0.05	0.14	0.07	0.07	0.32	0.10	0.06	0.05	<0.05	<0.05	<0.05	<0.05
	DOP	<0.05	<0.05	0.05	<0.05	0.08	0.08	0.26	<0.05	0.05	<0.05	0.15	0.05	<0.05	0.07
	TN	2.34	1.11	6.47	1.69	2.30	0.99	56.60	5.18	3.14	1.08	67.65	1.39	4.57	1.70
	PN	0.77	0.17	2.92	<0.05	0.69	<0.05	14.59	0.68	1.05	0.25	20.72	0.20	2.78	<0.05
	TDN	1.57	0.94	3.55	1.67	1.61	0.99	42.01	4.50	2.09	0.83	46.93*	1.19	1.79	1.66
	NO3	0.40	0.57	0.46	0.72	0.44	0.40	0.52*	0.43	0.51	0.51	0.73*	0.34	0.29	0.56
	NO2	<0.05	<0.05	<0.05	<0.05	<0.05	<0.05	<0.05	<0.05	<0.05	<0.05	<0.05	<0.05	<0.05	<0.05
	NH4	0.17	0.09	0.44	0.34	0.14	0.13	1.81	0.83	0.23	<0.05	1.81	<0.05	0.18	0.05
	DON	0.95	0.23	2.60	0.56	0.98	0.41	39.63	3.19	1.30	0.22	44.34	0.75	1.27	1.00

REFERENCES

Anderson, T.A., Guthrie, E.A., and Walton, B.T. (1993). Bioremediation in the rhizosphere. *Environmental Science and Technology,* 27, 2630-2636.

Arias, M. E., Brown, M. T., and Sansalone, J. J. (2013). Characterization of Storm Water–Suspended Sediments and Phosphorus in an Urban Catchment in Florida. *Journal of Environmental Engineering*, *139*(2), 277–288. https://doi.org/10.1061/(ASCE)EE.1943-7870.0000583.

Ayoub, G. M., Koopman, B., and Pandya, N. (2001). Iron and Aluminum Hydroxy (Oxide) Coated Filter Media for Low-Concentration Phosphorus Removal. *Water Environment Research*, *73*(4), 478–485.

Barrett, M. E. (2010). *Evaluation of sand filter performance*. Center for Research in Water Resources, University of Texas at Austin. Retrieved from https://utexas-ir.tdl.org/bitstream/handle/2152/10896/CRWR%20online%20report%2010-07.pdf?sequence=2

Barrett, M. E., Limouzin, M., and Lawler, D. F. (2013). Effects of Media and Plant Selection on Biofiltration Performance. *Journal of Environmental Engineering*, *139*(4), 462–470. https://doi.org/10.1061/ (ASCE)EE.1943-7870.0000551.

Berretta, C., and Sansalone, J. (2011). Speciation and Transport of Phosphorus in Source Area Rainfall?Runoff. *Water, Air, & Soil Pollution*, *222*(1–4), 351–365. https://doi.org/10.1007/s11270-011-0829-2

Benjamin, Mark M., and Lawler, Desmond F. (2013). Water Quality Engineering: Physical / Chemical Treatment Processes, Wiley, New Jersey.

Bertrand–Krajewski, J. L., Chebbo, G., and Saget, A. (1998) Distribution of pollutant mass vs volume in stormwater discharges and the first flush phenomenon. Water Res., 32 (8), 2341–2356.

Bratieres, K., Fletcher, T.D., Deletic, A., and Zinger, Y. (2008). Nutrient and sediment removal by stormwater biofilters: a largescale design optimisation study. Water Res. 42 3930–3940.

Brown, R. A., Birgand, F., and Hunt, W. F. (2013). Analysis of Consecutive Events for Nutrient and Sediment Treatment in Field-Monitored Bioretention Cells. *Water, Air, & Soil Pollution*, *224*(6). https://doi.org/10.1007/s11270-013-1581-6

Center for Watershed Protection (CWP) (2003). *Maryland Chesapeake and Atlantic Coastal Bays Critical Area 10% Rule Guidance Manual, Fall 2003*.

Chen, S., Ling, J., and Blancheton, J.-P. (2006). Nitrification kinetics of biofilm as affected by water quality factors. *Aquacultural Engineering*, *34*(3), 179–197. https://doi.org/10.1016/j.aquaeng.2005.09.004.

Chesapeake Bay Foundation (CBF) (n.d.). *Major River Watersheds of the Chesapeake Bay.* Accessed on 22 December 2016 at http://www.cbf.org/about-the-bay/maps/major-watersheds.

Collins, K.A., T.J. Lawrence, E.K. Stander, R.J. Jontos, S.S. Kaushal, T.A. Newcomer, N.B. Grimm, and M.L. Cole Ekberg (2010). Opportunities and Challenges for Managing Nitrogen in Urban Stormwater: A Review and Synthesis. Ecological Engineering 36:1507-1519.

Convergent. (n.d.). *Next Generation Bioretention: High Performance Modular Biofiltration Systems*.

Cronshey, R., McCuen, Richard H., Miller, Norman, Rawls, Walter, Robbins, Sam, and Woodward, Don (1986). *Urban hydrology for small watersheds*. US Dept. of Agriculture, Soil Conservation Service, Engineering Division. Retrieved from http://repositories.tdl.org/tamug-ir/handle/1969.3/24438.

Davis, A. P. (2007). Field performance of bioretention: Water quality. *Environmental Engineering Science*, *24*(8), 1048–1064. https://doi.org/10.1089/ees.2006.0190.

Davis, A. P., Shokouhian, M., Sharma, H., and Minami, C. (2006). Water Quality Improvement through Bioretention Media: Nitrogen and Phosphorus Removal. *Water Environment Research*, *78*(3), 284–293.

Davis, A. P., and McCuen, R. H. (2005). *Stormwater management for smart growth*. New York: Springer Science.

Davis, A. P., R. G. Traver, W. F. Hunt, R. Lee, R. A. Brown, and J. M. Olszewski. (2012). Hydrologic Performance of Bioretention Storm-Water Control Measures. *Journal of Hydrologic Engineering* 17(5):604-614.

Deletic, A. (1998) The first flush load of urban surface runoff. Water Res., 32 (8), 2462–2470.

Dietz, M. E., and Clausen, J. C. (2006). "Saturation to improve pollutant retention in a rain garden." Environ. Sci. Technol., 40(4), 1335–1340.

Eaton, A. D., Clesceri, L. S., Greenberg, A. E., and Franson, M. A. H., American Public Health Association., American Water Works Association., and Water Environment Federation. (1998). *Standard methods for the examination of water and wastewater*. Washington, DC: American Public Health Association.

Erickson, A. J., Gulliver, J. S., and Weiss, P. T. (2007). Enhanced Sand Filtration for Storm Water Phosphorus Removal. *Journal of Environmental Engineering*, *133*(5), 485–497. https://doi.org/10.1061/ ASCE 0733-9372 2007 133:5 485

Hallegraeff, G. M. (1993) A review of harmful algal blooms and their apparent global increase. Phycologia: March 1993, Vol. 32, No. 2, pp. 79-99.

Hartsig, T., and Szatko, A. (2012). *Performance Assessment of Two Stormwater Best Management Practices for Infiltration, Water Quality, and Vegetative Growth*.

Hathaway, J. M., Tucker, R. S., Spooner, J. M., and Hunt, W. F. (2012). A Traditional Analysis of the First Flush Effect for Nutrients in Stormwater Runoff from Two Small Urban Catchments. *Water, Air, & Soil Pollution*, *223*(9), 5903–5915. https://doi.org/10.1007/s11270-012-1327-x

Hatt, B.E., Fletcher, T.D., and Deletic, A. (2008). Hydrologic and pollutant removal performance of stormwater and biofiltration systems at the field scale. Journal of Hydrology 365: 310- 321.

He, J., Valeo, C., Chu, A., and Neumann, N. F. (2010). Characteristics of Suspended Solids, Microorganisms, and Chemical Water Quality in Event-Based Stormwater Runoff from an Urban Residential Area. *Water Environment Research*, *82*(12), 2333–2345. https://doi.org/10.2175/106143010X12681059117058

Hillel, D. (1998). *Environmental soil physics*. San Diego, CA: Academic Press.

Hsieh, C., and Davis, A. P. (2005). Evaluation and Optimization of Bioretention Media for Treatment of Urban Storm Water Runoff. *Journal of Environmental Engineering*, *131*(11), 1521–1531. https://doi.org/10.1061/ ASCE 0733-9372 2005 131:11 1521

Hsieh, C., Davis, A. P., and Needelman, B. A. (2007). Nitrogen Removal from Urban Stormwater Runoff Through Layered Bioretention Columns. *Water Environment Research*, *79*(12), 2404–2411.

Hunt, W. F., Davis, A. P., and Traver, R. G. (2012). Meeting Hydrologic and Water Quality Goals through Targeted Bioretention Design. *Journal of Environmental Engineering*, *138*(6), 698–707. https://doi.org/10.1061/(ASCE)EE.1943-7870.0000504

Irish, L., Lesso, W., Barrett, M. E., Malina, J. F., Charbeneau, R., and Ward, G. (1995). *An Evaluation of the Factors Affecting the Quality of Highway Runoff in the Austin, Texas Area* (No. CRWR 264). Center for Research in Water Resources, University of Texas at Austin.

Kadlec, R. H., and Knight, R. L. (1996). Treatment wetlands, CRC Press, Boca Raton, FL.

Kerkez, B., Gruden, C., Lewis, M., Montestruque, L., Quigley, M., Wong, B., Bedig, A., Kertesz, R., Braun, T., Cadwalader, O., Poresky, A., and Pak, C. (2016). Smarter Stormwater Systems. *Environmental Science & Technology*, *50*(14), 7267–7273. https://doi.org/10.1021/acs.est.5b05870.

Khorsha, G., and Davis, A. P. (2017). Characterizing Clinoptilolite Zeolite and Hydroaluminosilicate Aggregates for Ammonium Removal from Stormwater Runoff. *Journal of Environmental Engineering*, *143*(2), 4016082. https://doi.org/10.1061/(ASCE)EE.1943-7870.0001167.

Kim, H., Seagren, E. A., and Davis, A. P. (2003). Engineered Bioretention for Removal of Nitrate from Stormwater Runoff. *Water Environment Research*, *75*(4), 355–367.

Kreeb, L. B. (2003). *Hydrologic efficiency and design sensitivity of bioretention facilities* (Honor's Research). University of Maryland, College Park.

Lee, J. H., Bang, K. W., Ketchum, L. H., Choe, J. S., and Yu, M. J. (2002). First flush analysis of urban storm runoff. *Science of the Total Environment*, *293*(1), 163–175.

Lenth, J., Dugopolski, R., Quigley, M., Poresky, A., and Leisenring, M. (2010). Filterra Bioretention Systems: Technical Basis for High Flow Rate Treatment and Evaluation of Stormwater Quality Performance. *Americast Inc.: Ashland, VI, USA*. Retrieved from http://documents.northgeorgiawater.org/stormwater/post-construction-stormwater-technology-assessment-protocol/evaluated-products/filterra/Appendix_D_High_Flow_Rate_Whitepaper.pdf

Li, H., and Davis, A. P. (2009). Water quality improvement through reductions of pollutant loads using bioretention. *Journal of Environmental Engineering*, *135*(8), 567–576.

Li, L., and Davis, A. P. (2014). Urban Stormwater Runoff Nitrogen Composition and Fate in Bioretention Systems. *Environmental Science & Technology*, *48*(6), 3403–3410. https://doi.org/10.1021/es4055302

Li, Y., Lau, S., Kayhanian, M., and Stenstrom, M. K. (2005). "Particle size distribution in highway runoff." J. Environ. Eng., 131(9), 1267–1276.

Liu, J., and Davis, A. P. (2014). Phosphorus Speciation and Treatment Using Enhanced Phosphorus Removal Bioretention. *Environmental Science & Technology*, *48*(1), 607–614. https://doi.org/10.1021/es404022b.

Logan, B. E., Jewett, D. G., Arnold, R. G., Bouwer, E. J., and O'Melia, C. R. (1995). Clarification of Clean-Bed Filtration Models. *Journal of Environmental Engineering*, *121*(12), 869–873.

Lucas, W. C. and Greenway, M. (2008) Nutrient Retention in Vegetated and Non-vegetated Bioretention Mesocosms. J. Irrig. Drain. E-ASCE, 134 (5): 613-623.

Lucas, W. C. and Greenway, M. (2011). Hydraulic response and nitrogen retention in bioretention mesocosms with regulated outlets: part II–nitrogen retention. Water Environ Res. 2011 Aug;83(8):703-13.

Ma, Jia, Derek Berg, James H. Lenhart, John Pedrick, and Karel Tracy (2011). Field Study of Total Phosphorus Removal from Stormwater Runoff Using Adsorptive Filtration Media, *World Environmental and Water Resources Congress, Bearing Knowledge for Sustainability,* 649-656.

Manka, B. N., Hathaway, J. M., Tirpak, R. A., He, Q., and Hunt, W. F. (2016). Driving forces of effluent nutrient variability in field scale bioretention. *Ecological Engineering*, *94*, 622–628. https://doi.org/10.1016/j.ecoleng.2016.06.024.

McCuen, R. H. (2003). Smart growth: hydrologic perspective. *Journal of Professional Issues in Engineering Education and Practice*, *129*(3), 151–154.

McCuen, Richard H. (2005). *Hydrologic Analysis and Design,* 3rd edition, Pearson, New Jersey.

McCuen, R. H., and Bondelid, T. R. (1983). Estimating unit hydrograph peak rate factors. *Journal of Irrigation and Drainage Engineering*, *109*(2), 238–250.

Nakamoto, Nobutada, Nigel Graham, and Rolf Gimbel (2014). *Progress in Slow Sand and Alternative Biofiltration Processes,* International Water Association.

New York State Department of Environmental Conservation (NYSDEC) (2008). *Stormwater Design Manual.*

Northern Virginia Planning District Commission (NVPDC) (1992). *Northern Virginia BMP Handbook.*

Pitt, R., Field, R., Lalor, M., and Brown, M. (1995). Urban stormwater toxic pollutants: assessment, sources, and treatability. *Water Environment Research*, *67*(3), 260–275.

O'Neill, S. W., and Davis, A. P. (2012). "Water treatment residual as a bioretention amendment for phosphorus. I. Evaluation studies." J. Environ. Eng., 10.1061/(ASCE)EE.1943-7870.0000409, 318–327.

OptiRTC (n.d.). *Optimize Your Stormwater Infrastructure*. www.optirtc.com.

Peterson, I. J., Igielski, S., and Davis, A. P. (2015). Enhanced Denitrification in Bioretention Using Woodchips as an Organic Carbon Source. *Journal of Sustainable Water in the Built Environment*, *1*(4). https://doi.org/10.1061/ JSWBAY.0000800

Rajagopalan, R., Tien, C., Pfeffer, R., and Targos, G. (1982). Letter to the editor, *AlChE J.,* 28(5), 871-872.

Saget, A., Chebbo, G., and Bertrand–Krajewski, J. (1996) The first flush in sewer systems. Water. Sci. Technol., 33 (9), 101–108.

Sansalone J.J., Koran J.M., Smithson J.A. and Buchberger S.G. (1998). Physical characteristics of urban roadway soils transported during rain events, J. of Environ. Engineering, 124(5), 427-440.

Sansalone, J. J., and Cristina, C. M. (2004). First Flush Concepts for Suspended and Dissolved Solids in Small Impervious Watersheds. *Journal of Environmental Engineering*, *130*(11), 1301–1314. https://doi.org/10.1061/(ASCE)0733-9372(2004)130:11(1301).

Sansalone, J. J., and Kim, J.-Y. (2008). Transport of Particulate Matter Fractions in Urban Source Area Pavement Surface Runoff. *Journal of Environment Quality*, *37*(5), 1883. https://doi.org/10.2134/jeq2007.0495.

Sartor, J. D., G. B. Boyd, and F. J. Agardy (1974). Water pollution aspects of street surface contaminants. Journal (Water Pollution Control Federation):458-467.

Schnoor, J.L., Licht, L.A., McCutcheon, S.C., Wolfe, N.L. and Carriera, L.H. (1995) Phytoremediation: An Emerging Technology for Contaminated Soils. Environ. Sci. Technol., 29:318-323A.

Schueler, T. (1987), "Controlling Urban Runoff: A Practical Manual for Planning and Designing urban BMPs," Metropolitan Washington Council of Governments, Washington, DC.

Selbig, W.R., and Bannerman, R.T (2011). Characterizing the size distribution of particles in urban stormwater by use of fixed-point sample-collection methods: U.S. Geological Survey Open-File Report 2011–1052, 14 p.

Shang, C., Huang, P. M., and Stewart, J. W. B. (1990). "Kinetics of adsorption of organic and inorganic phosphates by short-range ordered precipitate of aluminum." Can. J. Soil Sci., 70(3), 461–470.

Soil Survey Staff, National Resources Conservation Service (NRCS). United States Department of Agriculture. *Web Soil Survey*. Accessed 17 August 2016 at https://websoilsurvey.sc.egov.usda.gov/.

Taylor, G. D., Fletcher, T. D., Wong, T. H. F., Breen, P. F., and Duncan, H. P. (2005). Nitrogen composition in urban runoff—implications for stormwater management. *Water Research*, *39*(10), 1982–1989. https://doi.org/10.1016/j.watres.2005.03.022.

Thermo Scientific (2010). *Nalgene Storm Water Sampler.* Retrieved from https://tools.thermofisher.com/content/sfs/brochures/D01640.pdf.

Urbonas, B. R. (1999). Design of a sand filter for stormwater quality enhancement. *Water Environment Research*, *71*(1), 102–113.

U.S. E.P.A. (2009). *National Water Quality Inventory: Report to Congress 2004 Reporting Cycle* (No. EPA 841-R-08-001). Washington, D.C.

USA Maryland Location Map (n.d.). Imaged obtained from Wikipedia Commons at https://commons.wikimedia.org/wiki/File:USA_Maryland_location_map.svg.

Van Buren, M.A., W.E. Watt, and J. Marsalek (1997). Applications of the Log-normal and Normal Distribtuions of Stormwater Quality Parameters, *Water Research,* 31(1), 95-104.

Vaze, J., and Chiew, F. H. (2002). Experimental study of pollutant accumulation on an urban road surface. *Urban Water*, *4*(4), 379–389.

Vaze, J., and Chiew, F. H. (2003). Study of Pollutant Washoff from Small Impervious Experiemental Plots. *Hydrogeochemistry and Water Chemistry*, *39*(6).

Weber, Walter J., Jr. (2001). *Environmental Systems and Processes: Principles, Modeling, and Design.* Wiley-Interscience, New Jersey.

Yan, Q., Davis, A. P., and James, B. R. (2016). Enhanced Organic Phosphorus Sorption from Urban Stormwater Using Modified Bioretention Media: Batch Studies. *Journal of Environmental Engineering*. https://doi.org/10.1061/(ASCE)EE.1943-7870 .0001073

Yao, K., Habiban, M.T., and O'Meila, C.R. (1971). Water and Wastewater Filtration: Concepts and Applications, *Environmental Science and Technology* 5(11), 1105-1112.

Young, G. K., Stein, S., Cole, P., Kammer, T., Graziano, F., and Bank, F. (1996). *Evaluation and Management of Highway Runoff Water Quality* (No. FHWA-PD-96-032). U.S. Department of Transportation.

Yu, S. L., and Stanford, R. (2007). Field evaluation of a stormwater bioretention filtration system. *Journal of Environmental Engineering and Management*, *17*(1), 63.

Zinger, Y., Blecken, G. T., Fletcher, T. D., Viklander, M., and Deletic, A. (2013). Optimising nitrogen removal in existing stormwater biofilters: Benefits and tradeoffs of a retrofitted saturated zone. Ecol. Eng. 2013, 51, 75−82.